Structure-Property correlations in ultra-high strain PLZT ceramics prepared via high energy mechanical milling

A thesis submitted

By

Ajeet Kumar

in partial fulfilment of the requirements for the award of the degree of

Doctor of Philosophy

in

Physics

School of Physics

University of Hyderabad

Hyderabad 500046

India

August 2016

DECLARATION

I hereby declare that the work embodied in this thesis entitled "**Structure-Property Correlations in ultra-high strain PLZT ceramics prepared via high energy mechanical milling"** is submitted to the University of Hyderabad in partial fulfilment for the award of **Doctor of Philosophy** in **Physics** is an original research work and results carried out by me under the joint supervision of **Prof. K. C. James Raju**, School of Physics, University of Hyderabad, Hyderabad, India and **Dr. A. R. James**, Scientist-F, Ceramics and Composites Group, Defence Metallurgical Research Laboratory, Hyderabad, India. To the best of my knowledge, this work is not submitted for any other degree in any University or Institute.

Ajeet Kumar

(12PHPH22)

Place: Hyderabad

Date:

CERTIFICATE FROM THE SUPERVISORS

This is to certify that the thesis entitled **"Structure-Property Correlations in ultra-high strain PLZT ceramics prepared via high energy mechanical milling"** is being submitted by **Mr. Ajeet Kumar** in partial fulfilment for the award of **Doctor of Philosophy** in **Physics** to the University of Hyderabad is a record of bonafide work carried out by him under our guidance and supervision at School of Physics, University of Hyderabad, Hyderabad, India and Ceramics and Composites Group, Defence Metallurgical Research Laboratory, Hyderabad, India. The results embodied in this thesis have not been submitted to any other University or Institute for the award of any degree or diploma.

Prof. K. C. James Raju
Supervisor

Dr. A. R. James, Sc-F
External supervisor

Date:

Date:

Dean
School of Physics, University of Hyderabad

Dedicated to

My Mother

Smt. Kamla Devi

List of contents

Acknowledgements

When I was first introduced to Physics, I wished that I could go to the end of this field. However, now I know that learning is a never ending process, but I am happy that at least academically I reached the pinnacle of this field. After getting a chance to fulfill my dream, from the first day to this day, the entire journey has been very fantastic, wonderful and a very important phase of my life.

First of all, I would like to thank my external supervisor Dr. A. R. James for his continuous support, encouragement, patience and guidance thorough out the Ph. D. program. Since I was new to the subject, he taught me all the basics from literature survey to experimental procedures. When I needed him for my research related problems to personal problems, he was always there to help me. His constant motivation, encouragement and discipline helped me to give my best.

I would like to thank my supervisor Prof. K. C. James Raju for believing in me, that I can do better. He polished my presentation as well as research skills and his valuable advice kept me focused. The discussions with him helped me to understand the research problems in different perspective. I admired him because of his continuous support.

I gratefully acknowledge the provision of funding for the research described in this thesis by Defence Metallurgical Research Laboratory, DRDO. I express my gratitude to former Directors of DMRL, Dr. G. Malakondaiah and Dr. Amol Ghokhle as well as the current Director Dr. S.V. Kamat, for giving the permission to carry out Ph.D. work and use the facilities of DMRL. I would also like to thank the Dean, School of Physics for giving me the opportunity to register for my Ph. D.

I would like to thank my doctoral committee members of UoH (Dr. S. Srinath and Dr. S.V.S. Nageswara Rao) and Research Council members of DMRL for their valuable and insightful suggestions.

I am grateful to Dr. V.V. Bhanu Prasad, Scientist 'G', DMRL, who gave me an opportunity to join his team as a research fellow and gave me access to all the facilities in the laboratory. I am thankful to Mr. M.L.V. Mahesh, Dr. N.V. Rama Rao, Mr. Vijaypal Shivran, Dr. P. Ghoshal, Mr. Premkumar and Mr. Mohan Rao from DMRL for technical discussion. Their valuable time, efforts, support and many fruitful discussions helped me throughout this research work.

I would like to thank the Prof. Rajeev Ranjan, IISc, Bangalore, Dr. B. Suresh, Dr. K. Suresh, ARCI, Hyderabad, Prof. G. Prasad, Osmania University, Hyderabad, Dr. K. Srinivas, ASL, Hyderabad and Dr. D. Pamu, IIT Guwahati for their constant support in the form of technical discussions and experimental help. Special thanks to Prof. Rajeev Ranjan for teaching me the basics of crystallography and Rietveld analysis and his Ph.D. scholar Dr. Ajay Kalyani for helping me in high temperature XRD measurements.

I would like to express my gratitude to all the faculty of the School of Physics, University of Hyderabad for sharing their knowledge and extending my knowledge base.

The support and efforts of the Ceramics and Composites Group (CCG) and the staff members of School of Physics, University of Hyderabad are gratefully acknowledged. Thanks are also due to all other admin and library staff from DMRL and UoH for their support in various aspects of work.

My special thanks to my colleagues and friends from DMRL Mrs. Rajlaxmi, Mr. Venkatramna, Mr. Venkatakrishnan, Mrs. Prasanna, Mr. Raghubir, Mr. V.S. Prasad, Mrs. Savita, Mr. Govind, Mr. Rakesh, Mr. Shivaji, Ms. Soumya, Mr. Rangaswami Reddy, Mr. Praveen, Mr. Rahul, Mr. Vikas and Mr. Deepak for constant motivation and support during the course of this work.

The support and motivation received from my lab mates Dr. Rambabu (IISc), Late Dr. Kiran, Mr. T. Anil, Mr. Ramakanth, Mr. E. Sivanaga Reddy, Mr. S. Bashaiah, Mr. Andrew Josheph, Mr. J.P. Gaud, Mr. Rahul Gayam, Mr. Sandeep Sharma, Mr. M. Alkhathy and friends Mr. Dhananjay, Mr. Paul Praveen, Mr. Shiva, Mrs. Rasmita, Ms. Ramya, Mrs. Preethi, Ms. Soumya, Ms. Uma, Mrs. Rasna, Dr. Suman Kalyan, Mr. Ravi, Dr. Alu, Mr. Sanjeeb, Mr. Naveen, University of Hyderabad from course work to research work is highly appreciated.

I am thankful to my friends Mr. Anil Kumar Saharan, Mr. Lokesh Sharma, Mr. Kishore, Dr. Shiv Kumar Barbar, Dr. Sardar Singh, Mr. Nakul, Mr. Vinay Pratap, Mr. Manish Sharma, Mr. Sunil Kumar, Mr. Prahlad, Mr. R. C. Jombos and Mr. Rajeev for their support at different stages of this research work.

Finally, I would like to thank my wife Pallavi and daughter Prakriti for their patience and understanding throughout this long journey. Their patience and calmness help me to focus on my work. I thank my brothers Mr. Vishal and Mr. Vikram, my sister Mrs. Renu, my sweet niece Riddhi and all my family members, for their continuous and enormous support and encouragement. Especial thanks to my grandmother and mother for their blessing, wishes.

List of figures

Chapter-I

Chapter-II

Chapter-III

Chapter-IV

Chapter-V

Chapter-VI

Chapter-VII

Chapter-VIII

List of tables

Chapter-I

Chapter-III

Chapter-IV

Chapter-V

Chapter-VI

Chapter-VII

Chapter-VIII

Synopsis

This thesis contains the research work on the investigation of ultra-high electrical (Dielectric, ferroelectric and piezoelectric) properties of La modified PZT ceramics. This work not only deals with the optimization of the amount of La substitution into the A-site of PZT system but also the processing parameters such as milling time, milling vials. With the help of a detailed X-ray investigation, the reasons behind the observed results are also explored. This work is divided into nine chapters, which deals with the different type of studies.

In **Chapter-1**, a brief introduction of piezoelectricity, ferroelectricity and their classification are given, which are directly related to this work. The objective of the present scheme of work is to synthesize and characterize smart materials such as soft lanthanum modified PZT ceramics by using high energy mechano-chemical ball milling technique which involves the optimization of La substitution in the PZT system as well as milling conditions (milling time, milling vials). On the one hand, the endeavor was to reduce the particle size while on the other hand, contamination had to be avoided since the properties of electro-ceramics are greatly affected by contaminants. The aim of this study is to understand the underlying Physics of Structure-Property Correlations of different compositions of PLZT ceramics by using different milling conditions and to improve the overall electrical properties of this material system. Overall the aim is to enhance the piezoelectric coefficients and electromechanical coupling factors of the materials by improving the microstructure of the PLZT ceramics. Apart from that another important objective of this study to ascertain the reason behind the ultra high piezoelectric properties of optimized PLZT ceramics. Some of the applications where PLZT ceramics offer advantages are high dielectric constant capacitors, piezoelectric sonar and ultrasonic transducers, radio and communication filters, medical diagnostic transducers, stereo tweeters, buzzers, gas ignitors, ultrasonic motors, electrooptic light valves, thin-film capacitors, and ferroelectric thin-film memories.

From the time of the discovery of piezoelectric ceramics, they have been widely studied for their use in different applications. Piezoelectric materials can be classified into two broad categories; lead based and lead free materials. As we know the toxic nature of the lead, forced researchers to search for the lead free materials. Recently, there has been a spurt of research on lead free piezoelectric ceramics. However, at present, there are no commercially available lead-free ceramics to completely replace lead based ceramics. Lead based materials still have importance because of their reliable, good and repeatable electrical properties. Lead based materials have significant practical and academic importance because of their excellent dielectric, ferroelectric and piezoelectric properties. Out of many lead based systems, Lead Zirconate Titanate (PZT) is an important material with high piezoelectric properties. The properties of PZT are further enhanced for specific applications by the addition of different dopants. Since at present, it is difficult to replace the lead based materials the immediate thrust is to minimize the lead that comes out into to the ambient as much as possible. In

this study substitution of Pb by suitable modifier in the PZT system not only enhances the electrical properties but is also a route to reduce the lead content. The highest electrical properties for PZT ceramics was achieved by off valent ion modification at the A-sites, in which La^{3+} substitutes pb^{2+} due to its comparable ionic size which is known as PLZT ceramics. While replacing divalent Pb^{2+} ions, trivalent La^{3+} ions generate vacancies at the A-site of the perovskite ABO_3 to neutralize the system, resulting in the increased electrical resistivity of the material. These donors also help to enhance domain reorientation, which results in the softening of PZT domain wall motion as well as easy reorientation of dipoles during poling. The La substitution into the PZT also modifies the morphotropic phase boundary (MPB); showing many beneficial effects on several basic properties. In this study PLZT ceramics have been engineered in such a way that it should be close to the MPB so as to show high piezoelectric properties. The general formula for PLZT is given by $(Pb_{1-x}La_x)(Zr_{1-y}Ti_y)O_3$.

Since electrical properties are greatly affected by the density of ferroelectric ceramics, complete densification (>95% of theoretical density) ensures achieving the maximized performance. In previous studies, dense PLZT ceramics were processed by using the cold and hot press techniques which involve the use of high temperature with prolonged sintering durations. Apart from that, hot pressing is time consuming and an expensive process. The above conditions lead to abnormal grain growth in ferroelectric ceramics which is detrimental to the performance of ferroelectric ceramics. Higher sintering temperatures not only lead to lead loss but also affect the electrical properties. Excess PbO is required to compensate for lead losses during high temperature sintering. Such additions are detrimental to the environment.

It has been one of the objectives of this work to reduce the overall processing temperatures and durations used in the synthesis of PLZT ceramics, viz. the calcination and sintering temperature and time. The importance of this can be understood from the fact that in the specific case of Pb-based ceramics, there is a tendency for volatilization of PbO at elevated temperatures when held at those temperatures for long durations. Since most of the lead loss happens at the time of processing, by a suitable materials engineering approach lead loss can be alleviated at the time of processing of the ceramics. This study is an endeavor along those lines. It was found that a combination of mechanical activation (high-energy mechano-chemical ball milling) with the cold isostatic process (CIP) could not only reduce processing temperatures and time but also circumvent the need to add excess PbO in the starting materials. At the same time, this could be done without compromising the high density of such ceramics due to this process. The mechanical activation method results in ultrafine powders with a narrow particle size distribution that can start reacting at room temperature itself and thereby reduce the processing temperature. The salient features of the processing technique are that (1) no excess PbO was added to the starting material because of lower calcination and sintering temperature that may be attributed to the very fine scale particle sizes after HEM ball milling and (2) no binder was

added in this process. This CIPing process has removed the binder addition and burnout step and avoided the contamination risk involved.

The properties of electro-ceramics are also greatly affected by the milling conditions. Preliminary studies show that to get the desired PZT/PLZT phase, ceramics were milled for long milling durations, up to 80 hours. Prolonged milling time increases the contamination risk. In this study ceramic powders were milled for much lesser times without compromising the properties of the ceramics, which, in turn, can reduce the contamination in the system. The selection of milling media such as milling vial and balls are also important. The use of metallic vials and balls can contaminate the ceramics powders resulting in the decrease in electrical properties. In this study two different ceramic vials viz. agate and zirconia vials were used for the ceramics synthesis. Based on the vial density, hardness, etc. results were explained. Use of zirconia vials and balls also reduce the contamination.

The electrical properties of the piezoelectric ceramics are influenced by the poling conditions. If the ceramics have low resistivity, the application of high poling field results in the electrical breakdown of the ceramics and sometimes physical breakdown is also possible. All of these, in turn, are resulting in the lowering of piezoelectric coefficients. Therefore optimum poling conditions should be identified. In this study, it was found that the ferroelectric material can be poled at $< 0.5\ E_c$, contrary to common practice of poling, which is far above the coercive field, without compromising the induced high piezoelectricity. This shows that poling of PLZT ceramics is possible at significantly reduced poling voltages which could be very advantageous if the samples have poor resistivity.

At the end of the thesis, the origin of ultra high piezoelectric properties is discussed using slow scan X-ray diffraction data. This XRD data was used for the crystallographic study using Rietveld refinement and the results are correlated.

In **Chapter-2**, a complete description of the synthesis, structural and electrical characterization is provided. It is well-known that the property of any material depends upon the processing route. Hence the steps for processing, processing equipment and the conditions must be carefully monitored and controlled for best results. High purity raw oxides of PbO, La_2O_3, ZrO_2 and TiO_2 powders (all from Sigma-Aldrich, USA, AR grade, purity >99.9%) were weighed according to the required stoichiometric formula. The reagents were ball milled in a Fritsch Pulverisette-5 (speed: 150 rpm, vials: agate and zirconium, balls: yttrium stabilized tetragonal zirconium balls, milling medium: distilled water) for different times viz. 1h, 2h, 3h, 5h, 7h and 10h. The milled powders were dried by using a heater, stirrer assembly and calcined in ambient air (800^oC, 4 hours, 5^oC/min). The PLZT calcined powders were filled in a rubber mold for cold isostatically pressing (300 MPa) in the form of cylindrical rods and these green cylindrical rods of PLZT ceramics were densified by sintering (1200^oC, 4 hours, 5^oC/min). The sintered PLZT cylindrical rods were cut into disks of <1

mm thick using an Isomet cutting machine. These ceramic disks were polished and electroded with conductive silver paste. It was ensured that all contacts were ohmic before any electrical characterization was performed.

Philips X'pert PW-3020, X-ray diffractometer with a monochromatic Cu-Kα radiation was used for phase analysis. Rietveld refinement studies were done with the help of FULL PROF software. The grain size of the fractured surface of sintered pellets was also examined with a SEM, LEO-440i scanning electron microscope. The density of the sintered PLZT ceramics was determined using the Archimedes' technique. Poled PLZT samples were used for the measurements of electromechanical and piezoelectric parameters. The piezoelectric charge coefficients (d_{33}) were determined using a d_{33} meter (SENSOR SS01 Piezo-d Meter, Canada). An LCR meter (Agilent E-4980A) was used for dielectric and resonance measurements. The polarization vs. electric field (P-E) and strain vs. electric field (S-E) measurements were traced using an advanced ferroelectric evaluation system of M/s aixACCT Systems, GmbH, Germany. TF 2000HS analyzer, FE-module and hysteresis software version v2.4.0.0 was used for the measurement. The FE-module consists of three amplifiers with an optimum signal to noise ratio. The method used to collect the data is the virtual ground feedback method, which is the highest precise technique for ferroelectric measurements.

The importance of structure-property correlations in piezo-ceramics cannot be under-stated. Since all the electrical properties (dielectric, ferroelectric and piezoelectric) of electro-ceramics are greatly affected by the microstructure. **Chapter-3** provides detailed structure-property analyses. In this chapter, the microstructure and the morphology of (i) different compositions of La modified $(Pb_{1-x}La_x)(Zr_{0.60}Ti_{0.40})O_3$ (PLZT x/60/40) and (ii) PLZT 8/60/40 ceramics that were milled for different time durations, were studied carefully. The effect of the novel approach of HEM and CIP results in the improved microstructure, confirmed by density, XRD and SEM studies. X-ray diffraction patterns were compared with the standard JCPDS files to confirm the perovskite phase formation. High energy milled PLZT powders show the partial perovskite phase formation, which indicates the partial chemical reaction at the milling stage itself. XRD patterns of the PLZT ceramics sintered at 1200^{o}C show single phase formation. SEM images of the milled powders show the agglomeration of particles, suggesting the fine scale size of milled powders. SEM images of sintered ceramics show dense and uniform grains. Higher density and more uniform grain distributions were found for the optimum PLZT composition. TEM studies were used for the 5 hours milled PLZT 8/60/40 ceramics which showed the particle size of PLZT 8/60/40 milled powders deviates from the spherical shape. The average particle size of milled powders, relative density and grain size of sintered compacts were found to be ~25 nm, 97.23% and ~1.45 μm, respectively.

In the **Chapter-4**, the dielectric properties of different compositions of PLZT ceramics are discussed. In the current study, the dielectric properties of the La^{+3} substituted PLZT x/60/40, especially PLZT 8/60/40 ceramics suggest that the La substitution affects the nature of the ferroelectric phase transition, which shows a deviation from normal to the diffuse type phase transition (DPT). The parameters of this DPT, such as the degree of deviation from Curie-Weiss law (ΔT_m), diffuseness empirical parameters γ and ΔT_{diff} were calculated for the different compositions of PLZT ceramics at 1kHz (for PLZT 8/60/40 ceramics it is carried out from 1 kHz to 500 kHz). The large value of γ ($1<\gamma<2$) and ΔT_{diff} at the said frequencies confirms the deviation from normal phase transition and the high degree of disorderliness in the material. The maximum value of dielectric constant ~2336 was found for the 5 hours milled PLZT 8/60/40 ceramics. Substitution of La^{+3} to the PZT system decreases the stability of the ferroelectric phases for the paraelectric and antiferroelectric phases resulting in a reduction of the T_c with increasing lanthanum. The reduction of T_c as a function of lanthanum substitution is also observed in this study. The decrease in transition temperature was found from 391^oC for PZT 60/40 to 129^oC for PLZT 10/60/40. To give more details about the diffuse phase transition of PLZT ceramics, resonance data were taken from room temperature to high temperature (~T_c), which was used for the calculation of electromechanical coupling coefficients. The existence of resonance phenomena above the dielectric maxima temperature for PLZT 8/60/40 ceramics suggests the DPT behaviour.

In **Chapter-5**, the ferroelectric properties (P-E and S-E hysteresis loops) of different compositions of PLZT ceramics (prepared for optimization of La substitution) as well as for the different milling conditions (optimization of milling vial and milling time) have been presented. The remnant polarization (P_r) and coercive field (E_c) were calculated from P-E hysteresis loops. The S-E hysteresis loops were used for the calculation of piezoelectric charge coefficient (d_{33}). In this study, in addition to the P-E hysteresis loops, current vs. electric field (I-E) curves were also used for the determination of E_c (the field corresponding to the domain switching current peak). Apart from P_r, E_c and d_{33}, some other important parameters such as internal macroscopic electric field (E_{in}), domain switching current (I_{max}), the squareness of P-E loops, strain hysteresis, normalized strain coefficient (S_{max}/E_{max}) were also calculated. These parameters help to study the behavior of ferroelectric materials. The optimized PLZT 8/60/40 composition that was milled for 5 hours in zirconia vials shows the highest value of P_r ~ 34 $\mu C/cm^2$, I_{max} ~ 2.06 mA, unipolar strain ~ 0.27%, hysteresis loss ~ 3%, an average d_{33} ~ 710 pC/N (calculated from unipolar S-E curves) and high shape symmetry with low E_c ~ 12 kV/cm. Temperature dependent P-E, S-E and I-E loops of PLZT 8/60/40 ceramics show the existence of P_r and I_{max} close to dielectric maxima temperature, which is one more evidence for the diffuse phase transition. High shape symmetry of P-E loops, low hysteresis loss in P-E as well as S-E loops and P_r at high temperature suggest the PLZT 8/60/40 ceramics are promising materials for high

temperature piezoelectric applications and successful optimization of synthesis conditions for these advanced ceramics.

Chapter-6 deals with the identification of optimum poling conditions. In order to obtain highest electrical properties in piezoceramics, the poling conditions should be optimized which can be done in three possible ways (1) Poling electric field (2) Poling time and (3) Poling temperature. In this chapter, all three conditions have been utilized for optimization and the results are presented. The effect of each of the three conditions on the dielectric, piezoelectric and ferroelectric properties are discussed. The dielectric constant (K), dielectric loss (D), piezoelectric charge (d_{33}) and electromechanical coupling coefficients (k_p) were measured at different combinations of poling parameters. Since the high strain and the high piezoelectric charge (d_{33}) of the electro-ceramics are interdependent, it is necessary to find the optimum poling conditions for electro-ceramics. Additionally, the effect of ceramic sample thickness on the said properties was also studied. It is a common practice to subject piezoelectric ceramics to electric fields well beyond their coercive fields, in order to pole them. However, in this study, it has been shown, that PLZT ceramics can be poled at ~5 kV/cm (< 0.5 E_c), half of the coercive field, without compromising the induced high piezoelectricity. This is evidenced by the values of K, D, d_{33} and k_p parameters. This shows that poling of PLZT ceramics is possible at significantly reduced poling voltages which could be very advantageous especially if the samples have poor resistivity. Optimum poling time was found to be 30 minutes which is much less compared to the normally employed time in hours. The poling temperature was varied from 75^{o}C to 120^{o}C while the T_c is ~200^{o}C. The effect of aging on the electrical properties was also studied for ceramics poled at 0.6 E_c and 3 E_c. The aging study also supports the poling of PLZT ceramics at a lower electric field.

In **chapter-7**, piezoelectric studies on different compositions of PLZT ceramics that were prepared by substituting La at the A-site of perovskite PZT and the effect of milling conditions on PLZT 8/60/40 composition are discussed in detail. The d_{33} and k_p are two important parameters to describe the electrical properties of piezo-ceramics. Whereas d_{33} is defined as the proportionality constant for the strain-electric field relation or charge generated per Newton force, k_p is related to the conversion of mechanical energy into electrical energy and vice-versa. High values of both d_{33} and k_p parameters decide the end application (actuator or transducer) of the electro-ceramics. The PLZT 8/60/40 composition is close to the MPB region. On account of this, it is expected that the increased number of directions of spontaneous polarization will help to improve the piezoelectric properties. The processing technique that was used here resulted in improved density while the ceramics retain their fine grain size, which in turn influence the domain wall motion and switching phenomena. All these factors help to improve the piezoelectric and electromechanical properties of PLZT ceramics. Piezoelectric studies of PLZT ceramic system which was milled for 5 hours in zirconia vial shows the highest piezoelectric coefficients ($d_{33} \cong 690$pC/N, $g_{33} \cong 28.48 \times 10^{-3}$ Vm/N) and electromechanical

coupling factors ($k_p \cong 75.8\%$, $k_{33} \cong 76.29\%$ and $k_{31} \cong 60.65\%$). The values of elastic compliances for the optimized PLZT ceramics were also found to be good.

In **Chapter-8**, the origin of ultra high strain and piezoelectric properties of PLZT ceramics are discussed from a crystallographic prospective with the help of Rietveld analysis. After detailed analysis from Chapter-3 to 6, it was confirmed that PLZT 8/60/40 ceramics which were milled for 5 hours in zirconia vial, show single and pure perovskite phase with a very dense micro-structure, uniform grain sizes with clearly visible grain shapes indicating the existence of a polycrystalline microstructure with average grain size <1.5 μm resulting in ultra high dielectric (K ~ 2336), ferroelectric ($P_r \sim 34\ \mu C/cm^2$, $E_c \sim 12$ kV/cm) and piezoelectric (strain ~ 0.29%, $d_{33} \sim 690$ pC/N, $k_p \sim$ 75%) properties. Since we know that the PLZT 8/60/40 ceramic composition is close to the MPB, even a slight change in phase can cause a huge variation in their electrical properties. This phase variation of PLZT ceramics can be detected by studying the XRD patterns. In this study, slow scan X-ray diffraction data were collected for PLZT samples from room temperature to 350^oC at a few spot temperatures. This XRD data is refined and analyzed by the Rietveld refinement method. The refined pattern shows the presence of two phases coexisting, instead of previously reported single tetragonal phase at MPB for PLZT 8/60/40 ceramics. These two phases had the tetragonal (P4mm) and monoclinic (Cm) symmetries. This structural change can be correlated with the ultra high piezoelectric strain in PLZT ceramics. The presence of the monoclinic phase helps for the rotation of polarization vector along the easy axis and is believed to be the reason for ultra high electrical properties such as high remnant polarization, strain, piezoelectric charge coefficients and electromechanical coupling factors with low coercive field and low strain-hysteresis loss.

In summary (**Chapter-9**), this thesis defines the series of experiments centered around a piezoelectric composition envisaged for high piezoelectric output and discussed in detail studies carried out to optimize the processing of such ceramics using HE-MCP and also scientifically designed experiments to show how the electrical properties could be enhanced. This chapter also enumerates the scope for further studies in this field of research.

Chapter-I

Introduction and Background

In this chapter, a brief introduction as well as the definitions of the important terms is given, which are directly or indirectly related to this work, such as piezoelectricity, ferroelectricity, etc. There is a brief discussion on the classification of piezoelectric and ferroelectric materials and the importance of perovskite structure. A brief review on lead based piezoelectric ceramics is also discussed.

1.1 Electro-ceramics and their classification

A ceramic material can be described as "an inorganic, non-metallic solid material, which is prepared by heating and cooling". These ceramics materials may possess amorphous, partly crystalline or crystalline structure **[1]**. Electro-ceramics are a class of ceramic materials which are used primarily for their electrical properties. As many electro-ceramics exhibit ferroelectric behavior, they are used in many electronic and optical applications. The application of these electro-ceramics depends on various factors such as raw materials, fabrication techniques and experimental procedures and so on.

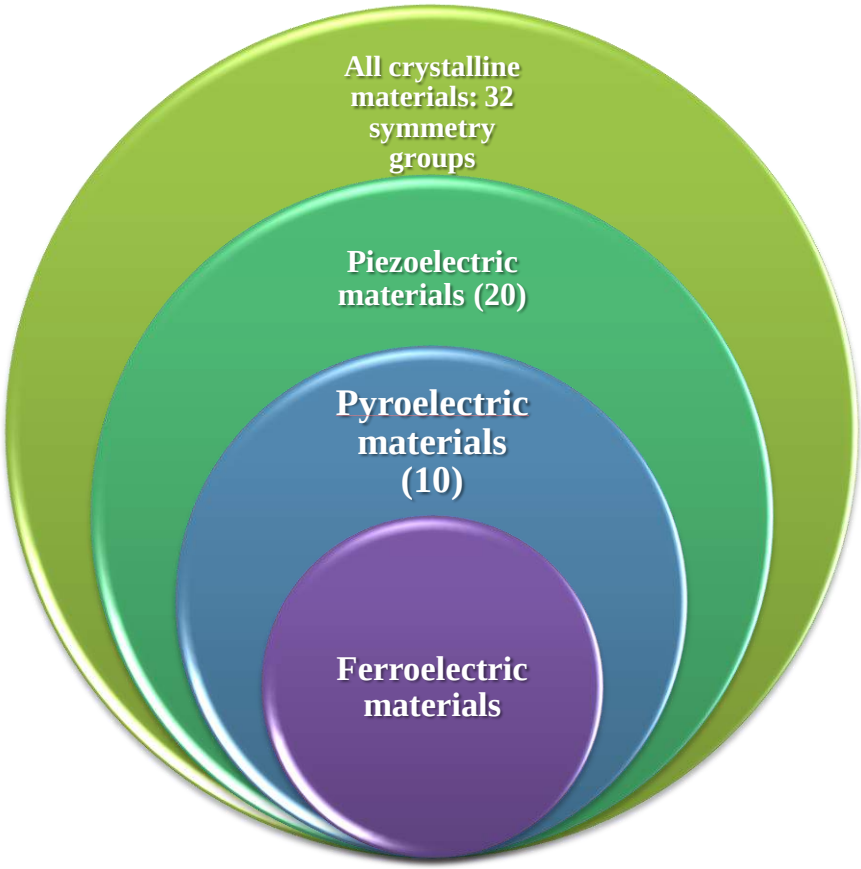

Fig. 1.1 *Classification of electro-ceramics.*

All crystalline materials can be classified into 32 different crystal classes or point groups based on their unit cell symmetry elements and show an electrostrictive material behavior. The electrostriction in material means that the material will change its length in proportion to the square of the applied electric field. The above mentioned symmetry elements are (1) axes of rotation, (2) a center of symmetry (3) mirror

planes and (4) combinations of above three, as discussed in the previous literature **[2]**. Out of 32 point groups, 11 point groups possess centrosymmetry and therefore do not show piezoelectricity. The remaining 21 crystal classes are not centrosymmetric, which is a necessary condition for the electro-ceramics to show the piezoelectricity. However, out of 21 non-centrosymmetric materials, 20 reveal the piezoelectric properties. The remaining one is not piezoelectric due to the other combinations of symmetry elements. The classifications of all the 32 crystal classes are shown in fig. 1.1.

1.2 Piezoelectricity and ferroelectricity

The piezoelectric effect was discovered by Jacques and Pierre Curie in 1880 while applying a mechanical pressure on the quartz and zinc blende. Piezoelectricity is defined as the linear correlation between mechanical stress or strain and electrical charge or voltage. All the materials which exhibit piezoelectricity are called as piezoelectric materials. In other words, piezoelectric materials can be polarized with the application of an electric field and mechanical stress. This effect is divided into two parts, direct and converse piezoelectric effect. The direct piezoelectric effect (generator) correlates the induced charge in the piezoelectric materials with a mechanical force, which was applied to the ceramic, whereas the converse piezoelectric effect (motor) describes the change in ceramic sample dimensions (expansion or contraction) with the application of an electric field **[3]**. This effect is linear in nature and reversible. The magnitude of the polarization depends on the magnitude of stress, and while the sign of the charge produced depends on the tensile or compressive stress **[2, 4-5]**.

Ferroelectrics are a subgroup of piezoelectrics, having a spontaneous polarization which is reversible with the direction of the applied electric field. The presence of a spontaneous (and switchable) macroscopic polarization is the defining property of ferroelectricity. Gray discovered in 1945 that domains within the grains could be oriented by the application of an external electric field. These ceramic materials act similar to a single crystal which shows high ferroelectric and piezoelectric properties. The special relationship between the ferroelectric and piezoelectric materials is "all poled ferroelectrics are piezoelectric, but not all piezoelectrics are ferroelectric" **[2]**. Ferroelectrics are further classified by four different structures such as bismuth layer structure ferroelectric (BLSF), Pyrochlore, tungsten bronze and the most important ABO_3 type perovskite structure as shown in fig. 1.2. Examples of these structures are Tungsten Bronze ($PbNb_2O_4$), Pyrochlore ($Cd_2Nb_2O_7$), Layer Structure ($Bi_4Ti_3O_{12}$) and the Oxygen Octahedral Perovskite structures (PT, PZ, PZT, PLT, PLZT, PLZST, PMN, PZN).

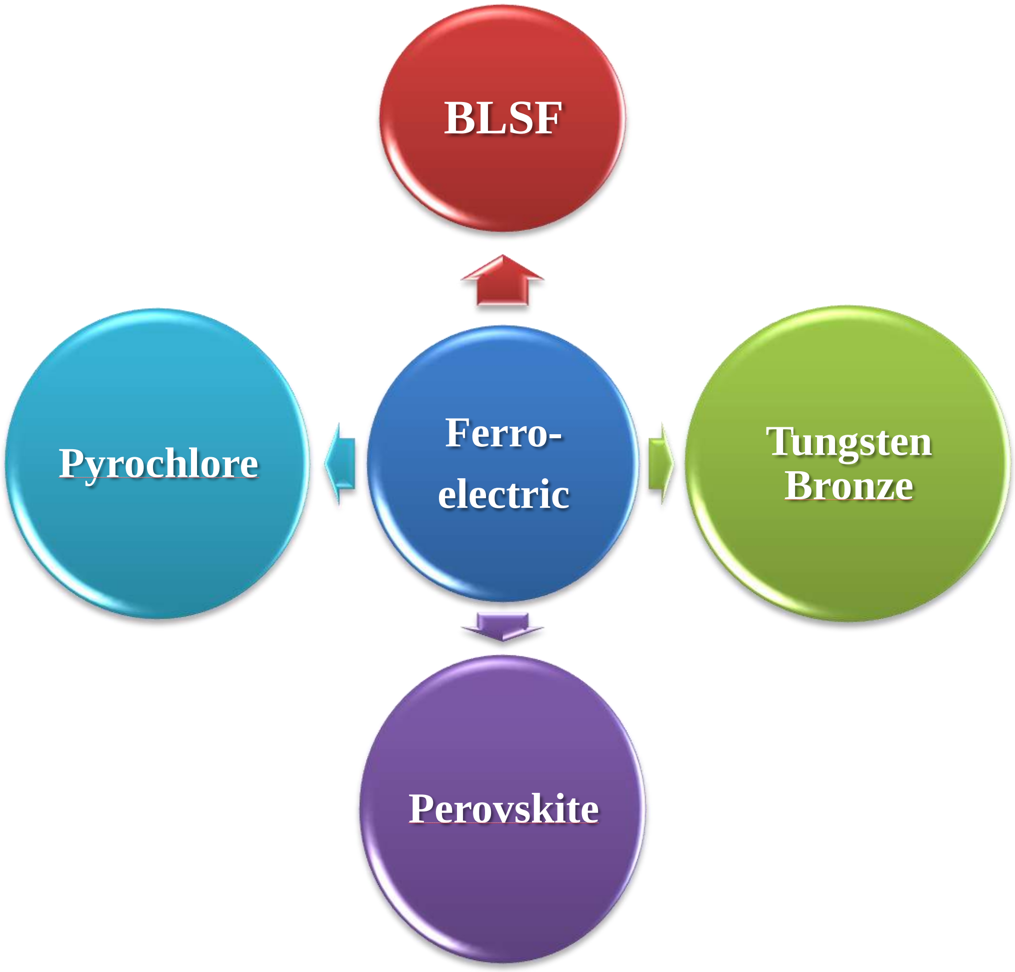

Fig. 1.2 *Classification of ferroelectric materials.*

1.3 The perovskite structure

The perovskite structure is an ABO_3 type of structure, which is the most common and important among piezoelectric materials. This structure has a simple cubic unit cell with large cations at the A-site corners and small cations at the B-site (body center) and oxygens at face centers. This structure is also called an oxygen octahedral structure. Fig. 1.3 shows the basic perovskite unit cell. A wide variety of cations at A and B positions can be substituted, and O also can be replaced by F, Cl, carbide, nitride, hydride and sulfide. Examples of this structure are $BaTiO_3$, $CaTiO_3$, $Pb(Zr,Ti)O_3$, $CsGeCl_3$, etc. **[6-9]**.

The stability of perovskite is described by Goldschmidt tolerance factor (t), which helps to quantify the degree of distortion in the unit cell. For the ideal cubic case, the relation between the cell axis 'a' and ionic radii (r_A, r_B and r_O) is given by

$$\boldsymbol{a} = \sqrt{2}(\boldsymbol{r_B} + \boldsymbol{r_O}) = \boldsymbol{r_A} + \boldsymbol{r_O} \quad \ldots\ldots (1)$$

The ratio of them 't' is called as the tolerance factor for the perovskite structure which is based on the ionic radii and ionic bonding and is given by

$$t = \frac{r_A + r_O}{\sqrt{2}(r_B + r_O)} \quad \text{..... (2)}$$

Where r_A, r_B and r_O are the ionic radii of the large cation, small cation and anion, respectively. t = 0.95 to 1 stand for the cubic perovskite structure and t > 1.0 is for the ferroelectrics **[10-12]**.

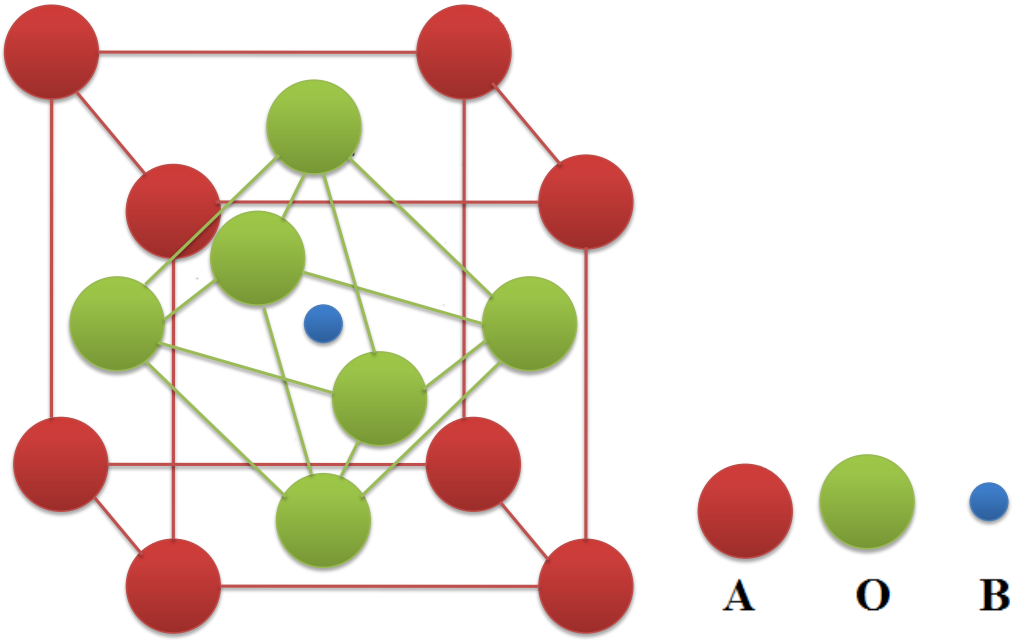

Fig. 1.3 *Perovskite structure of piezoelectric materials.*

1.4 Phase transition in ferroelectric ceramics

When ferroelectric materials are subjected to a temperature, they undergo structural phase transitions from a low temperature, low symmetry ferroelectric phase (for PLZT tetragonal symmetry) into a high temperature, high symmetry non ferroelectric paraelectric phase (for PLZT cubic symmetry) as shown in fig. 1.4. For ferroelectrics, phase symmetry is always lower than the paraelectric phase symmetry **13-15]**. The temperature point, at which the ferroelectric phase transition occur, is called the Curie point or Curie temperature, T_c. Above the Curie temperature, the dielectric permittivity of the materials decreases with an increase in temperature as per Curie-Weiss law **[16]**

$$\varepsilon = \varepsilon_o + \frac{C}{T - T_0} \quad \text{..... (3)}$$

Where C is the Curie constant, T_0 ($T_0 \leq T_c$) is the Curie-Weiss temperature.

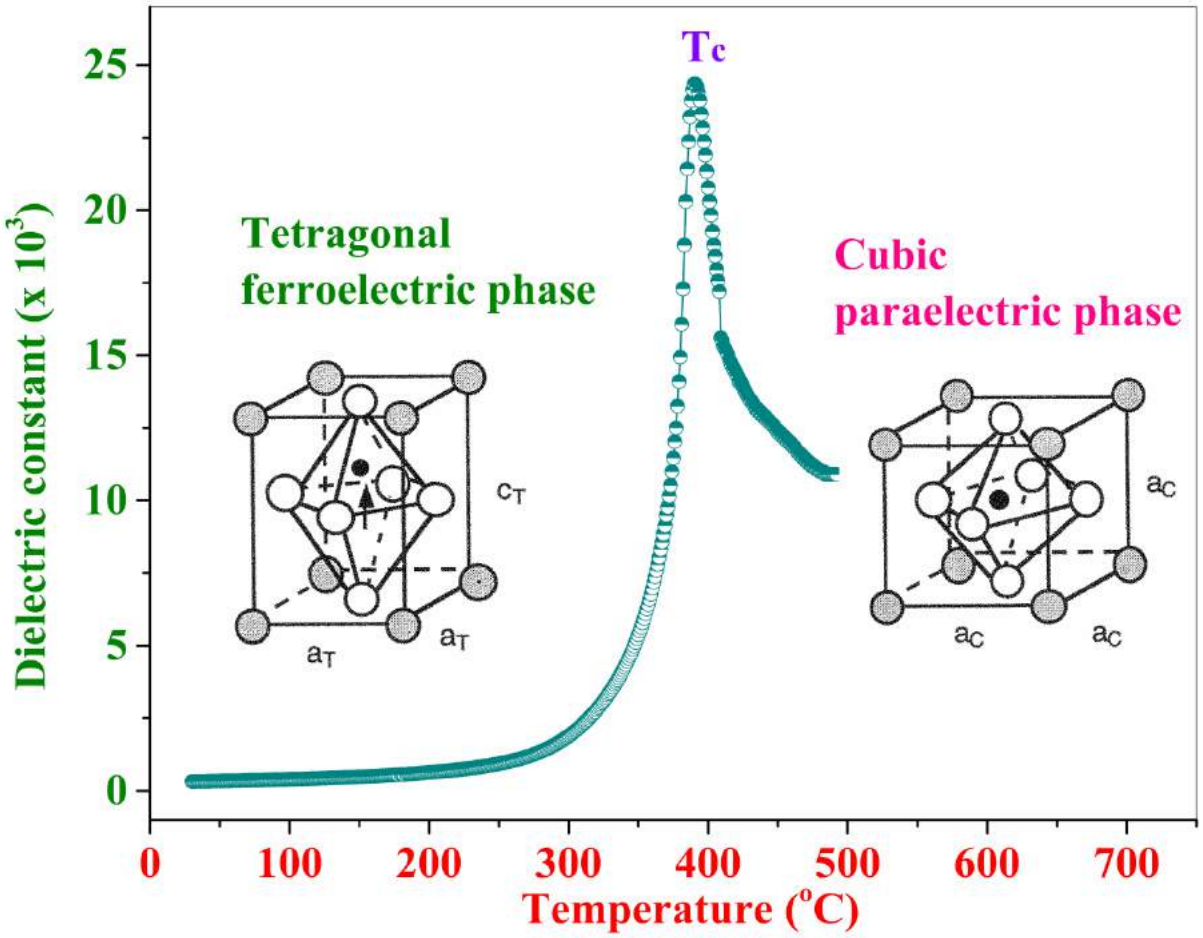

Fig. 1.4 *Illustration of the ferroelectric phase transition of ferroelectric materials from ferroelectric tetragonal phase to a paraelectric cubic phase with temperature.*

When the temperature is close to the Curie point, thermodynamic properties of materials such as elastic constant, dielectric constant, thermal constant and optical constant show an anomalous behavior due to distortion in the crystal structure. The Curie-Weiss temperature T_0 is different from the Curie point T_c. The Curie-Weiss temperature T_0 coincides with the transition temperature T_c in those ferroelectrics which undergoes a transition of the second order. For first order phase transition, the condition is $T_0 < T_c$.

1.5 Domains in ferroelectric ceramics

Ferroelectric ceramics possess small regions, in which all the electrical dipoles are aligned in the same direction (unidirectional polarization), called as ferroelectric domains. These domains in a ferroelectric crystal have a twin structure consisting of regions which have spontaneous polarizations with negative and positive polarity (fig. 1.5). This type of twin structure is called domain structure and the boundaries between the domains are called domain walls. By application of an electric field, the wall is displaced so that the volume of domains expands with the spontaneous polarization parallel to the electric field. If the field is very high, the whole crystal will have the spontaneous polarization parallel to the field. Such a crystal is a called as single domain crystal **[13, 17]**. The domains of ferroelectric materials are electrical analogs to the Weiss domains in ferromagnetic materials with some differences **[18]**.

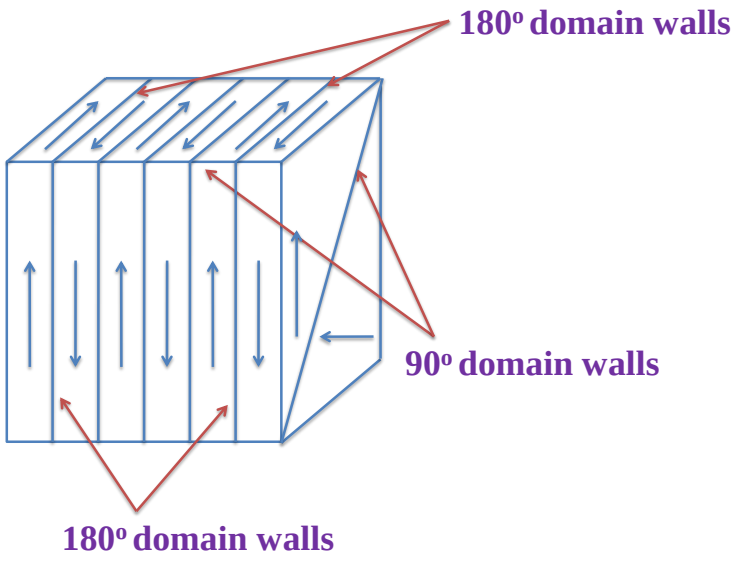

Fig. 1.5 *The schematic representation of 90° and 180° domain structures for tetragonal crystal.*

Above a material specific temperature, called the Curie point, the unit cell has a non ferroelectric (paraelectric) cubic symmetry (where the unit cell does not have a spontaneous polarization direction). The spontaneous polarization forms in the unit cell when the temperature is reduced below the Curie temperature. In this state the unit cell has a particular polarization direction that can be reoriented using the electric field. When ferroelectric materials are cooled from the paraelectric high symmetry phase to the ferroelectric low symmetry phase, domains form to minimize the electrostatic energy of the depolarizing field, which arises due to surface charge and elastic energy associated with mechanical constraints. Both 90^{o} and 180^{o} domain walls help reduce the effect of depolarization electric fields. However, elastic energy of the ceramics minimizes by the 90^{o} domain walls **[3]**. The ferroelectric and piezoelectric properties of electro-ceramics depend on the switching or domain response in the presence of an electric field.

1.6 Ferroelectric hysteresis loops

The difference in the nature of the domains in different ferroics (ferromagnetics, ferroelectrics and ferroelastics) helps them to exhibit their unique hysteresis phenomena with their respective driving external fields (magnetic field, electric field or stress). These loops can be used as a fingerprint to get information related to its electrical properties and structures as suggested by Jin et. al. [**19]**. For ferroelectrics, many characteristic parameters, such as spontaneous and remnant polarizations and the coercive field, can be directly extracted from the hysteresis loops. Ferroelectric materials show mainly three types of hysteresis loops Polarization vs. electric field (P-E), Strain vs. electric field (S-E) and Piezoelectric charge coefficient vs. electric field (d_{33}-E) hysteresis loops. However, in this chapter, the first two will be discussed in greater detail.

1.6.1 Polarization vs. electric field (P-E) hysteresis loops

The P-E hysteresis loops are the most important electrical characteristics of ferroelectric ceramics, which are similar to the magnetic hysteresis loop (B-H curve) of ferromagnetic materials. The term ferroelectric follows from the name ferromagnetic due to the similarity in the shape of B-H curve and P-E curve. For ferroelectrics, iron is not an important component compared to the ferromagnetics.

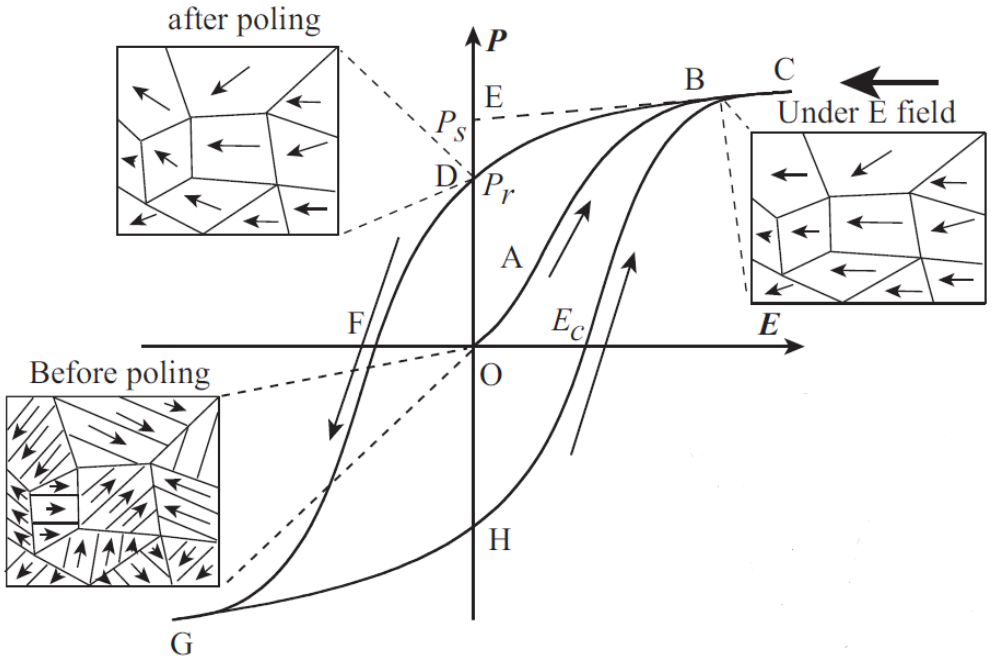

Fig. 1.6 *A typical P-E hysteresis loop in ferroelectric ceramics showing domain reversal or polarization rotation with a change in the external electric field* ***[19]***.

Fig. 1.6 shows the typical P-E hysteresis loop with important notations for ferroelectric ceramics. For an ideal ferroelectric system, the observed P-E hysteresis loops should show symmetry in their shape.

The positive and negative value of the remnant polarization (P_r) and coercive field (E_c) should be equal ($E_c = -E_c$ and $P_r = -P_r$). In reality, the shape of the ferroelectric hysteresis loops is affected by many factors such as material composition, preparation conditions, the thickness of the samples, mechanical stresses, the presence of charged defects, measurement conditions and thermal treatment.

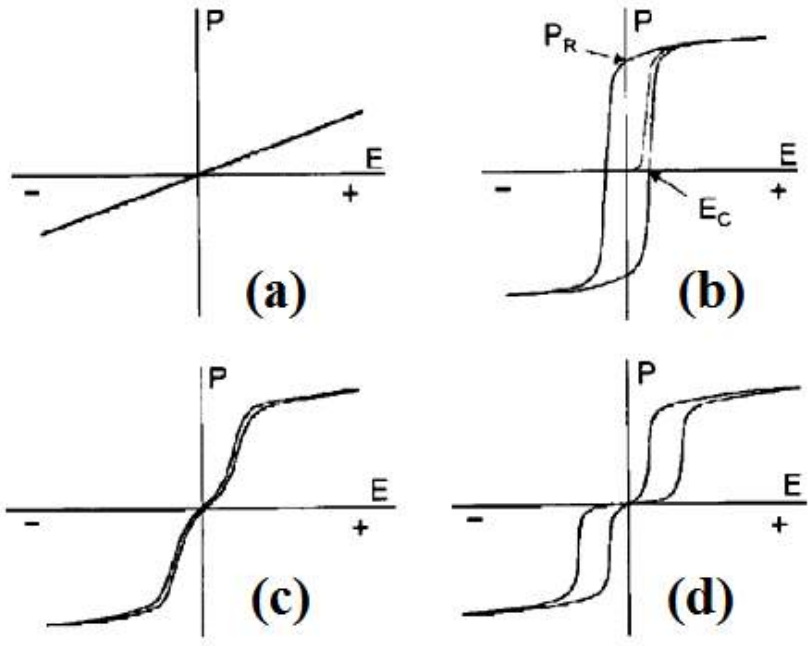

Fig. 1.7 *The hysteresis loops for (a) $BaTiO_3$ based capacitor (b) soft PZT (c) relaxor PLZT 8.6/65/35 and (d) antiferroelectric PSZT ceramics **[2]**.*

Hysteresis loops are the source of plentiful information to understand the true nature of ferroelectrics **[1]**. In fig. 1.7 (a) BT ceramics shows the linear P-E curve same as the capacitor, which means BT can be used as a linear capacitor. The square like P-E loop in fig 1.7 (b) reveals that the material has memory, whereas the loop in fig 1.7 (c) indicates no memory. The high remnant polarization of ferroelectrics can be related to the high internal polarizability, electromechanical coupling, strain and electrooptic activity. The coercive field (E_c), indicates the grain size of ceramics. The high and low E_c corresponds to small and large grain sizes, respectively. A high degree of loop squareness is related to better homogeneity and uniformity of grain size. An off-centered P-E loop from the zero voltage point indicates some degree of internal electrical bias caused by internal space charge or aging. Sharp edges of P-E loops indicate a high electrical resistivity of the materials **[20]**.

Apart from P-E hysteresis loops, current-electric field (I-E) loops are also important and informative for the ferroelectric materials. When an electric field is applied to a ferroelectric, along with the polarization, it also shows a current response. The total current generated from the ferroelectrics consists of different types of current signals. The first is due to the fast linear response of the dielectric and the current due to polarization switching **[3, 21]**. However, some other references show that the total current also has the weak leakage current (material dependent) component and displacement current **[22-**

23]. The effect of different current responses, rather than polarization switching current is visible in the low field region (fig. 1.8 (a) and (b)) but when the domain starts switching after crossing a threshold field, the domain switching current becomes more prominent. A peak in the I-E curve before reaching the maximum electric field is due to the switching of domains. Moreover, the magnitude of the peak current is higher than the current at maximum applied electric field **[24]**. The electric field corresponding to the domain switching current peak can be used as a coercive field.

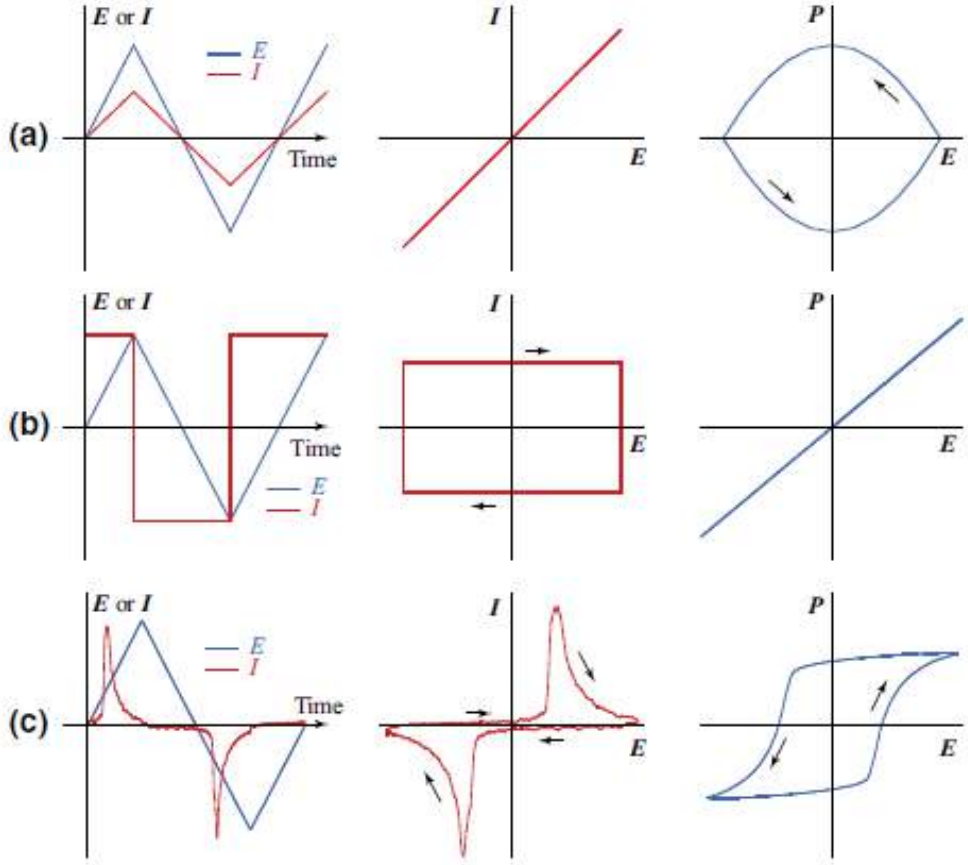

Fig. 1.8 *Schematic representation of E and I vs. time as well as P and I vs. E for (a) a linear resistor, (b) a linear capacitor and (c) a ferroelectric crystal, respectively* ***[19, 24]****.*

The existence of P-E hysteresis loops in ferroelectric ceramics is considered a necessary condition of ferroelectricity. However, every measured P-E loop, which gives the hysteresis, does not guarantee the existence of ferroelectricity. A lot of studies are available which shows that sometimes sample gives a false information regarding hysteresis that was mistaken for P-E hysteresis loop. The hysteresis loops, which was given by back-to-back diode combination is similar to ferroelectric P-E loops **[25]**. This combination may also give misleading dielectric anomalies due to Schottky like electrodes on non-ferroelectric materials. In fig. 1.9, a combination of a capacitor and a resistor gives the hysteresis features with increasing conductivity. However, these hysteresis loops are neither saturated nor show any switching current, giving false information about the ferroelectricity.

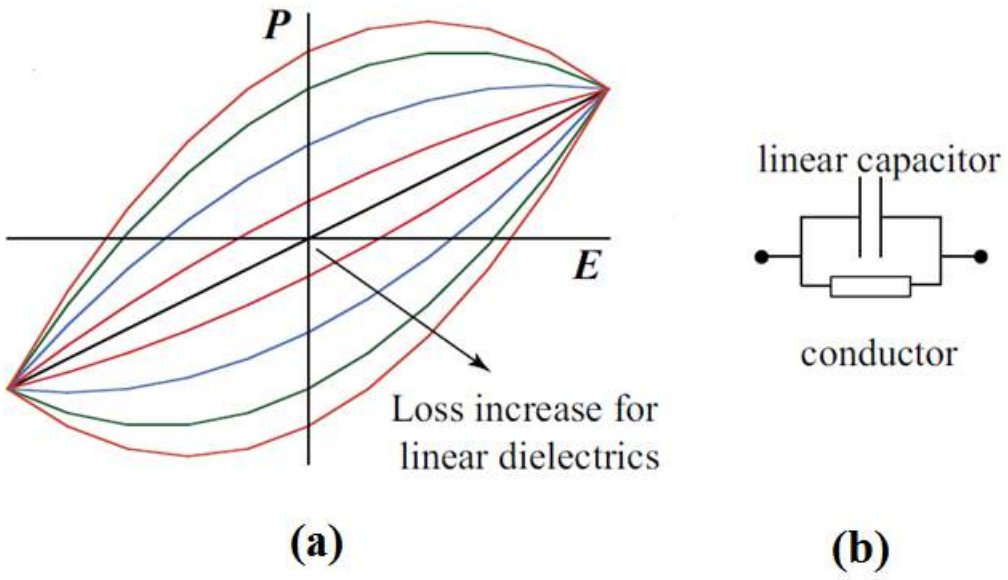

Fig. 1.9 *Schematic representation of P-E loops for (a) a linear capacitor with increasing conductivity (b) the corresponding equivalent circuits* ***[19]****.*

In his famous article 'Ferroelectrics go bananas" **[26]**, J.F. Scott went to more detailed explanation of P-E hysteresis loops, in which he showed that the P-E hysteresis, like a loop for the banana skin. Figure 1.10 (a) shows the charge versus voltage hysteresis curve for a silver paste electrode banana skin which is almost similar to many of the loops available in the literature. Figure 1.10 (b) shows the actual banana sample. From the above discussion, we can conclude that hysteresis in P-E loops alone does not confirm ferroelectricity. P-E hysteresis loop should show saturation and domain switching. I-E loops also can be used for the ferroelectricity confirmation, since domain switching peak is clearly visible in the I-E loops (fig. 1.8(c)).

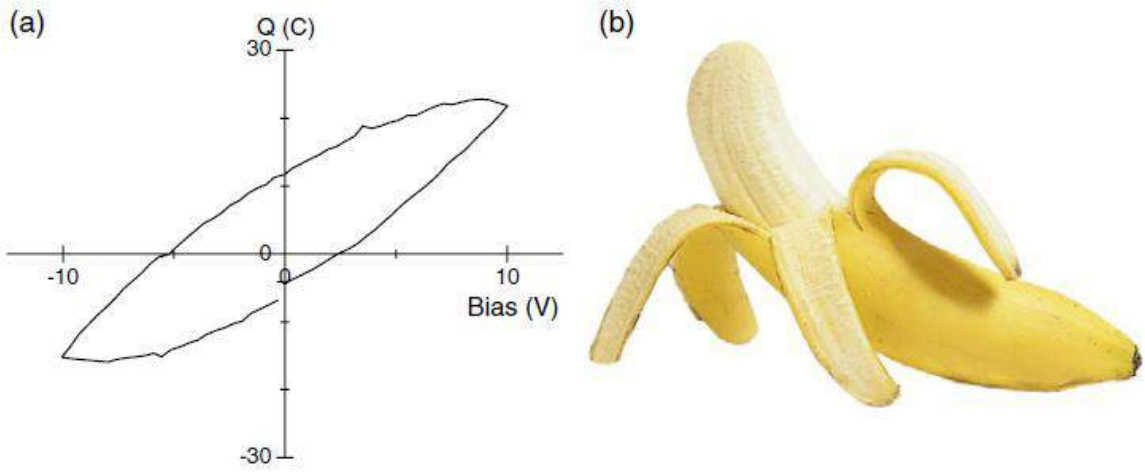

Fig. 1.10 *(a) Charge versus voltage loop for an electroded banana skin (b) real sample* ***[26]****.*

1.6.2 Strain vs. electric field (S-E) hysteresis loops

The measurement of an electric field induced unipolar and bipolar S-E hysteresis curves are also very important because these curves give the idea about piezoelectric properties of piezoelectric ceramics. With an application of the external electric field, ferroelectric materials also show strain-electric field hysteresis loops, in addition to the P-E hysteresis loops as shown in fig. 1.11 (a) and (b). The bipolar strain-electric field hysteresis loop resembles the shape of a butterfly, due to the converse piezoelectric effect of the lattice and the switching and movement of domain walls. In the presence of the low dc field, the S-E curves obey a linear relationship, corresponding to the piezoelectric effect. The switching of ferroelastic domain walls is believed to be due to the large hysteresis in bipolar S-E curves and the large negative strain in ferroelectrics. For unipolar S-E curves, large hysteresis is mainly due to the extrinsic contribution by domain switching. The hard ferroelectrics show asymmetric "butterfly" bipolar S-E curves and linear, hysteresis free unipolar S-E curves. The piezoelectric charge coefficient (d_{33}) can be calculated from the S-E hysteresis curves as shown in fig. 1.11 (b). However, in our study, unipolar S-E loops were measured. An average d_{33} can be defined as the slope of the unipolar S-E loops. The normalized strain coefficient (S_{max}/E_{max}) was also used to calculate the high field d_{33} for the PLZT electro-ceramics.

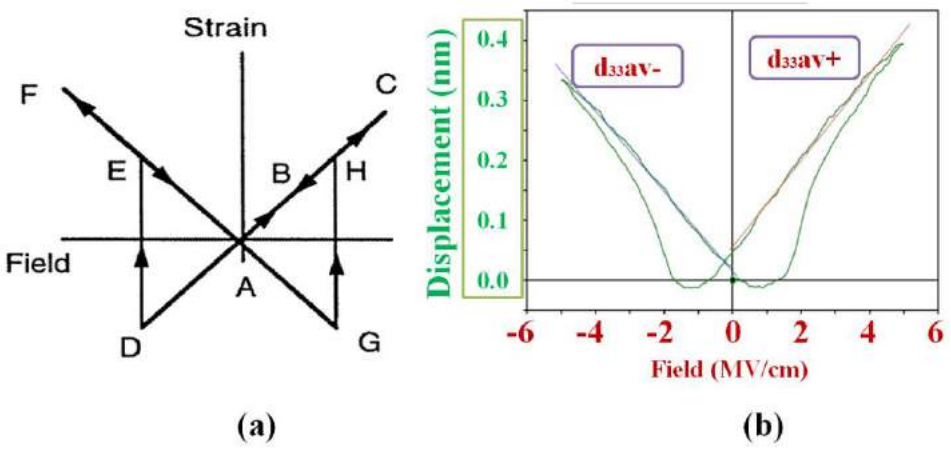

Fig. 1.11 *Strain-electric field hysteresis butterfly loop for (a) an ideal case with 180^o polarization reversal and (b) actual ferroelectric ceramics* ***[3, 22]****.*

1.7 Literature review on the importance of lead based piezoelectric materials

From the time of the discovery of piezoelectric materials especially lead based materials; they have been widely studied for their direct and indirect piezoelectric effects, useful in different applications (sensors and actuators) because of their reliable, repeatable and reasonably good electrical properties **[1, 2 and 27]**. They also found some application in the field of transducers and nano-positioners **[28-31]**. A significant number of research institutes were established all over the world, in which researchers are still

discovering new types of piezoelectric materials and exploring new dimensions in their applications. Piezoelectric materials also have a huge potential for their industrial and commercial applications. Some of their unusual properties and applications are piezoelectric sonar, ultrasonic motors, ultrasonic transducers, gas ignitors, radio communication filters, pyroelectric security surveillance devices, stereo tweeters, medical diagnostic transducers, buzzers, electrooptic light valves and positive temperature coefficient sensors **[32-36]**.

Piezoelectric materials can be classified into two broad categories; lead based and lead free materials. The toxic nature of lead, forced researchers to search for the alternatives (lead free materials). Recently, there has been a spurt of research on lead free piezoelectric ceramics for the improvement of their properties **[37-39]**. However, at present, Pb based ceramics are difficult to replace due to non availability of commercially lead-free ceramics. Lead based materials still have significant practical and academic importance because of their reliable, excellent and repeatable electrical properties (dielectric, ferroelectric and piezoelectric properties) **[40]**. The most important lead containing, solid-solution systems are divided into two categories, PZT based and PMN based ceramics. The most common examples of the PZT based ceramics are $(Pb,Ba)(Zr,Ti)O_3$, $Pb(Zr,Ti,Sn)O_3$, $(Pb,Sr)(Zr,Ti)O_3$, $(Pb,La)TiO_3$ and $(Pb,La)(Zr,Ti)O_3$[**2, 41-44**]. PMN and PMN material based studies are also reported by several researchers [**45-50**].

Out of all the above piezoelectric systems, PMN-PT ferroelectrics show high piezoelectric properties. Baek et. al. showed that PMN-PT ceramics possess very high piezoelectric strain and piezoelectric coefficients (termed as giant piezoelectricity) **[50]**. These huge strain levels and piezoelectric coefficients can be multiple times that of PZT ceramics **[25]**. These giant piezoelectric properties arise only under specific conditions. (1) To get the maximum piezoelectric response, the composition of PMN-PT should be near the morphotropic phase boundary (MPB). For bulk PMN-PT, this phase boundary occurs at ~33% PT (in the PMN-PT solid solution system). (2) PMN-PT should be in the pure perovskite form without any secondary phases. Synthesis of PMN-PT is known to be complex and typically one uses the complicated columbite precursor method making it an unviable material for practical applications **[49]**. It was therefore felt that using suitable materials engineering approaches, a relatively easy to synthesize material should be synthesized with electrical properties comparable with PMN-PT.

Out of the many lead based systems, Lead Zirconate Titanate (PZT) is an important material with high piezoelectric properties, which is known for a long time, since early 1950 **[1]**. These superior properties have been used for smart applications i.e. the development of sensors and actuators **[29-30]**. PZT is widely used to obtain good piezoelectric coefficients and is relatively easy to process. However, the properties of PZT can be further enhanced for the specific applications by the addition of different dopants or a modifier or other chemical constituents. Since at present, it is difficult to replace lead based materials, the immediate thrust is to minimize the lead that comes out into the ambient as much as possible. In this

study, the substitution of Pb by a suitable modifier in the PZT system not only enhances the electrical properties but is also a route to reduce the lead content. These dopants are mainly of two types namely 'soft' and 'hard'. Different types of modifiers are discussed here in brief.

Isovalent additives (A-site Pb^{2+} replaced by Ba^{2+} or B-site Zr^{4+} or Ti^{4+} replaced by Sr^{2+} or Sn^{4+}) to the PZT system, produce inhibited domain reorientation, lower dielectric loss, poorly developed hysteresis loops, low compliance and higher aging rates. On the other hand addition off-valent donors (A-site Pb^{2+} replaced by La^{3+} or B-site Zr^{4+} replaced by Nb^{5+}) increases the electrical resistivity of materials. The addition of small amounts of a donor dopant to a PZT ceramic formulation, are compensated by A-site metal (cation) vacancies in the crystal structure, which enhance the effects of extrinsic factors on the piezoelectric properties of the PZT ceramics. These off valent modified materials also are known as soft electro-ceramics **[1, 2]**. However, off-valent acceptors (B-site Zr^{4+} or Ti^{4+} replaced by Fe^{3+}) have limited lattice solubility in the base PZT system, creates oxygen (anion) vacancies in the crystal structure, which compensates the domain reorientation. The off-valent acceptor's modified ceramics are known as hard ceramics and show characteristics opposite to the soft ceramics, including less d_{33} and Curie points above 300°C. Hard ceramics are difficult to polarize or depolarize but more stable than soft ceramics. These ceramics show poorly developed hysteresis loops, lower dielectric constants, low dielectric losses, higher aging rates, low compliances and cannot produce large displacements. Hard ceramics are compatible with high mechanical loads and high voltages.

Based on the above description, many researchers have tried to prepare PZT ceramics, which are doped or substituted with different modifiers. The available literature was reviewed based on the electrical properties of modified PZT ceramics from the past two decades and are listed in table-1.1 **[51-64]**. There are reports on the modification of PZT ceramics with all the possible modifiers (Isovalent and off valent doners or accepters). Some of the modifiers are Nd, Nb, Sm, Eu, Gd, Dy, Er, Yb, Ca and Sr. PZT compositions were prepared with the said modifiers by using different processing techniques such as mortar pestle mixing, ball milling, attrition milling, co-precipitation and precursor methods. Khazanchi et. al. **[59]** reported the remnant polarization of ~27.7 μC/cm^2 with dielectric constant of ~1118 for the Eu substituted PZT ceramics (PEZT 4/65/35). The d_{33} of ~561pC/N was found for the $(Pb_{0.95}Nd_{0.05})(Zr_{0.58}Ti_{0.42})O_3$ composition by Jung et. al. **[51]**. Shannigrahi et. al. **[58]** has done the detailed study by substituting PZT with a number of modifiers and found the highest dielectric constant of ~2148 for $(Pb_{0.92}Nd_{0.08})(Zr_{0.60}Ti_{0.40})_{0.98}O_3$ ceramics. Apart from single substitution, many reports are also available in which, complex PZT ceramics were prepared with two or more modifiers **[55, 60, 63-64]**. Ceramics prepared by Singh et. al. **[63]** shows the improved P_r~32.5 μC/cm^2 and ceramics prepared by Texier et. al. **[55]** shows the high d_{33}~602 pC/N. However, due to their complex nature, repeatability for these ceramics cannot be ensured. In the case of PSZT ceramics the d_{33} and k_p were found to be ~289 pC/N and 58%, respectively **[1, 2]**.

Table-1.1 *Electrical properties of PZT ceramics modified with different dopants excluding lanthanum.*

S. No.	Compositions	Processing	Pr ($\mu C/cm^2$)	Ec (kV/cm)	Strain (%)	d_{33} (pC/N)	k_p (%)	K (1 kHz, RT)	T_c (^oC) (1 kHz)	Refs.
1	$(Pb_{0.95}Nd_{0.05})(Zr_{0.58}Ti_{0.42})O_3$	Mortar pestle mixed	-	-	-	561	-	-	260	[51]
2	$Pb_{0.97}Nd_{0.02}(Zr_{0.40}Ti_{0.60})O_3$	Ball milling	-	-	-	260	-	680	-	[52]
3	$Pb_{0.93}Nd_{0.07}(Zr_{0.60}Ti_{0.40})_{1-z/4}O_3$	Sol-gel	11.21	7.71	-	-	-	-	-	[53]
4	$(Pb_{0.95}Nb_{0.05})(Zr_{0.54}Ti_{0.46})O_3$	Ball milling	1.8	9	-	-	-	-		[54]
5	$Pb((Zr_{0.49}Ti_{0.51})_{0.94}Mn_{0.0252}Sb_{0.0192}W_{0.0156})O_3$ + 0.8758 wt% Ni	Ball milling	-	-	-	602	51	1061	-	[55]
6	2.4% Nb doped PZT (Zr/Ti=1.095) Sr=0% Sr=4%	Attrition milled	-	-	-	 410 392	-	-	 350 310	[56]
7	$Pb_{0.9725}$ $(Zr_{0.52}Ti_{0.48})_{0.945}Nb_{0.055}O3$	Mixed oxide (MO)	-	-	-	386	59.1	1529	443	[57]
8	$(Pb_{0.92}Nd_{0.08})(Zr_{0.60}Ti_{0.40})_{0.98}O_3$ $(Pb_{0.92}Sm_{0.08})(Zr_{0.60}Ti_{0.40})_{0.98}O_3$ $(Pb_{0.92}Eu_{0.08})(Zr_{0.60}Ti_{0.40})_{0.98}O_3$ $(Pb_{0.92}Gd_{0.08})(Zr_{0.60}Ti_{0.40})_{0.98}O_3$ $(Pb_{0.92}Dy_{0.08})(Zr_{0.60}Ti_{0.40})_{0.98}O_3$ $(Pb_{0.92}Er_{0.08})(Zr_{0.60}Ti_{0.40})_{0.98}O_3$ $(Pb_{0.92}Yb_{0.08})(Zr_{0.60}Ti_{0.40})_{0.98}O_3$	Sol-gel	8.84 7.58 5.41 8.31 6.75 10.78 -	6.61 5.58 5.28 3.11 3.97 7.22 -	-	269 151 53 - 84 75 -	-	2148 737 404 187 528 422 194	182 284 349 337 368 354 -	[58]
9	$(Pb_{0.96}Eu_{0.04})(Zr_{0.55}Ti_{0.45})_{0.99}O_3$	Mixed oxide (MO)	27.67	13.05	-	-	-	1118	327	[59]
10	$[Pb_{0.89}(Ba, Sr)_{0.11}](Zr_{0.52}Ti_{0.48})$ O_3+1 mol% Mn + 2 mol% F	Co-precipitation	28.1	10.8	-	370	68	2050	298	[60]
11	$(Pb_{0.97}Ca_{0.03})(Zr_{0.05}Ti_{0.95})O_3$	Precursor								[61]
12	$(Pb_{0.94}Sm_{0.06})(Zr_{0.65}Ti_{0.35})O_3$	Ball milling	35.8	-	-	172	42	685	260	[62]
13	$Pb(Zr_{0.588}Ti_{0.392}Fe_{0.01}Nb_{0.01})O_3$ $(Pb_{0.98}Sm_{0.02})((Zr_{0.588}Ti_{0.392}Fe_{0.01}Nb_{0.01})O_3$	Mortar pestle mixed	14.2 32.5	7.3 7.7	-	-	-	-	-	[63]
14	$Pb_{0.96}Sr_{0.04}(Mg_{1/3}Nb_{2/3})_{0.275}(Ni_{1/3}Nb_{2/3})_{0.1}Ti_{0.375}$ $Zr_{0.25}O_3$	Solid state reaction	-	-	-	362	-	2625	-	[64]

The highest electrical properties for PZT ceramics was achieved by off valent donor ion modification at the A-sites, in which Pb^{2+} substituted by La^{3+} due to its comparable ionic size is known as PLZT ceramics **[1, 65]**. La-modified PZT ceramics possess high dielectric and piezoelectric properties compared to the original PZT system because of the donor effect. While replacing divalent Pb^{2+} ions, trivalent La^{3+} ions generate vacancies at the A-site of the perovskite ABO_3 structure to neutralize the system. These vacancies counteract the natural p-type conductivity of the PZT ceramics, which results in the increase in electrical resistivity of the modified PZT materials. These donors also help to enhance domain reorientation, which results in the softening of PZT domain wall motion as well as easy reorientation of dipoles during poling. The electronic properties of La substituted PZTs are greatly enhanced as compared to the basic PZT system. La substitution to the PZT system is believed to lower the distortion of the unit cell, thereby promoting a single-phase, pore-free dense microstructure with the uniform grain growth **[43]**.

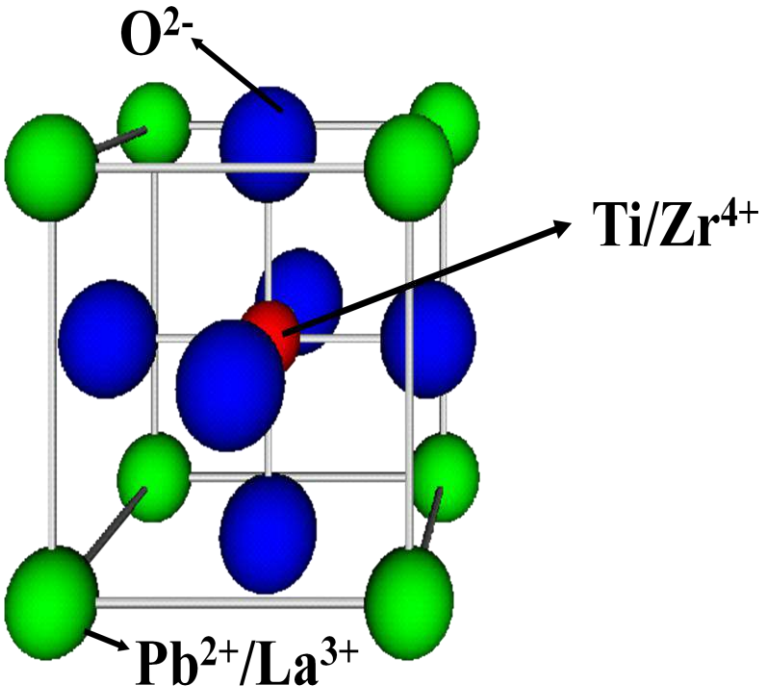

Fig. 1.12 Schematic representation of PLZT unit cell.

Adding La to the PZT system helps to maintain the extensive solid solution throughout the system. Due to the high solubility of lanthanum in the oxygen octahedral structure, the stability of the ferroelectric phases decreases in favor of the paraelectric and antiferroelectric phases. The PLZT ceramics are characterized by large dielectric constants, piezoelectric coefficients and electromechanical coupling factors. They also show high remnant polarization, permittivity and dielectric losses along with low

coercive field and mechanical quality factors. Soft PLZT ceramics produce larger displacements and wider signal band widths compare to the hard ceramics hence used primarily in sensing applications, rather than in power applications **[1-2, 43, 65-66]**. The general formula for the PLZT is given by $(Pb_{1-x}La_x)(Zr_{1-y}Ti_y)O_3$ and the schematic representation of the PLZT unit cell is given in fig. 1.12.

A brief literature review on the La modified PZT ceramics is given in table-1.2, in which the electrical properties of PLZT as well as for the modified PLZT are listed **[67-88]**. After studying the PLZT 8/60/40 ceramics, d_{33} of ~569 pC/N is reported by Shannigrahi et. al. **[58]**. The dielectric constant was also found to be good in the above study. The high remnant polarization ~58.1 μC/cm^2 and the coercive field ~7.10 kV/cm for $(Pb_{0.97}La_{0.03})(Zr_{0.60}Ti_{0.40})O_3$ ceramics was reported by Thakur et. al. **[84]**. There are also several reports on the different amount of lanthanum substitution with different Zr/Ti ratio. Comparative results of dielectric, ferroelectric and piezoelectric properties of these ceramics are given in table-1.2.

Many researchers also tried for further enhancement in the electrical properties of PLZT ceramics by doping them with different ions. Some of the dopants are K, Na, Cs, Bi, Fe, Al, Sb, Sr, etc. **[68-69, 74-77, and 79-81]**. The transition temperature of all of these ceramics decreases with an increase in La and any other dopants. Apart from above compositions, some of the very complex system with PLZT ceramics was also prepared **[31, 82]**. One of the system $[Pb_{1-x-y}La_xSr_y][(Zr_zTi_{1-z})_{1-x/4-5k/4}Nb_k]O_3$, y=1.50% was reported by Ramam et. al. **[82]** shows the P_r ~32.7 μC/cm^2, d_{33} ~498 pC/N and k_p~54% with dielectric constant of ~2385. One more complex composition was reported by Koduri et. al. **[31]**, in which PLZT ceramics were prepared by doping of x% PBLBiN ($Pb_{0.557}Ba_{0.38}La_{0.022}Bi_{0.02}Nb_2O_6$). We know that PLZT ceramics have a tetragonal structure and PBLBiN shows the tungsten bronze structure. The complex 0.94PLZT–0.06PBLBiN, composition, which was prepared by high energy mechanical ball milling, shows d_{33}~617 pC/N and k_p~59% with dielectric constant of ~2987.

After a thorough literature survey, it was found that there are only a few reports available on the effects of electric field induced strain on PLZT ceramics. This is indeed an important parameter in so far as it is needed for the estimation the d_{33} of the electro-ceramics. This being the case on account of the fact that the parameter is of paramount importance in evaluating the suitability of use of material for actuator applications. The $(Pb_{0.924}La_{0.076})(Zr_{0.70}Ti_{0.30})O_3$ composition reported by Zhang et. al. **[87]** shows the very less bipolar strain of ~0.3%. Despite many attempts by previous workers, a reliable process to develop ultra-high strain piezoceramics has met with only limited success, if at all, wherein it is essential to fabricate a material with a relatively simple composition as well as the process of fabrication. James et. al. has done significant work on the processing of PLZT ceramics to improve the electrical properties. All the important electrical parameters of PLZT ceramics such as remnant polarization, strain and piezoelectric charge coefficient were well reported **[89-93]**.

Table-1.2 *Electrical properties of PLZT and modified PLZT ceramics.*

S. No.	Compositions	Processing	P_r ($\mu C/cm^2$)	E_c (kV/cm)	Strain (%)	d_{33} (pC/N)	k_p (%)	K (1 kHz, RT)	T_c (^oC) (1 kHz)	Refs.
1	0.94PLZT–0.06PBLBiN	HEM	-	-	-	617	59.2	2987	242	[31]
2	$(Pb_{0.92}La_{0.08})(Zr_{0.58}Ti_{0.42})O_3$	Mortar pestle mixed	-	-	-	543	-	-	200	[51]
3	$(Pb_{0.92}La_{0.08})(Zr_{0.60}Ti_{0.40})_{0.98}O_3$	Sol-gel	21.90	6.65	-	569	-	3413	156	[58]
4	$(Pb_{0.90}La_{0.10})(Zr_{0.65}Ti_{0.35})O_3$	Sol-gel	-	-	-	-	-	990	92	[67]
5	$Pb_{0.9}(La_{0.99}K_{0.1})_{0.1}(Zr_{0.53}Ti_{0.47})_{0.975}O_3$	Sol-gel	-	-	-	-	-	1300	135	[68]
6	$Pb_{0.91}(La_{0.99}Na_{0.1})_{0.09}(Zr_{0.58}Ti_{0.42})_{0.9775}O_3$	Sol-gel	-	-	-	-	-	5700	89	[69]
7	$Pb_{0.91}(La_{0.95}Na_{0.5})_{0.09}(Zr_{0.65}Ti_{0.35})_{0.9775}O_3$	Sol-gel	-	-	-	-	-	2532	176	[70]
8	$(Pb_{1-z}La_z)(Zr_{0.60}Ti_{0.40})_{1-z/4}O_3$ Z=0.00 Z=0.05 Z=0.09 Z=0.12	Sol-gel	 7.69 7.00 6.20 2.89	 6.64 6.51 5.29 1.00	-	-	-	-	 359 250 116 55	[71]
9	$(Pb_{0.98}La_{0.02})(Zr_{0.535}Ti_{0.465})_{0.995}O_3$	Mortar pestle mixed	-	-	-	415	49	1030	371	[72]
10	$(Pb_{0.98}La_{0.02})(Zr_{0.54}Ti_{0.46})O_3$	Precursor route (PR)	45	11.1	-	-	-	-	-	[73]
11	$Pb_{0.90}(La_{0.99}Cs_{0.1})_{0.10}(Zr_{0.53}Ti_{0.47})_{0.975}O_3$	Pechini method	-	-	-	-	-	2319	116	[74]
12	$Pb_{0.91}La_{0.09}(Zr_{0.4}Ti_{0.6})O_3$	Mixed oxide	36.6	21.1	-	-	-	2500	-	[75]
13	$(Pb_{0.99}La_{0.01})(Zr_{0.52}Ti_{0.48})_{1-x/4}O_3$	Ball milled	-	-	-	-	48	1334	-	[76]
14	$Pb_{0.90}(La_{0.97}Bi_{0.3})_{0.10}(Zr_{0.65}Ti_{0.35})_{0.975}O_3$	Mixing	-	-	-	-	-	1322	178	[77]
15	$(Pb_{0.94}La_{0.6})(Zr_{0.65}Ti_{0.35})O_3$	Solid state reaction	16.0	2.95	-	-	-	3000	180	[78]
16	$[Pb_{0.92}(La_{0.91}Sb_{0.9})_{0.08}](Zr_{0.60}Ti_{0.40})O_3$	Solid state reaction	9.2	4.0	-	-	-	-	303	[79]
17	$[Pb_{0.90}(La_{0.93}Fe_{0.7})_{0.10}](Zr_{0.55}Ti_{0.45})_{0.975}O_3$	Solid state reaction	-	-	-	-	-	830	259	[80]
18	$[Pb_{0.92}(La_{1-z}Al_z)_{0.08}](Zr_{0.60}Ti_{0.40})_{0.98}O_3$ Z=0.0 Z=0.9	Sol-gel	-	-	-	 520 257	 29 43	 5700 5085	 163 356	[81]
19	$[Pb_{1-x-y}La_xSr_y][(Zr_zTi_{1-z})_{1-x/4-5k/4}Nb_k]O_3$, y=1.50%	Solid state reaction	32.66	-	-	498	53.8	2385	246	[82]
20	$(Pb_{0.97}La_{0.03})(Zr_{0.53}Ti_{0.47})O_3$	HEM	-	-	-	458	-	1880	-	[83]
21	$(Pb_{0.97}La_{0.03})(Zr_{0.60}Ti_{0.40})O_3$ $(Pb_{0.93}La_{0.07})(Zr_{0.60}Ti_{0.40})O_3$ $(Pb_{0.92}La_{0.08})(Zr_{0.60}Ti_{0.40})O_3$	Mortar pestle mixed	58.1 49.2 43.6	7.10 6.92 6.67	-	208 450 387	42.1 52.0 52.0	1210 1875 2511	320 221 188	[84]
22	PSLZT with 5 at% Sr and 1 at% La	Mixed oxide				640	56.0	1800		[85]
23	$(Pb_{0.92}La_{0.08})(Zr_{0.60}Ti_{0.40})O_3$	Ball milling	20.5	9.98				2785	145	[86]
24	$(Pb_{0.924}La_{0.076})(Zr_{0.70}Ti_{0.30})O_3$	Solid state reaction	26.41	7.76	0.30	410	-	-	96.4	[87]
25	$(Pb_{0.91}La_{0.09})(Zr_{0.65}Ti_{0.35})O_3 + 1\ \%MnO_2$	Ball milling	-	-	-	-	-	1430	218	[88]

Although there has been plentiful research on myriad Pb based systems, such as PMN-PT, which shows among the best, even so, PLZT ceramics attract a lot of attention, mostly on account of the ease of fabrication that it offers. PLZT ceramics have high remnant polarization (P_r), which can be used in memory applications. In addition, they possess low coercive fields (E_c), which helps in poling them easily. The high dielectric constant suggests the potential for using such ceramics for capacitor applications. The high electro-mechanical coupling coefficient (k_p) and high piezoelectric coefficient (d_{33}) values make it a good candidate for energy harvesting applications. Some of the applications where PLZT ceramics offer advantages are ultrasonic cleaners, non-destructive testing and imaging (NDT), ferroelectric thin-film memories, high dielectric constant, thin-film capacitors and electrocaloric effect as reported by several researcherers **[94-97]**. Apart from these applications, PLZT ceramics are easy to synthesize and can be used as an alternative to PMN-PT and any other complex material systems. PLZT system has less complexity than the latter, more repeatability and comparable in properties to other complex lead based systems showing high electrical property output. In short, we can say that PLZT ceramics possess all the compositional aspects of dielectric, ferroelectric, piezoelectric, electro-optic and pyroelectric properties.

The highest piezoelectric and dielectric properties of the piezoelectric ceramics are observed near the morphotropic phase boundary (MPB) **[2]**. La substitution into PZT also modifies the MPB; showing many beneficial effects on several basic properties. This study deals with the selection of optimum PLZT ceramics which should be close to the MPB and shows high electrical properties. The influence of lanthanum doping on the MPB of PZT ceramics was studied and reported by many researchers **[98-99]**. Depending upon the specific requirements for different applications of piezoelectric ceramics, various compositions of the Pb/La ratios may be chosen. Here the formula for PLZT x/60/40 is given by $(Pb_{1-x}La_x)(Zr_{0.60}Ti_{0.40})O_3$. Numerous reports are available on the doping of x at% of La^{3+} ions in the PZT system **[71, 79, and 100-104]**.

The electrical properties are greatly affected by the density of ferroelectric ceramics. Most of the applications require highly dense ferroelectric ceramics and >95% densification ensures the achieving of maximum performance **[5, 105]**. The high density of the PLZT ceramics was achieved by Haertling et. al. **[2, 43]** involving time consuming and an expensive hot pressing process in which calcined PLZT powders were first cold pressed and again hot pressed at high temperature and longer sintering durations (1250^{o}C for 16 hours). Such sintering conditions result in the abnormal grain or secondary grain growth, which are detrimental to the performance of PLZT ferroelectric ceramics. Higher sintering temperatures not only lead to lead loss, which compensates by excess PbO but also affects the electrical properties. Excess PbO addition is detrimental to the environment and performance of the PZT system. In other studies also, many researchers tried to get dense PLZT ceramics via different processing routes. However, all of these involves the use of high sintering temperatures along with longer processing times. Since most of the lead vaporization happens at the

time of processing of the lead based ceramics, by using the alternatives approaches of processing, the lead loss can be minimized.

The lead based ferroelectrics containing very fine scale powders with a narrow size distribution can be sintered at relatively low temperature, resolves the issue of lead volatility. For this purpose, nano-sized ferroelectric powders have been synthesized by several wet chemistry methods, such as sol-gel process, chemical co-precipitation, hydrothermal synthesis, thermal pyrolysis spray, micro-emulsion, molten salt and combustion, etc. **[5 and 105-106]**. Some of them are also reported in Tables-1.1 and 1.2. Numerous reports on various preparation methods for electro-ceramics are available, but the highest electrical properties were found for the high energy mechanically ball milled PLZT. This technique is superior to both the conventional solid state reaction and the wet chemistry based processing routes because it uses widely available and cost effective oxides as the starting materials. The process takes place at room temperature in properly sealed containers. This high energy ball milling technique also called as mechanical alloying, has been widely used to synthesize a wide range of fine nano-sized ceramic powders. The mechanochemically derived ceramic powders, which have high homogeneity and nano-meter scale size, demonstrate much better sinterability than those synthesized by wet chemical processes and the conventional solid state reaction. In this technique oxide precursors of the designed compounds are activated by mechanical energy compare to conventional solid-state reaction process, which requires heat energy.

The properties of electro-ceramics are also greatly affected by the milling conditions. Preliminary studies on the effect of high energy mechano-chemical (HEM) ball milling of PZT/PLZT ceramics were carried out by Kong et. al. **[4-5 and 105-106]**. To get the desired PZT/PLZT phase, ceramics were milled for long milling durations, up to 80 hours. Prolonged milling time increases the contamination risk. A detailed study should be carried out to select the high energy milling parameters for the improvement of ferroelectric and piezoelectric properties of ceramics. The ceramic powders should be milled for much lesser times without compromising the properties of the ceramics, which, in turn, can reduce the contamination in the system. The selection of milling media such as milling vial and balls are also important. The use of metallic vials and balls can contaminate the ceramic powders resulting in the decrease in electrical properties. Since the use of different ceramic vials viz. agate and zirconia vials for the ceramics synthesis can affect the electrical properties. The effect of milling media should be discussed based on the vial density, hardness, etc. Since raw oxides were used for the PLZT ceramics preparation and ZrO_2 is also one of the main oxides, it was felt that the use of zirconia vials and balls could reduce the contamination. Detailed studies are to be carried out. It is also important to highlight the fact that lead loss can be reduced substantially by carefully optimizing milling parameters (No excess PbO need to be added in the starting compositions).

The electrical properties of the piezoelectric ceramics are greatly influenced by the poling conditions. In the case of low resistive ceramics, the application of high poling electric field results in

the electrical breakdown of the ceramics and sometimes physical breakdown is also possible. All of these, in turn, are resulting in the lowering of piezoelectric coefficients. Therefore optimum poling conditions should be identified. Poling of PLZT ceramics should be done at reduced poling voltages, at a relatively lower temperature and shorter poling time, which could be very advantageous if the samples have high conductivity or poor resistivity. There are many available reports of poling of lead based or lead free compositions **[107-109]**. At the end, the origin of ultra high piezoelectric properties of PLZT ceramics will be discussed using slow scan X-ray diffraction data. This XRD data will be used for the crystallographic study using Rietveld refinement and the results will be correlated.

1.8 Motivation and main research objectives of the work

After a detailed description of the objective of this research in the previous section, the main motivation of the present study is described in this section. As discussed, due to the complex processing of materials with high electrical property output such as PMN-PT, the lanthanum substituted PZT system which is less complex to process and has almost equal piezoelectric and ferroelectric properties, was chosen for the detailed study. Akin to the other piezoceramics, PLZT ceramics also show their highest piezoelectric and dielectric properties near to the morphotropic phase boundary (MPB), since La substitution into the PZT also modifies the MPB. This motivates the search for an optimum PLZT composition, which should be close to the MPB by using suitable material engineering approach. Substitution of La not only improves the electrical properties but also helps to reduce the lead content in the parent system.

The high density of PLZT ceramics ensures the maximum performance. However, in order to obtain the high density, ceramics should be calcined and sintered at lower temperatures to avoid the lead loss. This can be done via suitable materials engineering. In this study, a combinatorial approach of high energy ball milling and cold isostatic pressing is proposed. HEM may result in a wide range of nano-sized fine ceramic powders, which react at room temperature via mechanical energy, lowering the heat treatment temperature. CIP typically at higher pressures than uniaxial pressing result in a high green density of ceramics, which is directly related to the final density. The main advantage of the processing technique are (1) PLZT ceramics were prepared at lower calcination and sintering temperature with no excess PbO in the starting material and (2) The PLZT ceramics discs was prepared without binder. This CIPing process has circumvented the necessity to add any binder and the burnout step and thereby alleviates the risk of contamination.

As we know all of the above processes, involve the extensive use of the milling process. Since the properties of electro-ceramics are also greatly affected by the milling conditions, a detailed study can help reduce the contamination in ceramic powders in the case of longer duration of milling

time and use of different milling media. In the present study, it was proposed that ceramics should be milled for different durations when different milling vials are used. Agate and Zirconia vials were chosen for the said studies. The high piezoelectricity in PLZT ceramics depends on the poling conditions. In this work, the identification of optimum poling conditions for PLZT ceramics is also proposed. Apart from above reasons, the optimized PLZT ceramic system shows ultra high piezoelectric coefficients. The main motivation of this thesis is to find the origin of these high properties.

The objective of the proposed scheme of work is to synthesize and characterize smart materials such as soft lanthanum modified PZT ceramics which involves the optimization of La substitution. It has been one of the objectives of this work to reduce the overall processing temperatures and durations used in the synthesis of PLZT ceramics, viz. the calcination and sintering temperature and time. The importance of this can be understood from the fact that in the specific case of Pb-based ceramics, there is a tendency for volatilization of PbO at elevated temperatures when held at those temperatures for long durations. In order to alleviate these issues, it was found that a combination of mechanical activation (high energy mechano-chemical ball milling) with the cold isostatic process (CIP) could not only reduce processing temperatures and time but also circumvent the need to add excess PbO in the starting materials. At the same time; it could be done without compromising the high density of such ceramics due to this process. The mechanical activation method results in ultrafine powders with a narrow particle size distribution that can react at room temperature itself and reduce the processing temperature. On the one hand, it would be the endeavor to reduce the particle size while on the other hand; contamination will have to be avoided since the properties of electro-ceramics are greatly affected by contaminants.

The aim is also to study the underlying Physics of Structure-Property correlations of different compositions of PLZT using different milling conditions and to improve the overall electrical properties of the piezo-ceramics studied. Overall the aim would be to enhance the piezoelectric charge coefficients and electro-mechanical coupling factors of the materials by improving the microstructure of the PLZT ceramics. Apart from that another important objective of this study to ascertain the reason behind the ultra high piezoelectric properties of optimized PLZT ceramics. In this study, it is proposed to synthesize (electrically) soft PLZT ceramics by high energy mechano-chemical ball milling using different milling media, such as agate, zirconia, etc. so as to enhance the reactivity of the constituent oxides and thereby reduce the calcination and sintering temperature. The study will involve optimization of milling durations. The phase evolution will be studied via X-ray diffraction data analysis, and the microstructure will be studied by SEM and TEM. The structure of the materials will be correlated with the electrical properties of the same at each stage of the study.

For all of the aforementioned reasons, materials engineering approach was used in a two pronged manner (1) To synthesize a material with properties comparable to PMN-PT. (2) To develop

a synthesis technique which is inexpensive but at the same time shows properties comparable to the complex hot pressing method. In doing so, it was attempted to find out the origin of ultra high piezoelectric properties of optimized PLZT ceramics, through a structural analysis using Rietveld refined XRD data collected at a different temperature.

References

[1] B. Jaffe, W.R. Cook Jr, and H. Jaffe, Piezoelectric Ceramics, (Academic Press New York) 1971.

[2] G.H. Haertling, J. Am. Ceram. Soc., **82[4]** (1999) 797.

[3] D. Damjanovic, Rep. Prog. Phy., **61** (1998)1267.

[4] L.B. Kong, T.S. Zhang, J. Ma and F. Boey, Progress in Materials Science, **53** (2008) 207.

[5] L.B. Kong, J. Ma, W. Zhu and O.K. Tan, J. Alloys and Comp., **322** (2001) 290.

[6] V.M. Goldschmidt, S.N.V. Akad, Oslo, I: Mat.-Naturv. Kl. No., **2**(1926) 8.

[7] H.D. Megaw, "Ferroelectricity in Crystals.", Methuen, London (1957).

[8] F.S. Galasso, Structure, Properties and Preparation of Perovskite Type Compounds, Pergamon Press, London (1969).

[9] H. Hahn and U.Z. Mutschke. Anorg. Allgem. Chem., **288** (1956) 269.

[10] E.A. Wood., Acta. Cryst., **4** (1951) 353.

[11] M.L. Keith and Roy, R. Am. Min., **39** (1954) 1.

[12] R.S. Roth, J. Res. Nat. Bur. Std., **58** (1957) 75.

[13] T. Mitsui, I. Tatsuzaki and E. Nakamura, An introduction to the physics of ferroelectrics, Gorden and Breach Science publication, London, (1976).

[14] M.E. Lines, A.M. Glass, Principles and Applications of Ferroelectrics and Related Materials, Oxford: Oxford University Press, (1977).

[15] F. Joan and G. Shirane, Ferroelectric Crystals, New York: Pergamon Press (1962)

[16] J.F. Nye, Physical properties of Crystals, Clarendon Press, Oxford (1990).

[17] A.V. Hippel, Rev. Modern Physics., **22** (1950) 221.

[18] A.J. Dekker, Solid State Physics, Mac Millian, NY (1991).

[19] L. Jin, F.Li and S. Zhang, J. Am. Ceram. Soc., **97[1]** (2014) 1.

[20] T.L. Jordan and Z. Ounaies, Piezoelectric ceramics characterization, ICASE, September (2001).

[21] T.M. Kamel and G. de With, J. Euro., Ceram. Soc., **28** (2008) 851.

[22] Hysteresis software version 2.4.0.0 user manual, aixACCT GmbH, Germany.

[23] B. Tareev, Physics of Dielectric Materials, English Translation, Meer Publishers, Moscow, Second Edition, Chapter-3 (1979).

[24] H. Yan, F. Inam, G. Viola, H. Ning, H. Zhang, Q. Jiang, T. Zeng, Z. Gao and M.J. Reece, J. Adv. Diel., **1 [1]** (2011) 107.

[25] L. Pintilie and M. Alexe, Appl. Phys. Lett. **87** (2005) 112903.

[26] J.F. Scott, J. Phys.: Condens. Matter **20** (2008) 021001.

[27] B. Jaffe, J. Am. Ceram. Soc., **41 [11]** (1958) 494.

[28] M. Hagiwara, H. Noguchi, T. Hoshina, H. Takeda, S. Fujihara, N. Kodama, and T. Tsurumi, Japanese J. Appl. Phys., **52** (2013) 09KD03.

[29] R. Dittmer, K.G. Webber, E. Aulbach, W. Jo, X. Tan and J. Rödel, Sensors and Actuators A, **189** (2013) 187.

[30] S. Priya, J.Electroceram., **19** (2007) 165.

[31] R. Koduri and M. Lopez, J. Mater Sci: Mater Electron, **19** (2008) 669.

[32] G. Busch, Ferroelectrics, **74** (1987) 267.

[33] W. Kanzig, Ferroelectrics, **74** (1987) 285.

[34] L.E. Cross and R.E. Newnham, History of Ferroelectrics, Ceramics and Civilization, Vol. III, High-Technology Ceramics-Past, Present and Future, American Ceramic Society, Westerville, OH (1987) 289.

[35] G. Busch, Ferroelectrics, **71** (1987) 43.

[36] J. Fousek, Ferroelectrics, **113** (1991) 3.

[37] L. Dong, D.S. Stone and R.S. Lakes, J. Appl. Phys., **111** (2012) 084107.

[38] W. Liu and X. Ren, Phys. Rev. Lett., **103** (2009) 257602.

[39] J. Rödel, W. Jo, K.T.P. Seifert, E.M. Anton, T. Granzow and D. Damjanovic, J. Am. Ceram.Soc., **92 [6]** (2009) 1153.

[40] B.G. Kim, S.M. Cho, T.Y. Kim and H.M. Jang, Phy. Rev. Lett., **86[15]** (2001) 3404.

[41] G. Shirane, K. Suzuki, and A. Takeda, J. Phys. Soc. Jpn., **7 [1]** (1952) 12.

[42] B. Jaffe, R. S. Roth, and S. Marzullo, J. Appl. Phys., **25 [6]** (1954) 809.

[43] G.H. Haertling and C.E. Land, J. Am. Ceram.Soc., **54** (1971) 1.

[44] S.T. Liu, J.D. Heaps and O.N. Tufte, Ferroelectrics, **3** (1972) 281.

[45] H. Ouchi, K. Nagano, and S. Hayakawa, J. Am. Ceram.Soc., **48 [12]** (1965) 630.

[46] L.E. Cross, S.J. Jang and R.E. Newnham, Ferroelectrics, **23** (1980) 187.

[47] S. Nomura and K. Uchino, Ferroelectrics, **50** (1983) 197.

[48] M.F. Yan, H.C. Ling and W.W. Rhodes, J. Mater. Res., **4 [4]** (1989) 930.

[49] S.L. Swartz and T.R. Shrout, Mater. Res. Bull., **17** (1982) 1245.

[50] S.H. Baek, M.S. Rzchowski and V.A. Aksyuk, MRS Bulletin, **37** (2012) 1022.

[51] S.C. Jung, H. B. Park, J. Kim, K. Kim and S.J. Kim, J. Korean Ceram. Soc., **31 [2]** (1994) 155.

[52] A. Garg, T.C. Goel, Mater. Sci. Eng. B, **60** (1999) 128.

[53] S.R. Shannigrahi, R.N.P. Choudhary and H.N. Acharya, Mater. Sci. Eng. B, **56** (1999) 31.

[54] M. Pereira, A.G. Peixoto and M.J.M. Gomes, J. Europ. Ceram. Soc., **21** (2001) 1353.

[55] N. Texier, C. Courtois, M. Traianids and A. Leriche, J. Europ. Ceram. Soc., **21** (2001) 1499.

[56] H. Zheng, I.M. Reaney, W.E. Lee, N. Jones and H. Thomas, J. Europ. Ceram. Soc., **21** (2001) 1371.

[57] S.Y. Chu, T.Y. Chen, I. Tsai and W. Water, Sensors and Actuators A, **113** (2004) 198.

[58] S.R. Shannigrahi, F.E.H. Taya, K. Yaoa and R.N.P. Choudhary, J. Europ. Ceram. Soc., **24** (2004) 163.

[59] R. Khazanchi, S. Sharma and T.C. Goel, J. Electroceram., **14** (2005) 113.

[60] B. Guiffard, E. Boucher, L. Lebrun and D. Guyomar, Mater. Sci. Eng. B, **137** (2007) 272.

[61] S. Sen, R.N.P Choudhary and P. Pramanik, Physica B, **387** (2007) 56.

[62] S.K. Pandey, O.P. Thakur, D.K. Bhattacharya, C. Prakash and R. Chatterjee, J. Alloys Comp., **468** (2009) 356.

[63] P. Singh, S. Singh, J.K. Juneja, K.K. Raina, R.P. Pant and C. Prakash, Integrated Ferroelectrics, **122** (2010) 23.

[64] Y. Zhao, Y. Zhang and X. Wang, J. Mater. Sci.: Mater. Electron, **24** (2013) 2240.

[65] H. Jaffe and D.A. Berlincourt, Piezoelectric Transducer Materials, Proc.IEEE, **53 [10]** (1965) 1372.

[66] G.H. Haertling, Piezoelectric and Electrooptic Ceramics in Ceramic Materials for Electronics, Editor R.C. Buchanan, Marcel Dekker, New York (1986) 135.

[67] K.L. Yadav and R.N.P. Choudhary, J. Mater. Sci. **28** (1993) 769.

[68] J. Mal and R.N.P. Choudhary, J. Phys. Chem. Solids, **l58 [3]** (1997) 421.

[69] H.R. Rukmini, R.N.P. Choudhary and V.V. Rao, , Mater. Chem. Phys., **55** (1998) 108.

[70] H.R. Rukmini, R.N.P. Choudhary and D.L. Prabhakara, Mater. Chem. Phys., **64** (2000) 171.

[71] S.R. Shannigrahi and R.N.P. Choudhary, J. Electroceram., **5 [3]** (2000) 201.

[72] A. Garg and D.C. Agrawal, Mater. Sci. Eng. B, **86** (2001) 134.

[73] M. Laurent, U. Schreiner, P.A. Langjahr, A.E. Glazounov and M.J. Hoffmann, J. Europ. Ceram. Soc., **21** (2001) 1495.

[74] R.N.P. Choudhary and J. Mal, Mater. Sci. Eng. B, **90** (2002) 1.

[75] Y. Zhang, A.L. Ding, P.S. Qiu, X. Y. He, X. S. Zheng, H.R. Zeng and Q.R. Yin, Mater. Sci. Eng. B, **99** (2003) 360.

[76] L. Pdungsap, N. Udomkanb, S. Boonyuen and P. Winotai, Sensors and Actuators A, **122** (2005) 250.

[77] R. Rai, S. Sharma and R.N.P. Choudhary, Solid State Comm., **133** (2005) 635.

[78] S. Singh, O.P. Thakur and C. Prakash, Synthesis, Def. Sci. J., **55 [3]** (2005) 349.

[79] S. Dutta, R.N.P. Choudhary and P.K. Sinha, J. Alloys Comp., **426** (2006) 345.

[80] R. Rai, S. Sharma, N.C. Soni and R.N.P. Choudhary, Physica B, **382** (2006) 252.

[81] S. Dutta, R.N.P. Choudhary and P.K. Sinha, J. Alloys Comp., **430** (2007) 344.

[82] K. Ramam and M. Lopez, Mater. Sci. Eng. B, **145** (2007) 41.

[83] B.P. Kumar, H.H. Kumar, D.K. Kharat and B.S. Murty, Mater. Chem. Phys. **112** (2008) 31.

[84] O.P. Thakur and C. Prakash, Integrated Ferroelectrics, **122** (2010) 100.

[85] V. Kalem, I. Cam and M. Timucin, Ceram. Inter. **37** (2011) 1265.

[86] O.G. Zaldıvar, A.P. Barranco, J.D.S. Guerra, M.E. Mendoza, F.C. Pinar and D.A. Hall, Physica B, **406** (2011) 1622.

[87] N. Zhang, Y. Feng and Z. Xu, Mater. Lett., **65** (2011) 1611.

[88] E.P. Delfin, J.E. García, A.V. García, F. Guerrero and J.A. Eiras, J. Europ. Ceram. Soc., **32** (2012) 1659.

[89] A.R. James, J. Subrahmanyam and K.L. Yadav, J. Phys. D: Appl. Phys., **39** (2006) 2259.

[90] A.R. James and J. Subrahmanyam, J. Mater. Sci.: Mater. Electron, **17** (2006) 529.

[91] A.R. James, B.S.S. Chandra Rao, M. Pathak, S.V. Kamat and J. Subrahmanyam, Nanotechnology, **19** (2008) 195201.

[92] A.R. James, B.S.S. Chandra Rao, S.V. Kamat, J. Subrahmanyam, K. Srinivas and O.P. Thakur, Smart Mater. Struct., **17** (2008) 035020.

[93] A.R. James and O.P. Thakur, Dielectric and Ferroelectric Reviews, Editors: S.S.N. Bharadwaja and R.A. Dorey, Research Signpost, Trivandrum, India, Ch-2 (2012) 33.

[94] Z. Liu, D. Shi, H. Zhou, L. Deng and K. Li, Ceram. Inter., **41 [1]** (2015) 941.

[95] G. Zhang, Z. Chen, B. Fan, J. Liu, M. Chen, M. Shen, P. Liu, Y. Zeng, Sh. Jiang and Q. Wang, APL Mater., **4** (2016) 064103.

[96] X. Li, Y.Yu, Z. Zheng, Ceram. Inter., **41 [1]** (2016) 490.

[97] H.R. Jo and C.S. Lynch, J. Appl. Phys. **119** (2016) 024104.

[98] M. Hinterstein, K.A. Schoenau, J. Kling, H. Fuess, M. Knapp, H. Kungl and M.J. Hoffmann, J. App. Phy., **108** (2010) 024110.

[99] S.H. Lee, C.B. Yoon, S.B.Seo and H.E. Kima, J. Mater. Res., **18 [8]** (2003) 1238.

[100] J.D.S. Guerra, J.E. Garcia, D.A. Ochoa, A.P. Barranco, O.G. Zaldivar, F.C. Pinar, J Mater. Sci., **47** (2012) 5715.

[101] F. Craciun, F. Cordero, I.V. Ciuchi, L. Mitoseriu and C. Galassi, J. Appl. Phys., **117** (2015) 184103.

[102] J.D.S. Guerra, A.C. Silva, R. Mcintosh, M.M. Hoque, R. Guo and A. S. Bhalla, Int. Ferroelectrics **166 [1]** (2015) 158.

[103] E.A. Falcão, J.A. Eiras, D. Garcia, I.A. Santos, A.N. Medina, M.L. Baesso, T. Catunda, R. Guo and A. S. Bhalla, Ferroelectrics **494 [1]** (2016) 33.

[104] S. Somwan, N. Funsueb, A. Limpichaipanit, A. Ngamjarurojana, Ceram. Inter., 42 [11] (2016) 13223.

[105] L.B. Kong, J. Ma and T.S. Zhang, J. Mater. Res., **16 [6]** (2001) 1636.

[106] L.B. Kong, W. Zhu and O.K. Tan, Mater. Lett., **42** (2000) 232.

[107] L. Zhang, Q. Sun, W. Ma, Y. Zhang and H. Liu, J. Mater. Sci: Mater. Electron, **23** (2012) 688.

[108] Y. Zhao, R. Huang, R. Liu and H. Zhou, Ceramics International, **38** (2012) 6067.

[109] S. Su, R. Zuo, S. Lu, Z. Xu, X. Wang and L. Li, Curr. Appl. Phys., **11** (2011) S120.

Chapter-II

Experimental techniques

2.1 Introduction

It is well-known that the properties of ceramic materials are mostly preparation dependent. The property of any material depends upon the way it is processed, so the steps for processing, the processing equipment and the conditions must be carefully monitored and controlled for best results. Much attention, therefore, is paid to the preparation of PLZT ceramics. The methods that are used for the mixing of raw oxides are mortar-pestle mixing and high energy mechano-chemical ball milling (Mechanical activation). A flow sheet describing the essential steps of processing and characterization is given in fig. 2.1. The mixing with mortar-pestle and HEM has many steps in common. However, they show differences at the powder forming and densification stages. Therefore careful attention has to be paid to the preparation of electro-ceramics.

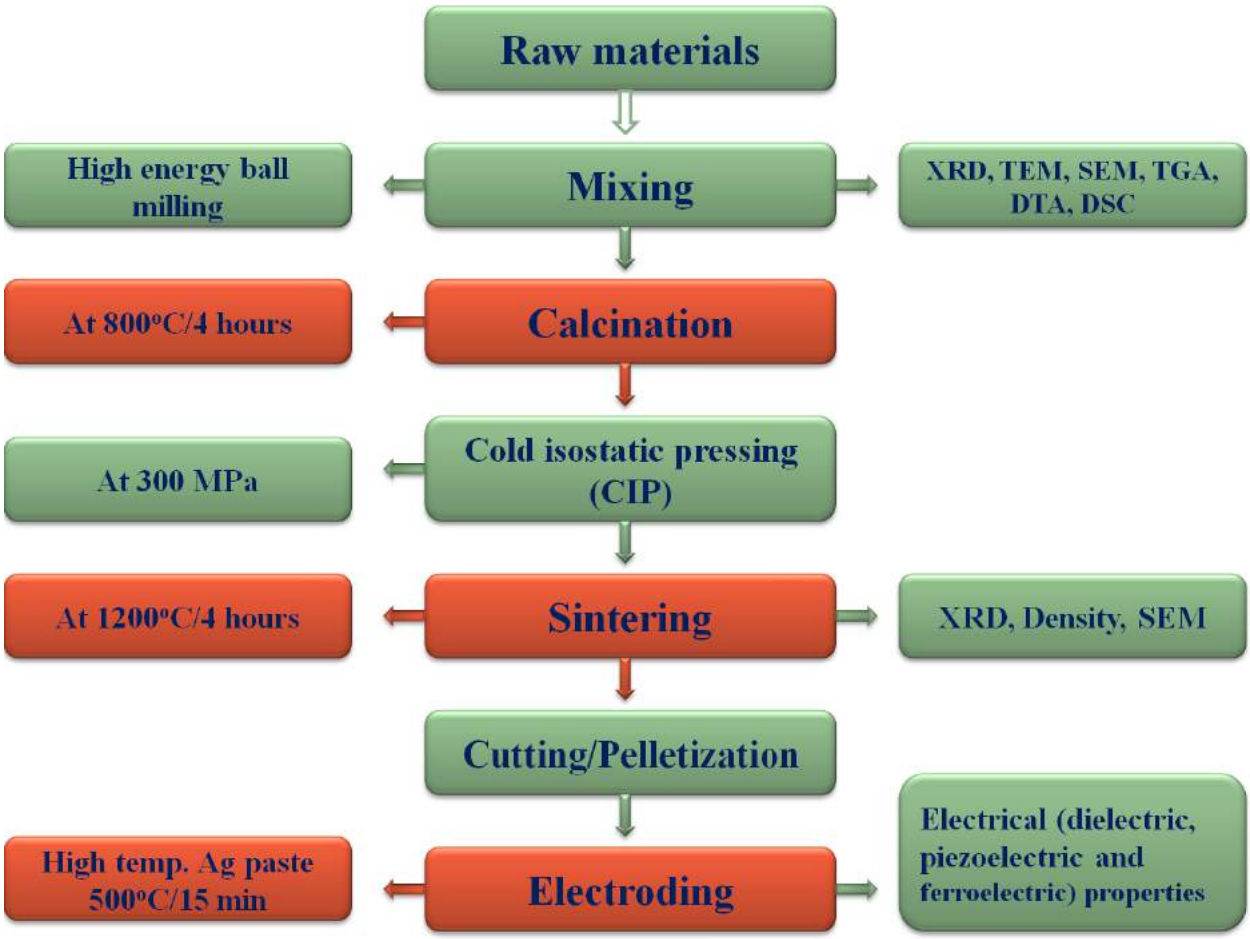

Fig. 2.1 *Flow chart for processing and characterization of PLZT ceramics.*

2.2 Types of synthesis methods for PLZT ceramics

The selection of a processing method to prepare the powders not only depends on the cost of the raw oxides but also on the end application. There are many methods available for synthesis of piezoelectric ceramics such as solid-state reaction (by using oxides or Mixed Oxide method) **[1]**, Pechini method **[2]**, hydrothermal processing **[3-4]**, sol-gel or **[5-6]**, co-precipitation technique **[7-9]**. Based on the desired properties any one of the above methods can be used for the ceramic preparation. Mainly two types of processing techniques are used for PLZT ceramics preparation namely co-precipitation method or solid-state reaction method.

2.2.1 Co-precipitation (CP) method

In this method, mutually soluble solutions were used as starting materials, which produced atomically homogeneous precursor solution that is precipitated while blending. Since the particle sizes of CP powders are finer than the mixed oxide (MO) powders, they are more reactive with relatively low calcination temperature, ~500°C for 1 h **[1]**. The optical quality PLZT ceramics required specially developed chemical CP processes involving liquid organometallic or inorganic precursors.

2.2.2 Mixed oxide method (Solid-state reaction)

The most adopted method to prepare piezoelectric ceramics is the most economical, mixed-oxide method **[1]**. This technique consists of wet milling (slurry form) of the individual oxides or other compounds, such as the nitrates and carbonates that decompose to the oxides during calcination (a solid-state chemical reaction at high-temperature) at 800° to 900°C. Solid-state reaction route further can be divided into two processes: mortar-pestle or high energy mechanochemical ball milling. HEM ball milling is advantageous over other methods due to the wide availability and low cost of starting materials. In this technique, desired ceramics are processed at room temperature with relatively simple operation. The use of other methods requires high calcination temperatures which are not suitable especially in the case of Pb-based electro-ceramics.

2.2.2.1 Mortar-pestle mixing

In this method, raw oxides of the desired composition are homogeneously mixed by using a mortar and pestle. There is no chemical reaction taking place between the raw materials. Thus mortar pestle mixed ceramic powders are to be calcined and sintered at high temperatures. Elevated temperature leads to a loss of volatile materials such as lead and bismuth, resulting in inferior electrical properties due to compositional non-stoichiometry.

2.2.2.2 High energy mechano-chemical ball milling (Mechanical activation)

It is reported and found that mechanical activation technique reduces the particle sizes, and yield enhanced electrical properties. The term milling is referred to as the breaking down of relatively coarse materials to the ultimate fineness. Mixing and milling are often processes, which are carried out simultaneously using one piece of equipment such as a ball mill. The principal aims of the milling process are to reduce the primary particle size which will result in increased reactivity of fine scale particles, to reduce the agglomerates size (ideally to primary particle size), to achieve the desired particle size distribution and to ensure that the scale of mixing is sufficiently small to guarantee that any subsequent calcination will produce the correct proportions of new and original phases **[10-11]**.

Fig. 2.2 *Fritsch Pulverisette P-5 two station planetary ball mill.*

Different types of milling equipment can be used to produce mechanically milled ceramic powders. They differ in their efficiency of milling, capacity and additional arrangement for cooling-heating, etc. Some important mills used for high energy mechanical milling include SPEX shaker mills, planetary mills, attritor ball mills, rod mills, vibrating frame mills, etc. Ball milling is extensively used for mixing and milling electronic ceramics. A Fritsch Pulverisette P-5 two station planetary ball mill that was used for milling the oxide powders for this work is shown in fig. 2.2.

Fig. 2.3 (a) and (b) schematically shows the milling process and mechanism that take place inside a milling bowl. The high energy mechano-chemical processing technique is a complex process, involving the rotation of milling bowl or vial in a planetary fashion, on a base plate of a mill (rotating in the opposite direction w.r.t. the bowls). The milling balls collide with each other as well as with the walls of the bowls. Planetary ball mills show high performance for grinding and pulverization of ceramic samples. A combination of impact and frictional forces results between the balls and vial which is responsible for size reduction of particles and at the same time for the micro-strains produced in them **[12]**. During this technique, the powder particles are repeatedly subjected to high impact energy. Thus, the mechanical milling provides the means to substantially increase reaction kinetics of the reduction reactions due to the fracturing of powder particles. Each collision is associated with the trapping of a small quantity of powder between either the balls themselves or the ball and walls of the vial **[10]**. If a medium like water is used, it is presumed that the energy of milling comes down on account of the viscosity of the liquid, but at the same time, this has the advantage that the liquid ensures that the powders are constantly in contact with the balls, thereby ensuring better milling efficiency. If dry conditions are used, there is a possibility that the powders might settle down at the bottom of the vial, whereas the balls only impact each other or the walls, without serving the purpose of milling the powders **[13]**.

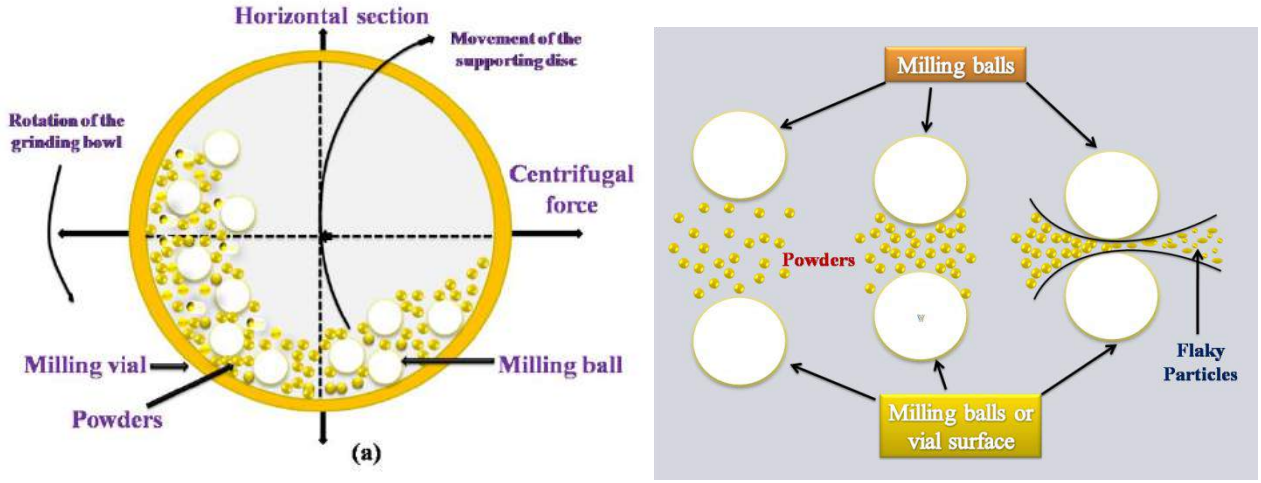

Fig 2.3 *(a) and (b) Schematic representation of the mechanism of a high energy planetary ball milling process* ***[10-11 and 13-14]****.*

Several factors which affect the milling process and play very significant roles in the fabrication of homogeneous materials are shown in fig. 2.4. Some of them are, type of mills (low energy and high energy mills), types of milling media, the milling tool materials, milling temperature, milling time, milling environment (dry milling or wet milling), milling atmosphere (air, nitrogen or an inert gas), milling media to powder weight ratio, etc. **[11]**. High energy ball milling process also has the few drawbacks such as the final powder product has too broad a particle size distribution,

promoting abnormal grain growth during sintering. This is largely due to the tumbling action of the media which leads to point contact only **[10-11]**. The milling media that was used for the milling process can induce impurities in the final product, which can directly affect the properties of electro-ceramics.

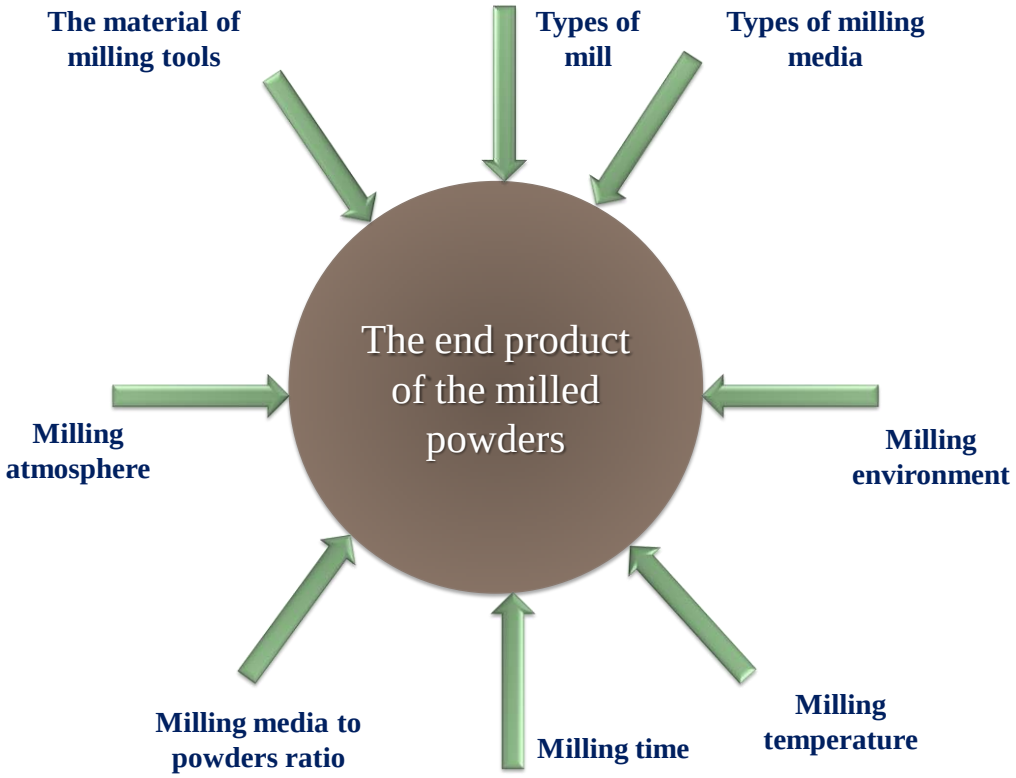

Fig. 2.4 *Schematic representation of the factors that affect the milling process* ***[10-11]****.*

2.3 Different steps of processing of PLZT ceramics

2.3.1 Raw material (Reagents)

Lead lanthanum zirconate titanate $(Pb_{1-x}La_x)(Zr_{0.60}Ti_{0.40})O_3$ ceramics hereinafter referred to as PLZT (x/60/40) were prepared using stoichiometric mixtures of PbO, La_2O_3, TiO_2 and ZrO_2 (all from Sigma-Aldrich, USA, AR grade, purity >99.9%) without any excess PbO. The particle size of raw oxides is in submicron range for the solid phase reactions to occur by atomic diffusion.

2.3.2 Weighing and mixing

The raw materials were weighed according to the stoichiometric formula. The reagents were mixed and milled by using high energy mechanical milling to produce the required chemical homogeneity. The powders were milled for different durations in agate vials (250 ml) or zirconium

vial (500 ml) with yttrium stabilized tetragonal zirconium (YTZ) balls (dia~3mm) by using Fritsch Pulverisette-5 (speed~150 rpm) (fig. 2.5). Distilled water was used as milling medium. The milling was stopped for 5 minutes after every hour to cool down the system. The milled powders were dried by using a heater, stirrer assembly.

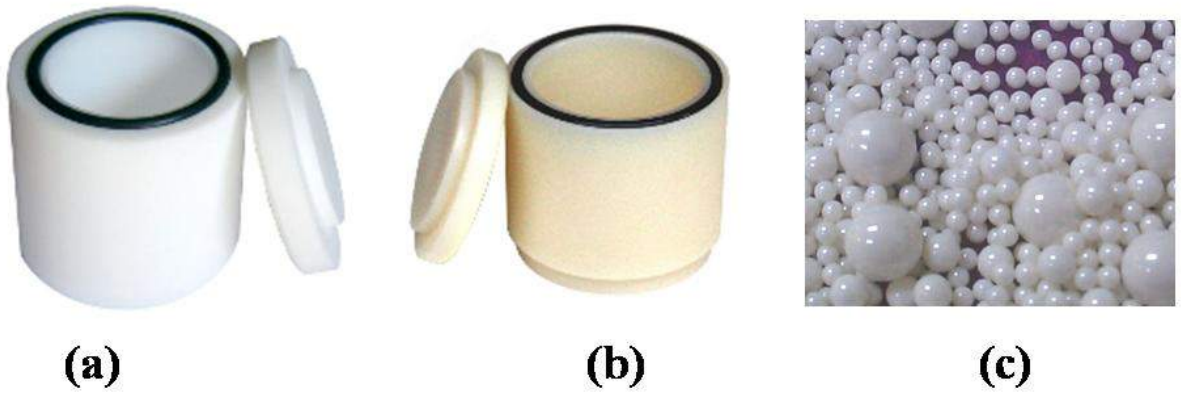

Fig. 2.5 *(a) Agate vial (b) zirconia vial and (c) zirconia balls.*

2.3.3 Calcination

After milling, ceramic bodies were calcined in granulated powder form. During this step, milled powders were calcined in ambient air at 800^{o}C for four hours with a heating rate of 5^{o}C per minute to activate the solid state reaction between the unreacted oxides to obtain the final perovskite phase. However, calcinations of PLZT ceramics at T>800^{o}C could lead to lead loss, resulting in detrimental effects on the electrical properties. Best electrical and mechanical properties can be achieved by using proper calcination conditions **[15]**. After calcination, the hard agglomerates were ground by milling of ceramics powders for a shorter duration. It prepares the reacted material for ceramic forming and helps to homogenize the compositional variations in the ceramic body. The ground powders were sieved by using a 100 mesh sieve.

2.3.4 Cold Isocratic Pressing (CIP)

Before sintering of electro-ceramics, green bodies should possess minimum density, which can be achieved by various techniques such as wet pressing, dry pressing, slip casting, cold isostatic pressing and extrusion. The choice of the method depends on the type of ceramic powder, desired shape, particle size distribution and state of agglomeration. In this study, the PLZT calcined powders were filled in a rubber mold and cold isostatically pressed (Ciped) in the form of a cylindrical rod at a pressure of 3 kbar (300 MPa). Fig. 2.6 (a) shows the schematic representation of the CIP process. Fig. 2.6 (b) and (c) shows the rubber mold setup used for CIP and the obtained green rod, respectively.

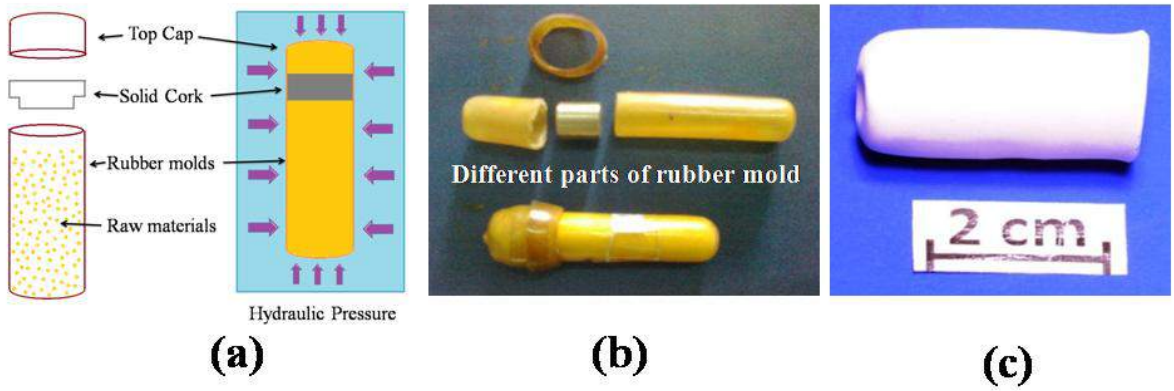

Fig. 2.6 *(a) Schematic representation of the cipping process (b) different parts of rubber molds (c) ciped green PLZT rod.*

2.3.5 Sintering

The sintering process, which involves the heat treatment of ceramic powder compacts at elevated temperatures for the diffusional mass transport, were used to get dense polycrystalline solids. This process is mainly used to reduce the porosity of the ceramics. After sintering improvement was found for the following parameters; elastic modulus, electrical and thermal conductivity, ceramic strength, fracture toughness, hardness, crystal structure, permeability to gasses and liquids, chemical composition, distribution of average grain size and pore size.

After compaction, the green cylindrical rod of PLZT ceramics (Fig. 2.6 (a)) was densified by sintering at 1200^{o}C for four hours at the heating rate of 5^{o}C per minute. In this process, reactions between the unreacted constituent phases (if any) take place. During high temperature sintering, in order to prevent PbO loss, a small crucible containing $PbZrO_3$ with 10% excess PbO was placed in a doubly sealed alumina crucible configuration. After the sintering process, the phase evolution was studied by X-ray diffraction and the microstructure was studied through SEM.

2.3.6 Grinding/Cutting/Polishing

The CIPed and sintered PLZT rods have an irregularity in their cylindrical shape (Fig. 2.6 (c)). The effect of irregular dimensions on the properties of ceramics can be minimized by grinding the sintered rod to a perfect cylindrical shape. Dimensioning and finishing of piezoelectrics are usually done by conventional grinding machinery with diamond as an abrasive medium. Figure 2.7(a) shows the ground cylindrical sintered PLZT rod. The ceramic sample geometries for measurement of the material's electrical properties were in conformity with the IEEE standards **[16]**. Sintered samples were cut into disks of <1 mm thickness using Isomet cutting machine shown in figure 2.7(b) resulting in disk shaped specimens as shown in figure 2.7(c).

Fig. 2.7 *(a) Sintered and ground rod into the shape of a perfect cylinder (b) Isomet cutting machine (c) ceramic pellets cut from PLZT rod.*

2.3.7 Electroding

The PLZT ceramic disks (fig. 2.7 (c)) were polished and both faces were electroded for electrical measurements. The electroding of the ceramic pellets was done using a high temperature conductive silver paste. Two coats of silver paste are required for good electroding. Silver paste is first applied on the surface of PLZT pellets and kept in an oven at 100^{o}C for 10 minutes and after that a second coat, followed by curing at 550^{o}C for 15 minutes (as per application note supplied by the manufacturer). The conductivity of each electrode was checked before any electrical characterization was performed. It was ensured that all contacts are ohmic.

2.4 Characterization techniques

The physical and chemical characteristics of ceramic powders strongly influence their behaviour during processing. The characterization of ceramic powders is very important since the understanding of phase constitution and transformation characteristics are critically dependent on them. The phase analysis, microstructure and morphological studies were done with the help of X-Ray diffraction (XRD), transmission electron microscopy (TEM), scanning electron microscopy (SEM) and density. TEM technique was used to measure the particle size of the milled ceramics. The SEM images can be used for the grain size measurements. The dielectric study was done to understand the nature of phase transitions. Ferroelectric and piezoelectric properties of the PLZT ceramics were also studied.

2.4.1 Structural and Morphological studies (XRD, SEM, TEM)

2.4.1.1 X-ray diffraction (XRD)

X-ray diffraction (XRD) is an important technique, which can be used to identify the crystalline phases present in materials. When an X-ray beam is directed onto a sample, some additional non-parallel beams emerge from the sample at different angles, which provides information about the lattice arrangements, orientations and geometry of atoms in the crystals. The non contact and non destructive nature of XRD makes it ideal for in situ studies. The intensities in XRD pattern provide quantitative information on the atomic arrangements at interfaces. These XRD patterns can be used to measure the structural properties such as phase composition, strain, epitaxy, crystallite size and defect structure. When an X-ray beam interacts with solid materials (powders or densified ceramics), it shows diffraction patterns, recorded by a diffractometer. For quantitative X-ray analysis, sample preparation can enhance the effectiveness by minimizing the effect of preferred orientation, texture, particle size broadening, and other material effects. Quantitative analysis should be carried out by calculating integrated line intensities, instead of using peak heights **[17]**.

When an X-ray beam penetrates the ceramic materials, which depend on upon the atomic number of the elements, it interacts with the electrons associated with the atoms. Some of these electrons are excited to high energy states. However, unexcited electrons oscillate with varying electric field and emit electromagnetic radiations, which have the same wavelength as the incident beam. The angular distribution of the emitted X-rays from the material can be predicted by summing the contributions from all the electrons. The net result is that constructive interference occurs and results in a strongly diffracted beam. The basis of X-ray diffraction is the Bragg's law, which describes the conditions for constructive interference of X-rays. The condition for constructive interference is given by equation-(1) **[**17**]**.

$$2d \sin\theta = n\lambda \quad \text{.....} \quad (1)$$

where d=lattice spacing, n=order of diffraction, λ=wavelength of X-rays, θ=angle between the incident and diffracting plane.

In general, the X-ray diffractometer has a basic X-ray tube, counter goniometer, sample holder and an electronic circuit panel with an automatic recorder. The counter tube is moved along the goniometric circle. The specimen is mounted at the center of the diffractometer and rotated by an angle about an axis of the material plane. The counter is attached to an arm rotating about an axis by an angle 2θ. The X-ray diffraction patterns are recorded in the computer with the help of suitable software. Fig. 2.8 (a) and (b) shows the Philips X'pert PW-3020 X-ray diffractometer experiment setup and X-ray diffraction geometry, respectively. The broadening of X-ray diffraction peaks provides a convenient method for determining particle sizes below ~0.1 μm **[18-19]**. As the crystal

size decreases, the width of the diffraction peak increases. The average particle size "P" is calculated using FWHM from the Scherrer formula.

$$P = \frac{K\lambda}{\beta \cos\theta} \quad \ldots\ldots\ldots\ldots\ldots\ldots\ldots\ldots\ldots\ldots\ldots\ldots\ldots\ldots (2)$$

where K = 0.89 (constant), λ = 1.5406 Å for CuKα radiation, β = Full Width at Half Maxima of maximum intensity peak.

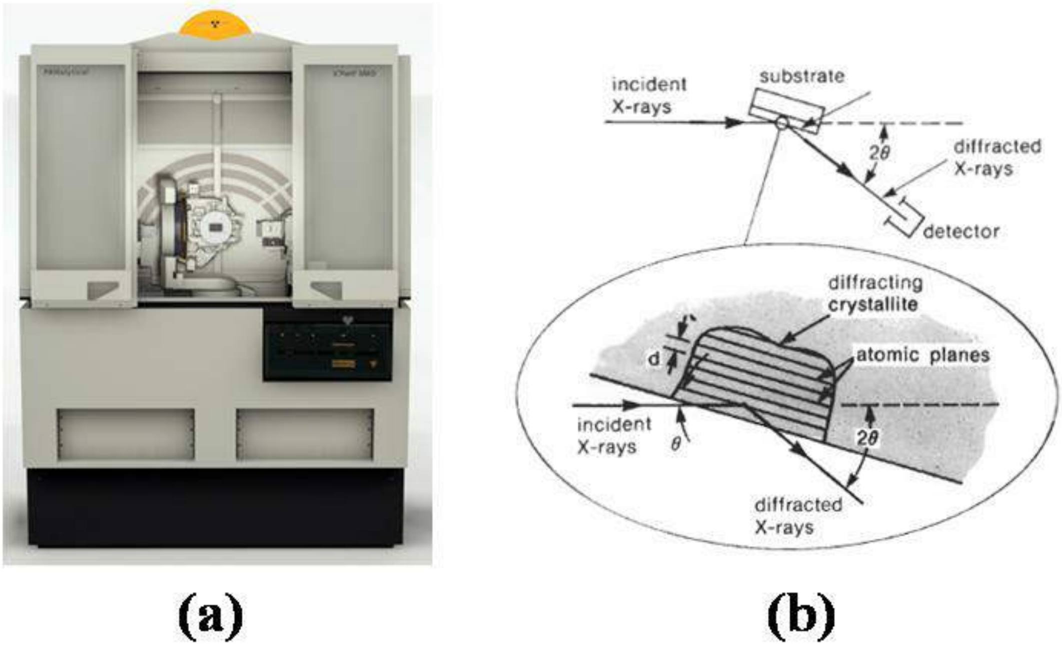

Fig. 2.8 *(a) A Philips X'pert PW-3020 X-ray diffractometer setup (b) X-ray diffraction geometry.*

2.4.1.2 Scanning electron microscopy (SEM)

In scanning electron microscopy (SEM), a high energy beam of electrons scans the material surface in a raster manner. The interaction between the electrons and the atoms of the materials generates the different types of signals such as back-scattered electrons (BSE), secondary electrons, and transmitted electrons, light (cathodoluminescence), characteristic X-rays and specimen current which give the information about the surface topography, electrical conductivity and composition. A beam of electrons which are reflected from the material by elastic scattering is called back scattered electrons (BSE). The relation between the atomic number (Z) of the materials and the intensity of the BSE signal help to provide information about the distribution of different elements. When the electron beam removes an inner shell electron, it causes a higher energy electron to fill the shell and release energy. This condition is responsible for the generation of characteristic X-rays which can be used to

identify the measure the abundance of elements and composition of the sample. The size and shape of the powder particles are determined by using SEM, which provides a highly magnified image of the material surface. The resolution of the SEM can be few nanometers with magnifications from 10-500,000. Not only the topographical information but also information about the composition near surface regions can be produced in the SEM.

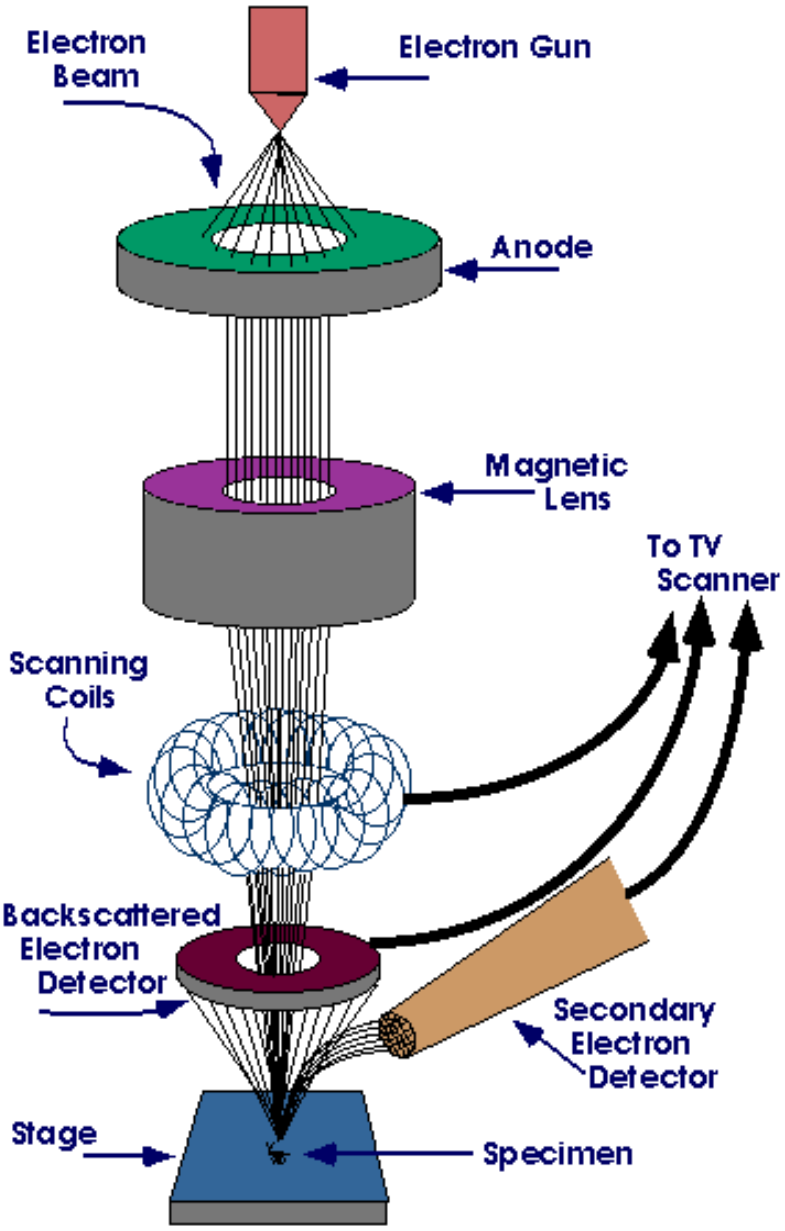

Fig. 2.9 *Schematic of a Scanning Electron Microscopy experimental setup.*

A schematic of a SEM is shown in Fig. 2.9 in which several types of sources can be used at the top of the microscope column for electrons generation. A differential voltage (typically, about 1 to 50 kV) in the electron gun accelerates the electrons down the column, which is in under vacuum. The electron beam is focused by variable strength electromagnetic lenses (X-axis and Y-axis

electromagnetic beam scanning coils) to a fine spot on the material surface. Various signals, generated from the material surface are detected by different types of detectors and the outputs of these detectors are electronically processed. The strong response signals from the material surface appear bright on the CRT, while the weak response signals appear dark. The images viewed on the CRT are recorded electronically **[20]**.

2.4.1.3 Transmission electron microscope (TEM)

TEMs are capable of higher resolution imaging due to the small de Broglie wavelength of electrons which enables examination of the fine details of the specimen. In this technique, a beam of electrons is transmitted through an ultra thin specimen and the interaction results in image formation which is again magnified and focused onto an imaging device such as a layer of photographic film, fluorescent screen or detected by a CCD camera. At lower magnification, the contrast of TEM images mostly depends on the absorption of electrons, composition and the thickness of the material. At higher magnifications, the intensity of the image is modulated by complex wave interactions.

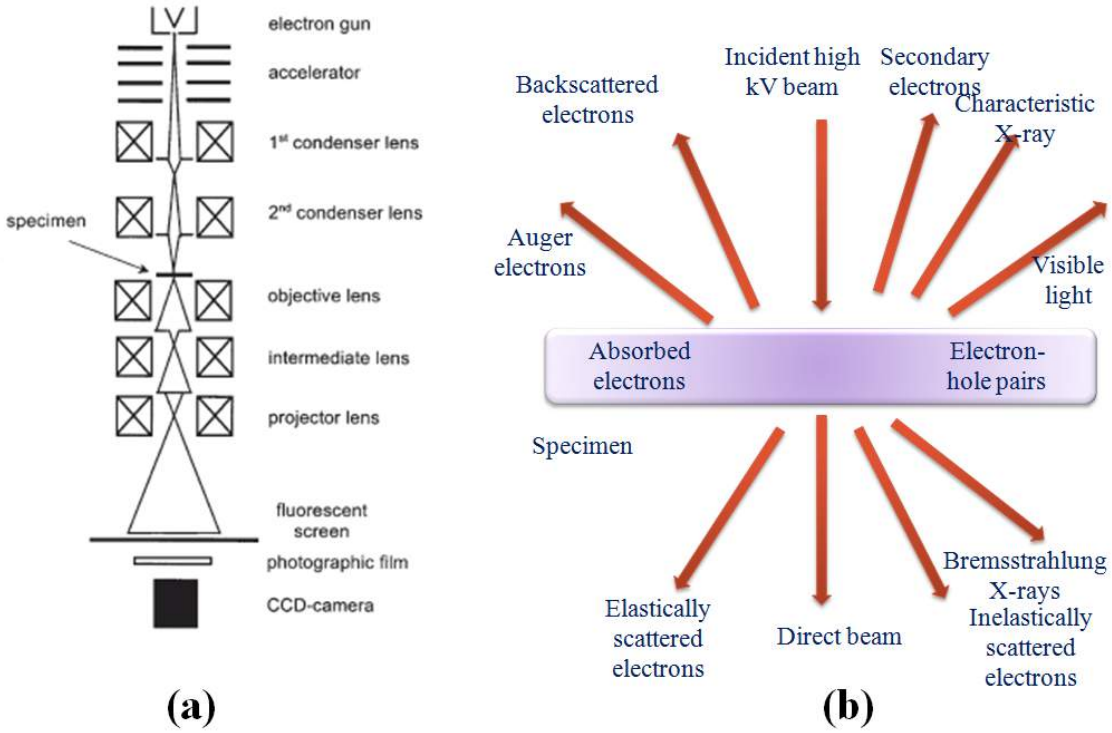

Fig. 2.10 *(a) Schematic of Transmission Electron Microscopy experimental setup (b) types of the signal generated in TEM.*

Fig. 2.10 (a) shows the schematic of a transmission electron microscope (TEM). Since the electrons are smaller than atoms, so it can see well below the atomic level. For TEM measurement specimens have to be very thin or electron transparent. A sufficient number of electrons must pass through the specimen in a reasonable time to give an interpretable image. The thickness of the samples will differ for TEM (100 nm) to HRTEM (50 nm). The requirement of thin specimens is a major limitation of the TEM. Fig. 2.10 (b) shows the materials response to the incident high energy electron beam. Many types of signals are generated when an electron beam passes through the ceramic samples. In order to get the best signal from the specimen, selection of electron source is very critical **[21]**. In this study, TEM was used to evaluate the size of PLZT powders. The powder samples for TEM observation were prepared by dispersing them in methanol and placing a few drops on a carbon-coated TEM grid. An FEI Tecnai 20G2 TEM was used for observation of the powders.

2.4.1.4 Density

High density with uniform microstructure is one of the most desirable features for PLZT based electro ceramics to obtain optimal electrical and mechanical properties. The density of the sintered PLZT ceramics is measured by using Archimedes principle using eq-(3). The theoretical density of PLZT ceramics is obtained from standard JCPDS file.

$$\boldsymbol{\rho_{exp}} = \frac{\boldsymbol{W_{dry}}}{\boldsymbol{W_{dry}} - \boldsymbol{W_{wet}}}\ \boldsymbol{\rho_l} \quad \ldots\ldots\ldots\ldots\ldots\ldots\ldots\ldots\ldots\ldots\ldots\ldots \text{(3)}$$

Where W_{dry} and W_{wet} are the weights of the PLZT ceramics in the air and, in the water, respectively, ρ_l is the density of water.

2.4.2 Dielectric studies

The Agilent E4980A Precision LCR meter, which is shown in fig. 2.11 (a), is used for evaluating the dielectric properties of the ceramic materials within a frequency range from 20 Hz to 2 MHz. Out of many modes of an LCR meter, the best mode is selected by considering the relative impedance magnitude of the reactance, series resistance (R_s) and parallel resistance (R_p). For the measurement of dielectric properties of PLZT ceramics, the desired mode was selected by setting the FUNC (C_p) on the MEAS SETUP page (display of the LCR meter, fig. 2.11 (b)). Generally, in the case of small capacitance (fig. 2.12 (a)), it yields large reactance, the effect of R_p has relatively more significance than R_s. The low value of R_s has negligible significance compared capacitive reactance. The parallel circuit mode (C_p-D) should be used only in case of a large capacitance.

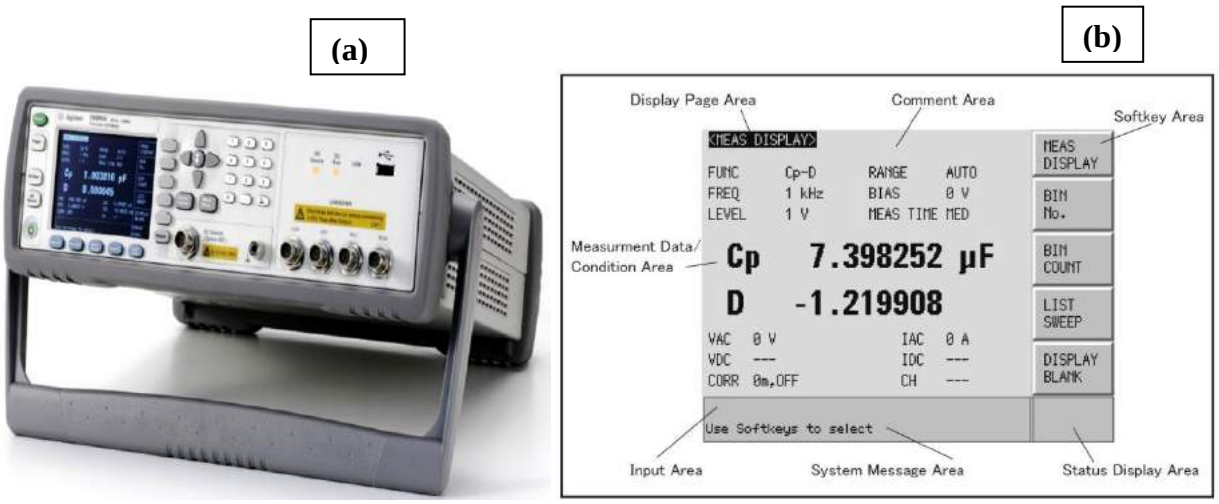

Fig. 2.11 *(a) Agilent E-4980A Precision LCR Meter (b) display format.*

Fig. 2.12 (b) represents the Parallel/Series circuit mode for capacitance measurement along with the measurement functions. Where C_s = Capacitance value measured using the series equivalent circuit model, C_p = Capacitance value measured using the parallel equivalent circuit model, Q = Quality factor, D = Dissipation factor, G = conductance, R_p = Equivalent series resistance measured using the parallel equivalent circuit model and R_s = Equivalent series resistance measured using the series equivalent circuit model. The LCR meter measures the capacitance-dissipation factor with an accuracy of ±0.05% in capacitance and ±0.0005 in a loss at all frequencies as mentioned in the LCR manual **[22]**.

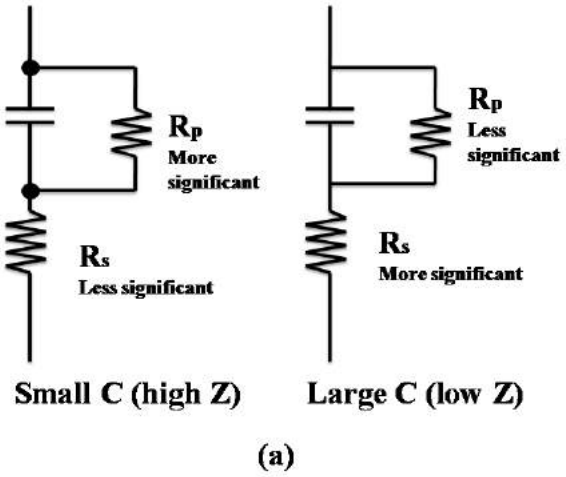

Circuit Mode	Measurement functions	Definition of D, Q and G
Cp mode 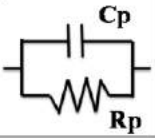	Cp-D Cp-Q Cp-G Cp-Rp	$D = 1/(2\pi fCpRp)$ $= 1/Q$ $G = 1/Rp$
Cs mode 	Cs-D Cs-Q Cs-Rs	$D = 2\pi fCsRs$ $= 1/Q$

(b)

Fig. 2.12 *(a) Capacitance circuit mode selection (b) Parallel/Series Circuit mode for capacitance measurement.*

The measured values of capacitance and admittance were used for the determination of the resonant and anti-resonant frequencies of the PLZT ceramics. The ceramics samples are loaded into the DUT (Device Under Test) for measuring the resonance. The DUT is then connected to the Agilent E4980A Precision LCR Meter. The capacitance-dissipation factor (C-D) values of the ceramic samples with respect to the frequency have been taken.

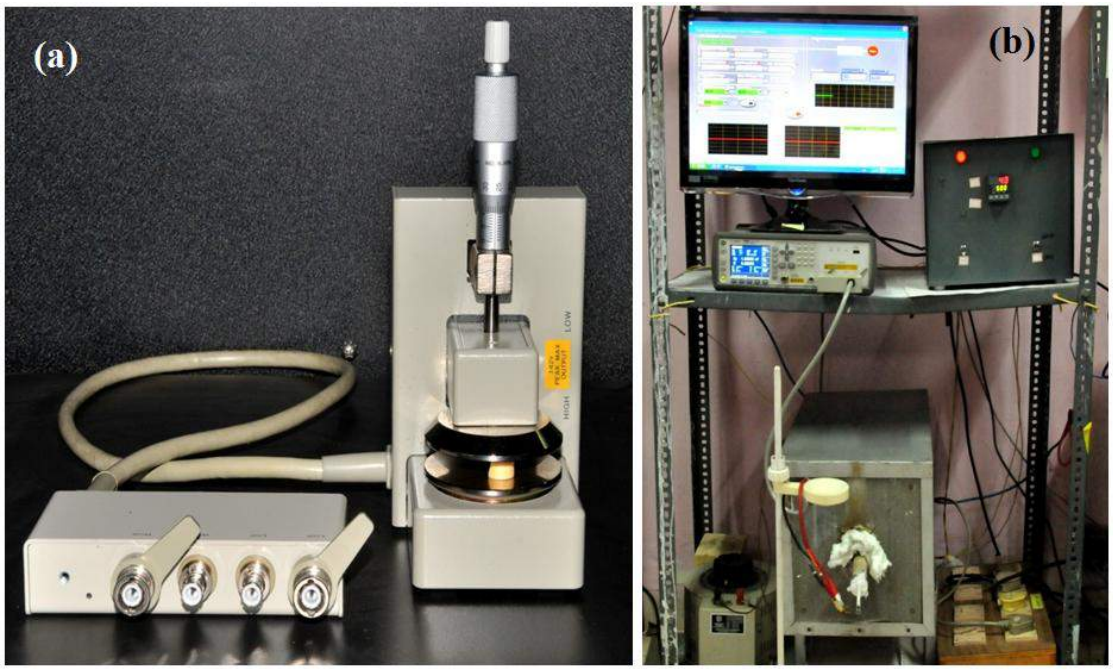

Fig. 2.13 *(a) Agilent sample holder for room temperature dielectric studies and (b) lab made temperature dependent dielectric studies setup.*

Fig 2.13 (a) shows the Agilent sample holder suitable for the room temperature dielectric studies. Ceramic samples were placed in between the two plates of the sample holder to measure the different parameters in the frequency range of 20 Hz to 2 MHz. Admittance vs. frequency data for the poled PLZT ceramics was used to calculate the coupling factors. Fig 2.13 (b) shows the lab made a setup for the temperature dependent dielectric studies. PLZT ceramics were placed in the high temperature sample holder which was inserted into the furnace and connected with an LCR meter. The temperature is controlled here by the PID controller. LCR meter and PID controller both are connected to the computer system and interfaced with a Labview program. The dielectric study for the ceramics is limited to the furnace temperature (maximum 650^{o}C) and four frequency points (from frequency range 20 Hz to 2 MHz).

2.4.3 Piezoelectric studies

In the ferroelectric ceramics, domains are randomly re-oriented and hence do not show any bulk piezoelectric property (fig. 2.14 (a)). The piezoelectric property in the ferroelectric ceramic can be induced by a 'poling process', in which a dc electric field with strength higher than the coercive field is applied to the ferroelectrics at a higher temperature. This process orients the spontaneous polarization within each grain of ceramics towards the direction of the applied field (fig 2.14 (b)), which leads to nonzero polarization. Due to symmetry restrictions, all the domains in a ceramic can

never get fully aligned along the poling axis. PLZT ceramics were poled using sample holders and poling set-up as shown in fig. 2.15 (a), (b) and (c) respectively. The DOW CORNING 704 silicone oil was used for the poling.

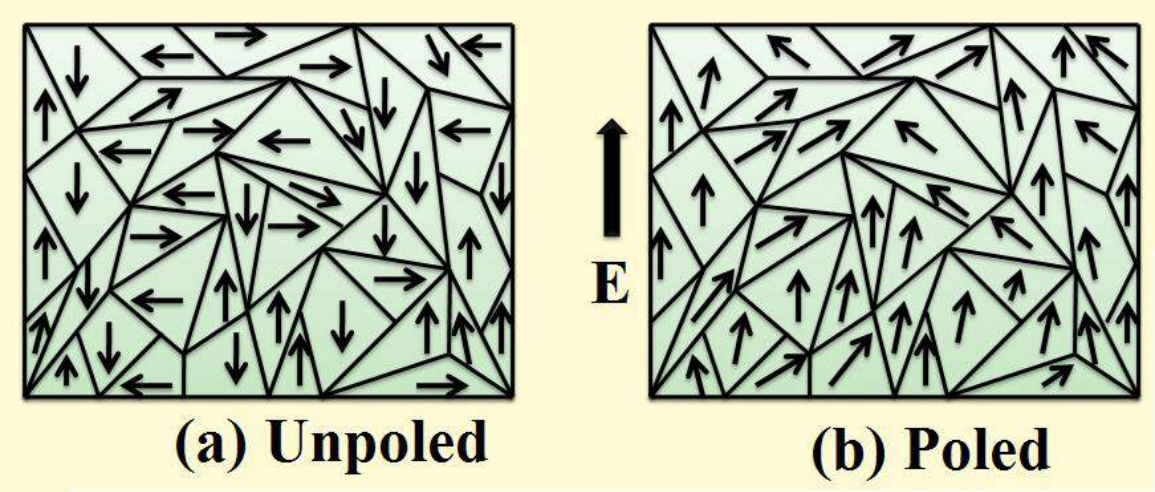

Fig. 2.14 *Alignment of domains in PLZT ceramics (a) in the absence of an electric field (b) in the presence of an electric field.*

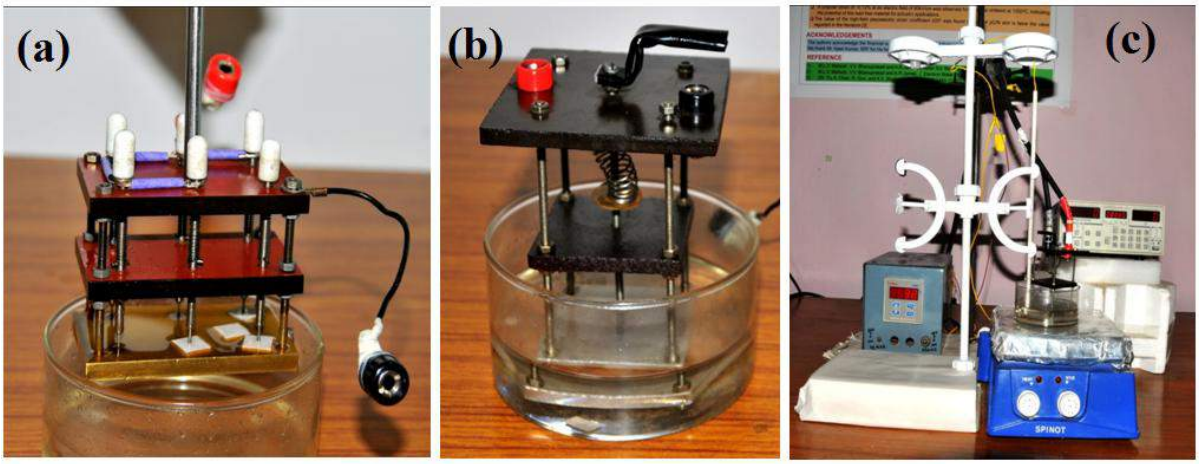

Fig. 2.15 *(a) and (b) Sample holder suitable for the poling of six samples and one sample, respectively (c) poling set-up used for poling.*

2.4.3.1 Piezoelectric coefficients (d_{33} and g_{33})

Fig. 2.16 (a) shows the SENSOR SS01 Piezo-d Meter, which was used for the piezoelectric charge coefficient measurements of poled PLZT ceramics. This meter operates on a slight variation of the basic Berlincourt principle (Fig. 2.16 (b)) which includes the use of V2.0vi software and a dynamic force of about 2N in the frequency range of 190 Hz. An internal force sensor senses the force

and is measured with appropriate signal conditioning. The voltage generated across the sample is captured and measured by a data acquisition card, and the d_{33} is calculated as

$$d_{33} = \frac{CV}{F} \quad \text{..... (4)}$$

where F is the applied force and V is the generated voltage. The capacitance connected in parallel with the test specimen is significantly higher than the capacitance of the sample element in order to provide the correct boundary condition for the measurement of d_{33} (at the constant electric field).

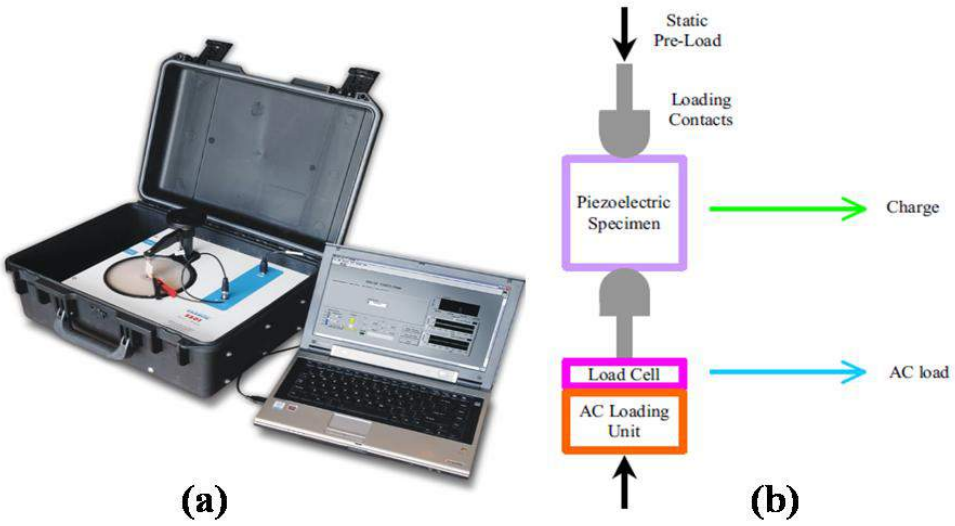

Fig. 2.16 *(a) SENSOR SS01 Piezo-d Meter (b) schematic diagram showing the components of a Berlincourt system.*

The piezoelectric voltage constant (g_{33}) can be calculated by using following equation

$$g_{33} = \frac{d_{33}}{\varepsilon_{33}} \quad \text{..... (5)}$$

where d_{33} is the piezoelectric charge coefficient and ε_{33} is the permittivity of the material.

2.4.3.2 Electromechanical coupling coefficients (k_p, k_{33} and k_{31})

Electromechanical coupling coefficients can be calculated by using the resonant and anti-resonant frequencies values from the admittance vs. frequency graph. The high electromechanical coupling factor shows the high effectiveness of ferroelectric in which a piezoelectric material converts mechanical energy into electrical energy or electrical energy into mechanical energy **[23-24]**. The planar coupling factor (k_p) was calculated by using the equation

$$\mathbf{k_p} = \sqrt{\frac{2.51(fa-fr)}{fr}} \quad \text{.....(6)}$$

Where f_r the resonant frequency and f_a anti-resonant frequency.

The longitudinal coupling factor (k_{33}) was calculated by using the equation

$$k_{33}^2 = \frac{\pi}{2}\frac{f_a}{f_r}\tan\left(\frac{\pi}{2}\frac{f_a-f_r}{f_a}\right) \text{ ..... (7)}$$

The coupling factor (k_{31}) was calculated by using the equation

$$k_{31}^2 = \frac{k_{33}^2}{1+k_{33}^2} \text{ ..... (8)}$$

where f_r the resonant frequency and f_a anti-resonant frequency.

2.4.3.3 Elastic compliances

Elastic compliances of the ferroelectrics are the ratio of a material's change in dimensions (strain) to an externally applied load (stress). These parameters show the inverse relation with the Young's modulus. For a given piezoelectric material, the parallel or perpendicular strain to the poling axis decides the elastic compliance along with electrical boundary conditions [**25-26**]. Here s^E is the compliance under a constant electric field (short circuit) and s^D is the compliance under a constant electric displacement (open circuit). The first subscript indicates the direction of strain; the second is the direction of stress. Elastic constants were calculated from the following equations:

$$s_{33}^D = \frac{1}{4\rho l^2 f_a^2} \ \mathbf{m^2/N} \text{ .....(9)}$$

$$s_{11}^E = \frac{1}{4\rho l^2 f_r^2} \ \mathbf{m^2/N} \text{ .....(10)}$$

$$s_{33}^E = \frac{S_{33}^D}{1-k_{33}^2} \ \mathbf{m^2/N} \text{ .....(11)}$$

$$s_{11}^D = \left(1-k_{31}^2\right) s_{11}^E \ \mathbf{m^2/N} \text{ .....(12)}$$

$$c_{33}^D = 4\rho l^2 \ f_a^2 \ \mathbf{N/m^2} \text{ ..... (13)}$$

$$c_{33}^E = \left(1-k_{33}^2\right) c_{33}^D \ \mathbf{N/m^2} \text{ ..... (14)}$$

where ρ = density of the material in kg/m^3, l = width of the ceramic, f_r = resonant frequency and f_a = anti-resonant frequency.

2.4.4 Ferroelectric studies

The polarization (P-E) and strain vs. electric field (S-E) measurement results were traced by using an advanced ferroelectric evaluation system of M/s aixACCT Systems, GmbH, Germany as shown in fig. 2.17. As per the recommendation of Yan et. al. **[27]**, triangular voltage waveform at a frequency of 1 Hz is used for the both measurements. Inset of the fig. 2.17 shows the Piezo Sample Holder Unit (PSHU) that allows testing of bulk ceramic samples of a wide variety of sample geometries from room temperature to 200^{o}C. A microcontroller Eurotherm 2416 is used as a temperature controller to heat up the PSHU. Ceramic samples with appropriate dimensions were placed in PSHU that is attached with an external high voltage Trek 610 HV 10 kV amplifier. The FE-module and TF 2000HS analyzer were used with hysteresis software version of v2.4.0.0.

Fig. 2.17 *Polarization and strain versus electric field measurement with aixACCT system with Piezo sample holder unit (PSHU)* ***[28]****.*

TF Analyzer 2000 consists of a basic unit and measurement modules, placed very close to the device under test, to increase the signal to noise ratio. FE-module probe head is designed for a variety of measurements such as dielectric (C-V) and ferroelectric hysteresis loops (S-E). The FE module consists of three amplifiers with an optimum signal to noise ratio. The measurement frequency is then limited by the drive limits of the amplifier. The current amplifier is used to select the current range with which the TF2000 measures. The current range should be close to the current response of the

ceramics during the measurement to fulfill the best measurement results. The current response depends on input parameters like frequency, amplitude, the measured sample material and geometry. A range between 10 pA and 1 A can be selected for a standard FE-Probe Head. Fig 2.18 shows a schematic diagram for the aixACCT ferroelectric hysteresis loop measurements system.

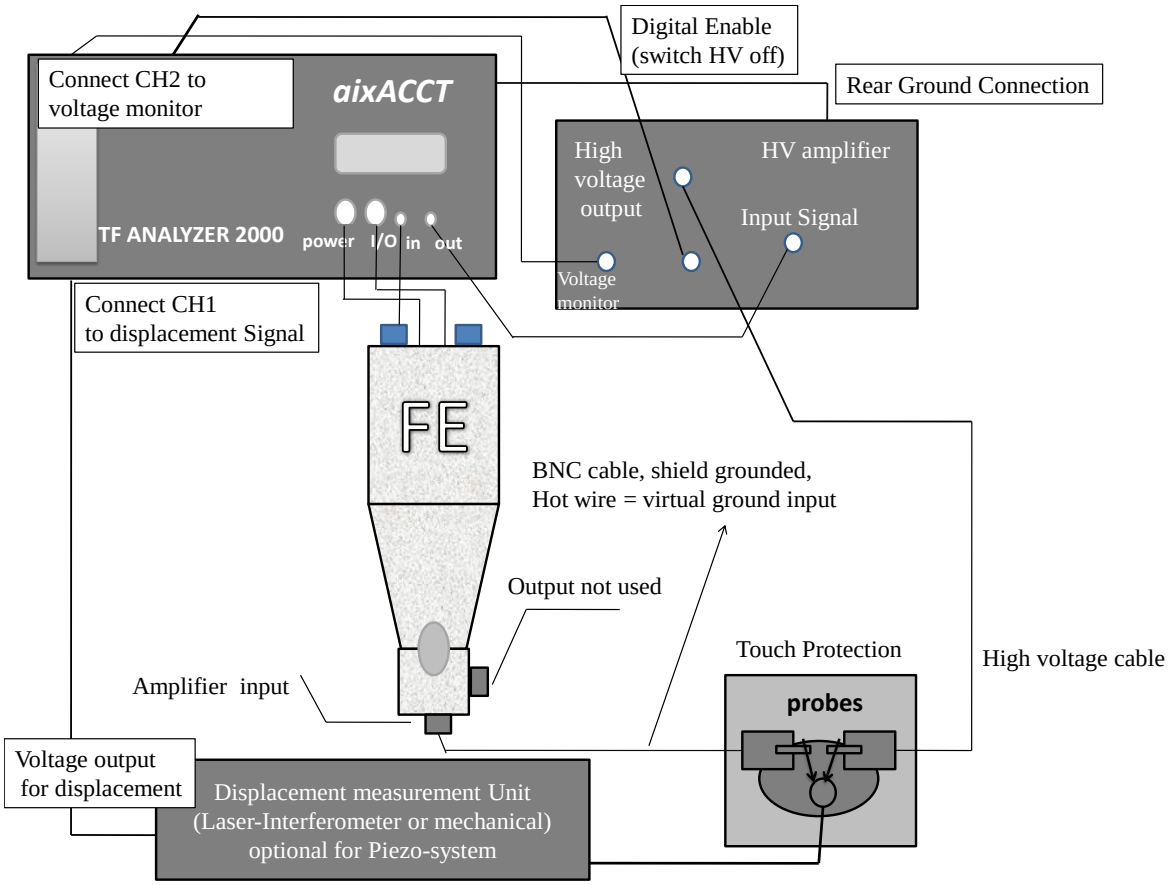

Fig. 2.18 *Schematic diagram for the aixACCT ferroelectric hysteresis loop tracer set up consisting of TF analyser, FE module, a high voltage amplifier and sample holder* ***[26]****.*

2.4.4.1 Polarization vs. electric field hysteresis loops (P-E)

The value of polarization at zero fields is called as remnant polarization (P_r) and the value of the necessary electric field which is required to bring the remnant polarization to zero is called as a coercive field (E_c). The aixACCT system uses a virtual ground feedback method (highest precise technique) to collect the data, which is realized by a current to voltage converter. This method reduces the influence of parasitic capacitance and back voltage known from the Sawyer-Tower measurement drastically and enables direct hysteresis measurements. For the measurements of P-E hysteresis loops current or charge response was recorded due to an applied electrical excitation voltage. The current, charge, frequency, applied voltage, and signal to noise ratio parameters needs to be estimated for

accurate measurements. The total polarization charge depends upon the material, geometry of the capacitor and the applied voltage. The magnitude of the current 'I' is given by the charge 'Q' and the change in voltage per time (slew rate). If 'P' is the polarization of the material, 'V' is the applied voltage and 'A' is the area of the ferroelectric capacitor then dV/dt describes the slew rate of the signal. The magnitude of the current flow during the polarization reversal process in ferroelectrics is given by the eq-(15) **[28]**. The switching process close to the coercive voltage V_c changes the (dP/dV) (in very short time) and increases the peak switching current.

$$\mathbf{Q = D.A \sim P.A}$$

$$\boldsymbol{I = \frac{dQ}{dt} = A.\frac{dP}{dV}\frac{dV}{dt}} \quad \text{..... (15)}$$

There exist three established methods to record the charge and current response of the sample for the measurements of P-E hysteresis loops. First, is Sawyer-Tower method (charge based), in which a reference capacitor is add in a series with the ferroelectric capacitor. The voltage drop at the reference capacitor is proportional to the polarization charge as defined by eq-(16) **[28]**

$$\mathbf{V = Q/C} \quad \text{..... (16)}$$

Among several drawbacks of this method include reference capacitor has to be adjusted for different ceramics, difficult to get precise reference capacitors and the addition of cable capacitance.

The second method is a Shunt method (current based) in which reference resistance (shunt resistor) is used. In this method, the switching current is measured as a voltage drop at the shunt resistor (V = R x I). The integration of this current gives the polarization charge **[38]**

$$\mathbf{Q = \int I\, dt} \quad \text{..... (17)}$$

The limitation of this method includes the dependency of resistance value on the sample capacitance and excitation frequency. The time constant of ferroelectric capacitor and shunt resistor influences the output at higher speed. The cable capacitance and the input capacitance of voltage measuring device are parallel to the reference resistor.

The third is a virtual ground method, which is based on current measurement using an operational amplifier with the feedback resistor. This method uses a current to voltage converter, whose output is connected to the inverting input of the operational amplifier via feedback resistance. The non inverting input is connected to ground. Both the inputs show the voltage difference in the range of microvolts which means the inverting input is virtually grounded with no back voltage. This method is suitable for the small capacitors measurement (cable capacitance is electrically ineffective) since both electrodes of the capacitor are kept at same potential **[28]**.

For an ideal ferroelectric parallel plate capacitor having lateral area 'A', the switched charge 'Q' is given by **[29]**

$$\mathbf{Q = 2\ P_r\ A} \quad \text{..... (18)}$$

However, for the real ferroelectric capacitor, conductivity always coexists with the capacitive ferroelectric samples (σ = electrical conductivity, E = applied field, and t = measuring time)

$$\mathbf{Q = 2P_r\ A + \sigma\ EAt} \quad \text{..... (19)}$$

For a non-ferroelectric linear dielectric Q is not zero but given by eq-(20). Since the dielectric loss is proportional to conductivity σ, equation (3) is said to describe a linear lossy dielectric.

$$\mathbf{Q = \sigma\ EAt} \quad \text{..... (20)}$$

2.4.4.2 Electric field induced strain hysteresis loops (S-E)

The application of an electric field to the ferroelectrics not only produces a polarization but also develops a large strain, which is linked to the converse piezoelectric effect of the lattice and switching and movements of domain walls. The electromechanical response can be measured either by applying an electrical excitation signal and measuring the samples mechanical displacement (S-E) or by applying a mechanical strain and recording the resulting charge displacement. The first method is commonly used as it allows the simultaneous electrical and electromechanical characterization. In the piezo measurement (PZM) electric field induced displacement or stain in ceramics sample was captured by an additional external displacement sensor which is a laser interferometer. This combination allows a comfortable and comprehensive investigation of the piezoelectric or electrostrictive displacement. The influence of process parameters can be examined on the shape of the resulting butterfly curve. The measurement parameters such as excitation signal frequency and its amplitude can be varied.

The aixACCT ferroelectric was used for the S-E measurement which consists of an SIOS laser interferometer of class 2M. The direction of applied electric field and the measurement direction (of displacement) are the same. Fig. 2.19 shows the set up for the measurement of electric field induced strain. The S-E measurement set up consists of a sample holder, LASER beam, mirror and the adjustment screws. With the help of the adjustment screws at the mirror, it is possible to move the LASER beam to each position on the top electrode. Consequently the reflected beam shifts as well. Therefore it is easy to adjust the reflected spot at the center of the aperture. Wave length of LASER light is 632 nm and the resolution of the system is 1 nm.

Fig. 2.19 *The aixACCT ferroelectric S-E hysteresis loop setup with sample holder, LASER source, mirror and adjustment screws* ***[26]***.

In this present study unipolar S-E hysteresis curves were used to calculate the piezoelectric charge coefficient (d_{33}) of the piezoelectric materials. The slope of the S-E curves in lower field region shows the d_{33} of the piezo-ceramics. Strain hysteresis in S-E curves can be calculated by using the equation

$$\textbf{Strain hysteresis}\ (\%) = \frac{\Delta x}{x_{max}} \times 100 \quad \ldots\ldots\ldots\ldots\ldots\ldots\ldots\ldots\ (21)$$

where x_{max} is the maximum strain of ceramics at the maximum applied field and Δx is the difference between the strain at ½ E_{max} field in both directions.

References

[1] G.H. Haertling, J. Am. Ceram. Soc., **82** (1999) 797.

[2] M. Deluca, C.A. Vasilescu, A.C. Ianculescu, and D.C. Berger, J. Eur. Ceram. Soc., **32** (2012) 3551.

[3] W.J. Dawson, Am. Ceram. Soc. Bull., **67 [10]** (1988) 1673.

[4] B.W. Lee and S.B. Chob, J. Eur. Ceram. Soc., **25** (2005) 2009.

[5] X.G. Tang, J. Wang, X.X. Wang, and H.L.W. Chan, Solid State Commun., **131** (2004) 163.

[6] S. Roy, A.R. James, S. Bysakh and J. Subrahmanyam, Metals Mater. Process, **19** (2007) 143.

[7] G.H. Haertling and C.E. Land, Ferroelectrics, **3** (1972) 269.

[8] K.S. Mazdiyasni, Am. Ceram. Soc. Bull., **63 [4]** (1984) 591.

[9] S.B. Reddy, K.P. Rao and M.S.R Rao, Scri. Mater., **57** (2007) 591.

[10] M. Sherif, E. Eskandarany, Mechanical alloying for Fabrication of advanced engineering materials, Noyes Publications, William Andrew Publishing, New York, U.S.A. (2001).

[11] C. Suryanarayana, Progress Mater. Sci., **46** (2001) 1.

[12] A.K. Nath, K.C. Singh, Physica B, **405** (2010) 430.

[13] A.R. James and O.P. Thakur, Dielectric and Ferroelectric Reviews, Editors: S.S.N. Bharadwaja and R.A. Dorey, Research Signpost, Trivandrum, India, Ch-2 (2012) 33.

[14] P.S. Gilman and J.S. Benjamin, Ann. Rev. Mater. Sci., **13** (1983) 279.

[15] A. Bergmann, G. Fritz and O. Glatte, J.Appl. Cryst., **33** (2000) 1212.

[16] IEEE 1988 An American national standard, IEEE standard of piezoelectricity (New York: ANSI/IEEE) Std 176 (1987).

[17] M.F.C. Ladd and R.A. Palmar, Structure Determination by X-ray Crystallography, New York: Plenum Press (1985).

[18] B.D. Cullity, Elements of X-Ray diffraction, 2nd ed., Addison-Wesley Reading, MA (1978).

[19] H.P. Klug and L.F. Alexander, X-Ray Diffraction procedures for polycrystalline and amorphous materials, John Wiley & Sons, New York (1974).

[20] C.R. Brundle, C.A. Evans, S. Wilson, Encyclopedia of materials, materials characterization series, Manning Publications Co. (1992).

[21] D.B. Williams and C.B. Carter, Transmission electron microscopy: A text book for material science, Plenum Publishing corporation, New York.

[22] Agilent E4980, A Precision Impedance Analyzer Data Sheet, Agilent Technologies.

[23] B. Jaffe, Piezoelectric Ceramics, J. Am. Ceram. Soc. **41 [11]** (1958) 494.

[24] B. Jaffe, W.R. Jr. and H. Jaffe; Piezoelectric Ceramics, Academic Press New York (1971).

[25] W.A. Smith, proc. 6th Int. Symp. Ampl. Ferroelectrics, (1986) 249.

[26] L. Swartz, IEEE Trans. Electrical Insulation, **25** (1990) 935.

[27] H. Yan, F. Inam, G. Viola, H. Ning, Q. Jiang, T. Zeng, Z. Gao and M. J. Reece, J. Adv. Diel., **1** (2008) 107.

[28] Hysteresis software version 2.4.0.0 user manual, aixACCT GmbH, Germany.

[29] J F Scott, J. Phys.: Condens. Matter. **20** (2008) 021001.

Chapter-III

Phase analysis, Micro-Structural and morphological studies of PLZT ceramics

3.1 Introduction

It is well known that the electrical properties (dielectric, ferroelectric and piezoelectric) of all electro-ceramics are greatly affected by the microstructure. A small variation in the microstructure of electro-ceramics can change the above properties. The improvement or worsening of the electrical properties depends upon the type of changes in micro-structure and morphology of ceramics. It is always suggested that a careful examination of the microstructure and morphology of ceramics should precede the electrical property studies. Ceramics should fulfill certain minimum structural requirements such as pure phase, grain size and density to make them electrically viable.

In this chapter, PLZT ceramics were investigated for their micro-structural and morphological properties based on their density, phase formation and microstructure. As discussed in Chapter-1 (Introduction) different amounts of lanthanum were substituted in the A-site of the PZT parent system. Different compositions of lanthanum modified $(Pb_{1-x}La_x)(Zr_{0.60}Ti_{0.40})O_3$ (here in after referred to as PLZT x/60/40) were studied carefully and the optimum PLZT system was found. To understand the effect of La substitution in the PZT system, it was necessary to synthesize the basic (un-modified) PZT system. Properties of all La modified PZT compositions were compared with the base composition of $Pb(Zr_{0.60}Ti_{0.40})O_3$ (PZT 60/40) system. The optimum PLZT composition was milled by changing the milling parameters such as milling media and milling time. For the milling time studies, it was also necessary to synthesize and study the basic system, not subjected to high energy mechano-chemical processing (HE-MCP) by mixing the powders using a mortar & pestle.

XRD patterns were used to confirm the perovskite phase formation of the ceramics. Measured XRD patterns were compared with the standard JCPDS file to assign the h,k,l values to each and every peak. To study the effect of lanthanum substitution, milling vial and milling time, these XRD patterns are very helpful. XRD pattern of the PLZT ceramics sintered at 1200^oC show a single phase formation. SEM images of the milled powder show the agglomeration of particles due to their fine scale sizes. SEM images of sintered ceramics show dense and uniform grains for most of the ceramics. Higher density and more uniform grain distributions were found for the optimum PLZT system. Details of these studies are presented in this chapter.

3.2 Literature survey

From the time of the discovery of piezoelectric materials, they have been widely studied for their usefulness in various applications. Piezoelectric materials can be classified broadly as lead based materials and lead free materials. Out of several lead based systems, PLZT ceramics is prepared by substitution of La^{3+} ions, in place of Pb^{2+} ions at the A-sites of the perovskite PZT, which attracts a

lot of attention due to their high reliable and repeatable dielectric, ferroelectric, piezoelectric, electro-optic and pyroelectric characteristics suitable for various sensor, actuator and transducer applications **[1-3]**.

All the said properties mentioned above arise due to the donor effect. While replacing divalent Pb^{2+} ions, trivalent La^{3+} ions generate vacancies at the A-site of the perovskite PZT to neutralize the system. La^{3+} substitution to the basic PZT system softens the domain walls and also modifies the morphotropic phase boundary (MPB). The highest dielectric and piezoelectric properties of the piezoelectric ceramics are observed close to the MPB **[1]**. The influence of lanthanum doping on the MPB of PZT was studied by Hinterstein et. al. **[4]**. Depending upon the specific applications of piezoelectric ceramics, various compositions differing in Pb/La ratios may be chosen. Here the formula for PLZT x/60/40 is given by $(Pb_{1-x}La_x)(Zr_{0.60}Ti_{0.40})O_3$. To get the best properties, the La substitution in the PZT solid solution should be optimized in such a way that optimum PLZT ceramics composition is near the MPB **[5-12]**.

The choice of a specific PLZT composition depends on their uses in final applications. There are a variety of PLZT compositions available and studied in detail. Some compositions are good for the one specific application and some are suitable for another. PLZT 9/65/35 ceramics shows high transparency and hence are suitable for electro-optic applications. PLZT ceramics close to the MPB show high electrical (ferroelectric and piezoelectric) properties. Some of them show ultra-high strain and high piezoelectric charge coefficient (d_{33}). In this study, different PLZT compositions were studied, and the processing parameters were optimized in such a way that they show optimum electrical properties. These ultra-high strain ceramics can be used for sensors and actuators.

Most of the applications require highly dense ferroelectric ceramics and >95% densification ensures the achieving of maximum performance **[5, 13-14]**. The high density of the PLZT ceramics was achieved by Haertling et. al. **[1, 5]** involving time consuming and expensive hot pressing process in which calcined PLZT powders were first cold pressed and again hot pressed at high temperature and for longer sintering durations (1250^oC for 16 hours). Such sintering conditions result in the abnormal grain or secondary grain growth, which are detrimental to the PLZT performance. Higher sintering temperatures are not only lead to lead loss, which compensates by excess PbO but also affects the electrical properties. Excess PbO addition is detrimental to the environment and performance of the PZT system. The lead based ferroelectrics containing very fine scale powders with a narrow size distribution can be sintered at relatively low temperature, resolves the issue of lead volatility. For this purpose, nano-sized ferroelectric powders of PLZT ceramics have been synthesized by high energy mechanically ball milled PLZT. In this technique oxide precursors of the designed compounds are activated by mechanical energy compare to conventional solid-state reaction process, which requires heat energy **[13-14]**.

The substitution of lanthanum in the PZT system and the milling conditions affect the density, phase formation and microstructure of the ceramic material. Based on the above study, PLZT

compositions and milling conditions can be optimized. For the optimization of milling time and to obtain the best properties it is necessary to mill the powder for an optimum duration of time. Shorter milling times cannot trigger the required chemical reaction and on the other hand, excess milling may cause contamination of the electro-ceramic powders.

3.3 Preparation of PLZT 8/60/40 ceramics without milling (Mortar-pestle mixing)

Since the properties of the PLZT electro-ceramics are greatly affected by the milling parameters specially milling time, to know the specific effects of milling on these powders, it is prudent to synthesize and characterize PLZT ceramics that were not subjected to HE-MCP as well. So the raw oxide powders of PLZT ceramics were mixed using a mortar and pestle. The remaining processes for mortar-pestle mixed ceramics were the same as was used for high energy ball milled ceramics.

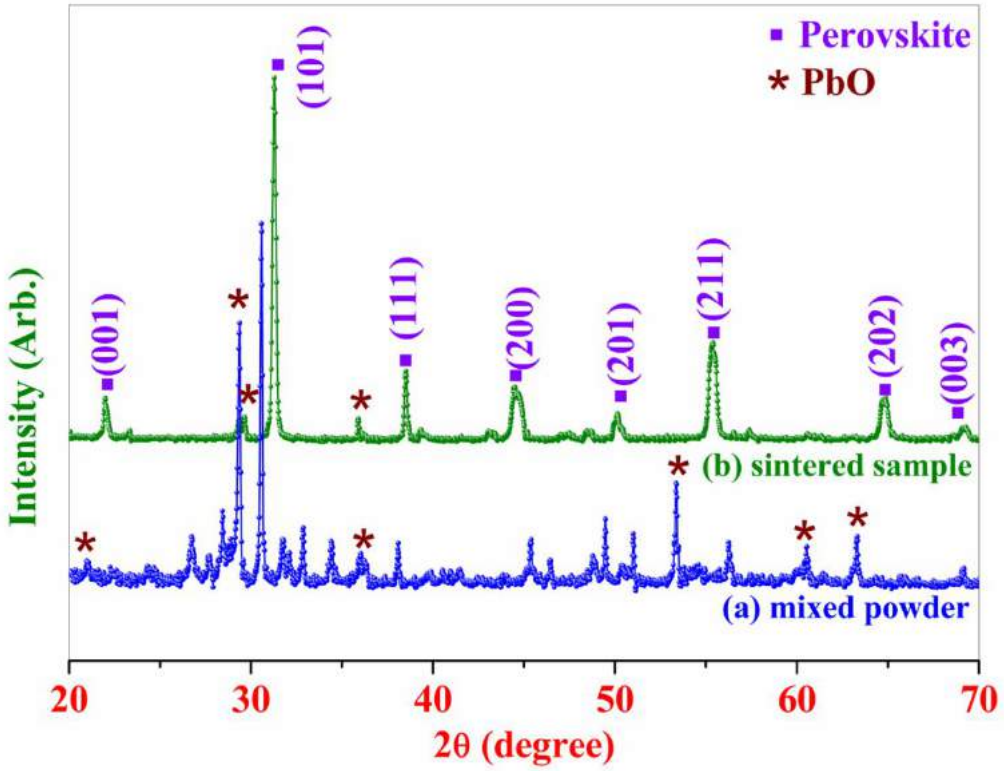

Fig. 3.1 *X-Ray diffraction patterns for the PLZT 8/60/40 (a) mortar pestle mixed powders and (b) sintered ceramics.*

The mortar pestle mixed powders of PLZT 8/60/40 were characterized using X-ray diffraction and SEM techniques. Fig. 3.1 (a) and 3.2 (a) shows the XRD pattern and SEM images of PLZT 8/60/40 mortar pestle mixed powders. The XRD pattern of PLZT mixed powders shows peaks corresponding to the raw materials with no trace of the perovskite phase. Peaks related to raw oxides

are clearly visible. Fig. 3.1 (a) shows the particles of mixed powders are agglomerated and SEM is not able to find the average particle size. Fig. 3.1 (b) and 3.2 (b) shows the XRD pattern and SEM image of sintered PLZT ceramics, respectively. Most of the PbO peaks in sintered PLZT disappeared when compared to the as-mixed powders. Few peaks related to PbO are seen in the XRD pattern of sintered PLZT compact along with the perovskite phase, indicating that the ceramics need to be sintered at higher temperatures. The average crystallite size for mortar-pestle prepared PLZT 8/60/40 ceramics was found to be ~36 nm using the Scherrer formula.

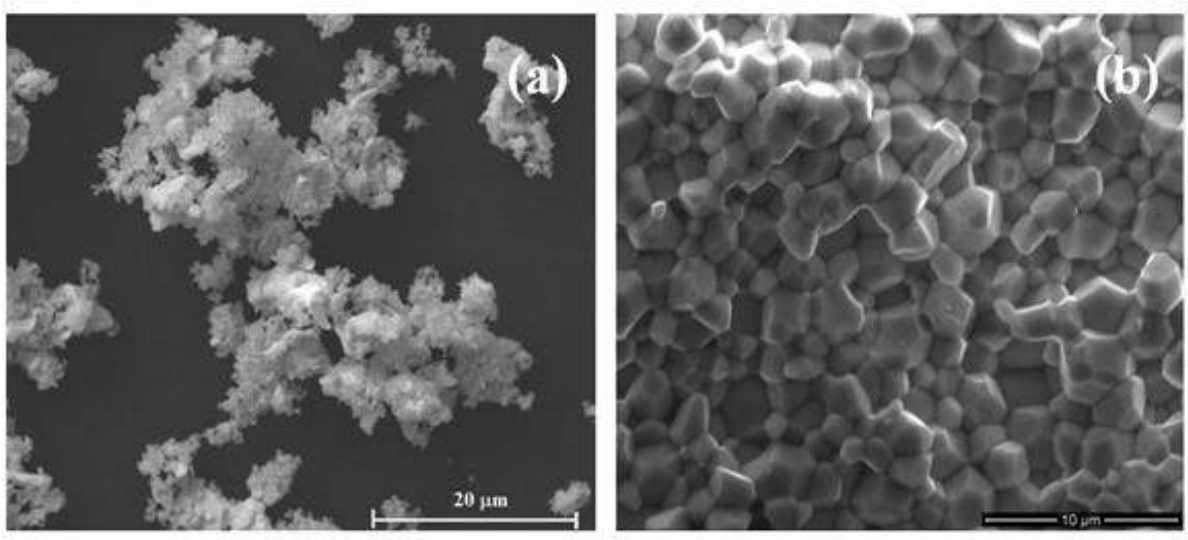

Fig. 3.2 *Scanning electron microscopy images for PLZT 8/60/40 (a) mortar pestle mixed powders and (b) sintered fractured surface of ceramic.*

From the SEM image of a fractured surface of sintered PLZT 8/60/40 ceramics, it is clear that the ceramics have a uniform grain size distribution and dense microstructure. The average grain size was found to be <1.85 µm. The density of the sintered PLZT 8/60/40 electro-ceramic was measured by the Archimedes' method and found to be > 95% relative to the theoretical density.

3.4 Density of PLZT ceramics

The optimum mechanical and electrical properties of PZT and PLZT based ceramics are not only (high) density dependent but also affected by uniform microstructure. Since the properties of the electro-ceramics are also highly density dependent so ceramics should have the minimum density to perform the electrical measurements. The density of the sintered PLZT ceramics is calculated by using the Archimedes principle. The equation that was used for the calculation of experimental density is given in chapter-2. The theoretical density of PLZT is obtained from standard JCPDS file.

3.4.1 Optimization of La substitution in PZT (PLZT) ceramics

La substituted PZT ceramics $(Pb_{1-x}La_x)(Zr_{0.60}Ti_{0.40})O_3$ for different compositions (PLZT x/60/40; x=0.00, 0.02, 0.04, 0.07, 0.08, 0.09, 0.10) were synthesized via combinatorial approach by high energy mechano-chemical ball milling method and cold isostatic pressing (CIP). The cipped pellets of PLZT x/60/40 ceramic were sintered and density was calculated. Effects of La substitution on the density of PLZT ceramics were studied in this chapter. Fig. 3.3 shows the change in experimentally calculated and relative density for PLZT x/60/40 ceramics, as a function of lanthanum substitution. Fig. 3.3 shows the PLZT 8/60/40 ceramic system exhibiting higher density than other systems. The density of the PLZT x/60/40 ceramics is given in Table-3.1.

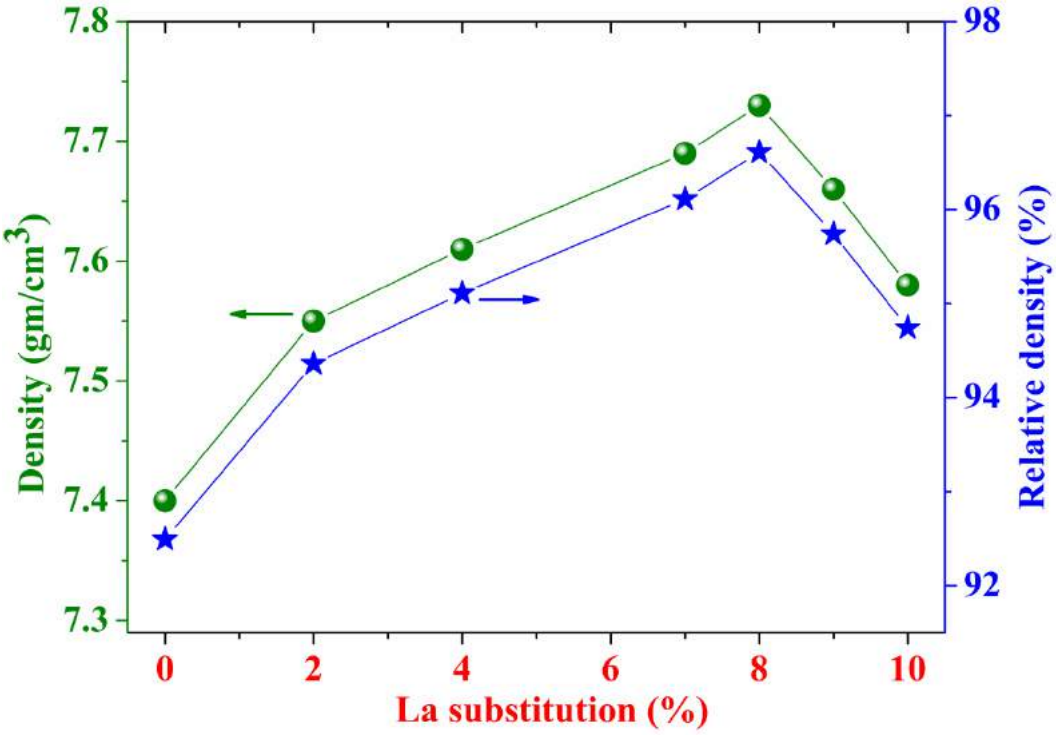

Fig. 3.3 *Changes in measured and relative density of PLZT ceramics as a function of La substitution.*

Table-3.1 *Density of PLZT x/60/40 ceramics.*

Compositions	Density (gm/cm^3)	Relative density (%)
PZT 60/40	7.40	92.49
PLZT 2/60/40	7.55	94.36
PLZT 4/60/40	7.61	95.11
PLZT 7/60/40	7.69	96.11
PLZT 8/60/40	7.73	96.61
PLZT 9/60/40	7.66	95.74
PLZT 10/60/40	7.58	94.74

3.4.2 PLZT 8/60/40 ceramics milled with different vials

From the last section 3.4.1, it is clear that the PLZT composition that was prepared by the substitution of 8% of lanthanum at the A-site of PZT (PLZT 8/60/40) shows the highest relative density (96.61%). Encouraged by this result, this composition was used to study the effect of milling vials on the characteristics of the same. PLZT 8/60/40 was milled by using different milling vials, made of agate and Zirconia, respectively. The density of PLZT 8/60/40 ceramics milled with different vials is given in Table-3.2. It shows that PLZT 8/60/40 ceramics milled with Zirconia vials have better density than that milled in agate vials.

Table-3.2 *Density of PLZT 8/60/40 ceramic milled with different vials.*

Milling vials	Density (gm/cm^3)	Relative density (%)
Agate vial	7.73	96.61
Zirconia vial	7.78	97.23

3.4.3 PLZT 8/60/40 ceramics milled for different durations

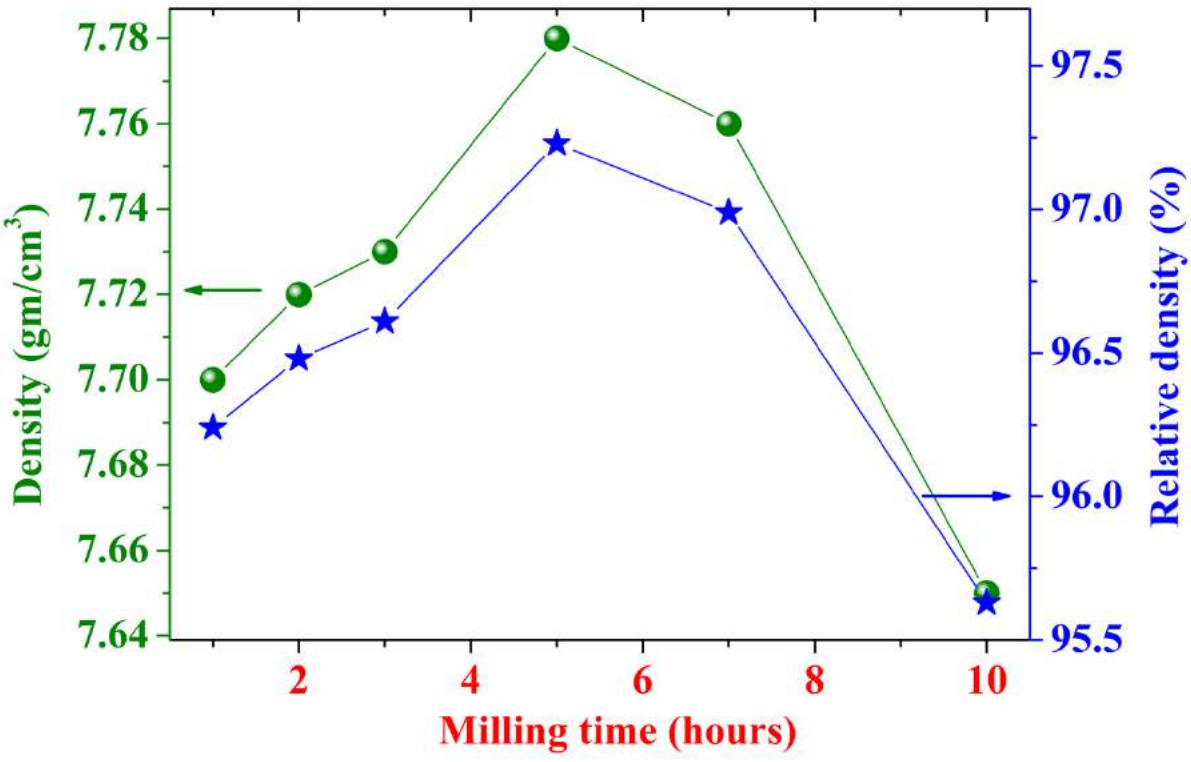

Fig. 3.4 Changes in measured density and relative density of PLZT 8/60/40 ceramics as a function of milling time.

The optimized composition of PLZT ceramic was milled for different durations using mechanical activation method. The density of electro-ceramics is also affected by the milling time similar to the other milling parameters, as discussed in Chapter-1. In this study, the density was measured for PLZT 8/60/40 ceramic, which was ball milled for different durations for the optimization of milling time. Fig. 3.4 shows the variation in the density of PLZT 8/60/40 ceramic as a function of milling time. PLZT 8/60/40 ceramics, which was milled for 5 hours shows the highest density. The density of PLZT 8/60/40 ceramics milled for different durations is given in Table-3.3.

Table-3.3 *Density of PLZT 8/60/40 ceramic milled for different durations.*

Milling durations	Density (gm/cm^3)	Relative density (%)
1h	7.70	96.24
2h	7.72	96.48
3h	7.73	96.61
5h	7.78	97.23
7h	7.76	96.99
10h	7.65	95.63

3.5 Phase analysis and structural properties

In this section, XRD patterns were taken for all La substituted PZT compositions as well as for PLZT 8/60/40 composition, which was milled for different durations. These XRD patterns were obtained for both as milled powders and sintered compacts.

3.5.1 Optimization of La substitution in PZT (PLZT) ceramics

The as milled powders and the sintered pellets of La substituted PZT were characterized using XRD technique. Fig. 3.5 shows the XRD patterns of the as milled powders of PLZT x/60/40 ceramics. The XRD results for the as milled PLZT x/60/40 ceramics, which were prepared via high-energy mechanical milling indicated that milled powders are highly reactive giving rise to perovskite phase during milling itself, as shown in fig. 3.5. The (001), (101), (200) and (201) peaks pertaining to the perovskite structure of PLZT 8/60/40 are seen to be prominent in the XRD patterns for the milled powders.

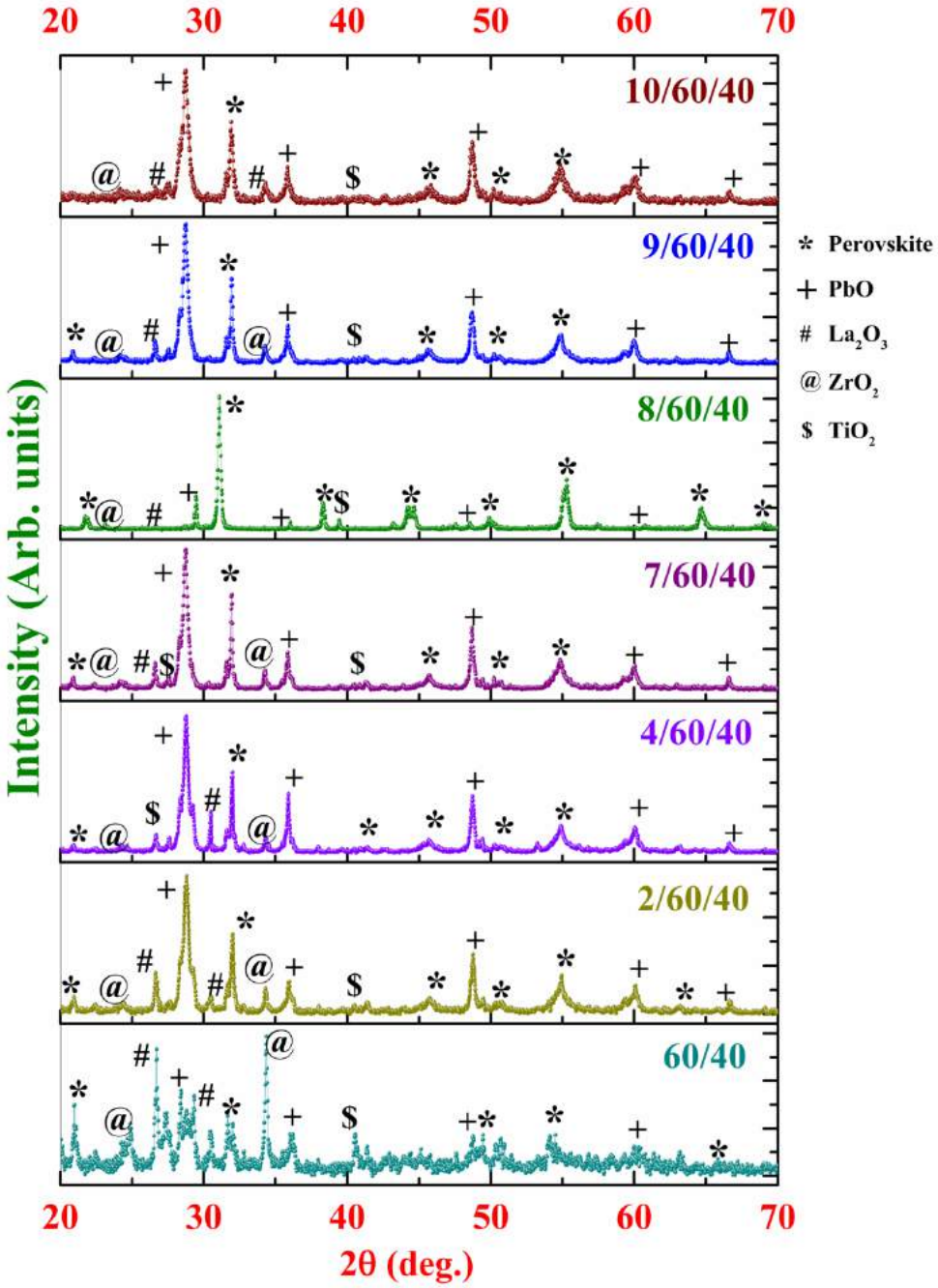

Fig. 3.5 *X-ray diffraction patterns for as milled powders of PLZT x/60/40 ceramics prepared via high energy ball milling technique.*

From fig. 3.5, it is also observed that as the lanthanum substitution increases, there is a commensurate increase in perovskite phase. PLZT 8/60/40 composition shows almost the complete transformation to the perovskite phase when compared with other systems. In the XRD patterns of PLZT x/60/40 ceramics, along with the perovskite peaks, other peaks are also observed that are corresponding to the raw materials. All the peaks were matched by using their respective JCPDS cards.

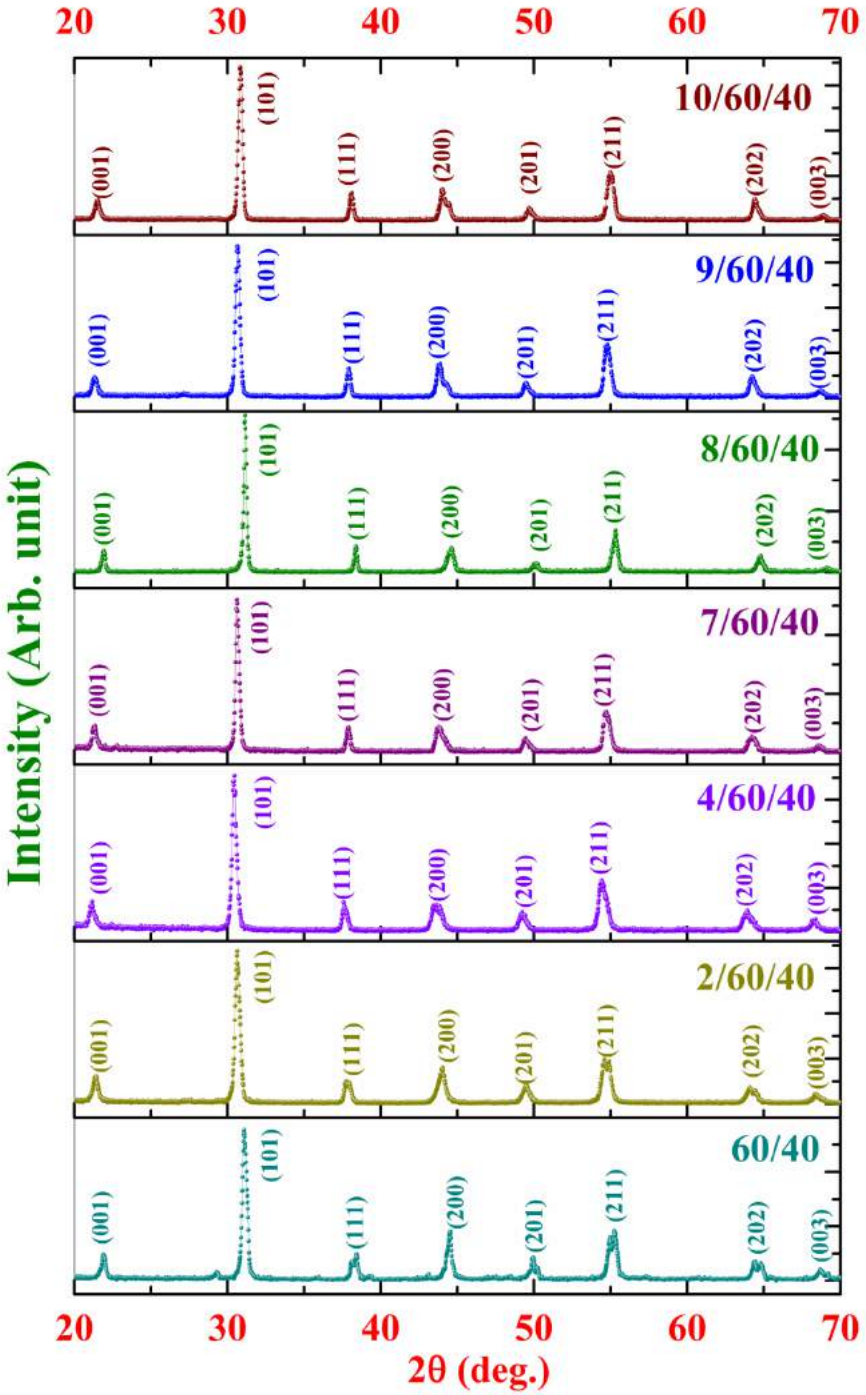

Fig. 3.6 *X-ray diffraction patterns for sintered compacts of PLZT x/60/40 ceramics prepared via high energy ball milling technique.*

Fig. 3.6 shows the XRD patterns of sintered PLZT x/60/40 ceramics. After sintering, the disappearance of the peaks of PbO and other raw materials that were unreacted after milling indicates completion of the chemical reactions that leads to the phase transformation into the desired perovskite PLZT phase. The perovskite phase formation is confirmed by comparing the XRD patterns with JCPDS (53-0698) file. The peaks pertaining to the perovskite structure of PLZT 8/60/40 are seen to be prominent in the XRD data for both milled powders and sintered samples.

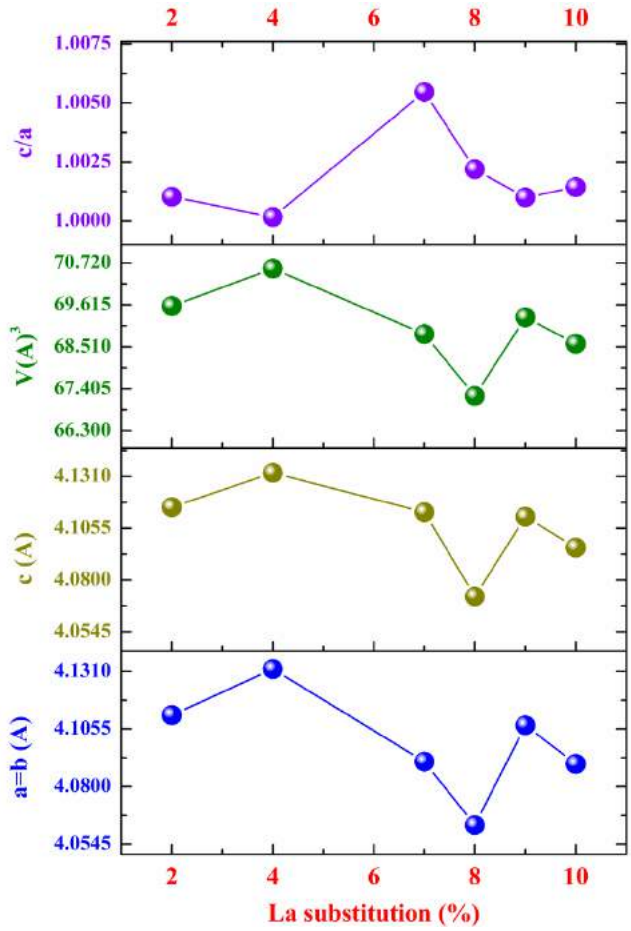

Fig. 3.7 *The lattice parameters, volume and c/a ratio of the unit cell of sintered PLZT x/60/40 ceramics.*

From fig. 3.7 it is very clear that the structure of the PLZT unit cell is changing with the amount of La substitution. Fig. 3.7 shows the lattice parameters ('a' and 'c'), volume and c/a ratio for the sintered PLZT x/60/40 unit cell as a function of La substitution. Lattice and volume of the unit cell decrease as the La substitution increases, reaches its minimum value at 8% substitution, and then increases thereafter. PLZT 7/60/40 ceramics show the maximum value of c/a ratio. A variation in c/a ratio of the unit cell directly affects the electrical properties of electro-ceramics **[15]**. The broadening of X-ray diffraction peaks was used for the calculation of average crystallite size. The average crystallite size (P) for PLZT x/60/40 with different La substitution was calculated by using the Scherrer equation (Chapter-2).

Fig. 3.8 shows the variation in FWHM or β, the average crystallite size and lattice strain for maximum intensity (101) peak of PLZT x/60/40 ceramics as a function of La substitution. Both the FWHM and average crystallite size values are interdependent. The crystallite size is inversely proportional to the peak width. As the crystallite size decreases, the width of the diffraction peak increases and vice versa. Fig. 3.8 gives us an idea about the crystallinity of the perovskite PLZT ceramics, with the pattern of FWHM and average crystallite size indicating a change in crystallinity.

PLZT 8/60/40 ceramics show the maximum crystallite size and minimum lattice strain. All the measured and calculated structural parameters of PLZT x/60/40 ceramics are given in Table-3.4.

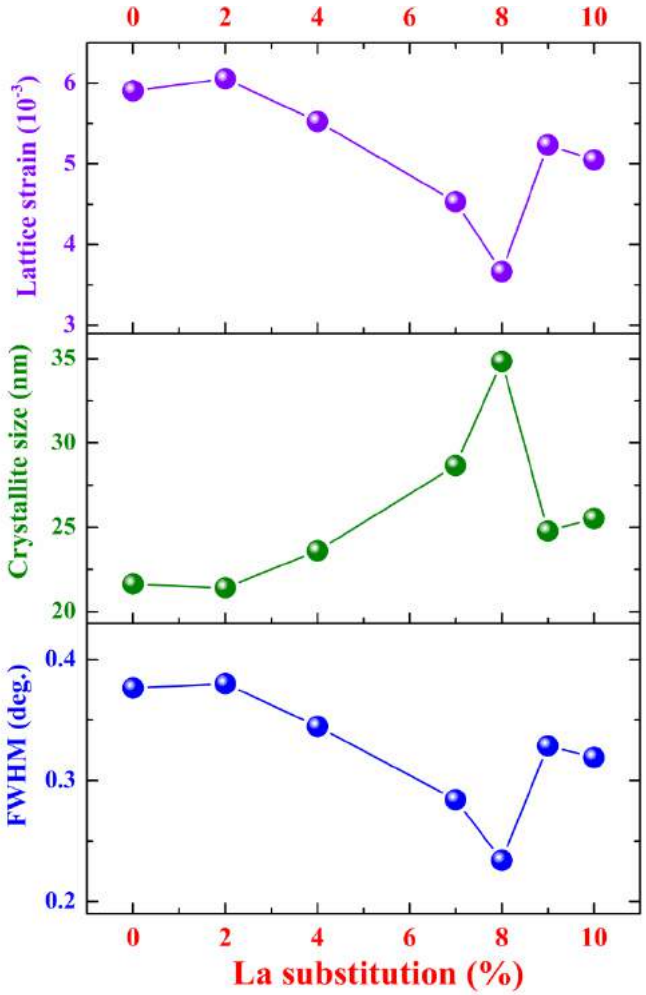

Fig. 3.8 *Variations of full width at half maxima (FWHM), crystallite size and lattice strain at maximum intensity (101) peak for PLZT x/60/40 ceramics.*

Table-3.4 *Structural parameters of PLZT x/60/40 ceramics.*

Compositions	a (Å)	c (Å)	V (Å)^3	P (nm)	β (deg.)	Strain
PZT 60/40	4.0669	4.0935	67.7079	21.6	0.3765	0.0059
PLZT 2/60/40	4.1116	4.1159	69.5810	21.4	0.3801	0.0061
PLZT 4/60/40	4.1321	4.1327	70.5732	23.6	0.3447	0.0055
PLZT 7/60/40	4.0911	4.113	68.8448	28.7	0.2841	0.0045
PLZT 8/60/40	4.0629	4.0719	67.2163	34.8	0.2341	0.0037
PLZT 9/60/40	4.1071	4.1112	69.2878	24.8	0.3286	0.0052
PLZT 10/60/40	4.0901	4.0959	68.5912	25.5	0.3191	0.0051

3.5.2 PLZT 8/60/40 ceramics milled with different vials

From XRD studies of different compositions, it is clear that the PLZT composition that was prepared by the substitution of 8% of lanthanum at the A-site of PZT (PLZT 8/60/40) shows relatively good structural properties. PLZT 8/60/40 was further milled using different milling vials viz. agate and Zirconia. All the structural parameters are given in Table-3.5. Results show that the PLZT 8/60/40 ceramics milled in Zirconia vials have better density than agate milled ceramics.

Table-3.5 *Structural parameters of PLZT 8/60/40 ceramic milled with different vials.*

Milling vials	a (Å)	c (Å)	V $(Å)^3$	P (nm)	β (deg.)	Strain
Agate vial	4.0629	4.0719	67.2163	34.8	0.2341	0.0037
Zirconia vial	4.0596	4.0635	66.9671	23.3	0.3505	0.0055

3.5.3 PLZT 8/60/40 ceramics milled for different durations

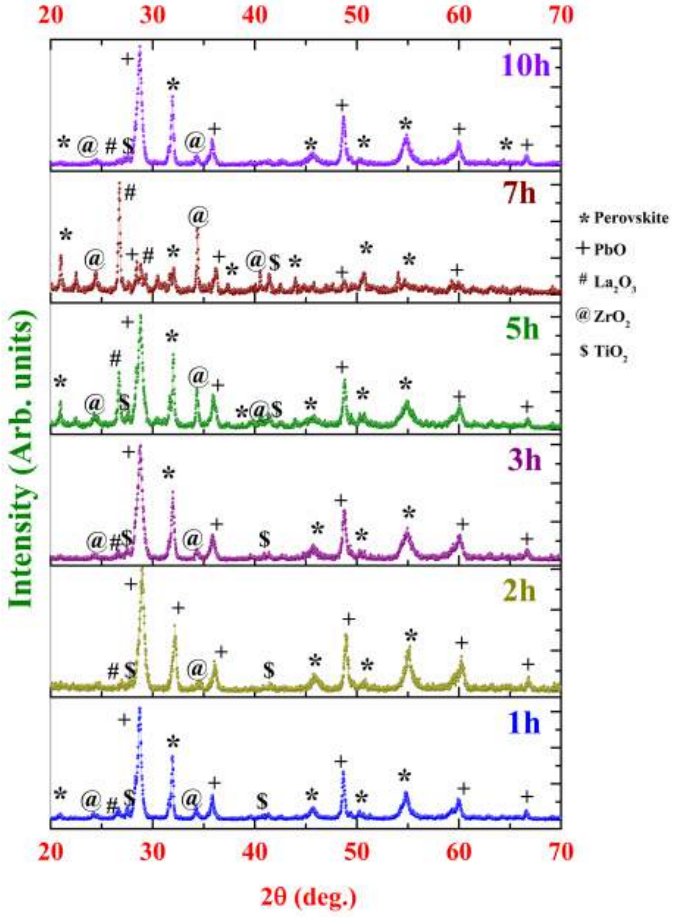

Fig. 3.9 *X-ray diffraction patterns for as milled powders of PLZT 8/60/40 ceramics milled for different durations with high energy ball mill.*

Fig 3.9 and 3.10 showed the XRD pattern of as milled powders and sintered PLZT 8/60/40 ceramics, respectively, which were milled for different durations. As seen in fig. 3.9, as milled powders also show some peaks pertaining to the perovskite phase. The (001), (101), (200) and (201) peaks pertaining to the perovskite structure of PLZT 8/60/40 are seen to be prominent in the XRD data for as milled powders. These peaks are proof of the chemical reaction of raw oxides at the milling stage that results in partial perovskite phase formation.

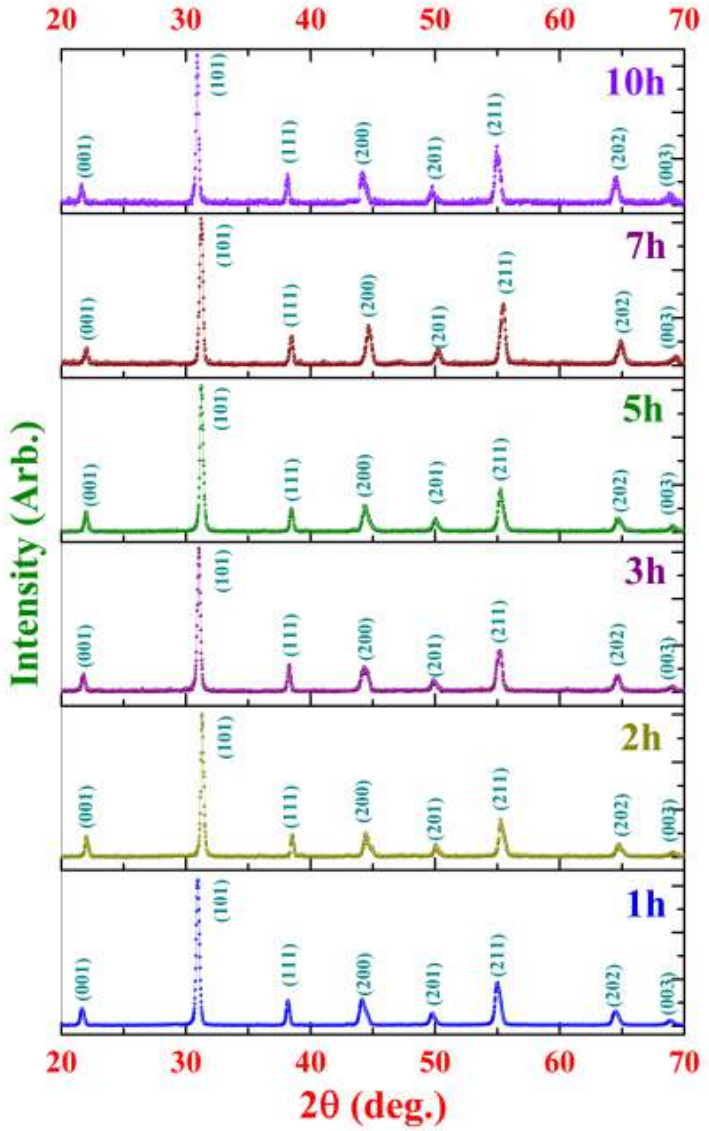

Fig. 3.10 *X-ray diffraction patterns for sintered PLZT 8/60/40 ceramics prepared from high energy ball milled powders, milled for different durations.*

Fig 3.10 shows the XRD patterns for the sintered compact of PLZT 8/60/40 ceramics. The disappearance of the unreacted PbO and other raw oxide peaks, prominently present in the XRD pattern of as milled powders show that the reaction of raw oxides is completed only after sintering. Unreacted oxides react completely during sintering. No other phases were detected in sintered PLZT,

indicating that the remaining oxides in the samples already reacted leading to the formation of the perovskite phase. During the heat treatment of compacted ceramics, the reaction of the oxides takes place and a complete phase transformation perovskite PLZT phase is taken place.

Fig. 3.11 shows that the structure of the PLZT unit cell is changing as a function of milling time. Fig. 3.11 shows the lattice parameters ('a' and 'c'), volume and c/a ratio for the sintered PLZT 8/60/40 ceramics milled for different durations. Lattice parameters and volume of the unit cell decreases as the milling time increases, reaches its minimum value at 7 hours, and then increases. PLZT 8/60/40 ceramics milled for 7 hours exhibit the maximum value of c/a ratio.

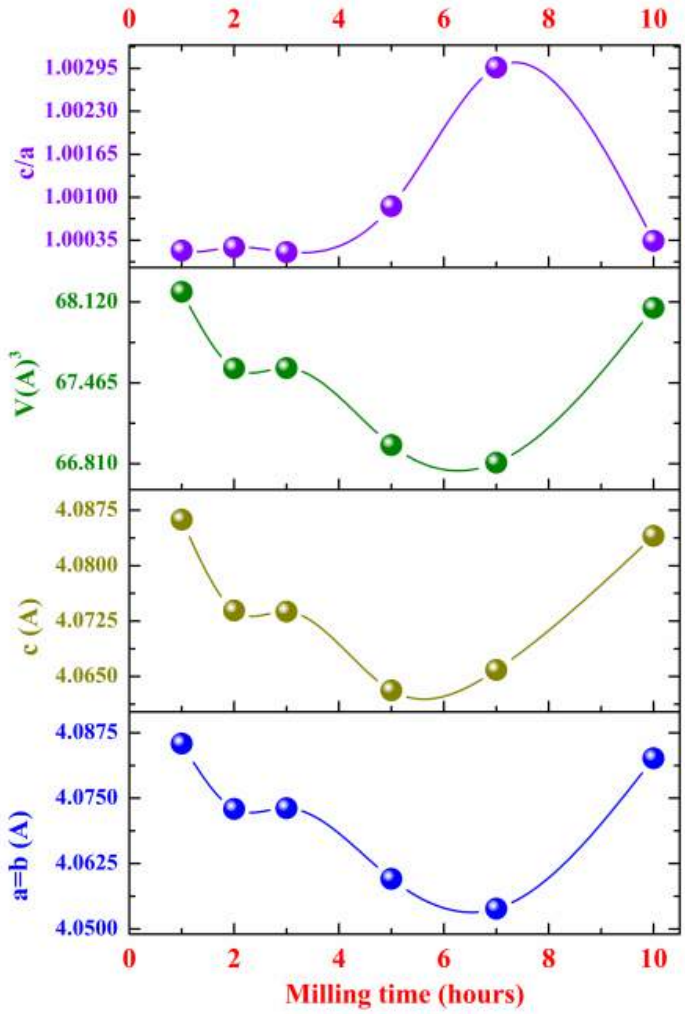

Fig. 3.11 *The lattice parameters, volume and c/a ratio of the unit cell of sintered PLZT 8/60/40 ceramics as a function of milling time.*

From the broadening of X-ray diffraction peaks, the average crystallite size for PLZT 8/60/40 milled for different durations was calculated using Scherrer equation (Chapter-2). Fig. 3.12 shows the variation in full width at half maxima (FWHM or β), the average crystallite size and lattice strain for maximum intensity (101) peak of PLZT 8/60/40 ceramics as a function milling time. Since FWHM

and average crystallite size are interdependent, crystallite size is inversely proportional to the peak width. As the crystallite size decreases, the width of the diffraction peak increases and vice versa. All the measured and calculated structural parameters for the PLZT 8/60/40 ceramics milled for different durations are given in Table-3.6.

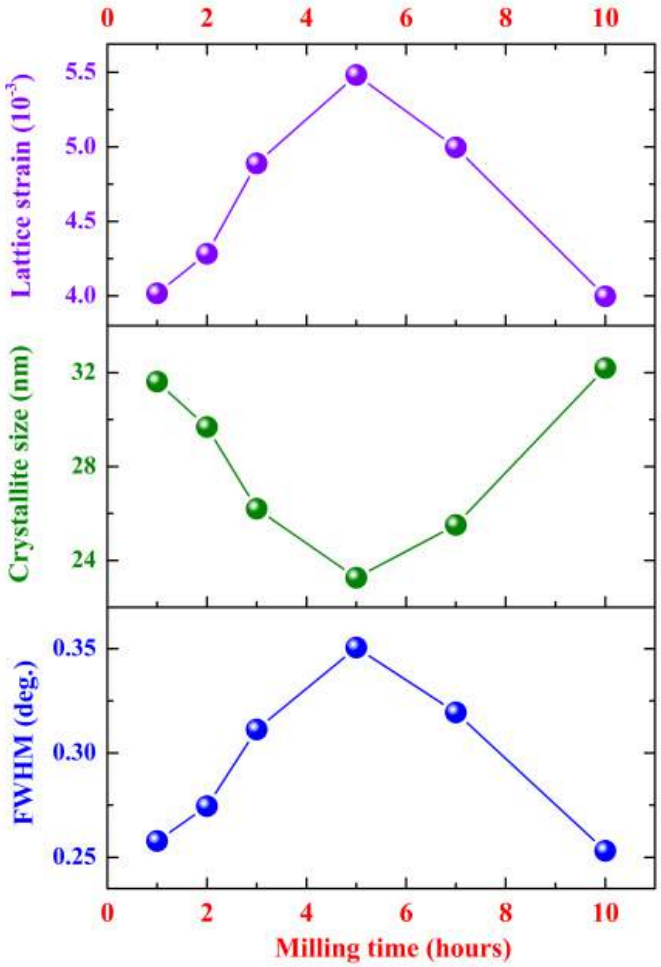

Fig. 3.12 *Variation in FWHM, crystallite size and lattice strain at maximum intensity (101) peak for sintered PLZT 8/60/40 ceramics as a function of milling time.*

Table-3.6 *Structural parameters of PLZT 8/60/40 ceramic milled for different durations.*

Milling durations	a (Å)	c (Å)	V $(Å)^3$	P (nm)	β (deg.)	Strain
1h	4.0854	4.0862	68.20253	31.61102	0.25781	0.0040
2h	4.0729	4.0739	67.58194	29.68312	0.27452	0.0043
3h	4.0731	4.0738	67.58443	26.20099	0.31127	0.0049
5h	4.0596	4.0631	66.96115	23.26396	0.35054	0.0055
7h	4.0539	4.0659	66.81811	25.50921	0.31946	0.0050
10h	4.0826	4.0840	68.07241	32.19395	0.25316	0.0040

3.6 Micro-structural and morphological studies

Scanning electron microscopy (SEM) was used for the micro-structural and morphological studies. SEM images were taken for the PZT ceramics substituted with different amounts of La and PLZT 8/60/40 ceramics milled for different durations. SEM images of PLZT ceramics give an idea about the grain size, shape, micro-structure and density. Along with the XRD analysis, SEM studies are also very important for electro-ceramics.

3.6.1 Optimization of La substitution in PZT (PLZT) ceramics

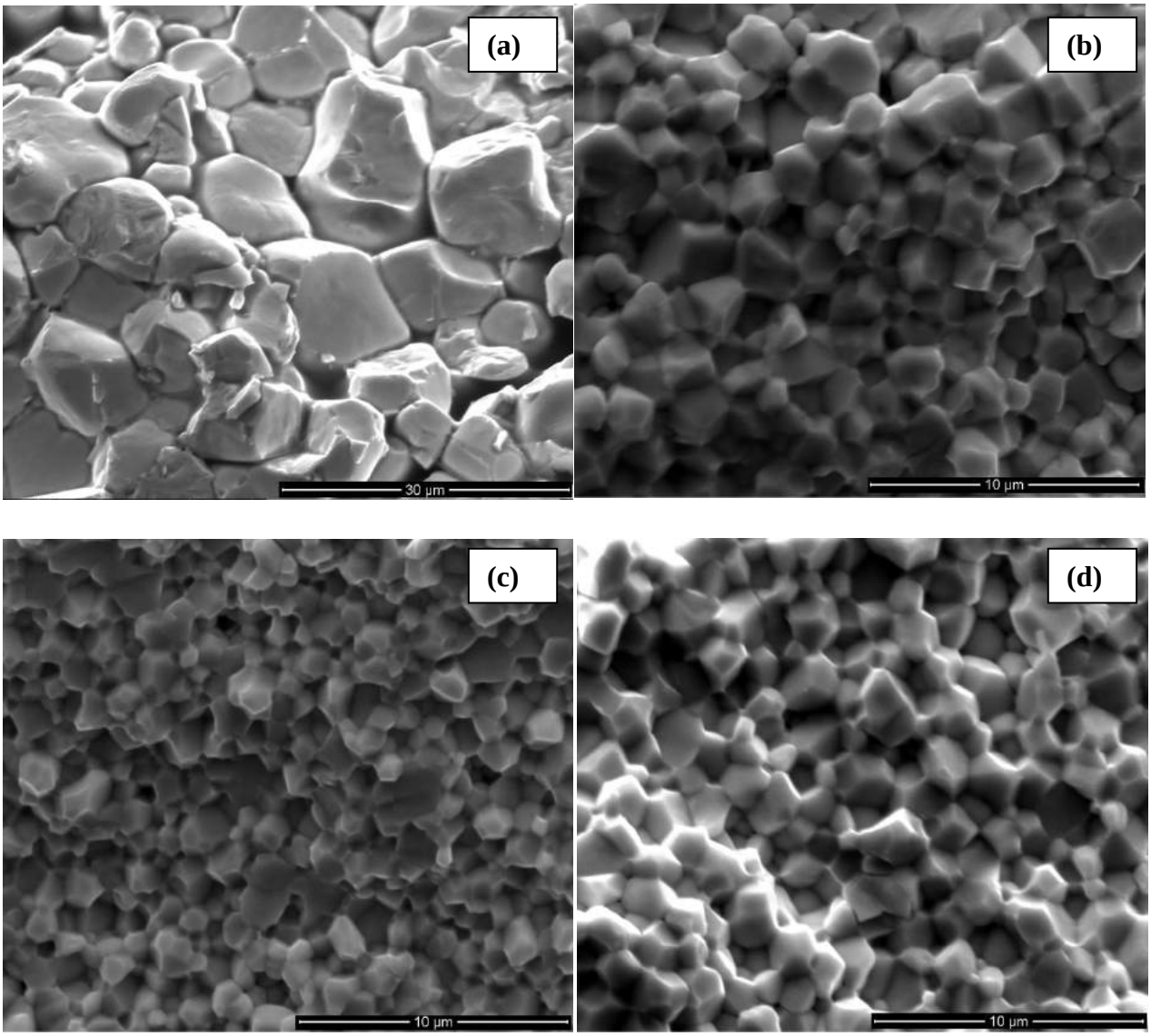

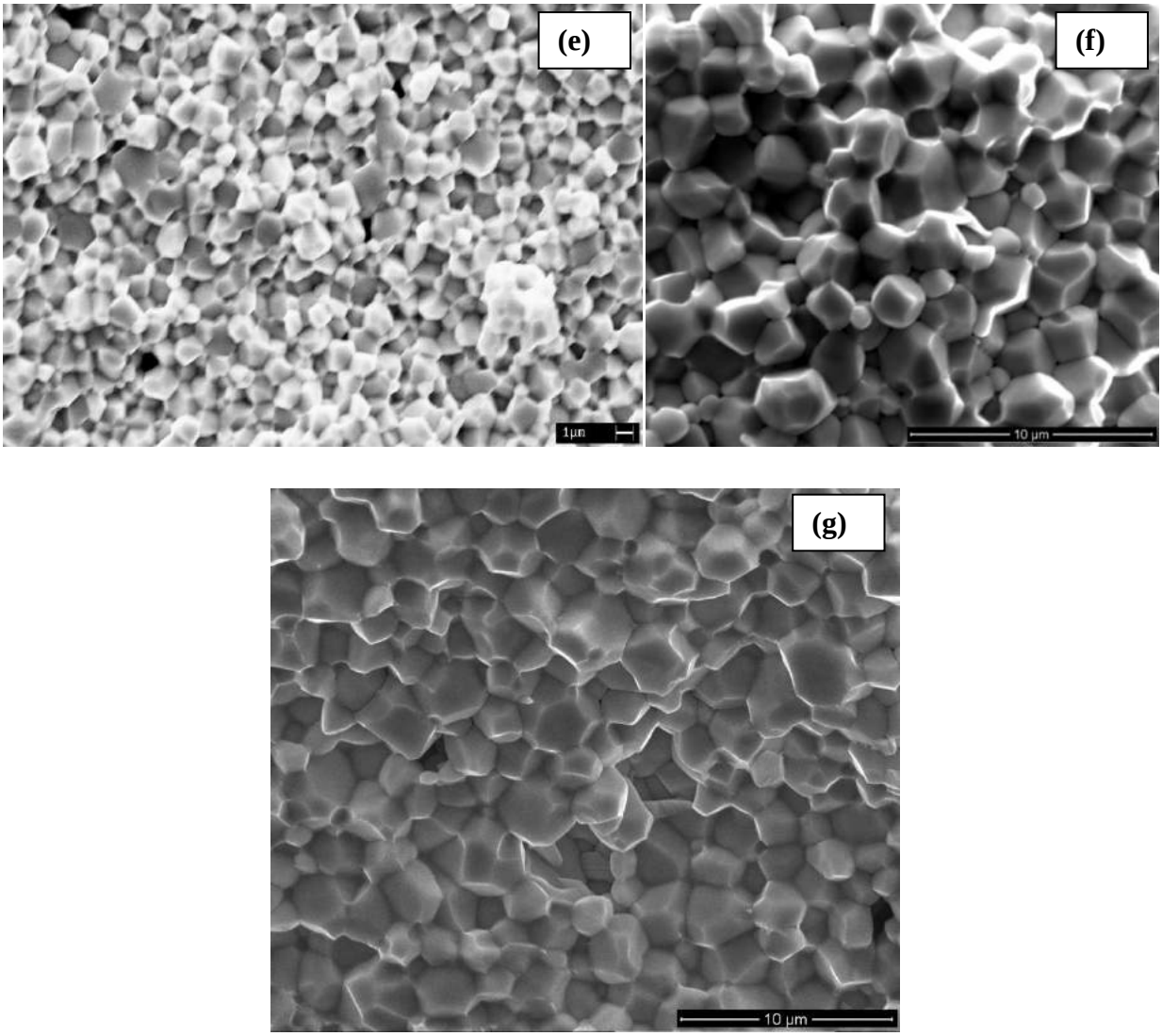

Fig. 3.13 *SEM images of sintered PLZT x/60/40 ceramics as a function of lanthanum substitution (a) 0% (b) 2%, (c) 4%, (d) 7%, (e) 8%, (f) 9%, and (g) 10%.*

Fig. 3.13 shows the SEM images of PLZT ceramics that was prepared with different amounts of lanthanum substitution. The base composition of PZT shows larger grains compared to La substituted ones with a less dense microstructure. The grain shapes for the PZT system was also not uniform and this also has an effect on the electrical properties. With an increase in the amount of lanthanum substitution in the PZT system, grain size decreases, and ceramics show improved microstructure and uniform grain size. The fractured surface of sintered PLZT x/60/40 compositions shows uniform grain sizes, a dense microstructure with clearly visible grain shapes. The grain size of electro-ceramics has a great effect on their dielectric, ferroelectric and piezoelectric properties. Fig. 3.13 shows the SEM micrograph of the sintered pellet of PLZT 8/60/40 ceramics indicating a very dense structure with a uniform grain size. Grain shapes and the grain boundaries of PLZT ceramics are clearly visible, indicating the existence of a polycrystalline microstructure. The average grain size was found to be ~1.3 µm.

Fig. 3.14 shows the change in average grain size of sintered PLZT x/60/40 ceramics as a function of La substitution. For the basic PZT system, the average grain size was found to be ~9 µm. When the lead is substituted by lanthanum at the A-site of PZT, a sharp decrease in grain size was observed. After reaching the minimum value ~1.3 µm for PLZT 8/60/40 ceramics, grain size again increases. The average grain sizes for PLZT x/60/40 ceramics are given in Table-3.7.

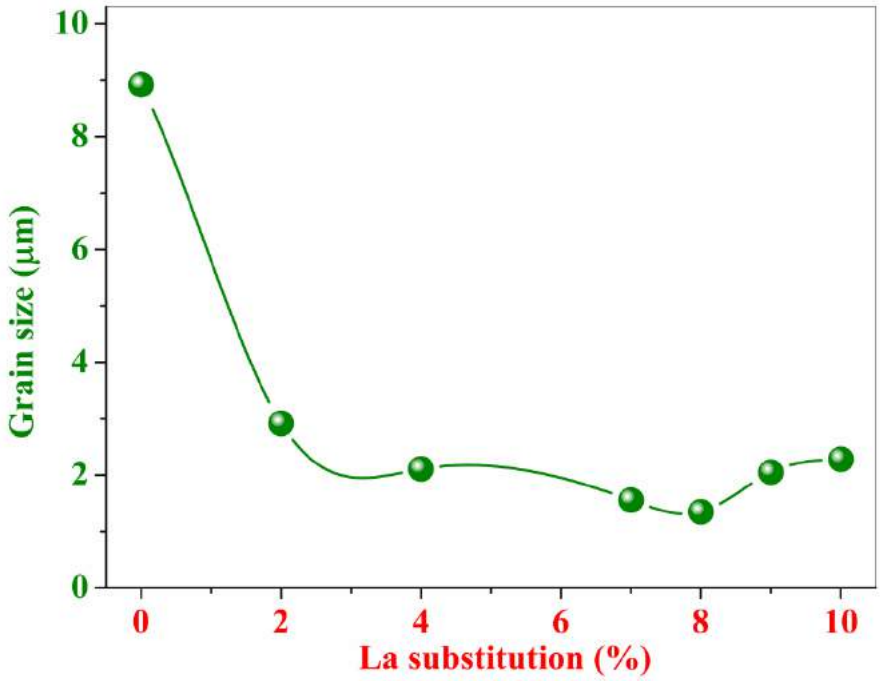

Fig. 3.14 *Variation in average grain size of PLZT x/60/40 ceramics as a function of La substitution.*

Table-3.7 *Average grain size of PLZT x/60/40 ceramics.*

Compositions	Grain size (µm)
PZT 60/40	8.92
PLZT 2/60/40	2.92
PLZT 4/60/40	2.11
PLZT 7/60/40	1.56
PLZT 8/60/40	1.35
PLZT 9/60/40	2.05
PLZT 10/60/40	2.28

3.6.2 PLZT 8/60/40 ceramics milled with different vials

SEM images of the different compositions of PLZT ceramics shows that average grain size is less for the PLZT 8/60/40 ceramics which was prepared by the 8% of La substitution at the A-site of PZT. PLZT 8/60/40 was further milled using different milling vials, viz. agate and zirconia. Average

grain size is given in Table-3.8. Results show that the agate and zirconia vial milled PLZT 8/60/40 ceramics have almost the same grain size.

Table-3.8 *Average grain size of PLZT 8/60/40 ceramic milled with different vials.*

Milling vials	Grain size (μm)
Agate vial	1.35
Zirconia vial	1.45

3.6.3 PLZT 8/60/40 ceramics milled for different durations

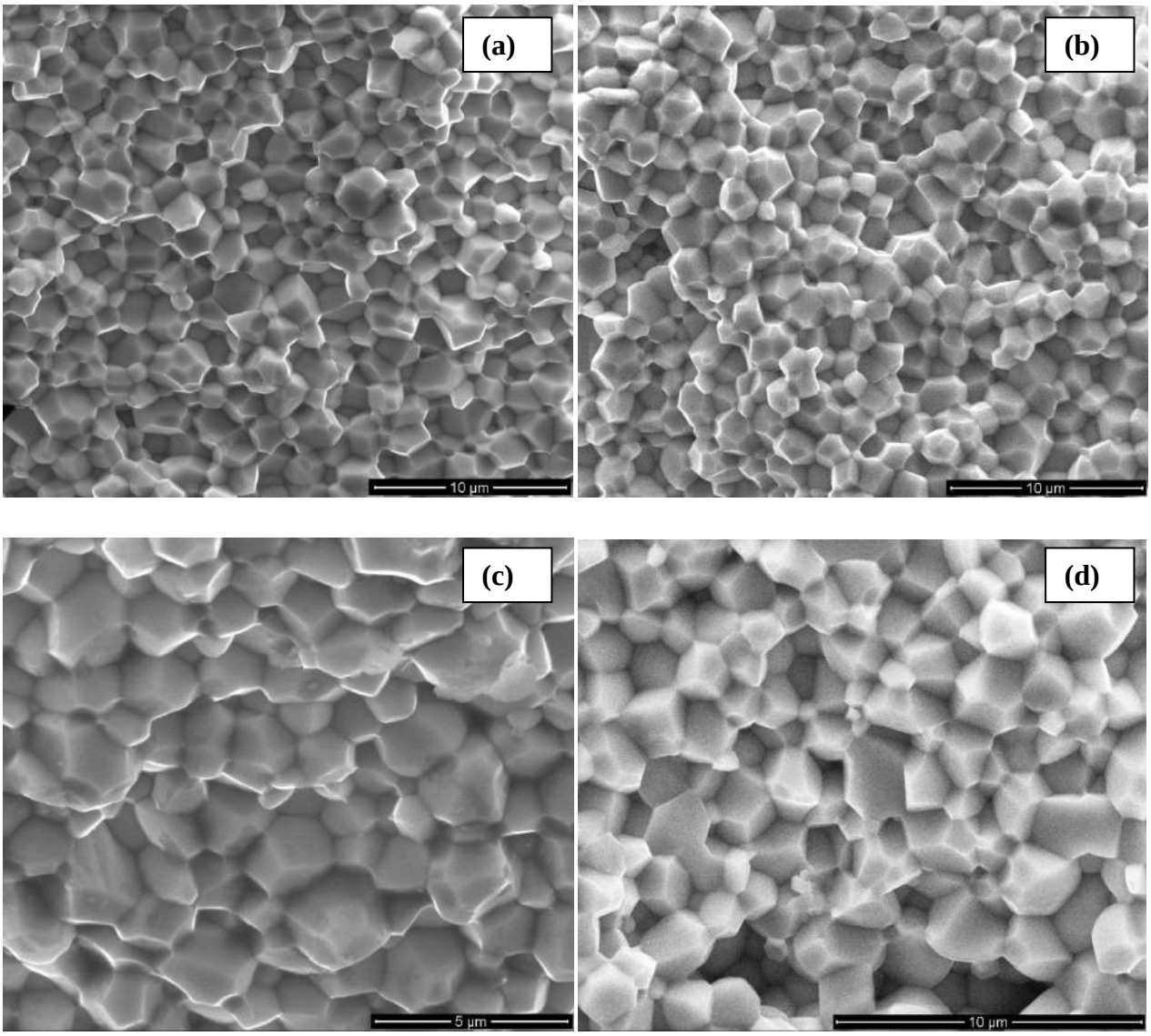

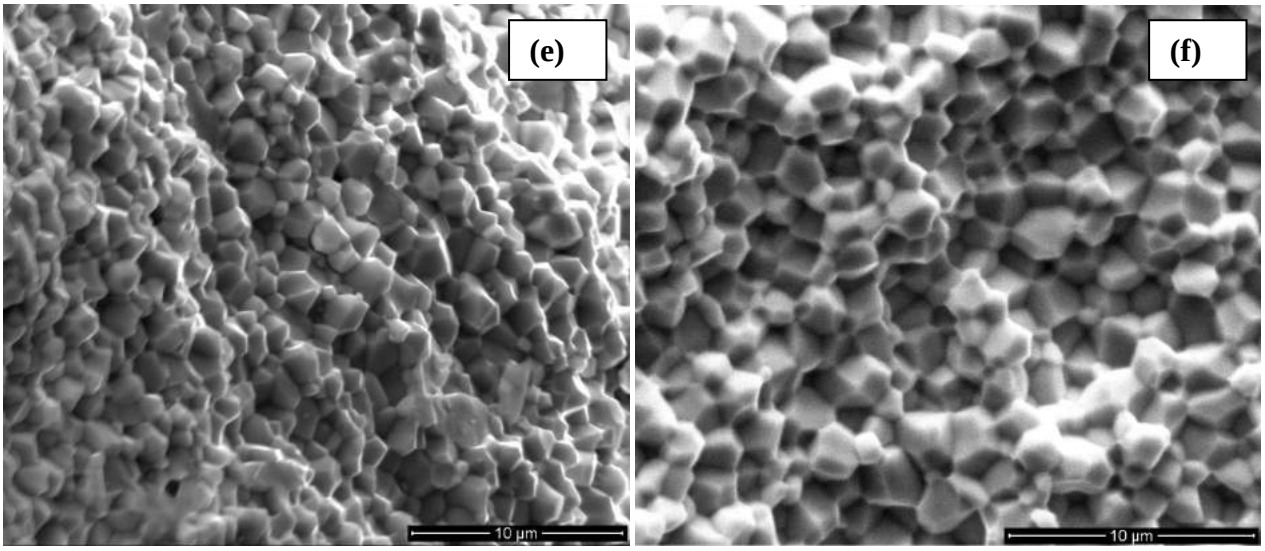

Fig. 3.15 *SEM images of sintered PLZT 8/60/40 ceramics milled for (a) 1h (b) 2h, (c) 3h, (d) 5h, (e) 7h and (f) 10h.*

Fig. 3.15 shows the SEM images of PLZT 8/60/40 ceramics milled for different durations. All the images show almost equal grain sizes, however, if one measure by the line intercept method, there are small changes in the grain sizes. Fig. 3.15 shows the SEM micrographs of the sintered pellet of PLZT 8/60/40 ceramics, which were prepared by using milled powders, milled for different milling times, indicating a dense structure and uniform grain size. PLZT 8/60/40 ceramics shows clearly visible grain shapes which confirm the polycrystalline microstructure. Fig. 3.15 show that when the milling time increases, grain size decreases, reaching a minimum value and thereafter rising again. PLZT 8/60/40 ceramics milled for 5 hours shows the minimum grain size of ~1.45 µm.

Since PLZT 8/60/40 ceramics milled for 5 hours shows the best microstructure, the as milled powder of this composition is examined by microscopic techniques for the particle size measurements. SEM images of as milled powders show agglomerated particles **[16]**. TEM images were also taken for the milled powders of PLZT 8/60/40 ceramics for microstructure examination of the material. The TEM image of the as milled powders shows that the particle size of PLZT 8/60/40 deviates from the spherical shape and is non-uniform with a broadly distributed particle size range. The size of high energy ball milled powders is in the nano-meter range. The reduction in particle size results in an increase in the surface to volume ratio making the particles highly reactive and causing an agglomeration between the particles (Fig. 3.16). The sol-gel process results in spherical particles whereas MCP results in elongated/flaky particles on account of the high impaction forces resulting in mechanical deformation of the same **[10, 17]**. The average particle size of PLZT ceramics was calculated from the TEM image was found to be ~25 nm. During the milling process, the mechanical energy is applied to PLZT powders by high strength collision and high pressure impact between the

milled powder and milling media. The pressure generated from mechano-chemical milling is high enough to break down the particles of the PLZT powder to nano-meter size.

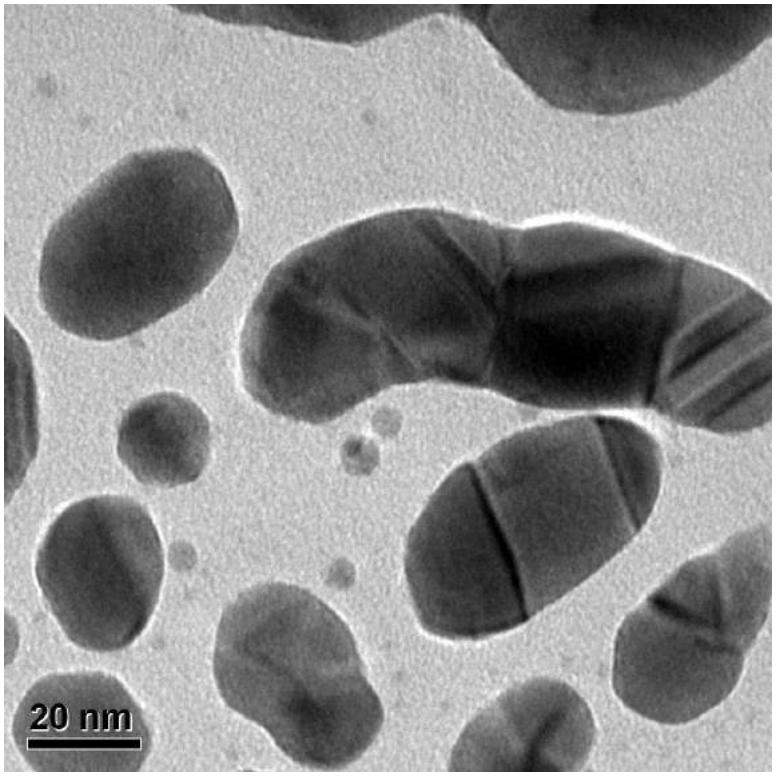

Fig. 3.16 *TEM image of PLZT 8/60/40 milled powders.*

3.7 Discussion

Figs. 3.3 and 3.4 show the changes in density as a function of lanthanum substitution and milling time. For both cases, at first, the density increases get its highest value and then decreases. Change in density with La substitution can be explained based on the solubility of La ions in the PZT lattice, which is a function of composition and depends on the amount of lead titanate (PT). The solubility limits of intermediate compositions are proportional to their Zr/Ti ratios **[1]**. The solubility of lanthanum in the PZT ceramics increases as a function of lanthanum substitution, resulting in modification of the MPB. PLZT 8/60/40 ceramics show the highest density (fig. 3.3), best structural parameters (section 3.5.1), clear and visible grain boundary (fig. 3.13) and fine grains (fig. 3.14). All of the above properties are related to the solubility of lanthanum. After 8% lanthanum substitution, the said properties decrease/showing saturation.

Figs. 3.5 and 3.9 show the XRD patterns of as milled powder of PLZT x/60/40 ceramics and PLZT 8/60/40 ceramics, milled for different durations, respectively. In both figures, XRD patterns show the partial perovskite phase formation, as can be clearly seen from some of the peaks. High

energy mechano-chemical milling results in very fine scale size and highly reactive nano-powders. The use of HEM milling process enhances both mixing of the raw materials and reduction in their sizes. These milled powders with high surface free energy become highly reactive, thus giving rise to perovskite phase during milling itself, as can be seen in the figure. The XRD results of as milled PLZT ceramics (Figs. 3.5 and 3.9) prepared via high-energy mechanical milling indicate that the HEM technique provides enough energy to refine the size of the starting oxides of ceramics at the initial stage of milling. The mechanically refined milled powders become more and more reactive due to increasing in their surface to volume ratio.

The milling was done at room temperature. Powders synthesized by high energy milling possess particle sizes in the nano meter scale. Generally, high energy mechanical milling process can be divided into three stages. The first stage is related to the refinement of starting oxide powders in both particle and crystallite size. This procedure also results in amorphous phase formation. The second stage of milling process corresponds to the formation of phase nuclei and subsequent crystallization of the desired PLZT phase. At the last stage, synthesized PLZT powders are affected by further milling, which results in structural defects and disorder of milled PLZT powders.

Figs. 3.6 and 3.10 show the XRD patterns of sintered compacts of PLZT x/60/40 ceramics and PLZT 8/60/40 ceramics, milled for different durations, respectively. Both the figures show the disappearance of the unreacted PbO and other oxide peaks that were present in XRD pattern of as milled ceramics. During the heat treatment of compact PLZT ceramics, the reaction between the unreacted oxides takes place and a complete phase transformation into perovskite PLZT phase is formed. No other phases were detected in sintered PLZT, indicating that the remaining oxides in the samples already got reacted leading to the formation of the perovskite phase.

As already discussed, the solubility of lanthanum in the PZT lattice depends on the amount of La%. Fig. 3.7 shows that the unit cell parameters of PLZT ceramics change as a function of lanthanum substitution. The lattice defects and strains in the PLZT materials change as a function of lanthanum substitution which may affect the structural properties. Lattice strains and the unit cell parameters also changed with La substitution and these have an effect on the volume of the unit cell. The increase in lattice parameters and unit cell volume result in a lattice relaxation. Previously for the niobium-doped PZT, the lattice distortion along the tetragonal c-axis was found to be strongly reduced as the grain size is decreased when compared to the a-axis dimension **[18]**. In this study too, the decrease in unit cell volume as seen in fig. 3.7 can be understood on the basis of grain sizes. When a ferroelectric ceramic undergoes a paraelectric to a ferroelectric phase transition, its internal stress increases, which results in the above mentioned dimensional changes. In fine grained ferroelectrics, the mutually clamped spontaneous unit cell distortion not only reduces the intrinsic polarization but also increases the internal stresses **[19]**.

Fig. 3.8 shows that the PLZT 8/60/40 ceramics have the minimum lattice strain and maximum crystallite size. Optimal lanthanum substitution at the A-site of the PZT ceramics results in lattice relaxation which decreases the lattice strain. All the aforementioned reasons are sufficient for the binding of crystallites in clusters leading to an increase in their size. After 8% La substitution, the decrease in crystallite size may be the result of a change in crystal structure, resulting in defects again leading to increasing in strain and decrease in crystallite size. From the Scherrer formula it is clear that when the average crystallite size increases, the Full Width at Half Maxima decreases.

Figs. 3.11 and 3.12 show the structural parameters of PLZT 8/60/40 ceramics as a function of milling time. The change in the unit cell parameters can be explained by grain size variation. Fig. 3.12 shows that the PLZT 8/60/40 ceramics milled for 5 hours have the minimum crystallite size and maximum lattice strain.

Figs. 3.13 and 3.15 show the SEM micrographs of the fractured surface of sintered PLZT x/60/40 ceramics and PLZT 8/60/40, that were milled for different durations. The addition of La also affects the microstructure of the ceramics. SEM images of the fractured surface of La modified PZT show that the grain size decreased when compared to unmodified PZT ceramics **[11]**. It was deemed that minute chemical inhomogeneities on the A and B sites of the perovskite prevented the growth of grains. Another possibility would be the formation of secondary phases on a very small scale at the grain boundaries. Fig. 3.14 shows grain size variation for the different compositions of PLZT ceramics. A small change in the grain size of PLZT 8/60/40 ceramics milled for different durations can be attributed to the reaction kinetics and solubility of the modifier in the parent PZT system.

The grain size of the PLZT ferroelectric ceramics is a very important factor which affects the tetragonality (c/a ratio), dielectric constant, phase transition temperature (T_c), remnant polarization, piezoelectric and pyroelectric coefficients. Ferroelectric and piezoelectric properties directly depend on the grain size of the ceramics and fine grained ceramics show the good properties when compared with conventional ceramics **[20]**. The grain size dependence on the dielectric, ferroelectric and piezoelectric properties of PLZT 8/60/40 ceramics were reported by Kamel et. al. **[21]**.

The grain size of electro-ceramics affects the extrinsic contribution to piezoelectricity, ferroelectric domain wall motion and switching of domain walls, which is directly related to the electric field induced polarization and strain in the ferroelectric ceramic materials. Domain wall switching is highly affected by the quality of presence of intergranular phases, grain boundaries and porosity **[22]**. The uniform grain sizes, clear and visible grain boundaries and lack of porosity in the PLZT materials may be the reasons for the good properties exhibited. The extrinsic piezoelectricity in PZT ceramics is highly dependent on the chemical composition, especially the amounts and types of modifying dopants **[23]**.

3.8 Summary

Effect of lanthanum substitution of the A-site of PZT ceramics is studied. Based on the density, XRD and SEM result PLZT 8/60/40 composition was optimized. This optimized PLZT 8/60/40 ceramic system was again milled with different milling vial and for different durations. PLZT 8/60/40 ceramics milled for 5 hours with Zr vials gave the highest density and best microstructure. As milled PLZT powders also show the partial perovskite phase, which proves the partial chemical reaction at milling stage itself. PLZT 8/60/40 composition was also successfully prepared with the conventional mortar pestle mixing/grinding method and properties of this system were compared with the high energy milled (HEM) PLZT 8/60/40. Properties for the PLZT 8/60/40 milled (HEM) ceramics are found to be better than PLZT 8/60/40 mortar pestle mixed ceramic.

References

[1] G.H. Haertling, J. Am. Ceram. Soc., **82** (1999) 797.

[2] B. Jaffe, W.R. Cook Jr. and H. Jaffe, Piezoelectric Ceramics, Academic Press, New York, Ch.1 (1980).

[3] K. Uchino, Acta. Mater., **46 [11]** (1998) 3745.

[4] M. Hinterstein, K.A. Schoenau, J. Kling, H. Fuess, M. Knapp, H. Kungl and M.J. Hoffmann, J. Appl. Phys., **108** (2010) 024110.

[5] G.H. Haertling and C.E. Land, J. Am. Ceram. Soc., **54** (1971) 1.

[6] A.R. James, J. Subrahmanyam and K.L. Yadav, J. Phys. D: Appl. Phys., **39** (2006) 2259.

[7] A.R. James, J.P. Praveen, M.P. Kumar and V.V.B. Prasad, Mater. Res. Bul., **47 [11]** (2012) 3459.

[8] A.R. James and J. Subrahmanyam, J. Mater. Sci: Mater. Electron., **17** (2006) 529.

[9] L. Pdungsap, N. Udomkan, S. Boonyuen and P. Winotai, Sensors and Actuators A, **122** (2005) 250.

[10] S. Dutta, R.N.P. Chaudhary and P.K. Sinha, J. Alloys Comp., **430** (2007) 344.

[11] S.R. Shannigrahi and R.N.P. Chaudhary, J. Electroceram., **5 [3]** (2000) 201.

[12] J.D.S. Guerra, J.E. Garcia, D.A. Ochoa, A.P. Barranco, O.G. Zaldivar and F.C. Pinar, J. Mater. Sci., **47** (2012) 5715.

[13] L.B. Kong, J. Ma and T.S. Zhang, J. Mater. Res., **16 [6]** (2001) 1636.

[14] L.B. Kong, J. Ma, W. Zhu and O.K. Tan, J. Allo. Comp., **322** (2001) 290.

[15] F. Gao, X. Dong, C. Mao, F. Cao and G. Wang, J. Am. Ceram. Soc., **94 [12]** (2011) 4162.

[16] A. Kumar, V.V.B. Prasad, K.C.J. Raju, R. Sarkar, P. Ghoshal and A.R. James, Defence Science Journal, Submitted.

[17] S. Roy, A.R. James, S. Bysakh, J. Subrahmanyam, Metals Mater. Proces., **19 [1-4]** (2007) 143.

[18] C.A. Randall, N. Kim, J.P. Kucera, W. Cao, and T.R. Shrout, J. Am. Ceram. Soc., **81 [3]** (1998) 677.

[19] N. Kim, Grain Size Effect on the Dielectric and Piezoelectric Properties in Compositions Which are Near the Morphotropic Phase Boundary of Lead Zirconate Titanate Based Ceramics; Ph.D. Thesis, The Pennsylvania State University (1994).

[20] W. Hackenberger, M.J. Pan, V. Vedula, P. Pertsch, W.Cao, C. Randall, T.R. Shrout, SPIE Conf. on Smart Mater. Tech., San Diego, CA, March Proc. SPIE 3324 (1998) 28.

[21] T.M. Kamel and G. de With, Grain size effect on the poling of soft $Pb(Zr,Ti)O_3$ ferroelectric ceramics, J. Euro. Ceram. Soc., 28 (2008) 851-61.

[22] D. Damjanovic, Rep. Prog. Phy., **61** (1998)1267.

[23] W. Cao, C.A. Randall, J. Phys. Chem. Solids, **57 [10]** (1996) 1499.

Chapter-IV

Dielectric studies on PLZT ceramics

4.1 Introduction

In this chapter, the dielectric properties of different compositions of PLZT ceramics were studied for the optimization of La substitution at the A-site of PZT ceramics as well as the milling parameters such as milling vial and milling duration. As discussed in chapter-3, the highly reactive nature of the nano size HEM milled PLZT powders enables the formation partial perovskite phase at room temperature which is confirmed by XRD patterns. The use of cold isostatic pressing for the compaction of fine scale nano PLZT powders results in a higher density > 98% with dense and closely packed microstructure as shown in SEM images of sintered PLZT ceramics. All of these micro-structural improvements help in achieving the optimum dielectric properties.

In this present study dielectric measurements for the PLZT ceramics suggest that the La modification affects the nature of the ferroelectric phase transition of PZT and deviates towards diffuse type phase transition (DPT). Some of the parameters, which describes the DPT, such as the degree of deviation from the Curie-Weiss law (ΔT_m), diffuseness empirical parameters γ and ΔT_{diff} were calculated for the different compositions of PLZT ceramics at 1kHz as well as for PLZT 8/60/40 ceramics at various frequencies. The value of γ ($1<\gamma<2$) and the large value of ΔT_{diff} at measured frequencies confirms the deviation of phase transition and the high degree of disorderliness in the material.

4.2 Literature survey

As we know that physical properties of ABO_3 type materials can be affected by a suitable ionic substitution at different atomic sites. The adjustment in the composition ratio of different cations leads to a very sensitive zone, called as the MPB, which is separated by two or more phase regions. For PZT solid solutions, optimum piezoelectric activity was found in the region which is separated by tetragonal (P4mm) and rhombohedral (R3c) phases **[1]**. The La modified PZT system (PLZT) shows many fold improvement in dielectric, ferroelectric, electro-optic, pyroelectric and piezoelectric properties **[1-2]**. However, high solubility of La in the oxygen octahedral PZT structure decreases the stability of the ferroelectric phases in favor of the paraelectric and antiferroelectric phases and phase diagram shows a reduction of the T_c with increasing La content **[3-4]**.

PZT ceramics show a normal phase transition with a narrow dielectric peak at the transition temperature (T_c) **[4-7]**. However, some other lead based systems such as modified PZT (PLZT x/65/35) **[6-11]** and PMN based systems show the relaxor type phase transition **[12-13]**. Not only the above mentioned lead based ceramics but also some other material lead free systems such as BZT-BCT **[14]**, Zn-doped BCZT **[15]** and BS-NBT-PT **[16]** shows the deviation from the normal phase transition. Substitution of La on the A-site of PZT system modifies the MPB **[17]**, which results in the

deviation from the normal phase transition to diffuse type phase transition (DPT). Improved electrical properties were observed for the PLZT ceramics which shows the broadened dielectric peak at the transition temperature. This broadened phase transitions can be attributed to structural disorder and compositional fluctuations in the PLZT solid solutions **[18]**.

The effect of A or B sites modification of PZT ceramics on the dielectric properties by different single or double dopants was reported by several researchers **[5, 19-26]**. However, PLZT x/60/40 ceramics, which shows an incomplete or diffuse type phase transition, is not well explained. The aim of this chapter is the investigation of dielectric properties of off-valent La^{+3} donor substitutions in PZT ceramics. The nature of the ferroelectric phase transition of PLZT x/60/40 ceramics will be also discussed.

4.3 Frequency dependence of dielectric properties of PLZT ceramics

Frequency dependent dielectric constants and losses studied are very important and used here to see the effect of (i) La substitution in PLZT x/60/40 ceramics and (ii) PLZT 8/60/40 ceramics that were milled for different durations with the help of Agilent E-4980A LCR from 20 Hz to 2 MHz frequency range.

4.3.1 Compositional dependence of dielectric properties of PLZT ceramics

Fig. 4.1 shows the change in dielectric constant (hereinafter referred as K) and loss as a function of frequency, respectively for the basic PZT ceramic system as well as La^{+3} substituted (2 to 10%) in the frequency range from 20 Hz to 2 MHz. The rate of change in the dielectric constant and loss with respect to the frequency was found to be almost same for all PLZT compositions. However, 8% lanthanum substituted PLZT ceramics show the high dielectric constant in the frequency range from 20 Hz to 2 MHz (Fig. 4.1).

Fig. 4.2 shows the room temperature dielectric constant and dielectric loss graph for PLZT ceramics as a function of lanthanum substitution. Both the parameters show a change with an increase in lanthanum substitution. From fig. 4.2 it is clear that the dielectric constant increases with lanthanum substitution and its maximum value was found for the PLZT 8/60/40 ceramics and then comes down. Fig. 4.2 shows a significant, drop in the dielectric loss for 8% La substituted PZT ceramics, where the dielectric constant is highest. PLZT 8/60/40 system show ~6 times increase in room temperature dielectric constant compared to the basic PZT system. All the room temperature measured dielectric parameters are listed in Table-4.1.

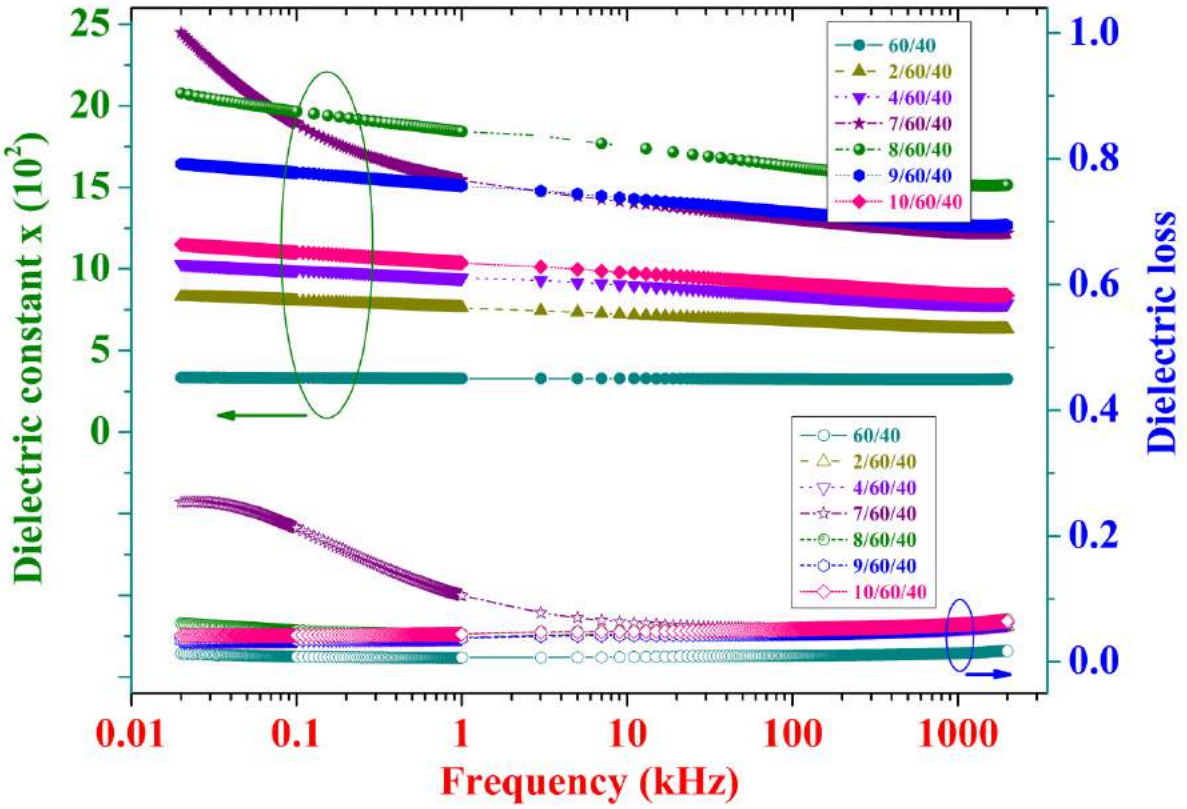

Fig. 4.1 *Room temperature dielectric constant and loss vs. frequency graph over 20 Hz to 2 MHz for PLZT x/60/40 ceramics.*

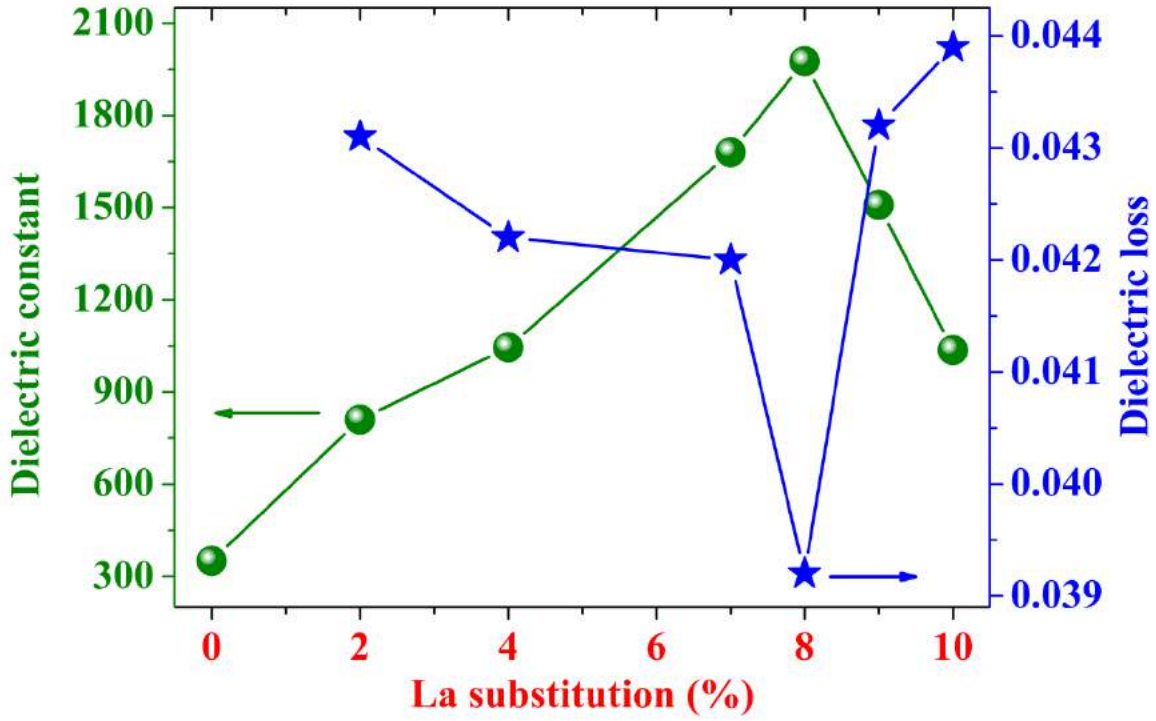

Fig. 4.2 *Room temperature dielectric constant and loss of PLZT x/60/40 ceramics, measured at 1 kHz.*

Table-4.1 *Room temperature dielectric properties of PLZT x/60/40 ceramics, measured at 1 kHz.*

Compositions	K	D
60/40	350	0.0077
2/60/40	811	0.0431
4/60/40	1045	0.0412
7/60/40	1681	0.0425
8/60/40	1976	0.0392
9/60/40	1509	0.0432
10/60/40	1036	0.0439

4.3.2 PLZT 8/60/40 ceramics milled in different vials

In the previous section, we found that PLZT 8/60/40 ceramics that was prepared by 8% La substitution in the A-site of basic PZT system shows the highest dielectric constant and lowest dielectric loss. This composition was further used to study the effect of milling vials on the dielectric properties by milling PLZT 8/60/40 using different milling vials made of agate and zirconia, respectively. Dielectric constant and loss for PLZT 8/60/40 ceramics milled with different vials are given in Table-4.2 shows that ceramics milled in zirconia vials have better properties than agate milled ceramics.

Table-4.2 *Room temperature dielectric properties of PLZT 8/60/40 ceramic milled with different vials, measured at 1 kHz.*

Milling vials	K	D
Zirconia vial	2336	0.0425
Agate vial	1976	0.0392

4.3.2 PLZT 8/60/40 ceramics milled for different time durations

Fig. 4.3 shows the dielectric constant and dielectric loss vs. frequency within the frequency range from 20 Hz to 2 MHz for the PLZT 8/60/40 ceramics milled for different time durations (1h to 10h). The figure also shows that the rate of change dielectric constant and loss with respect to the frequency is almost same for the PLZT 8/60/40 ceramics milled for different durations, however, 5 hours milled PLZT ceramics show the better properties.

Fig. 4.4 shows the change in room temperature dielectric constant and dielectric loss graph for PLZT ceramics as a function of milling time. The highest dielectric constant and low dielectric loss were found for the PLZT 8/60/40 ceramics that was milled for 5 hours. All the room temperature measured dielectric parameters are listed in Table-4.3.

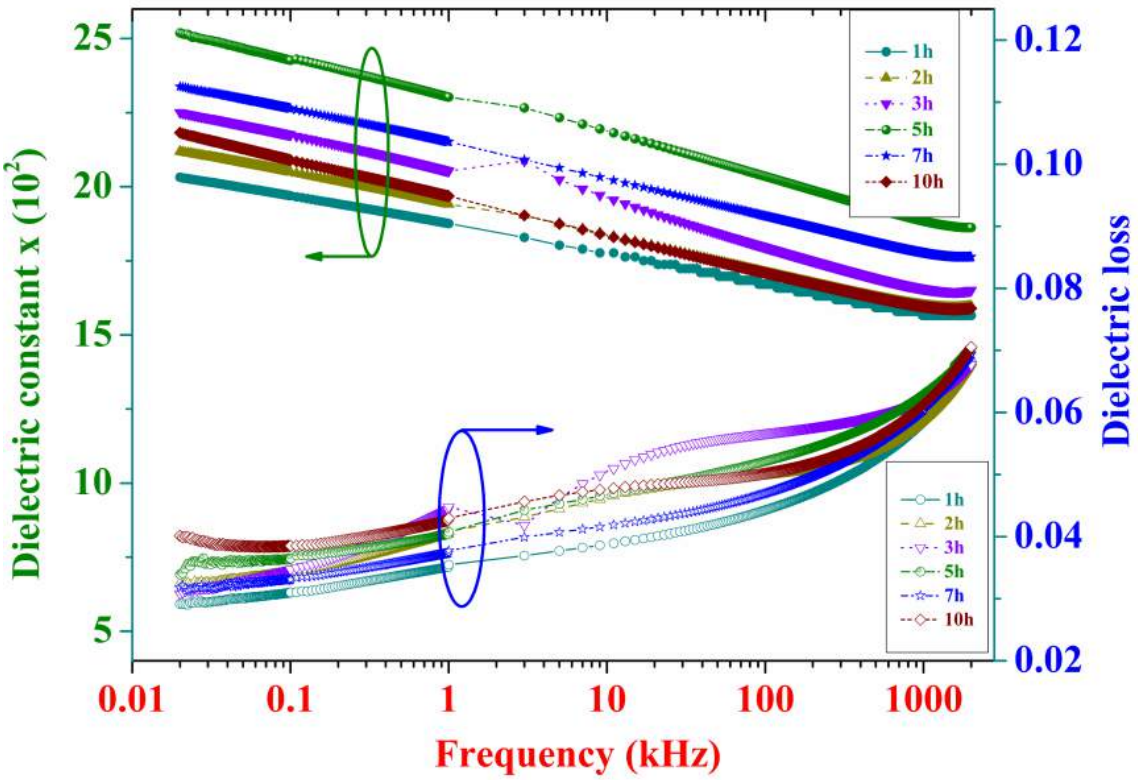

Fig. 4.3 *Room temperature dielectric constant and loss vs. frequency graph over 20 Hz to 2 MHz for PLZT 8/60/40 ceramics milled for different time durations.*

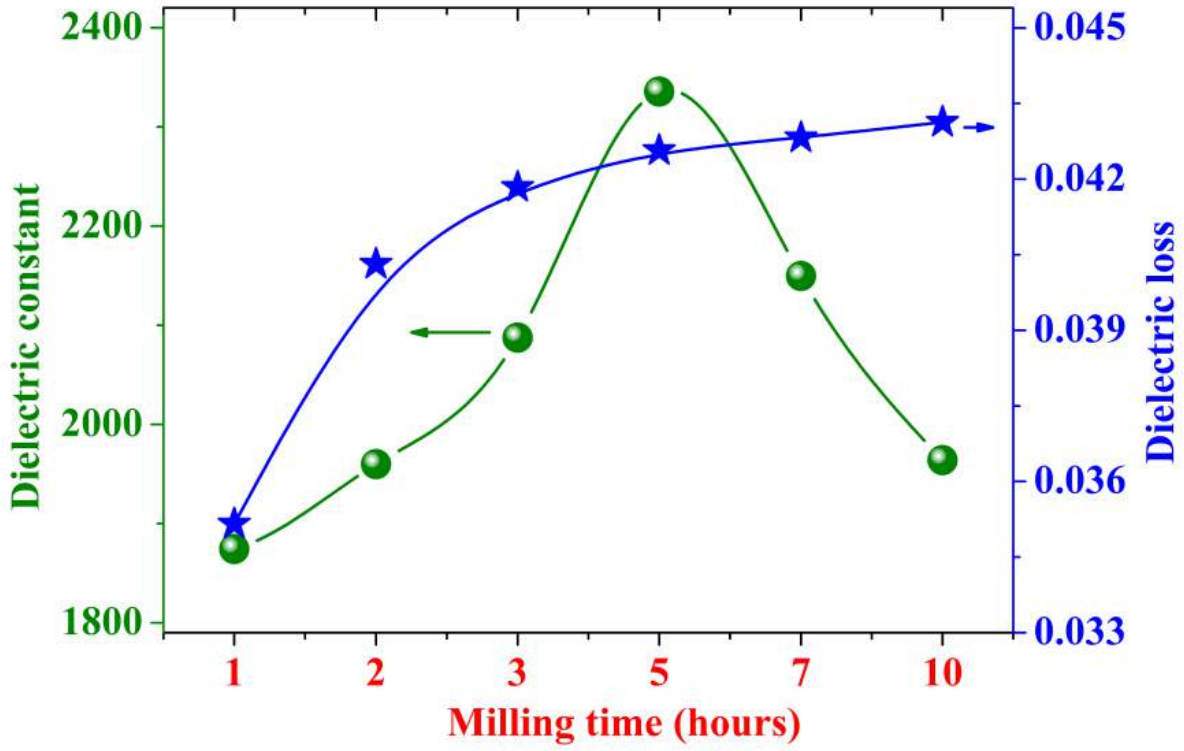

Fig. 4.4 *Room temperature dielectric constant and loss for PLZT 8/60/40 ceramics milled for different time durations, measured at 1 kHz.*

Table-4.3 *Room temperature dielectric properties of PLZT 8/60/40 ceramics milled for different durations and measured at 1 kHz.*

Milling durations	K	D
1h	1874	0.0352
2h	1960	0.0403
3h	2088	0.0418
5h	2336	0.0426
7h	2150	0.0428
10h	1964	0.0431

4.4 Temperature dependent dielectric property studies and the nature of phase transition of PLZT x/60/40 ceramics

In previous section 4.3, it was confirmed that the La substitution affects the room temperature dielectric properties of PZT ceramics. In this section, the temperature dependent dielectric studies are done to determine the nature of the ferroelectric phase transition of PLZT ceramics.

4.4.1 Compositional dependence of the dielectric properties of PLZT ceramics

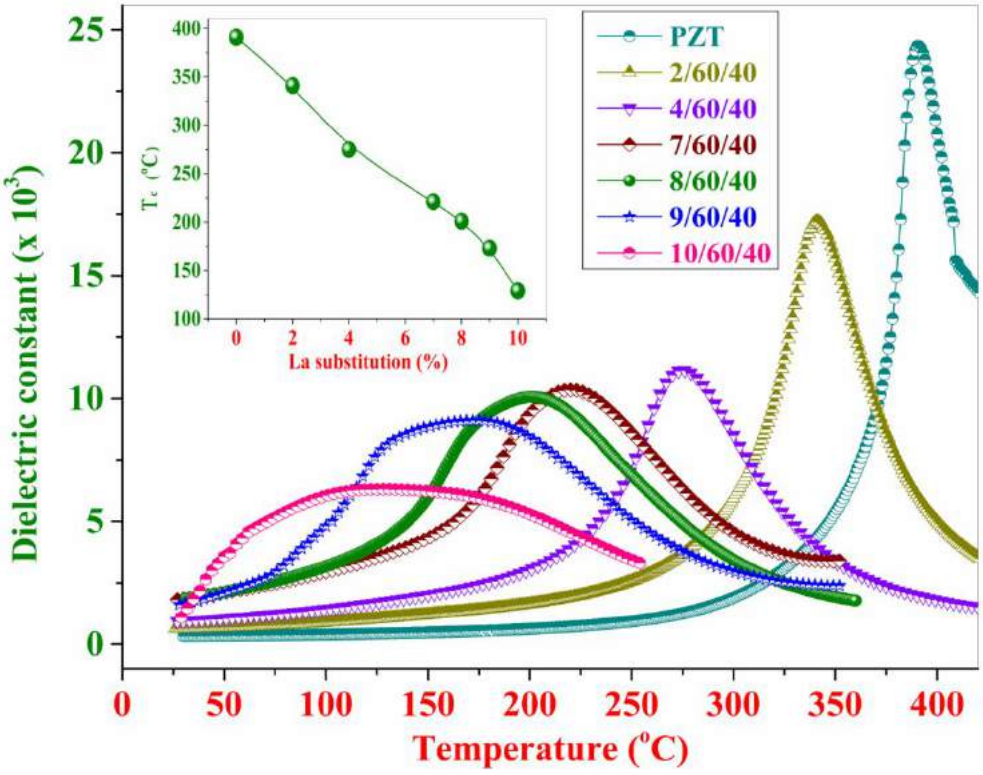

Fig. 4.5 *Dielectric constant vs. temperature graph for PLZT x/60/40 ceramics, measured at 1 kHz. Inset of the fig. shows the change in transition temperature with lanthanum substitution.*

Figs. 4.5 and 4.6 show the temperature dependent dielectric constant and loss for the lanthanum substituted PZT ceramics, respectively. From fig. 4.5 it is clear that basic PZT system shows paraelectric to ferroelectric phase transition at very high transition temperature (T_c=T_m~391^oC) with a sharp peak. As the lanthanum substitution increases in the PZT system, this sharp peak becomes broader and broader owing to the fact that lanthanum substitution affects the phase transition, shifting towards diffuse type phase transition. Inset of the fig. 4.5 shows the change in transition temperature as a function of La content in PLZT ceramics. The transition temperature of PLZT ceramics reduces as a function of increasing lanthanum substitution.

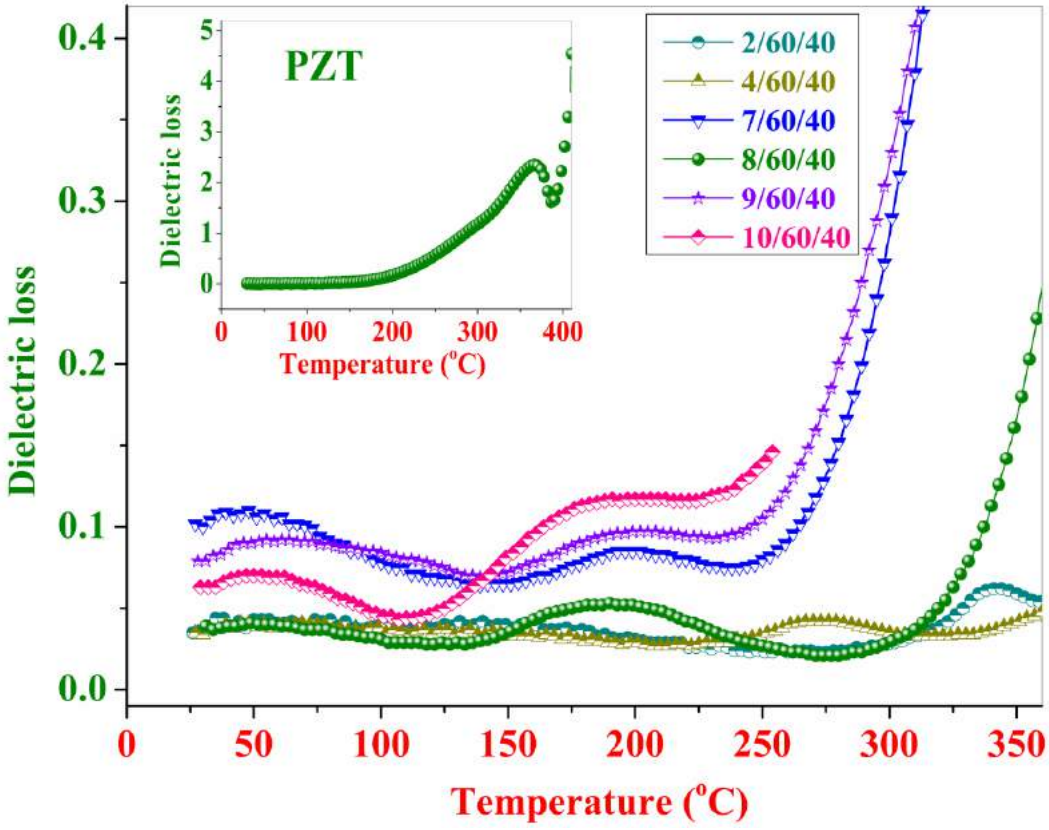

Fig. 4.6 *Dielectric loss vs. temperature graph for PLZT x/60/40 ceramics, measured at 1 kHz. Inset of the fig. show the temperature dependent dielectric loss of PZT system.*

Fig. 4.6 showed the change in the dielectric loss as a function of temperature for different compositions of PLZT ceramics and was found less for the lanthanum substituted PLZT ceramics when compared with PZT ceramics (Inset of the fig. 4.6).

Fig. 4.7 and 4.8 show the dielectric constant and dielectric loss for different PLZT compositions, measured across transition temperature with varying frequencies. Basic PZT ceramics shows a very high dielectric constant (~24345) at dielectric maxima temperature when compared with La modified PZT. The value of dielectric loss for lanthanum substituted PLZT at T_c was found to be less (Fig. 4.8).

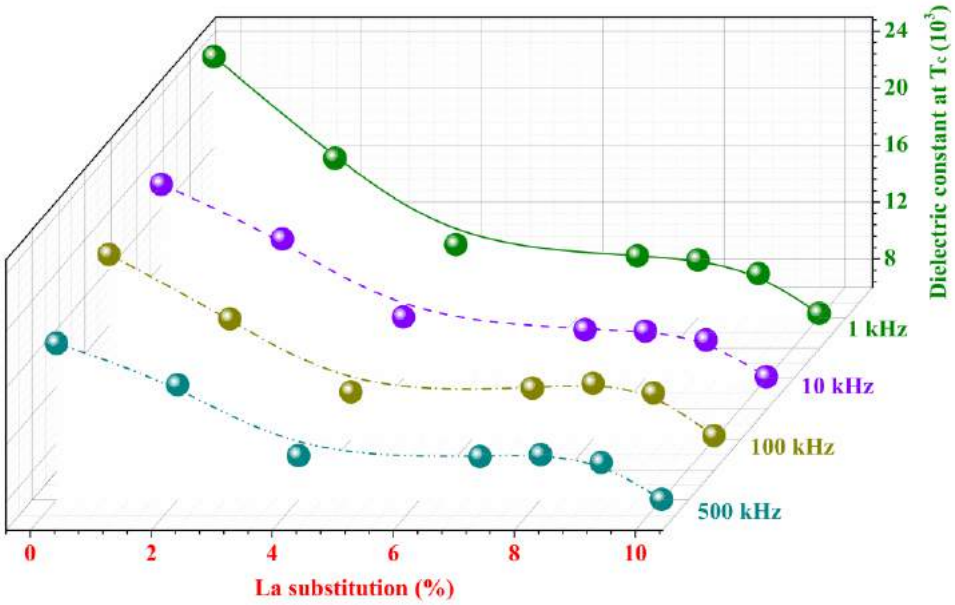

Fig. 4.7 *Change in dielectric constant as a function of lanthanum substitution measured at transition temperature for 1 kHz, 10 kHz, 100 kHz and 500 kHz.*

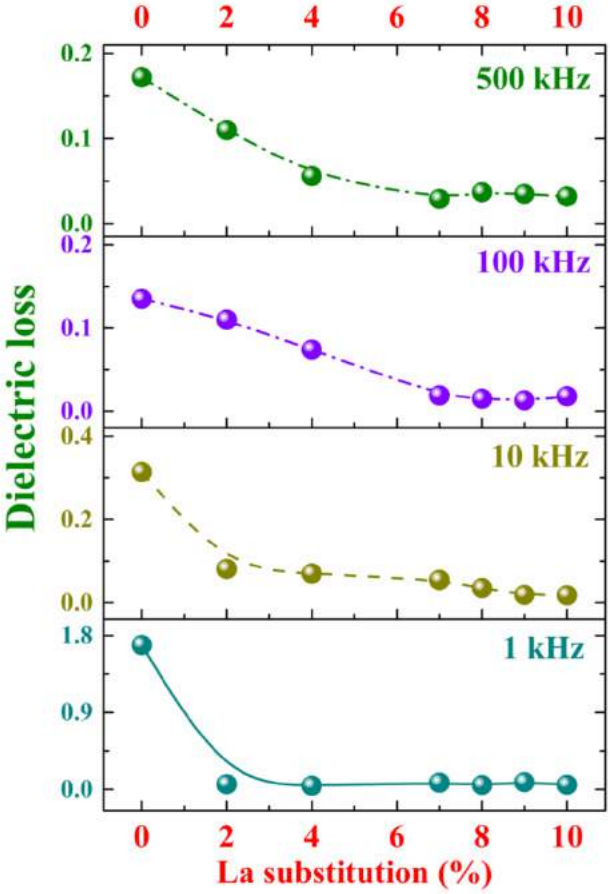

Fig. 4.8 *Change in the dielectric loss as a function of lanthanum substitution measured at transition temperature for 1 kHz, 10 kHz, 100 kHz and 500 kHz.*

Since the dielectric constant vs. temperature curve for the lanthanum substituted PLZT ceramics shows the broad peak, it suggests the deviation from the normal phase transitions. The equation used to evaluate parameters like ΔT_m which reflect the degree of deviation from the Curie-Weiss law is defined as

$$\mathbf{\Delta T_m = T_{cw} - T_m} \quad \text{..... (1)}$$

where T_{cw} denotes the temperature from which permittivity starts to deviate from the Curie-Weiss law and T_m represents the corresponding temperature of the maximum dielectric constant.

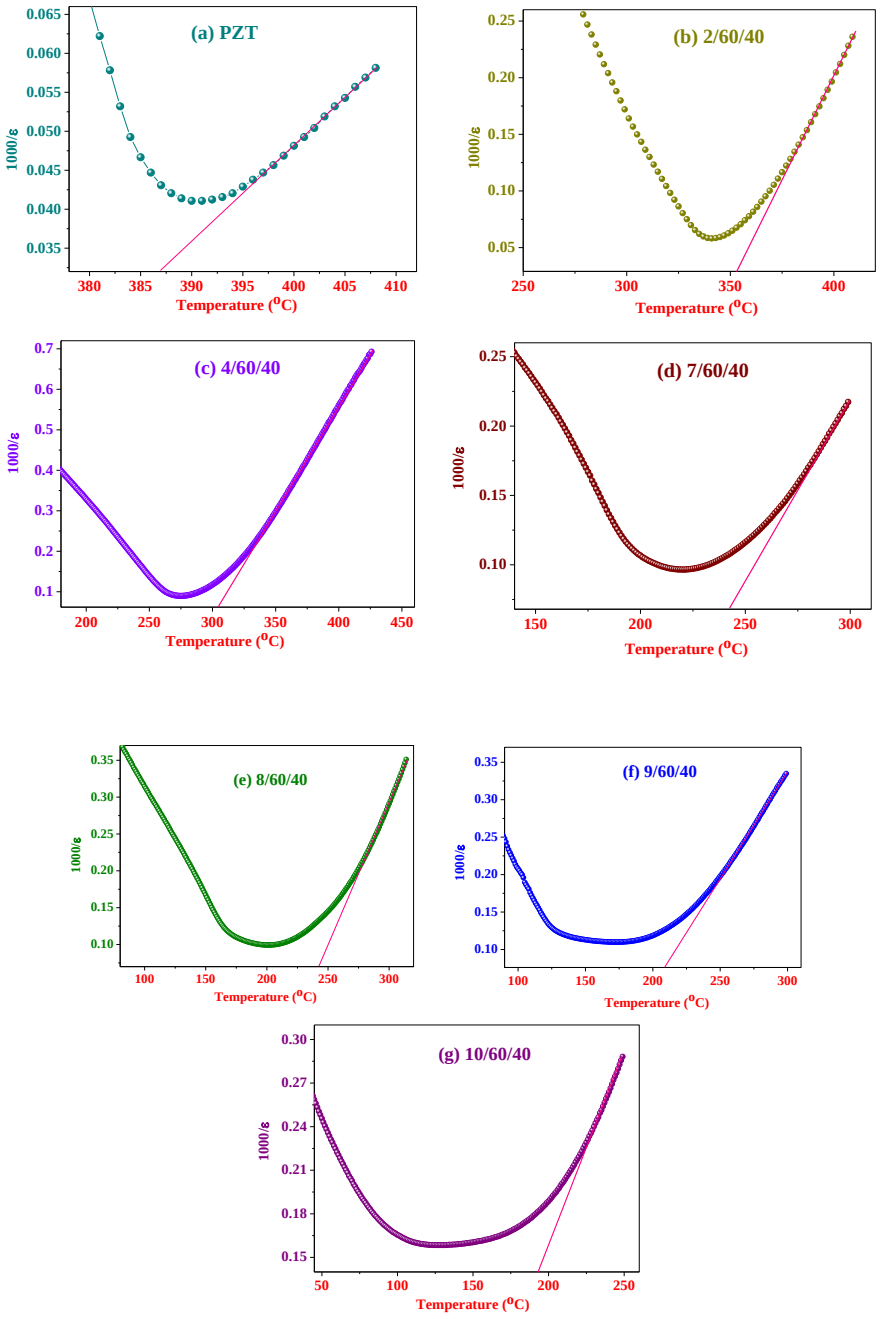

Fig. 4.9 *Reciprocal of the dielectric constant w.r.t. temperature for PLZT x/60/40 ceramics at 1 kHz.*

The reciprocal of dielectric constant as a function of temperature is shown in figs. 4.9 (a) to (g) for different compositions of PLZT ceramics. All the graphs were plotted at a frequency of 1 kHz. The linear fitting in dielectric constant vs. temperature graph, above transition temperature, provides plentiful information pertaining to the diffused transition behavior of PLZT x/60/40 ceramics. The linear fit of all composition (4.9 (a)-(g)) shows that the temperatures corresponding to the dielectric maxima (T_m) and the intercept of linear fitting on temperature axis do not coincide. This indicates a deviation from the normal phase transition. The deviated phase transition can be described as DPT or relaxor type phase transition, which will be discussed here.

To confirm the true nature of ferroelectric phase transition for PLZT x/60/40 ceramics, several parameters were calculated by using eq-(1) and discussed. The values of T_{cw} and ΔT_m were calculated for the PLZT x/60/40 ceramics and are given in Table-4.4. Fig. 4.10 shows the change in said parameters as a function of lanthanum substitution. Fig. 4.10 shows that the ΔT_m, which reflects the degree of deviation from the Curie-Weiss law, is increasing as lanthanum substitution increases.

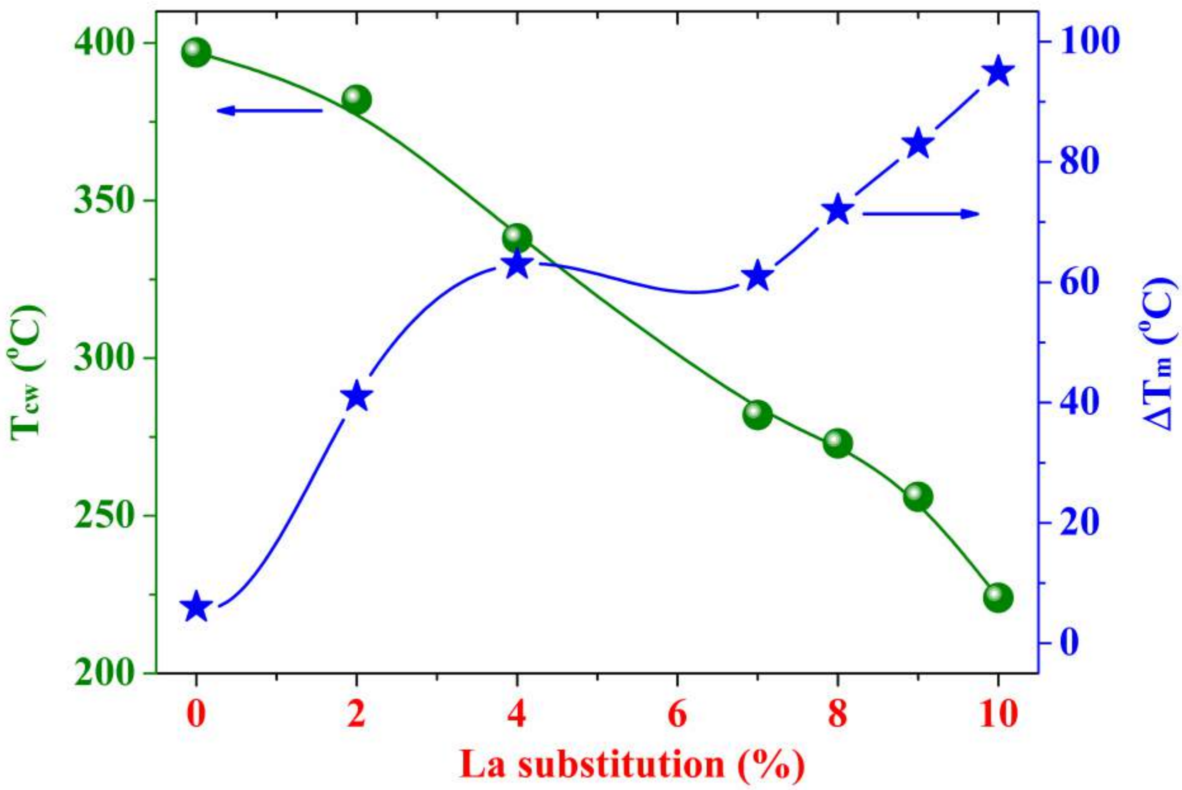

Fig. 4.10 *Change in the parameters related with the deviation from normal phase transition as a function of lanthanum substitution.*

The degree of diffuseness (γ) in the dielectric peak of PLZT ceramics can be quantified by using a modified empirical expression, which was proposed by Uchino et al. **[27]** as given in eq-(2),

$$\frac{1}{\varepsilon} - \frac{1}{\varepsilon_{max}} = \frac{(T - T_{\varepsilon max})^{\gamma}}{C_1} \quad \text{.......................................} (2)$$

where ε and ε_{max} are the dielectric constants at temperature T (T > T_c) and transition temperature (T_c), respectively. C_1 is a Curie like constant and γ is a diffuseness parameter, which gives information about the phase transition. The slope of the linear curve fit $\ln(1/\varepsilon - 1/\varepsilon_{max})$ vs. $\ln(T - T_m)$ was used for the calculation of diffuseness parameter. γ = 1 stands for the normal Curie-Weiss behaviour with sharp phase transition, while γ = 2 represents the complete relaxor type phase transition **[27-28]**.

The plots between $\ln(1/\varepsilon - 1/\varepsilon_{max})$ and $\ln(T - T_m)$ for the PLZT x/60/40 ceramics, which was used to determine the value of γ, are shown in fig. 4.11 (a) to (g). The value of γ from 1.49 to 1.98 (< 2) for PZT and PLZT 10/60/40 systems, respectively, confirms the occurrence of diffuse phase transitions in this material. There is a clear deviation from the Curie-Weiss type of phase transition. The large value of γ (Table-4.4) confirms the shifting of first-order to second-order phase transition and the presence of high degree of disorder in the material **[29-30]**.

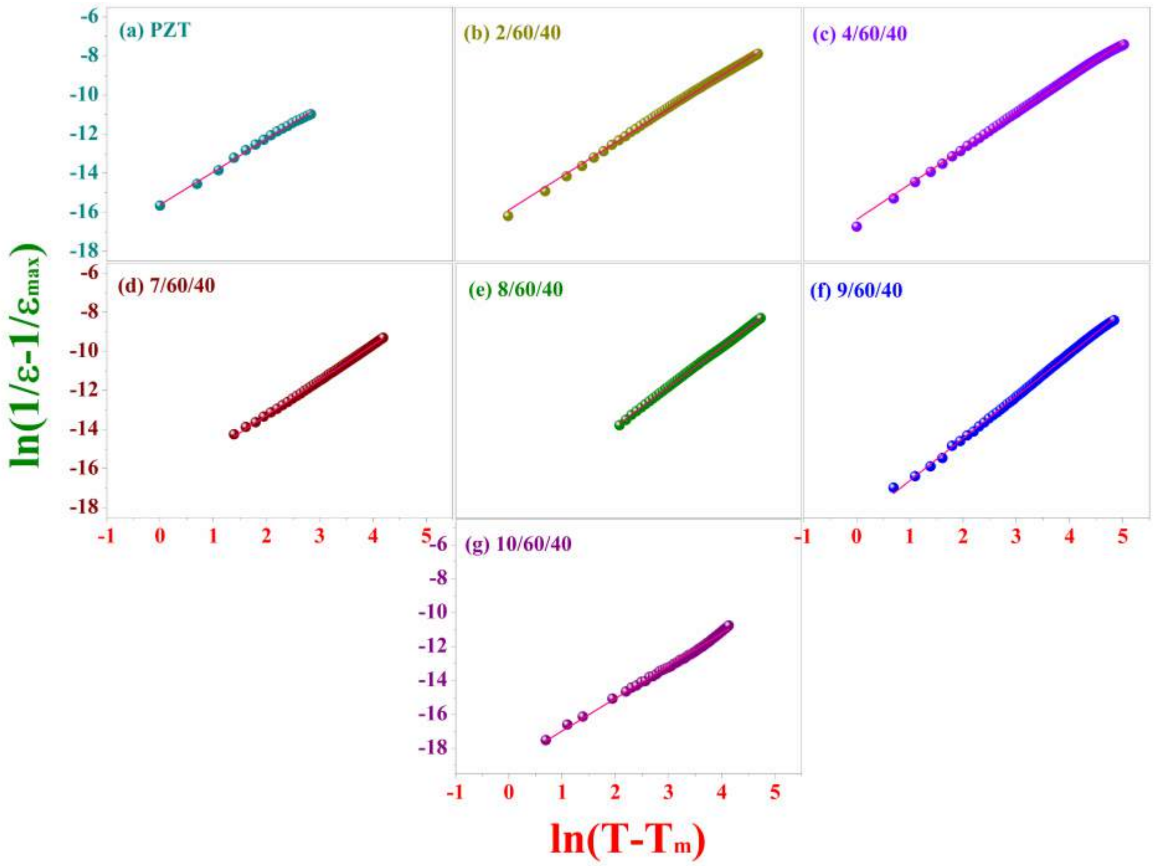

Fig. 4.11 *Fitting with empirical Curie-Weiss law for the PLZT x/60/40 ceramics at 1 kHz.*

The diffuseness of the phase transition can be described by an empirical parameter ΔT_{diff}, defined by eq-(3) **[31]**.

$$\Delta T_{diff} = T_{0.9\varepsilon max} - T_{\varepsilon max} \quad \ldots\ldots\ldots\ldots\ldots\ldots\ldots\ldots\ldots\ldots (3)$$

where $T_{0.9\varepsilon max}$ is the temperature corresponding to the 90% of the maximum dielectric constant, in the high-temperature side and $T_{\varepsilon max}$ is the temperature corresponding to the dielectric maxima peak. The calculated values of the empirical parameter for the different compositions of PLZT ceramics are given in Table-4.4. Fig. 4.12 shows the change in the diffuseness parameter γ and empirical parameter ΔT_{diff} as a function of lanthanum substitution. Both the parameters show an increase in their value as lanthanum substitution increases.

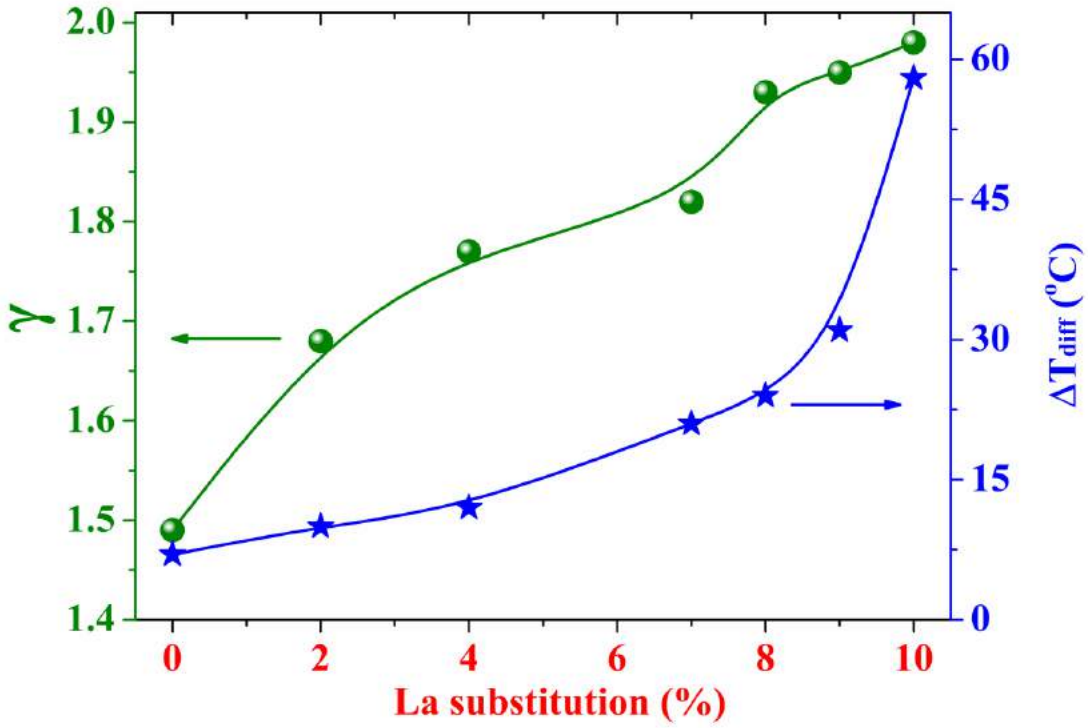

Fig. 4.12 *Change in the diffuseness parameter γ and empirical parameter ΔT_{diff} for PLZT x/60/40 ceramics, measured at 1 kHz.*

Table-4.4 *Temperature dependent dielectric properties of PLZT x/60/40 ceramics, measured at 1 kHz.*

Compositions	T_c (°C)	K (T_c)	D (Tc)	T_{cw} (°C)	ΔT_m (°C)	γ	ΔT_{diff} (°C)
60/40	391	24345	1.69	397	6	1.49	7
2/60/40	341	17211	0.061	382	41	1.68	10
4/60/40	275	11150	0.042	338	63	1.77	12
7/60/40	221	10364	0.079	282	61	1.82	21
8/60/40	201	10065	0.051	273	72	1.93	24
9/60/40	173	9102	0.086	256	83	1.95	31
10/60/40	129	6312	0.054	224	95	1.98	58

The temperature coefficient of permittivity (TC_ε) is defined as

$$TC_\epsilon = 100\frac{\epsilon_T - \epsilon_{RT}}{\epsilon_{RT}} \quad \text{..... (4)}$$

where $\in_T$ is the permittivity at any temperature T and $\in_{RT}$ is its room temperature value. The relative variations of the dielectric permittivity for different compositions of PLZT ceramics within the temperature range of 30˚C to 400˚C at 1 kHz are shown in fig. 4.13. Inset of the figure 4.13 shows the $TC_{\in}$ coefficient for the PZT system, which is very sharp when compared with La modified PZT compositions. The broadness of $TC_{\in}$ vs. temperature curves for different PLZT compositions also confirms diffuse phase transition.

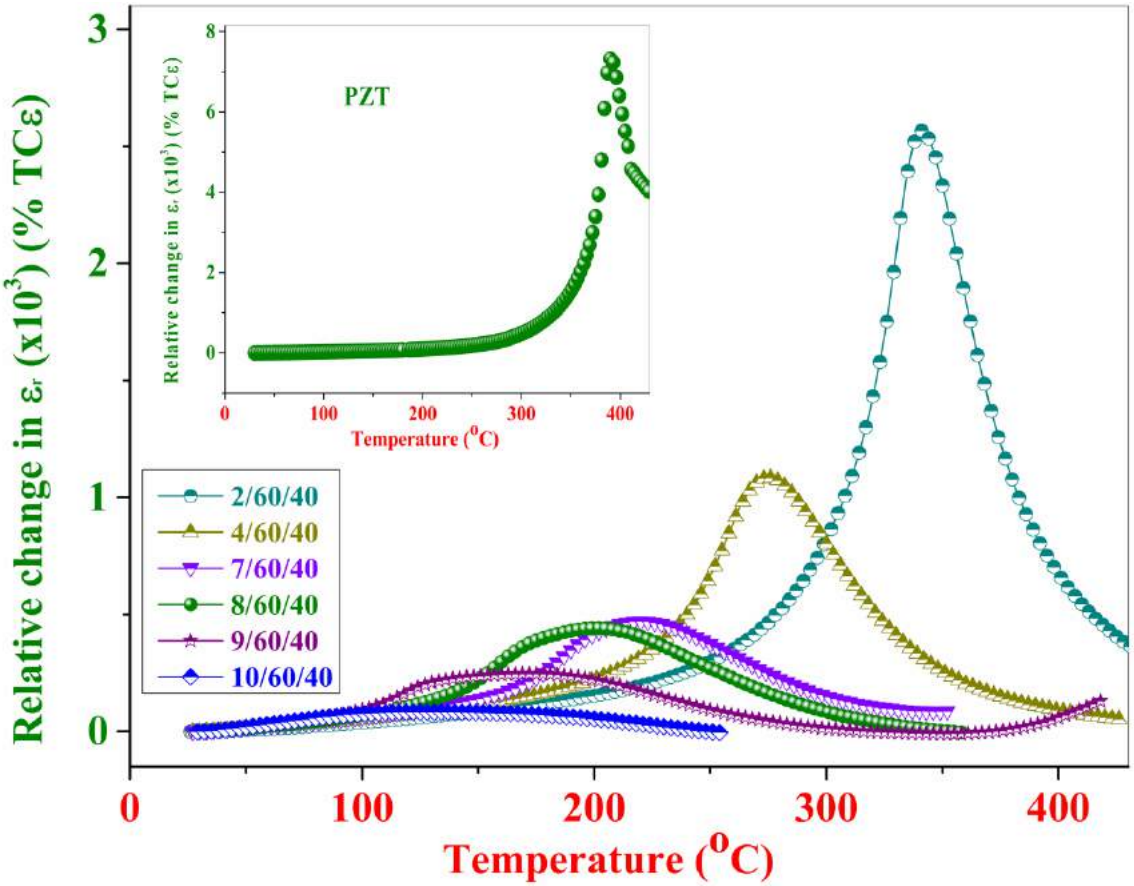

Fig. 4.13 *Variation of % $TC_{\in}$ for PLZT x/60/40 ceramics as a function of temperature at 1 kHz.*

4.4.2 PLZT 8/60/40 ceramics milled for 5 hours with zirconia vials

The dielectric studies for the PLZT 8/60/40 ceramics as a function of temperature at different frequencies was done to understand the nature of the ferroelectric phase transition. Figs. 4.14 (a), (b) and (c) show the dielectric constant and dielectric loss vs. temperature graphs of PLZT 8/60/40 ceramics at different frequencies (1 kHz to 500 kHz). Figs. 4.14 (a), (b) and (c) show the broadened dielectric constant vs. temperature curve rather than a sharp and narrow peak (as in normal ferroelectrics) around T_c, which is one of the most important characteristics of a disordered perovskite structure with a diffuse phase transition.

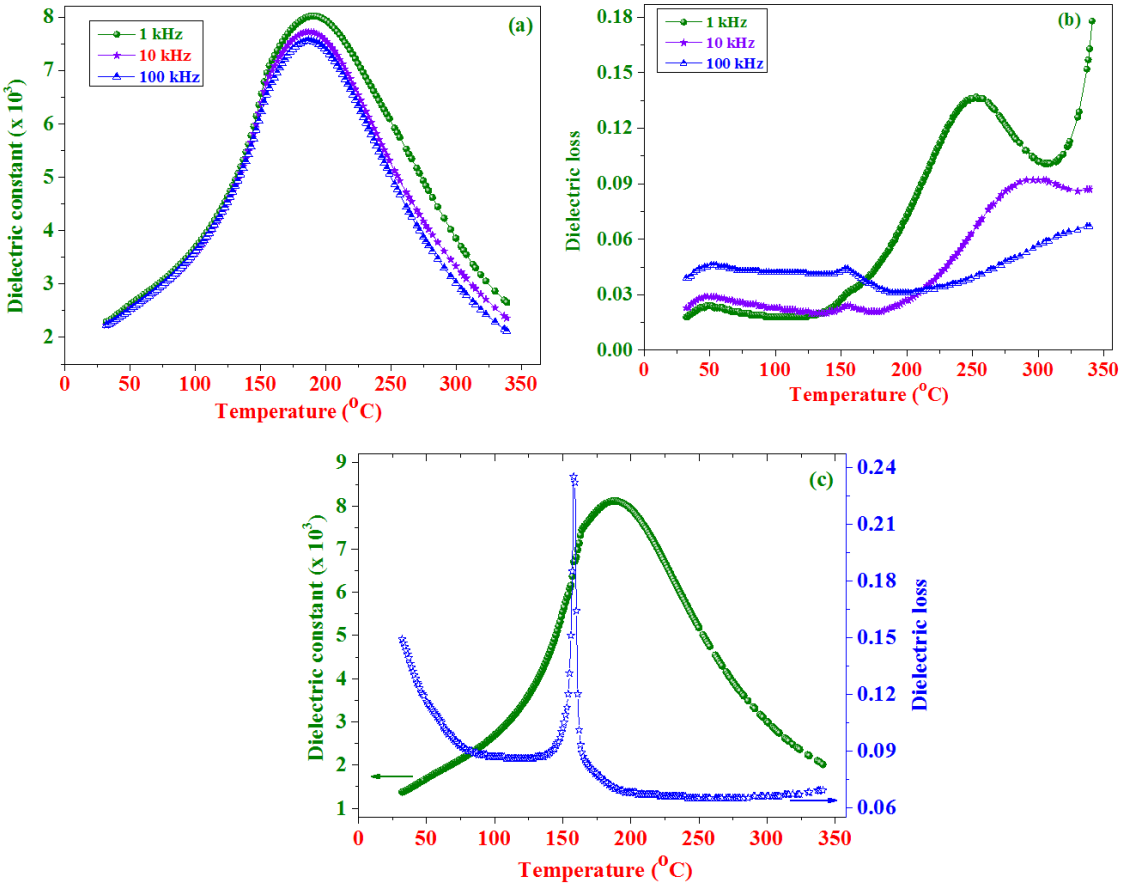

Fig. 4.14 *(a) Dielectric constant and (b) dielectric loss vs. temperature curves at various frequencies from 1 kHz to 100 kHz for PLZT 8/60/40 ceramics. Fig. (c) shows the dielectric constant and loss vs. temperature curve at a frequency of 500 kHz.*

Figs. 4.15 (a) to (d) show the reciprocal of dielectric constant as a function of temperature at different frequencies ranging from 1 kHz to 500 kHz.The linear fitting for the reciprocal of dielectric constant at temperatures above T_c gives more information about DPT behavior of PLZT ceramics. The linear fitting for the reciprocal of dielectric constant shows the dielectric maxima temperature and the intercept of linear fitting on temperature axis do not coincide, which is clear indication of deviation from the normal to DPT or relaxor type phase transition. Just as in the case of PLZT x/60/40 ceramics in the previous section 4.4.1, here also several parameters which are related to the diffusive transition of relaxor nature were calculated and discussed by using the eq-(1) and are given in Table-4.5.

Figs. 4.16 (a) to (d) show the plots between the $\ln(1/\varepsilon - 1/\varepsilon_{max})$ vs. $\ln(T - T_m)$ for PLZT 8/60/40 ceramics at different frequencies. A linear relationship was observed for different frequencies. The slope of the fitted $\ln(1/\varepsilon - 1/\varepsilon_{max})$ vs. $\ln(T - T_m)$ curves was used to determine the value of γ, which was found to be 1.98, 1.95, 1.97 and 1.94 (< 2) for frequencies of 1 kHz, 10 kHz, 100 kHz and 500 kHz, respectively. This large value of γ (Table-4.5) is the confirmation of the deviation from the Curie-Weiss type phase transition to DPT phase transition for PLZT 8/60/40 ceramics **[29-30]**.

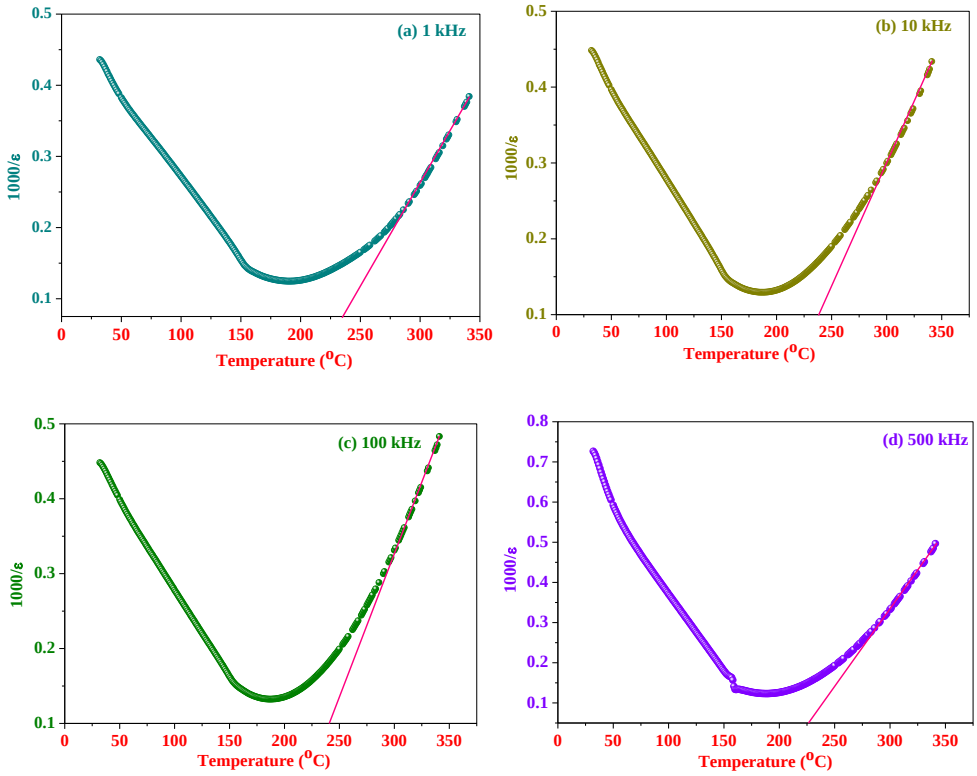

Fig. 4.15 *Reciprocal of the dielectric constant w.r.t. temperature for the PLZT 8/60/40 ceramics at various frequencies (a) 1 kHz (b) 10 kHz (c) 100 kHz and (d) 500 kHz.*

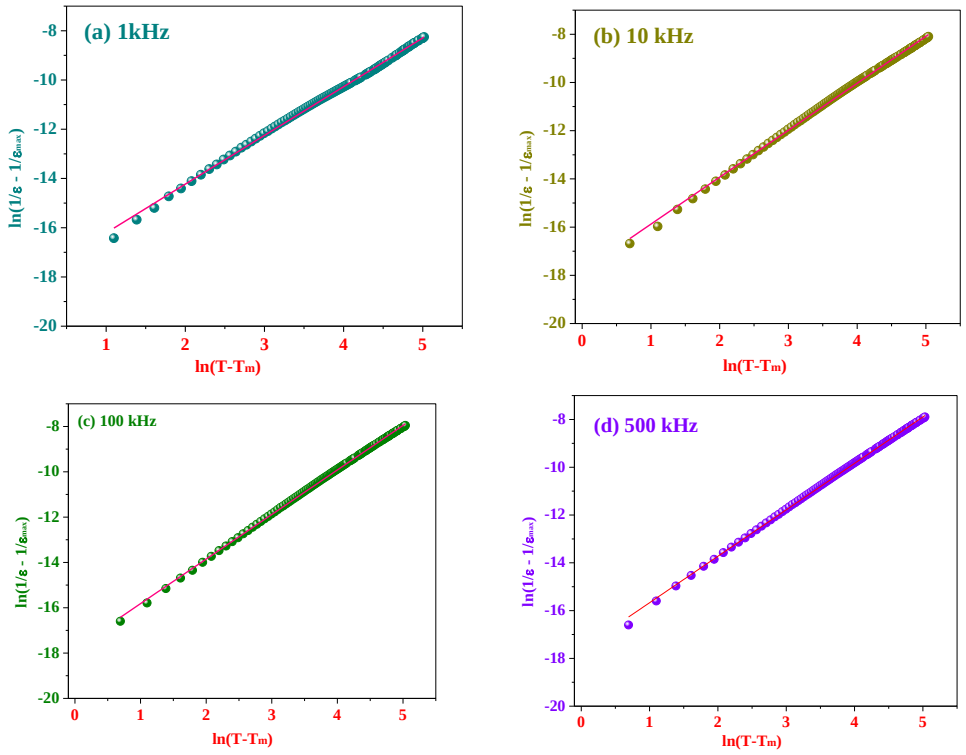

Fig. 4.16 *Fitting with empirical Curie-Weiss law for the PLZT 8/60/40 ceramics at different frequencies (a) 1 kHz (b) 10 kHz (c) 100 kHz and (d) 500 kHz.*

Table-4.5 *Dielectric properties for PLZT 8/60/40 5h milled ceramics*

Parameters	1 kHz	10 kHz	100 kHz	500 kHz
γ	1.98	1.95	1.97	1.94
ΔT_{diff}	33	39	29	26
T_{cw}	286	291	295	282
ΔT_m	96	104	108	94

4.5 Discussion

The variation in dielectric constant and loss with frequency for both cases (first different compositions of PLZT ceramics (Fig. 4.1) and second PLZT 8/60/40 ceramics milled for different durations (Fig. 4.3)) shows that these parameters decrease with increasing frequency (up to 1 kHz). This shows a dispersion in the lower frequency range, which almost stabilizes at higher frequency region. The dielectric dispersion at lower frequencies can be attributed to the space charge polarization arising from fine changes in the micro-structural features (impurities, porosity, density and grain structure) and due to non-stoichiometry which can occur due to PbO loss. At higher frequency, very little change (independent of frequency) was found in dielectric constant and loss with frequency. Thereafter, dispersion in the ceramics is due to the Maxwell-Wagner **[32-33]** type interfacial polarization. The dielectric constant for polar materials is explained by contributions of multiple components of polarizability like deformational (electronic and ionic) and relaxational (oriental and interfacial) polarization. The orientation polarization decreases as frequency increases since it takes more time than electronic and ionic polarization. This decreases the value of dielectric constant at lower frequencies, approaching a constant value at a higher frequency, which is related to the interfacial polarization **[34]**.

From figs. 4.2 and 4.4, it is clear that the PLZT 8/60/40 ceramics milled for 5 hours show the better dielectric properties than the rest of the compositions. These results can be attributed to the improvement in the microstructure (density, grain size and uniformity in grain size) along with intrinsic factors like the grains behaving more like strain free crystals. The dielectric constant of ferroelectric ceramics usually increases with increasing density. PLZT ceramics having a very fine (nano-meter region) and large grain sizes (micrometer region) showed lower dielectric constant **[28]**. In the case of PLZT ceramics having very fine grains, the magnitude of the dielectric constant gradually decreased probably due to the diminished mobility of the domain walls, which shows that at optimum conditions, ceramics have fewer defects and vacancies. The unclamped dipoles inside the grains are free to respond to the oscillating electric field with minimum restrictions yielding a higher dielectric constant with a lower value of the dielectric loss.

Figs. 4.5, 4.6 and 4.14 (a)-(c) shows the temperature dependent dielectric properties of the different compositions of PLZT ceramics and 5 hours milled PLZT 8/60/40 ceramics, respectively. These studies help to understand the nature of the ferroelectric phase transition of PLZT ceramics. Fig. 4.5 shows that an increase in the lanthanum substitution results in an increase in the broadening of the dielectric constant-temperature curve. It is also apparent from fig. 4.14 (a) and (c) that the variation of dielectric constant with temperature (30-350˚C) at different frequencies (1 kHz to 500 kHz) is a broadened curve rather than a sharp peak at T_c, which shows a disordered perovskite structure with the diffuse phase transition. This peak broadening in PLZT ceramics is believed to be due to compositional fluctuations and/or substitutional disordering in the arrangement of cations in one or more crystallographic sites of the structure, which leads to microscopic or nanoscopic heterogeneity in the compounds, with different local Curie points **[18, 23-24]**. These compositional fluctuations occur when Pb^{+2}, Zr^{+4} and Ti^{+4} are replaced by La^{+3}. The changes are ascribed to the lead vacancies (Donor dopants such as W^{6+}, Nb^{5+}, La^{3+}, Th^{4+}, Ta^{5+}, B^{3+} and Sb^{5+} cause Pb-vacancies by substituting a higher valence ion for Pb^{2+}) and the resulting increase in domain wall mobility **[25]**. Substitution of La^{+3} to the A-site of the PZT system enhances the domain reorientation. It also maintains the solid solution throughout the system. La modification in the PZT system decreases the stability of the ferroelectric phases for the paraelectric and antiferroelectric phases, which results in a reduction of the T_c with increasing lanthanum **[3]**. The reduction of T_c as a function of lanthanum substitution is also observed in this study as shown in the inset of fig. 4.5.

In this study, the value of peak dielectric constant obtained is found to be less when compared with the previous reports of PLZT, which was measured at 10 kHz with grain sizes > 4 μm **[25]**. This may be due to fine grain sizes (< 1.5 μm) of the PLZT ceramics. As we know that the decrease in grain sizes increases the dilution effect exerted by the increasing number of non-ferroelectric grain boundaries, which results in the decrease in the magnitude of the dielectric constant. Figs. 4.14 (a) and (c), show a small shift in Curie temperature as a function of frequency and the temperatures of peak dielectric constant and peak dielectric loss do not coincide. This temperature difference can be the consequence of temperature dependent relaxation near Curie temperature indicated by the Kramers-Krönig relation **[18]**.

Figs. 4.6 and 4.14 (b)-(c) shows the change in the dielectric loss as a function of temperature for PLZT x/60/40 ceramics and 5 hours milled PLZT 8/60/40 ceramics, respectively. The dielectric loss for the lanthanum substituted PLZT ceramics was found to be less (Fig. 4.6) compared to the PZT ceramics (Inset of fig. 4.6). The variation of dielectric loss with temperature for PLZT 8/60/40 ceramics from 1 kHz to 500 kHz is shown in figs. 4.14 (b) and (c). The dielectric loss of PLZT 8/60/40 ceramics was found to be very less for frequencies from 1 kHz to 100 kHz except for 500 kHz. Generally, for the electro-ceramics, dielectric loss increases as a function of temperature and frequency. The dielectric loss for the electro-ceramics is a measure of the residual charge on a capacitor after discharge. This phenomena is attributed to the polarization relaxation mechanism of

the ceramics. Usually, dielectrics with higher dielectric constant, which have more polarizing mechanisms show higher dielectric loss than lower K materials. The increase in the dielectric loss as a function of temperature is attributed to the increase in conduction current of the electro-ceramics. The conduction current can be divided into residual current or leakage current and absorption current. The dielectric material, under the application of dc voltage for a sufficiently long time, shows a constant leakage current known as a residual current.

Some of the perovskite oxides electro-ceramics, for example, titanates (BT, PZT and PLZT) does not have the charge balanced ratio (anions to cations). This condition leads to the imperfect stoichiometry in ceramics, which again results in the formation of charge carriers. This can be explained by the following example in which a Pb^{2+} cation is replaced by a La^{3+} cation, which leaves a net negative charge. This net negative charge shows a temperature dependent definite random mobility. The combined effect of all the defects, inhomogeneities, space charge formation, etc. produces a conduction current, which also results in dielectric losses. Generally, dielectric losses, in dielectric materials occur due to rotations and internal friction of dipolar molecules. The energy loss in the molecular transfer from one to another position is also one of the main reasons of dielectric losses. Since the dipole mechanism in electro-ceramics is a temperature and frequency dependent phenomena hence the dielectric loss caused by the dipole mechanism obtain its maximum value at a certain temperature and definite frequency. The change in the dielectric loss of electro-ceramics as a function of temperature and frequency is related to the effects of various polarization mechanisms. However, when the temperature of the ceramics rises, the resulting drop in viscosity experienced by the rotating dipoles exert a double effect on the amount of losses. These losses occur not only due to an increase in the degree of dipole reorientation but also the friction between the rotating dipoles. There is a reduction in energy required to overcome the resistance of the viscous medium. In a polar substance with an increase in temperature, not only do the dipole reorientation losses increase but also electrical conduction losses **[35]**.

The dielectric loss was found to be very low except for the frequency at 500 kHz, which shows an unusual dielectric loss peak. It was also found that with an increase in frequency, dielectric constant of the PLZT 8/60/40 ceramics at transition temperature show a decrease except for 500 kHz frequency at which the dielectric constant slightly increases. Since for the dielectric studies poled PLZT ceramics was used, which show the resonance effect due to the poling phenomenon. The resonance phenomena at high temperature will be given in Chapter-7.

The electro-ceramics, which show the broad dielectric peak at their transition temperature, revealed that high temperature piezoelectric activity, well above the dielectric maxima. The diffuse phase transition occurs in a temperature range called as the Curie range, above which ceramics do not show any ferroelectricity **[18]**. The existence of polarization, after dielectric maxima temperature for the materials showing DPT and relaxor phase transition, can be explained on the basis of the existence of Polar Regions. The relaxor behavior in ferroelectrics is believed to be the consequence of the

presence of dynamic polar nano-regions which are ever more active and are of fine scale in the vicinity of T_m in a classical relaxor system. With an increase in temperature, the direction of a net polarization (P_s) fluctuates or becomes very dynamic. The short-range interactions between the Polar Regions control the fluctuations of P_s, leading to its freezing at a characteristic temperature far below the T_m **[36]**.

4.6 Summary

Dielectric properties for the La^{+3} substituted PLZT x/60/40 and PLZT 8/60/40 ceramics, which were prepared by high energy mechano-chemical ball milling at different durations, were studied in detail. The temperature dependent dielectric measurements for the PLZT x/60/40 and PLZT 8/60/40 ceramics suggest that the La substitution affects the nature of ferroelectric phase transition of PZT. The PLZT Ceramics shows a deviation from normal to the diffuse type phase transition (DPT). This diffuse phase transition for the PLZT ceramics is explained based on many parameters such as the diffuseness parameter (γ), the degree of deviation from Curie-Weiss law (ΔT_m) and empirical parameters (ΔT_{diff}). All the said parameters were calculated at various frequencies from 1 kHz to 500 kHz by using different equations and fitting curves. The large value of diffuseness parameter (γ) ($1<\gamma<2$) and empirical parameters (ΔT_{diff}) for PLZT ceramics at different frequencies confirms the deviation from normal phase transition and the high degree of disorderliness in the material.

References

[1] B. Jaffe, W.R. Cook Jr., and H. Jaffe, Piezoelectric Ceramics, Academic Press, New York, Ch.-1 (1980).

[2] G.H. Haertling and C.E. Land, J. Am. Ceram. Soc., **54** (1971) 1.

[3] G.H. Haertling, J. Am. Ceram. Soc., **82** (1999) 797.

[4] M. Prabu, I.B. Shameem Banu, S. Gobalakrishnan and M. Chavali, J. Alloys Comp., **551** (2013) 200.

[5] R. Rai, S. Sharma, N.C. Sonia and R.N.P. Choudhary, Physica B, **382** (2006) 252.

[6] M. Plonska and Z. Surowiak, Molecular and Quantum Acoustics, **27** (2006) 207.

[7] S.K.S. Parashar and K. Parashar, Integ. Ferroelectrics, **121** (2010) 106.

[8] F. Fang, H. Gui and X. Zhang, Ferroelectrics, **175** (1996) 233.

[9] P.S. da Silva Jr., M. Venet and O. Florencio, J. Alloys Comp., **647** (2015) 784.

[10] R. Rai, S. Mishra and N.K. Singh, J.Alloys Comp., **487** (2009) 494.

[11] N. Kumar, P. Tirupathi, B. Kumar, M. Pastor, A.C. Pandey and R.N.P. Choudhary, Adv. Mater. Lett., **6[4]** (2015) 284.

[12] G.A. Smolenskii, A.I. Agranovskaya, Sov. Phys. Solid State (Eng. Transl.), **1 [10]** (1960) 1429.

[13] S.H. Baek, M.S. Rzchowski and V.A. Aksyuk, MRS Bulletin, **37** (2012) 1022.

[14] W. Wang, L.D. Wang, W.L. Li, D. Xu, Y.F. Hou and W.D. Fei, J. Alloys Comp., **624** (2015) 284.

[15] Z. Zhao, X. Li, H. Ji, Y. Dai and T. Li, J. Alloys Comp., **637** (2015) 291.

[16] Z. Yao, Z. Song, H. Liu, H. Hao, M. Cao and Z. Yu, J. Alloys Comp., **577S** (2013) S488.

[17] W.Z. Zhu, A. Kholkin, P.Q. Mantas and J.L. Baptista, J. Mater. Sci., **36** (2001) 4089.

[18] M.E. Lines and A.M. Glass, Principles and Applications of Ferroelectrics and Related Materials, Oxford: Oxford University Press (1977).

[19] R.N.P. Choudhary and J. Mal, Mater. Sci. Eng. B, **90** (2002) 1.

[20] A.K. Shukla, V.K. Agarwal, I.M.L. Das and J. Singh, Bull. Mater. Sci., **34[1]** (2011) 133.

[21] M. Adamczyka, L. Kozielski, A.L. Czekaj and D. Czekaj, J. Alloys Comp., **509** (2011) 6452.

[22] A.P. Barranco, J.D.S. Guerra, O.G. Zaldívar, F.C. Piñar, M.E. Mendoza, D.A. Hall and E.B. Araújo, Solid State Comm. **149** (2009) 1308.

[23] P. Goel, K.L. Yadav and A.R. James, J. Phys. D: Appl. Phys., **37** (2004) 3174.

[24] K.L. Yadav and R.N.P. Choudhary, Bull. Pure Appl. Sci.D, **14** (1995) 23.

[25] S.L. Fu, S.Y. Cheng and C.C. Wei, Ferroelectrics, **67** (1986) 93.

[26] S.R. Shannigrahi and R.N.P. Chaudhary, **5[3]** (2000) 201.

[27] K. Uchino and S. Nomura, Ferroelectrics Lett., **44 [3]** (1982) 55.

[28] D. Viehland and M. Wutting, L.E. Cross, Ferroelectrics, **120** (1991) 71.

[29] S.C. Jung, H.B. Park, J. Kim, K. Kim and S.J. Kim, J. Kor. Ceram. Soc., **31** (1994) 155.

[30] S.R. Shannigrahi, F.E.H. Tay, K. Yao and R.N.P. Choudhary, J. Eur. Ceram. Soc., **24** (2004) 163.

[31] K. Uchino, S. Nomura, L.E. Cross and R.E. Newnham, Phase Transitions, **2 [1]** (1981) 1.

[32] J.C. Maxwell, Electricity and Magnetism, Oxford University Press, London (1973).

[33] K.W. Wagner, Annals of Physics, **40** (1993) 818.

[34] S. Upadhyay and D. Omprakash, Bull. Mater. Sci., **19 (**1996) 513.

[35] B. Tareev, Physics of Dielectric Materials, English Translation, Meer Publishers, Moscow, Second Edition, Ch. 3 (1979).

[36] A. Bootchanont, N. Triamnak, S. Rujirawat, R. Yimnirun, D. P. Cann, R. Guo and A. Bhalla, Ceram. Inter. **40** (2014) 14555.

Chapter-V

Ferroelectric property studies on PLZT ceramics

5.1 Introduction

The present study deals with two types of ferroelectric hysteresis loops, polarization (P-E) and strain vs. electric field (S-E). Both hysteresis loops were traced using a sophisticated instrumentation system of M/S aixACCT GmbH Germany, based on the virtual ground method. All the necessary details, related to the measurement system are already given in Chapter-2. P-E hysteresis loops were used to calculate the remnant polarization (P_r) and coercive field (E_c) while S-E hysteresis loops were used for the calculation of piezoelectric charge coefficients (d_{33}). These values help to study the behavior of ferroelectric materials. A poling procedure is required to make the PLZT ceramics piezoelectrically active. Previous reports suggest that the PLZT 8/60/40 ceramics can be poled by applying an external electric field (poling electric field), higher than the coercive field.

In this chapter, the ferroelectric properties of different compositions of PLZT ceramics were studied that would help for the optimization of La substitution at the A-site of PZT ceramics. The effect of milling parameters such as milling vial and milling duration on the ferroelectric properties of the optimized PLZT system, P-E, S-E and related parameters were further measured. Generally, P-E hysteresis loop data are used for the evaluation of the coercive fields. However, current vs. electric field (I-E) curves also can be used for the same. In I-E curves, the field responsible for domain switching current peak is called the coercive field.

In this present study, not only the P-E and S-E loops were studied but also I-E loops were measured to support P-E studies. Apart from P_r, E_c and d_{33}, some other important parameters such as internal macroscopic electric field (E_{in}), domain switching current (I_{max}), the squareness of P-E loop, strain hysteresis, normalized strain coefficient (S_{max}/E_{max}) were also calculated. The polarization and strain vs. electric field hysteresis loop of PLZT 8/60/40 ceramics was measured at a different temperature in the temperature range of 30^{o}C to 170^{o}C. Temperature dependent ferroelectric studies are useful for the better understanding of ferroelectric phase transitions in PLZT 8/60/40 ceramics.

5.2 Literature survey

Ferroelectric hysteresis loops (P-E and S-E) are the source of important key information, which are required for the understanding of ferroelectric materials **[1]**. These studies reveal the true nature of the materials and help to confirm the ferroelectric behavior of the PLZT ceramics. The P-E hysteresis loops of ferroelectrics are the one of the most important electrical characteristics due to their similarity with the magnetization versus magnetic field loops of ferromagnetics. For ferroelectrics, iron is not an important component compared to the ferromagnetics. The value of P_r and E_c depends upon the type of dopants and modifiers. For lead based ferroelectrics the value of P_r changes from 30 to 40 μC/cm^2, whereas E_c varies from ~2 kV/cm to near electrical breakdown (~125 kV/cm) **[2]**.

In ferroelectrics, the fraction of switched domains or polarization reversal is described by uniform random nucleation of reversed domains according to the Kolmogorov-Avrami-Ishibashi (KAI) model with a single field domain-switching time t_0 under different voltages (V) **[3-6]**

$$\boldsymbol{p(t) = 1 - e^{-(t/t_0)^n}} \quad \text{..... (1)}$$

where t is the time elapsed after the application of the external field E, n=material parameter, which is related to the dimension of domain growth (n = 2 for 2D growth and n = 3 for 3D growth).

The Landau-Ginzburg (LG) mean field theory of ferroelectricity helps in the prediction of the intrinsic coercive field, which is responsible for the polarization reversal in ferroelectric materials **[7]**. This predicted the value of intrinsic E_c which is caused by localized nucleation of domains with reversed polarization is always larger than the experimentally measured value of the E_c for real ferroelectrics **[8-9]**. The Gibbs free energy density G can be described by the LG expansion in terms of electrical polarization P **[7, 10]**, which gives the intrinsic polarization hysteresis function P(E) for a given ferroelectric state (T_c). The ferroelectrics show the stable polar state below the phase transition temperature.

In the presence of an external electric field, ferroelectric materials also show strain-electric field hysteresis loops. The bipolar strain-electric field hysteresis loop which resembles the shape of a butterfly occurs due to the converse piezoelectric effect of the lattice as well as switching and movement of domain walls. In the presence of the low dc field, the S-E curves obey a linear relationship, corresponding to the piezoelectric effect. The switching of ferroelastic domain walls is believed to be due to the large hysteresis in bipolar S-E curves and the large negative strain in ferroelectrics **[11]**. The equation of state relating the electric and elastic variables can be written for converse piezoelectric effect **[1]**

$$\mathbf{S = s^E T + d E} \quad \text{..... (2)}$$

where S = strain, s = material compliance, T = stress, d = piezoelectric coefficient and E = applied electric field.

Polar or pyroelectric and ferroelectric materials show spontaneously formed electric dipole moment in the absence of an external electric field. The associated polarization is called spontaneous polarization (P_s), which can occur only in materials with a unique polar axis. In ferroelectrics, the direction of P_s can be switched by an external electric field. All ferroelectric materials are pyroelectric, but only some pyroelectric materials are ferroelectric. The pyroelectric effect is defined by the change in the P_s with temperature **[11]** (where p_i (C m^{-2} K^{-1}) is the pyroelectric coefficients):

$$\boldsymbol{p_i = \frac{\partial P_{s,i}}{\partial T}} \quad \text{.....(3)}$$

Eq-(3) can be rewritten as

$$\mathbf{D_i = \Delta P_{s,\,i} = p_i \Delta T} \ldots\ldots\ldots\ldots\ldots\ldots\ldots\ldots\ldots\ldots\ldots\ldots \quad (4)$$

where D_i is the induced surface charge density due to the temperature change ΔT.

La^{+3} substituted PZT (PLZT) at the MPB is one of the most important materials for the ferroelectric actuators, which properties are highly temperature dependent. The change is temperature is due to varying ambient conditions as well as from the generation of heat by the inner losses **[12-15]**. Heat generation in fuel injection systems, account for up to 40% of primary energy, in which temperature conditions varies from -40 to 150^{o}C. The dependence of electro-mechanical properties on temperature is a serious issue, which forces researchers to change in the design of actuators, should be handled carefully. For the design of materials for different application not only the temperature stability of the electrical properties but also an understanding of the governing mechanisms of temperature characteristics are required. The temperature dependendent piezoelectric studies in PZT ceramics under low field conditions are reported by several researchers **[17-20]**. In this chapter, the effect of temperature on the P-E, S-E and piezoelectric coefficients are discussed in detail.

5.3 Ferroelectric (P-E and S-E) properties of mortar-pestle mixed PLZT 8/60/40

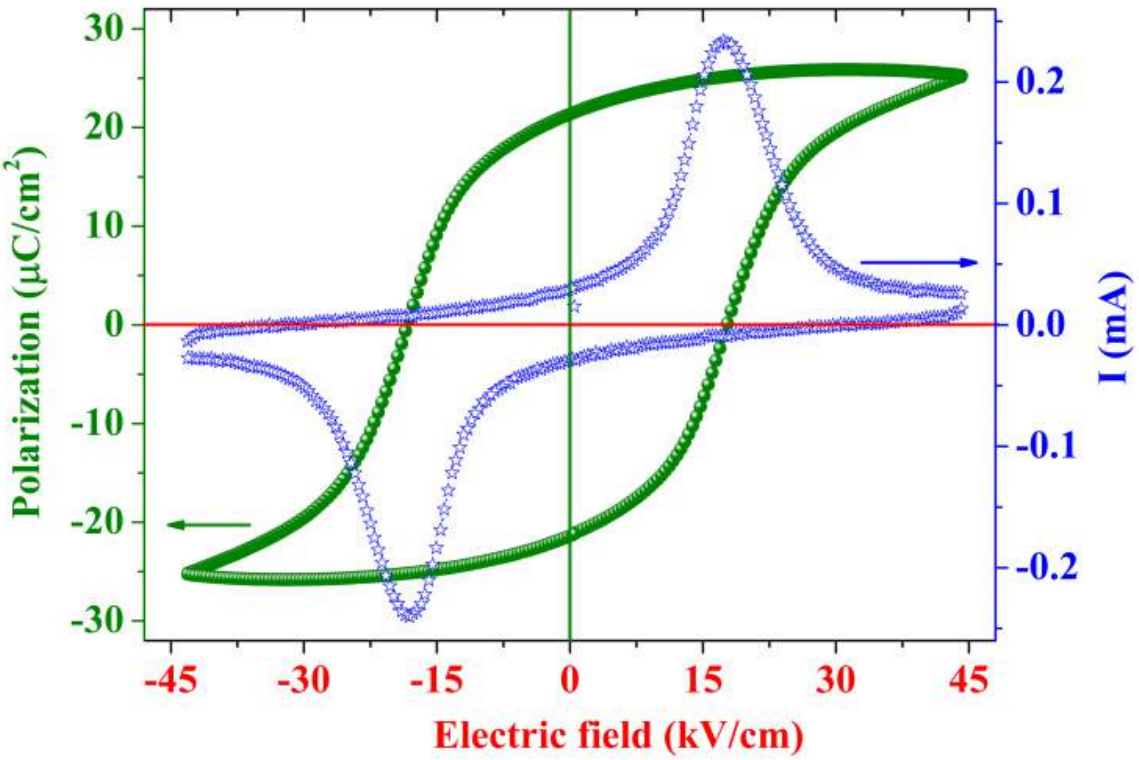

Fig. 5.1 *P-E and I-E curve with domain switching current peaks for mortar pestle prepared PLZT 8/60/40 unpoled ceramic measured at 45 kV/cm, 1 Hz and 25^{o}C.*

To know that how the milling time affects the ferroelectric properties of ferroelectric materials, P-E and S-E hysteresis loops were also measured for the mortar and pestle prepared PLZT 8/60/40 ceramics. Figs. 5.1 and 5.2 show the P-E, I-E and S-E hysteresis loops of mortar pestle prepared ceramics.

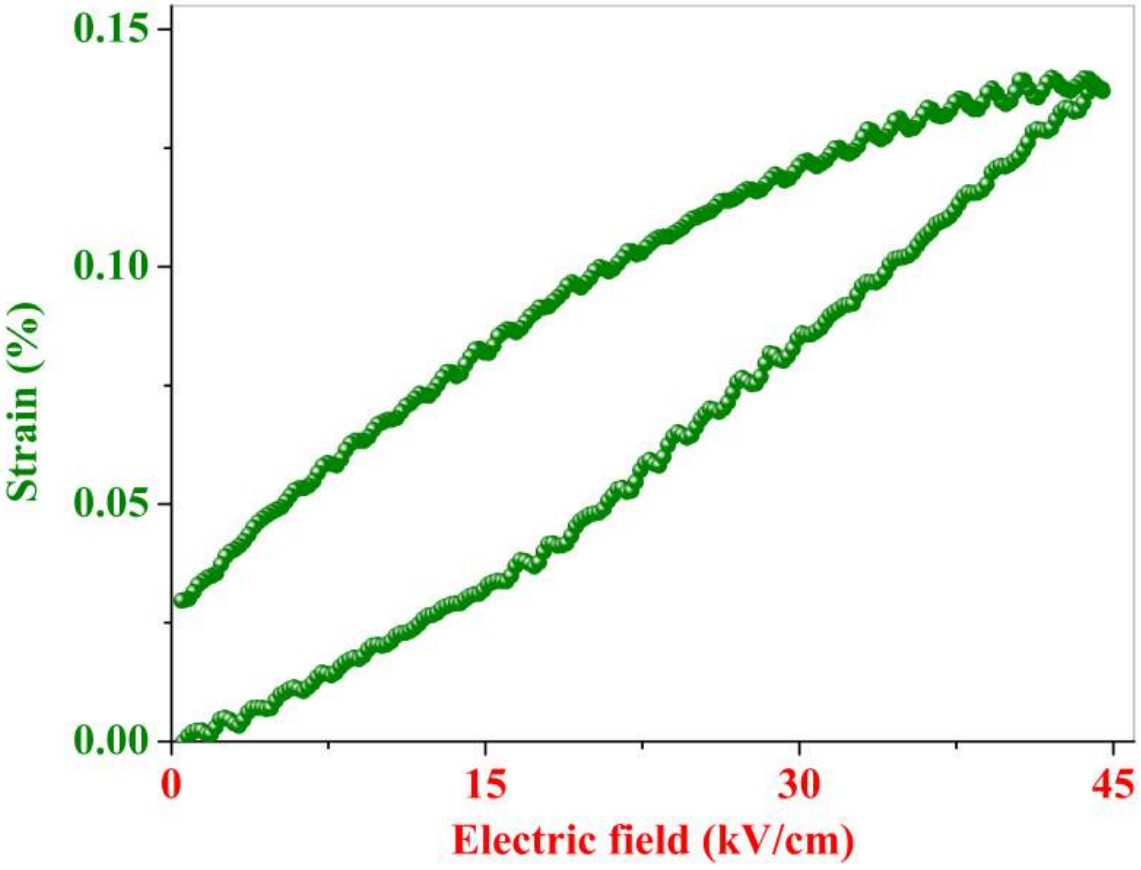

Fig. 5.2 *Unipolar S-E hysteresis curve of mortar pestle prepared PLZT 8/60/40 poled ceramics measured at 45 kV/cm, 1 Hz and 25°C.*

5.4 Polarization vs. electric field (P-E) hysteresis loops studies

5.4.1 Compositional dependence of P-E loops in PLZT system

La substituted PZT ceramics $(Pb_{1-x}La_x)(Zr_{0.60}Ti_{0.40})O_3$ (PLZT x/60/40; x=0.00, 0.02, 0.04, 0.07, 0.08, 0.09 and 0.10) were synthesized via high energy ball milling and cold isostatic pressing. Effects of La substitution on the P-E and I-E curves were discussed in this section. Fig. 5.3 shows the polarization vs. electric field hysteresis curves for different compositions of PLZT ceramics. The loops illustrate the change in polarization with respect to the applied electric field. Fig. 5.3 shows that the shape of P-E loops of PLZT ceramics changes as a function of lanthanum substitution. The PLZT

8/60/40 system shows the typical well-saturated P-E hysteresis loop with highest shape symmetry, squareness and well shaped in comparison to the other systems.

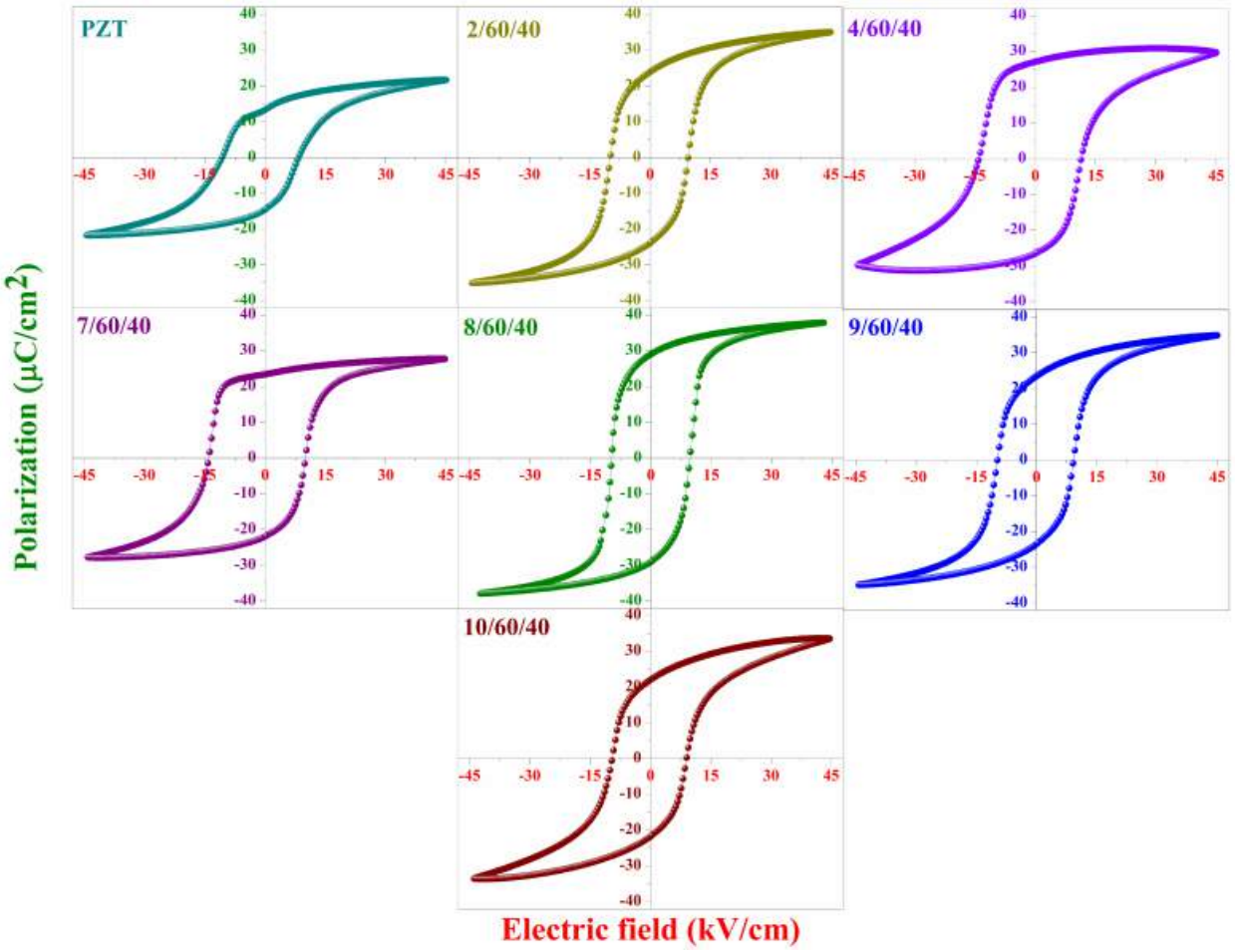

Fig. 5.3 *P-E hysteresis curves for unpoled PLZT x/60/40 ceramics measured at 45 kV/cm, 1 Hz and 25°C.*

Figs. 5.4 and 5.5 show the change in P_r and E_c of PLZT x/60/40 systems as a function of applied electric field. All PLZT compositions were subjected to the same electric field of 45 kV/cm. Fig. 5.4 shows that with an increase in the electric field, remnant polarization of PLZT ceramics increases rapidly. The value of P_r gets saturated due to the alignment of domains. The coercive field curve also follows the same path and shows the similar saturation and switching field characteristics (fig. 5.5). From figs. 5.4 and 5.5, it is clear that the change in P_r and coercive field E_c for PLZT 8/60/40 ceramics is more linear in low electric field region and is also linear in the high electric field region. However, it also shows saturation in this part with respect to other ceramic compositions.

Fig. 5.6 shows the change in both P_r and E_c as a function of La substitution measured at 45 kV/cm. The maximum value of remnant polarization (~29.1 μC/cm^2) was found for the PLZT 8/60/40 ceramics. On the other hand PLZT 8/60/40 ceramics also show the low coercive field (~9.4 kV/cm).

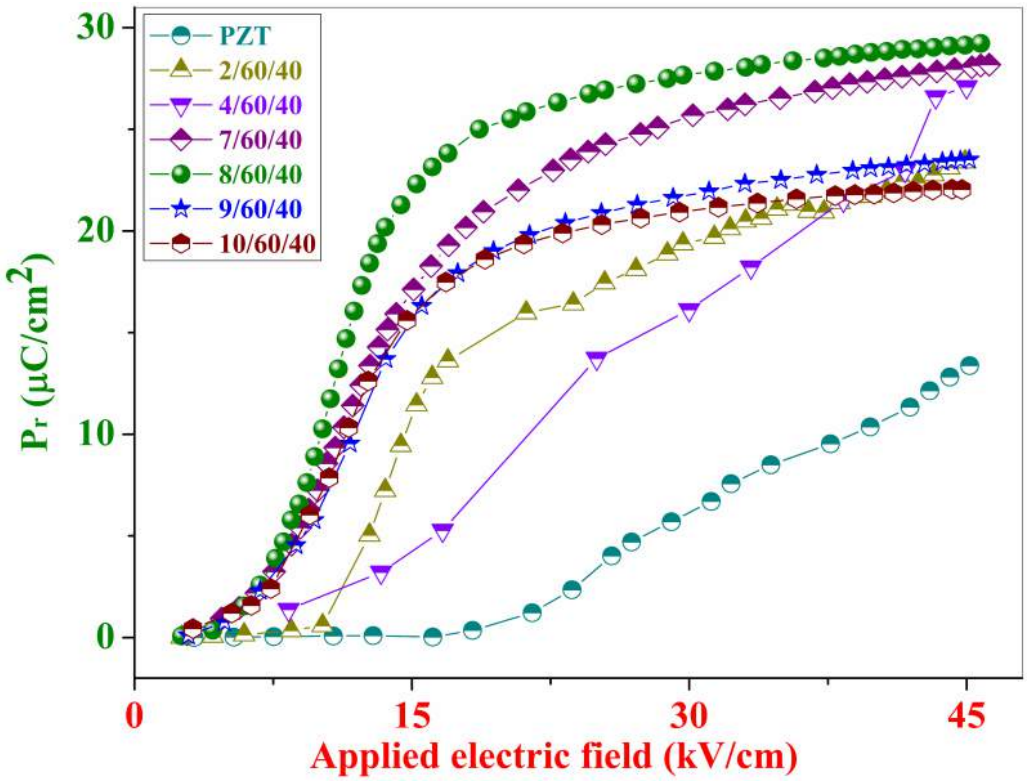

Fig. 5.4 *Variation in remnant polarization as a function of applied electric field for different compositions of unpoled PLZT ceramics measured at 1 Hz and 25°C.*

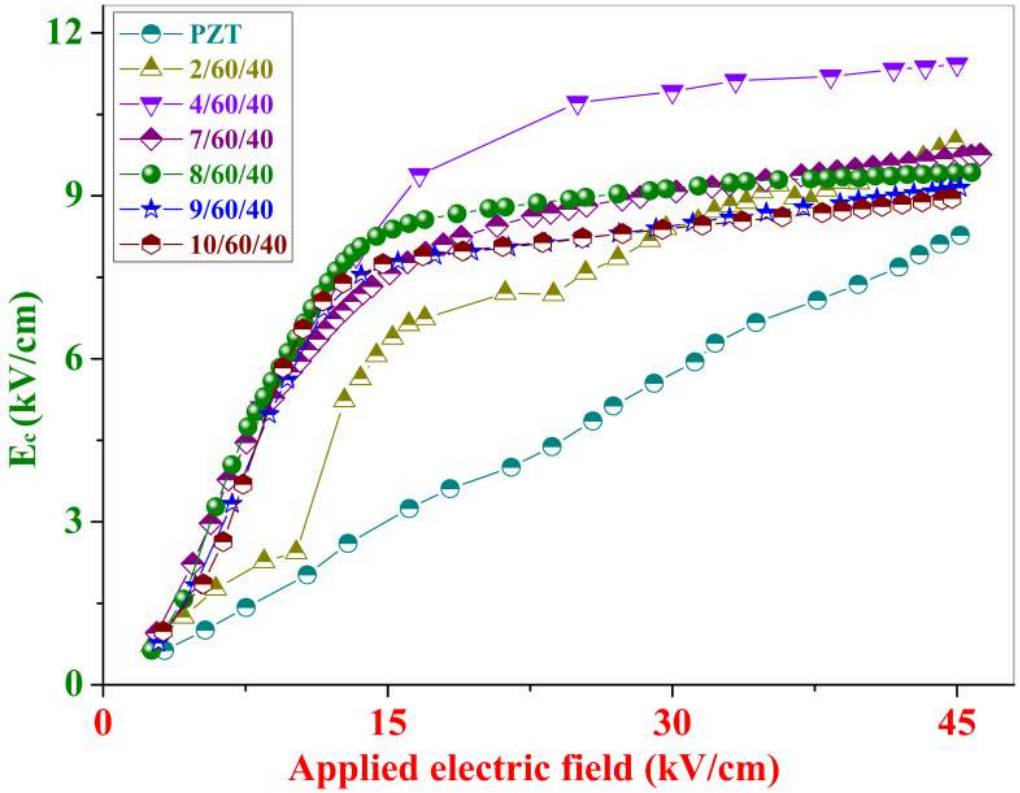

Fig. 5.5 *Variation in the coercive field as a function of applied electric field for different composition of unpoled PLZT ceramics measured at 1 Hz and 25°C.*

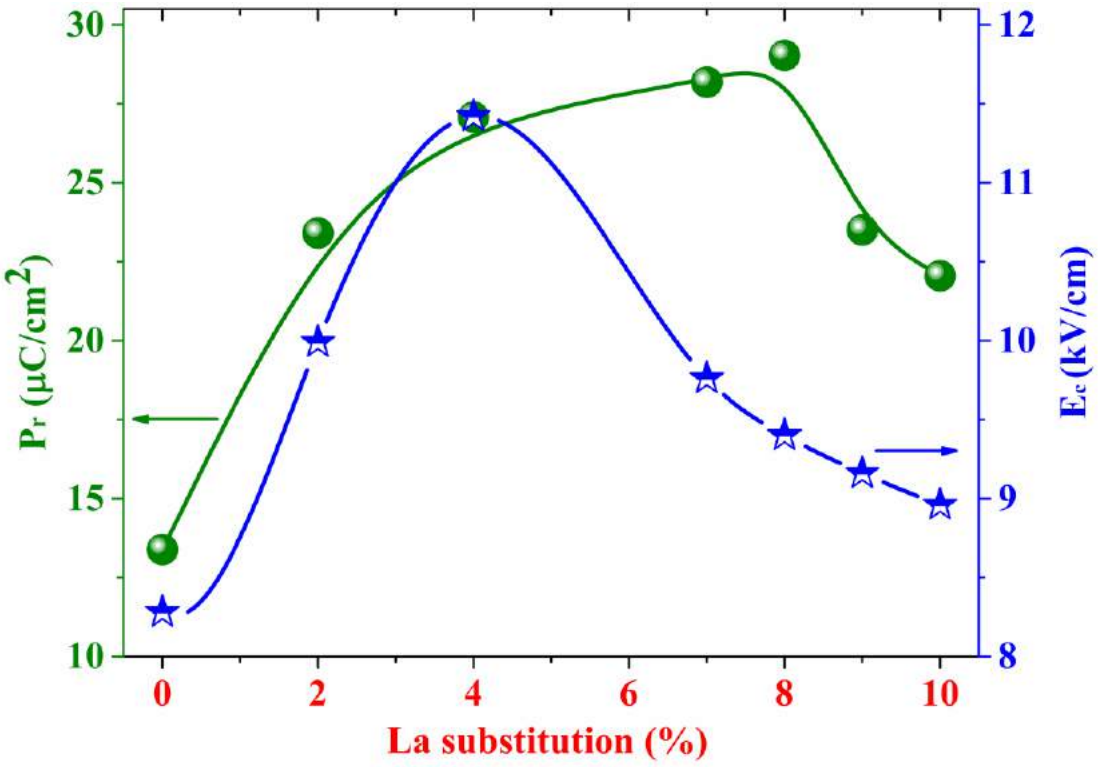

Fig. 5.6 *Change in P_r and E_c as a function of lanthanum substitution of unpoled PLZT ceramics measured at 45 kV/cm, 1 Hz and 25°C.*

The electric field, which is necessary to bring the remnant polarization (P_r) to zero is called the coercive field (E_c). The coercive field of ferroelectrics can be evaluated from the P-E hysteresis loop. It is also important that the E_c that is determined from the intercept of the polarization of P-E hysteresis loop with the electric field axis is not an absolute threshold field **[11, 21]**. Due to the above reason current vs. electric field (I-E) curves also can be used for the measurement of E_c.

When an electric field is applied to a ferroelectric, along with the polarization, it also shows the current response. This current response consists of different types of current signals and is equal to the total current generated from the ferroelectrics. D. Damjanovic suggested that the total current consists of two parts. The first part is mainly due to the fast linear response of the dielectric and the second is due to polarization switching **[11]**. However, some other references show that the total current also has the weak leakage current (material dependent) and displacement current **[22-23]**. Fig. 5.7 shows the current vs. electric field loops for the PLZT 8/60/40 ceramics.

The effect of different current responses, rather than polarization switching current is visible in the low field region but when the domain starts switching after crossing a threshold field, domain switching current become more prominent. The occurrence of a peak in the current signal before reaching the maximum electric field indicates domain switching in ferroelectrics. The magnitude of this domain switching peak current is much higher than the component of total current at the maximum applied electric field **[24]** in saturated I-E loops. The electric field, which is corresponding to the domain switching current peak in I-E loops is identified as the coercive field.

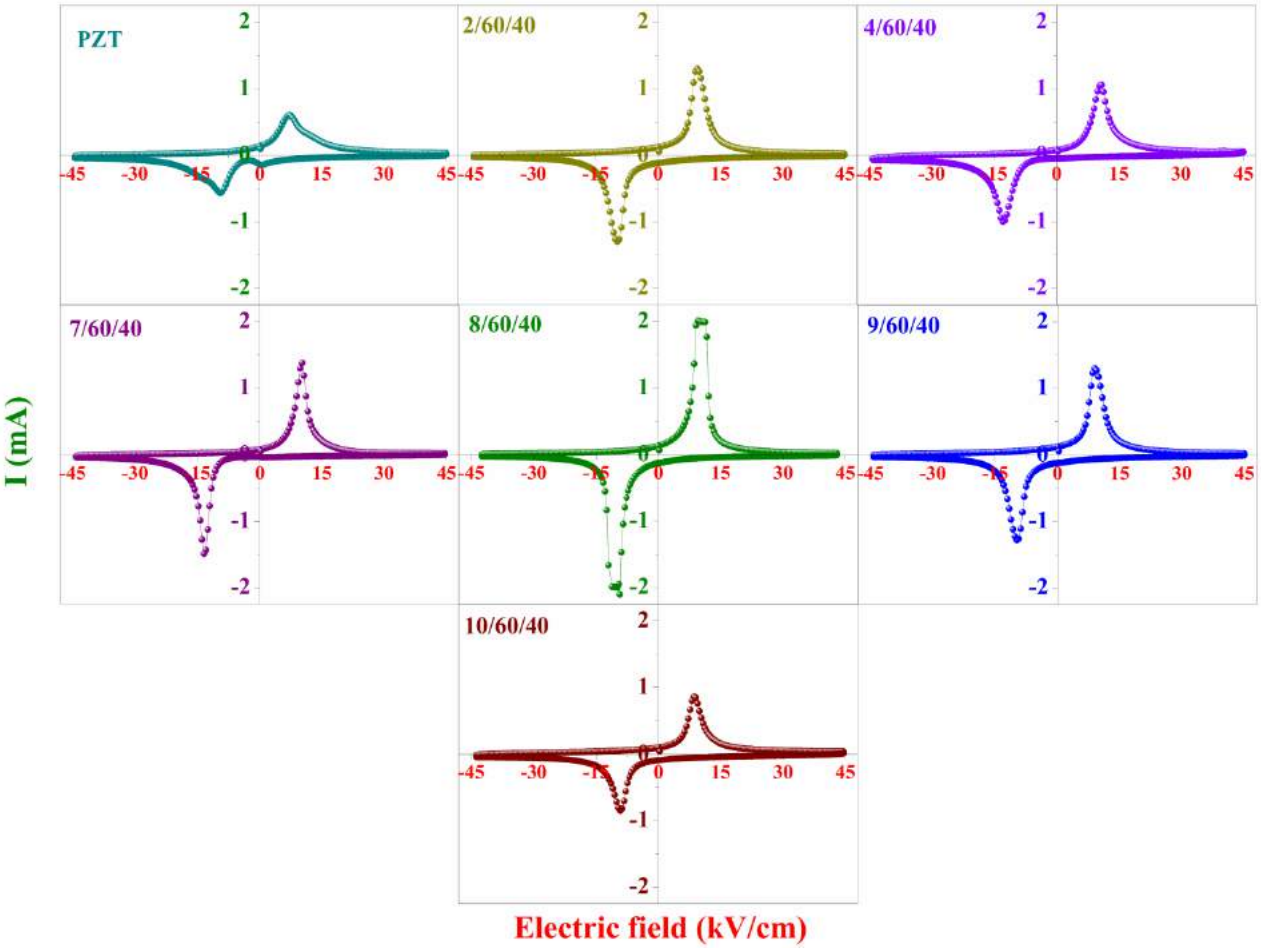

Fig. 5.7 *I-E curves for the unpoled PLZT x/60/40 ceramics measured at 45 kV/cm, 1 Hz and 25^{o}C.*

The variation of domain switching current peak with respect as a function of applied electric field of PLZT x/60/40 ceramics is shown in fig. 5.7. The domain switching current measured during switching voltage cycles is different from the leakage current which is generated when the ceramic is exposed to a particular voltage. The peaks were observed in both forward and reverse directions, confirming the ferroelectric nature of the ceramics **[25]**. Figs. 5.7 and 5.8 show that the magnitude of domain switching current (I_{max}) is changing as a function of lanthanum substitution. The maximum value of domain switching current was found to be ~2 mA for PLZT 8/60/40 ceramics. All the important ferroelectric parameters of PLZT x/60/40 ceramics are listed in Table-5.1.

For an ideal ferroelectric system, the observed P-E hysteresis loops should show symmetry in their shape. The positive and negative value of the remnant polarization (P_r) and coercive field (E_c) should be equal ($E_c = -E_c$ and $P_r = -P_r$). In reality, the shape of the ferroelectric hysteresis loops is affected by many factors such as material composition, preparation conditions, the thickness of the samples, mechanical stresses, the presence of charged defects, measurement conditions and thermal treatment. The high leakage currents in the ceramic sample can affect the shape of the hysteresis loop, especially at high voltages and low frequencies.

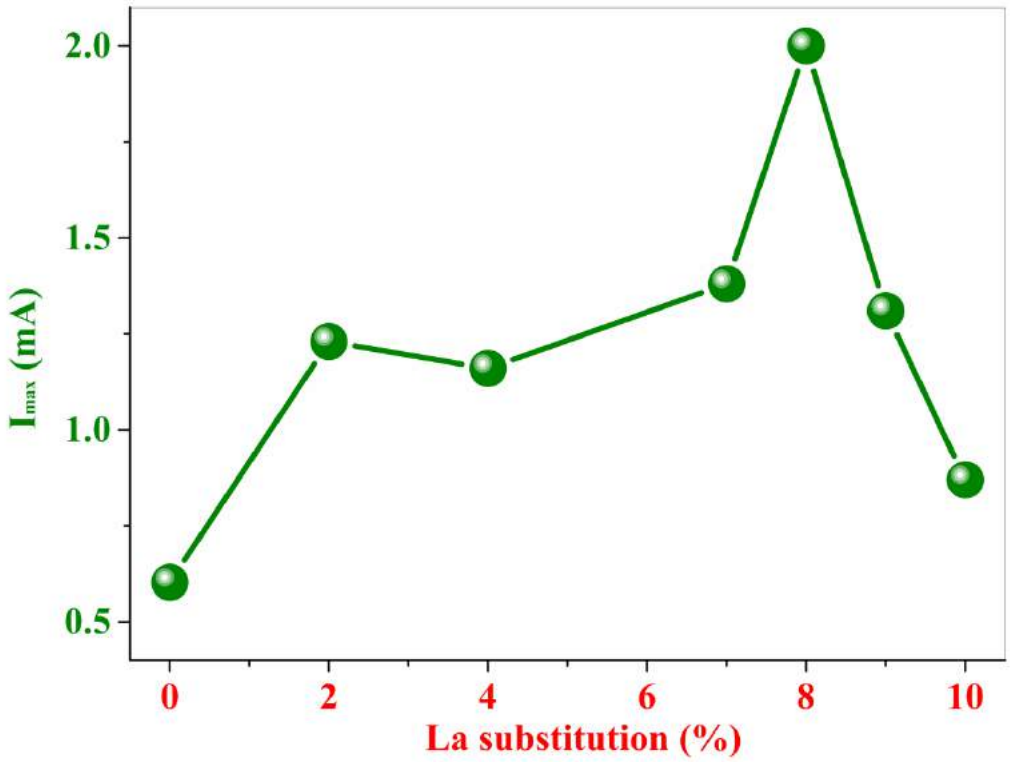

Fig. 5.8 *Change in the value of domain switching current peak as a function of lanthanum substitution of unpoled PLZT ceramics measured at 45 kV/cm, 1 Hz and 25°C.*

It is to clarify that the symmetry in this chapter does not reflect the crystal symmetry and only represents the symmetry of P-E hysteresis loop. In this study, we have also observed that different compositions of PLZT ceramics show the deflection from symmetry in their P-E hysteresis loops. These deflection magnitudes are expressed by the terms E_{in} and (P_{r+} + P_{r-}). The term E_{in} is called as a macroscopic internal electric field that can be calculated by eq-(5) **[26]**.

$$\boldsymbol{E_{in}} = \frac{\boldsymbol{E_{c+}} + \boldsymbol{E_{c-}}}{\mathbf{2}} \quad \text{..... (5)}$$

where E_{c+} and E_{c-} represents the positive and negative coercive field.

Eq-(5) also can be written in terms of voltage. The change in coercive voltage is called the voltage shift in the P-E hysteresis loop. Voltage shift means a difference between positive coercive voltage V_{c+} and negative coercive voltage V_{c-} and can be used to show the asymmetry in the shapes of P-E loops. The term $V_{c,\,shift}$ is defined as **[22]**:

$$\boldsymbol{V_{C,shift}} = \frac{\boldsymbol{V_{c+}} + \boldsymbol{V_{c-}}}{\mathbf{2}} \quad \text{..... (6)}$$

Both equations (5) and (6) have the same meaning for ferroelectrics and show the shift from their ideal P-E shape. However, in this chapter, we from now on will use the term E_{in}.

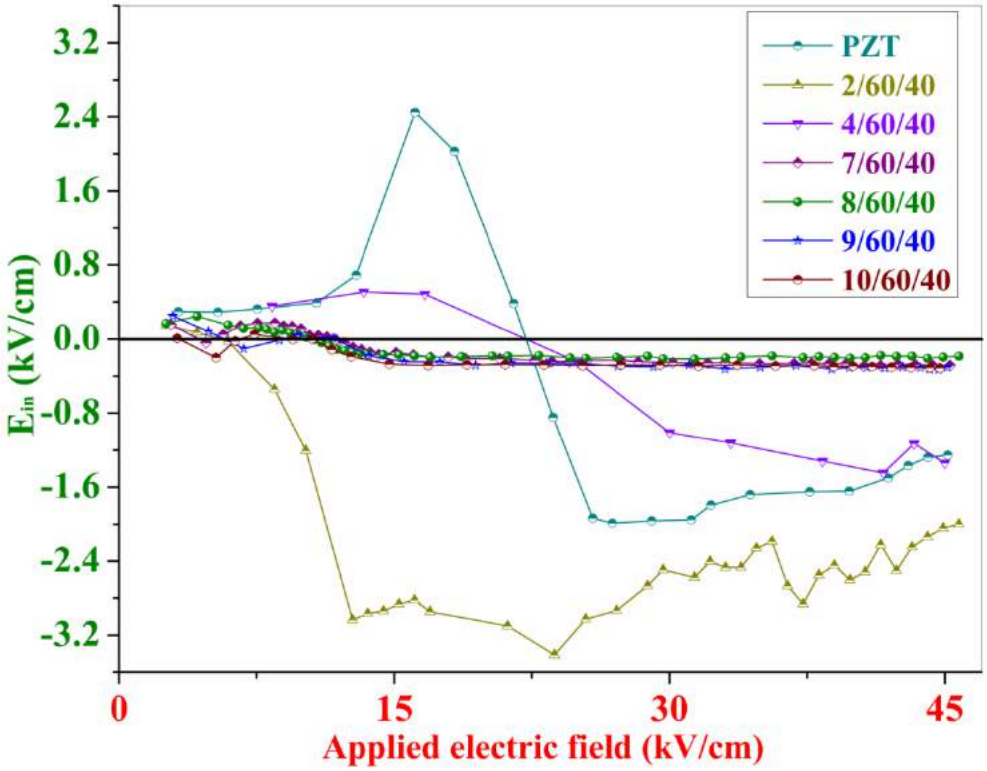

Fig. 5.9 *Change in the shape symmetry of P-E loops, calculated from the coercive field of unpoled PLZT x/60/40 ceramics measured at 45 kV/cm, 1 Hz and 25°C.*

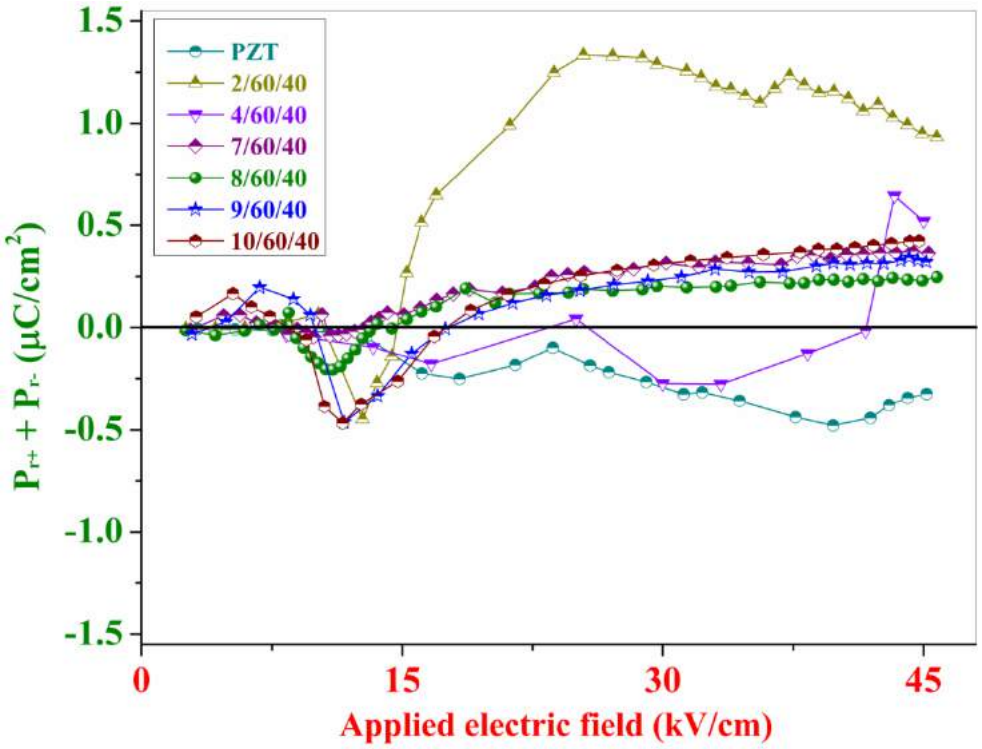

Fig. 5.10 *Change in the shape symmetry of P-E loops, calculated from the remnant polarization of unpoled PLZT x/60/40 ceramics measured at 45 kV/cm, 1 Hz and 25°C.*

Figs. 5.9 and 5.10 show the change in the symmetry of P-E hysteresis loops for different compositions of PLZT ceramics. More the deviation of respective parameters from X-axis more is the asymmetry in the P-E hysteresis loops. Less deviation shows that positive and negative part of both remnant polarization and coercive field are almost equal. Both the figs. confirm that the P-E loop of PLZT 8/60/40 ceramics is more symmetric than remaining compositions. Fig. 5.11 shows the change in parameters E_{in} and $(P_{r+} + P_{r-})$, as a function of lanthanum substitution of unpoled PLZT ceramics. Fig. 5.11 confirms that the 8% lanthanum substituted PZT ceramics (PLZT 8/60/40) have the minimum value of E_{in} and $(P_{r+} + P_{r-})$, which are related to highly symmetric P-E hysteresis loop.

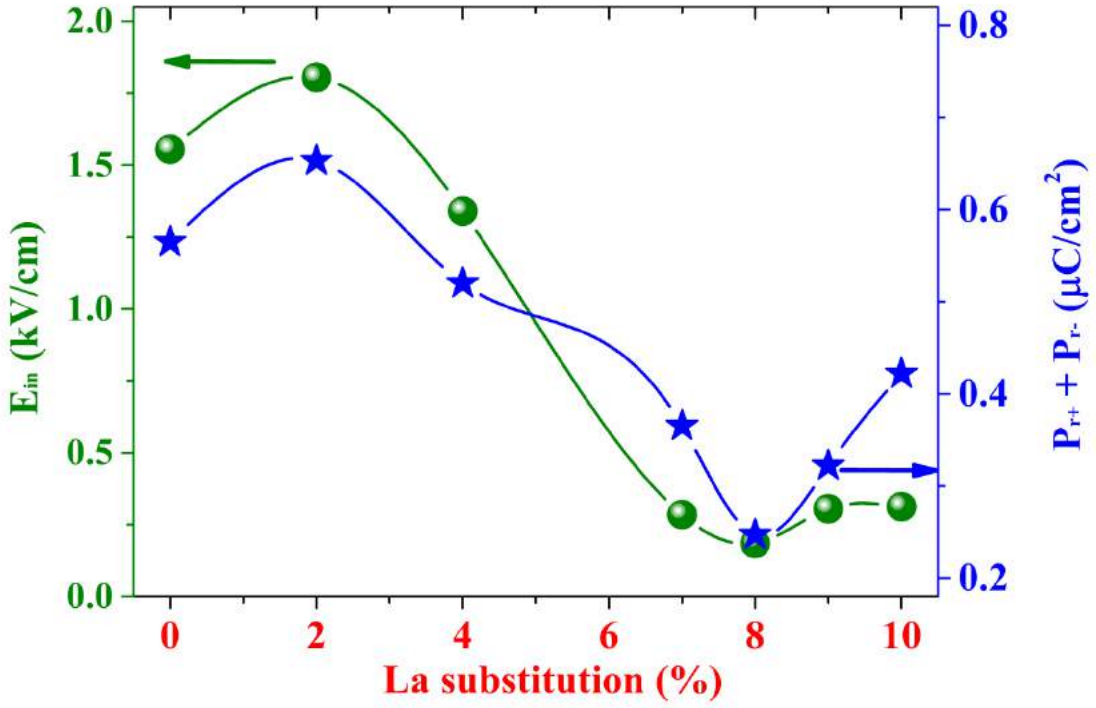

Fig. 5.11 *Change in E_{in} and $(P_{r+} + P_{r-})$ as a function of lanthanum substitution of unpoled PLZT ceramics measured at 45 kV/cm, 1 Hz and 25°C.*

Table-5.1 *Ferroelectric properties of PLZT x/60/40 ceramics measured at 45 kV/cm.*

Compositions	P_r (μC/cm^2)	E_c (kV/cm)	I_{max} (mA)
PZT 60/40	13.4	8.3	0.63
PLZT 2/60/40	23.4	10.0	1.03
PLZT 4/60/40	27.1	11.4	1.06
PLZT 7/60/40	28.2	9.8	1.36
PLZT 8/60/40	29.1	9.4	2.00
PLZT 9/60/40	23.5	9.2	1.31
PLZT 10/60/40	22.1	8.9	0.87

5.4.2 PLZT 8/60/40 ceramics milled with different vials

In the last section 5.4.1, it was shown the effect of lanthanum substitution on the ferroelectric properties of PZT ceramics and we found that PLZT 8/60/40 ceramics that was prepared by 8% La substitution in the A-site of basic PZT system shows the highest remnant polarization, highest domain switching current value and low coercive field. This composition also shows an improvement in the shape of P-E loop. The composition PLZT 8/60/40 was further used to study the effect of milling vials on the ferroelectric properties. PLZT 8/60/40 ceramics were milled by using different milling vials made of agate and zirconia, respectively. Some of the important ferroelectric properties of PLZT 8/60/40 ceramics milled with different vials are given in Table-5.2. It shows that PLZT 8/60/40 ceramics milled with zirconia vials have better properties than agate milled ceramics.

Table-5.2 *Ferroelectric properties of PLZT 8/60/40 ceramics milled with different vials, measured at 45 kV/cm.*

Milling vials	P_r (μC/cm^2)	E_c (kV/cm)	I_{max} (mA)
Zirconia vial	34.1	11.98	2.06
Agate vial	29.1	9.40	2.00

5.4.3 PLZT 8/60/40 ceramics milled for different durations

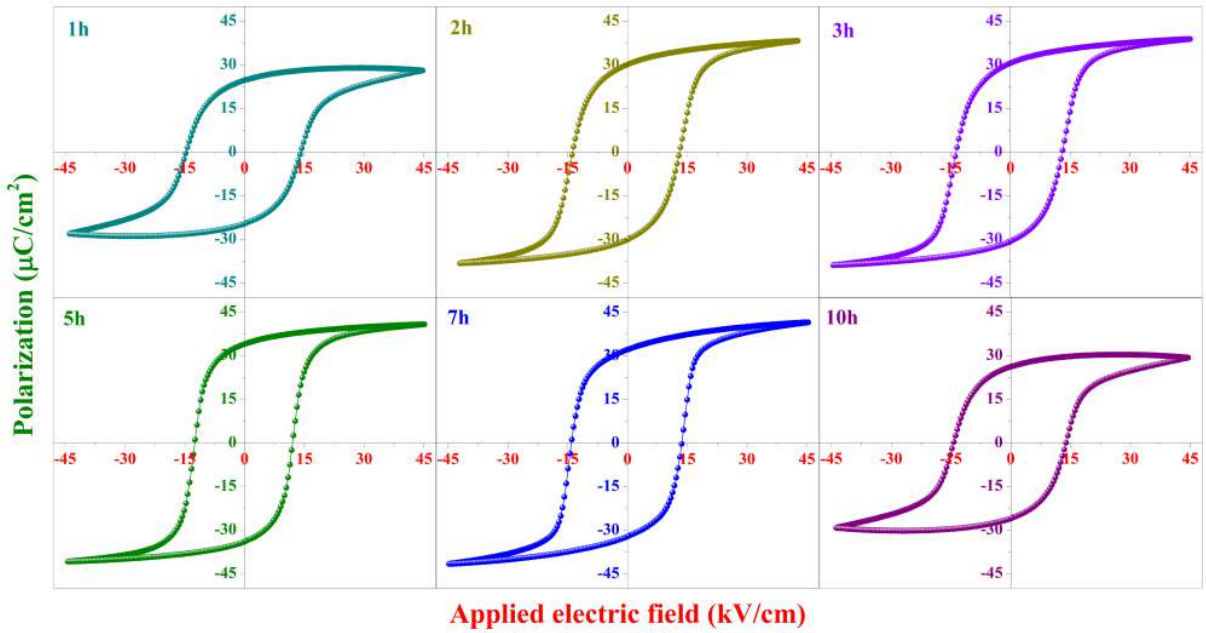

Fig. 5.12 *P-E hysteresis curves for mechano-chemically processed unpoled PLZT 8/60/40 ceramics milled for 1h, 2h, 3h, 5h, 7h and 10h measured at 45 kV/cm, 1 Hz and 25°C.*

In section 5.4.1, ferroelectric properties of PLZT x/60/40 ceramics were studied. Same ferroelectric studies were also done for PLZT 8/60/40 ceramic samples, milled for different durations. Fig. 5.12 shows the change in the shape of P-E loops of PLZT ceramics as a function of milling time. PLZT 8/60/40 ceramic system that was milled for 5 hours shows well-saturated, symmetric electric field induced ferroelectric polarization hysteresis loops with the highest squareness.

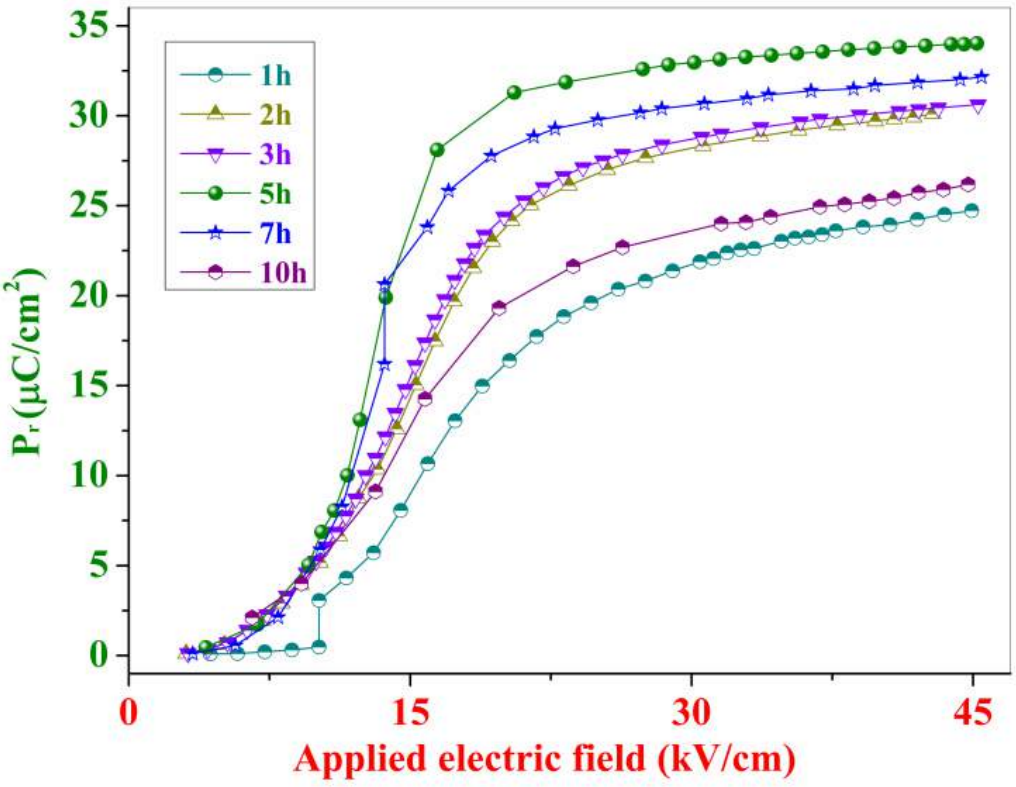

Fig. 5.13 *Variation in the remnant polarization as a function of applied electric field for PLZT 8/60/40 ceramics milled for different durations, measured at1 Hz and 25^{o}C.*

Figs. 5.13 and 5.14 show the change in remnant polarization (P_r) and coercive field (E_c) as a function of applied electric field of PLZT 8/60/40 electro-ceramics, milled for different durations. The maximum amplitude of applied electric field to study the effect of milling time on the ferroelectric properties of PLZT 8/60/40 ceramics was fixed at 45 kV/cm. From the figs. 5.13 and 5.14, it can be seen that the remnant polarization and coercive field values increase rapidly with the electric field and get saturated due to the alignment of domains. These saturation and switching field characteristics are similar to the figs. 5.4 and 5.5. The change in P_r and E_c (Figs. 5.13 and 5.14) for PLZT 8/60/40 ceramics, milled for 5 hours is more linear in both the low as well as high electric field region and show high saturation in the high electric field region.

Fig. 5.15 shows the change in P_r and E_c as a function of milling time, measured at 45 kV/cm. Maximum remnant polarization (~34.1 μC/cm^2) and minimum coercive field (~12 kV/cm) values were found for the 5 hours milled PLZT 8/60/40 ceramics.

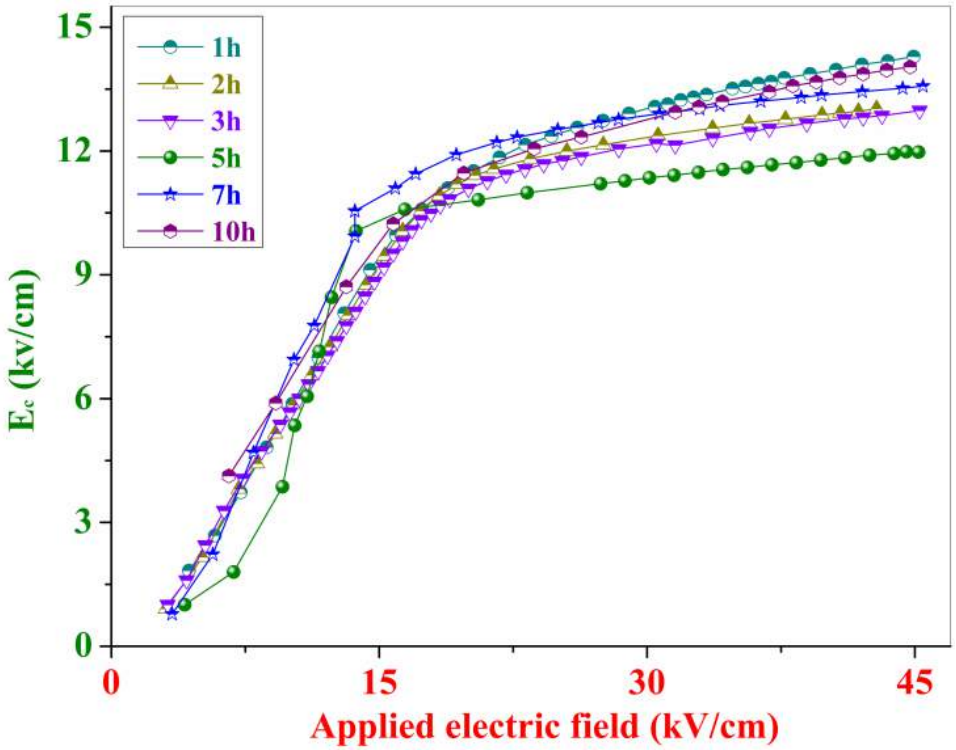

Fig. 5.14 *Variation in the coercive field as a function of applied electric field for PLZT 8/60/40 ceramics milled for different durations, measured at1 Hz and 25°C.*

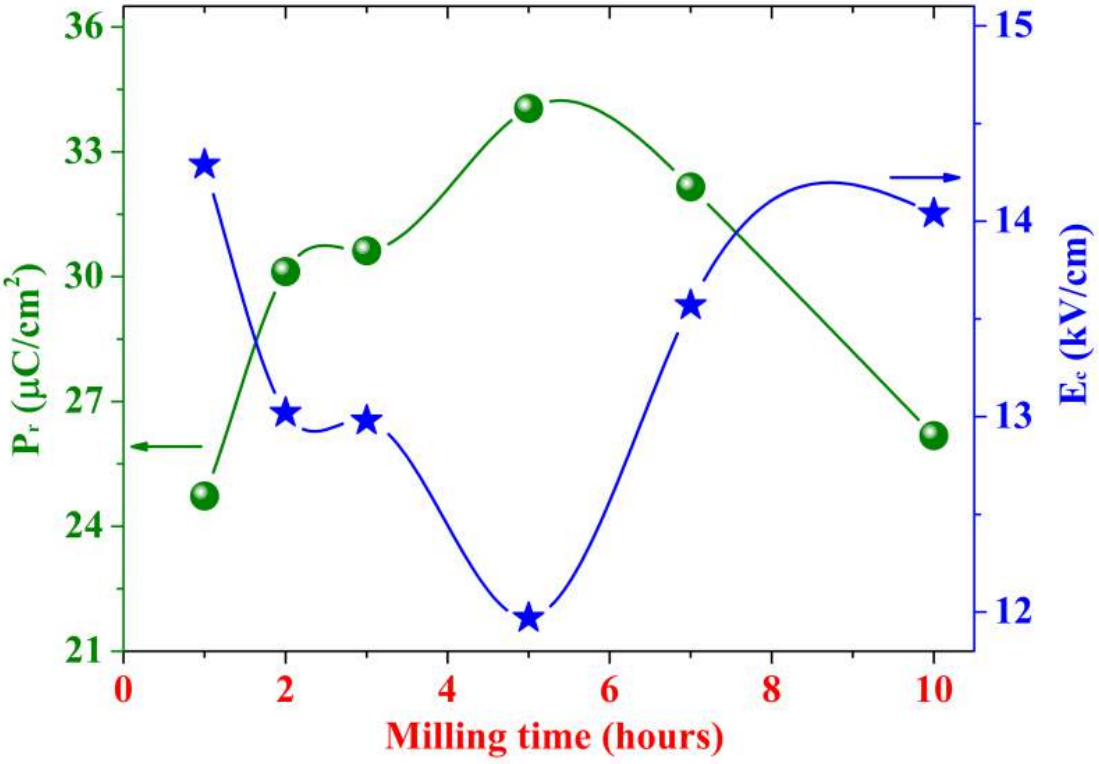

Fig. 5.15 *Change in P_r and E_c of unpoled PLZT ceramics as a function of milling time, measured at 45 kV/cm, 1 Hz and 25°C.*

Along with P-E hysteresis loops, current vs. electric field (I-E) curves were also measured for PLZT 8/60/40 ceramics that were milled for different durations. Fig. 5.16 shows I-E curves for PLZT 8/60/40 ceramics, milled for 1h, 2h, 3h, 5h, 7h and 10h, respectively. The domain switching peaks confirm the ferroelectric nature of the ceramics. Fig. 5.17 shows the change in the magnitude of domain switching current as a fintion of milling time.

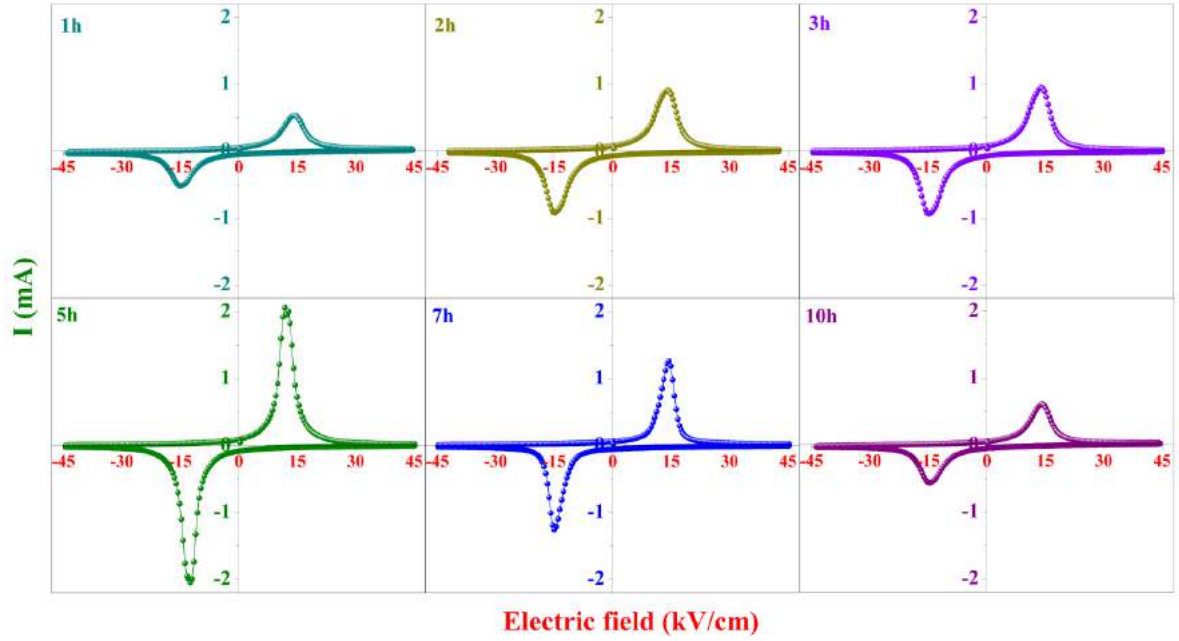

Fig. 5.16 *Current vs. electric field curves for mechano-chemically processed unpoled PLZT 8/60/40 ceramics milled for 1h, 2h, 3h, 5h, 7h and 10h, measured at 45 kV/cm, 1 Hz and 25°C.*

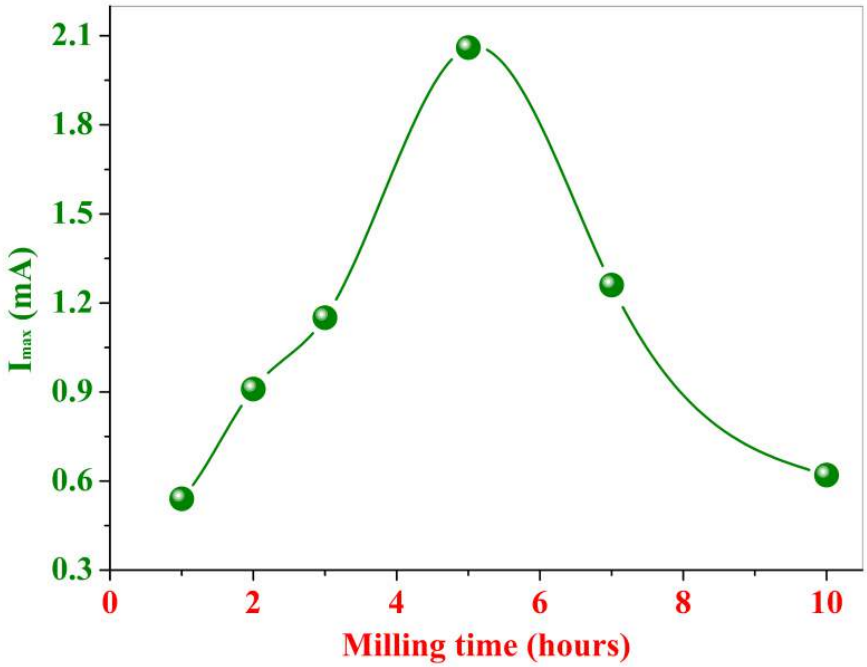

Fig. 5.17 *Change in domain switching current peak value as a function of milling time of unpoled PLZT ceramics measured at 45 kV/cm, 1 Hz and 25°C.*

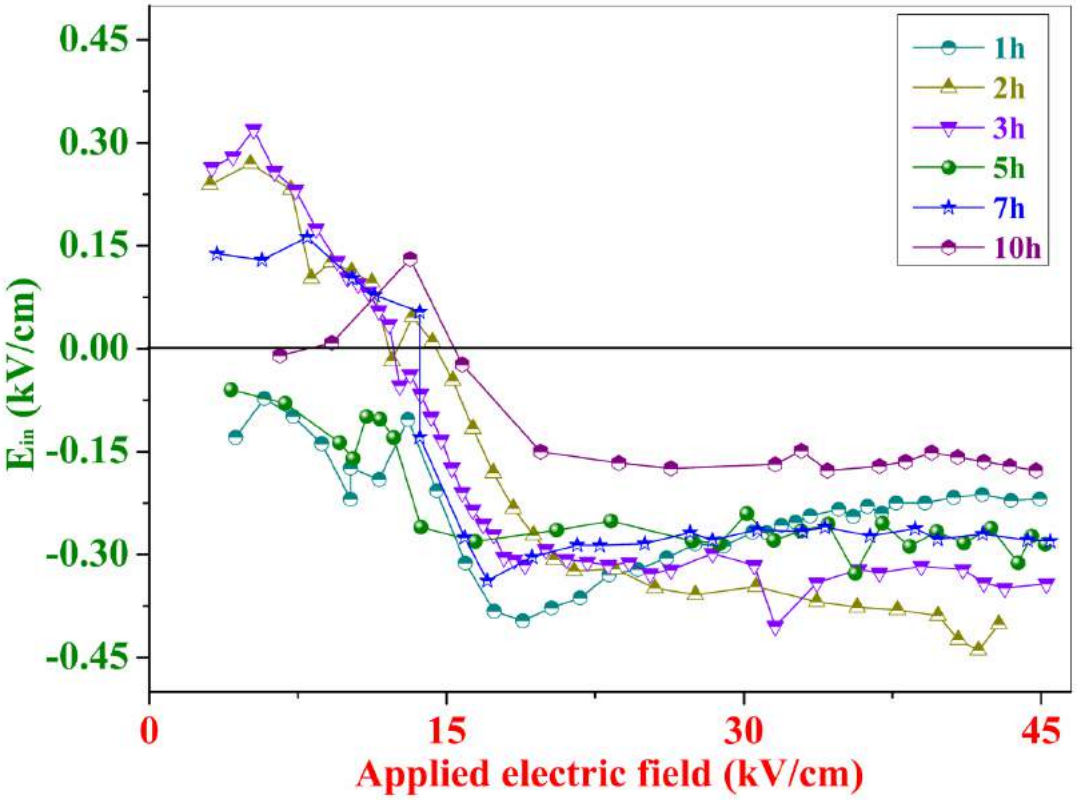

Fig. 5.18 *Change in the shape symmetry of P-E loops, calculated from the coercive field of unpoled PLZT ceramics, milled for different durations, measured at 45 kV/cm, 1 Hz and 25°C.*

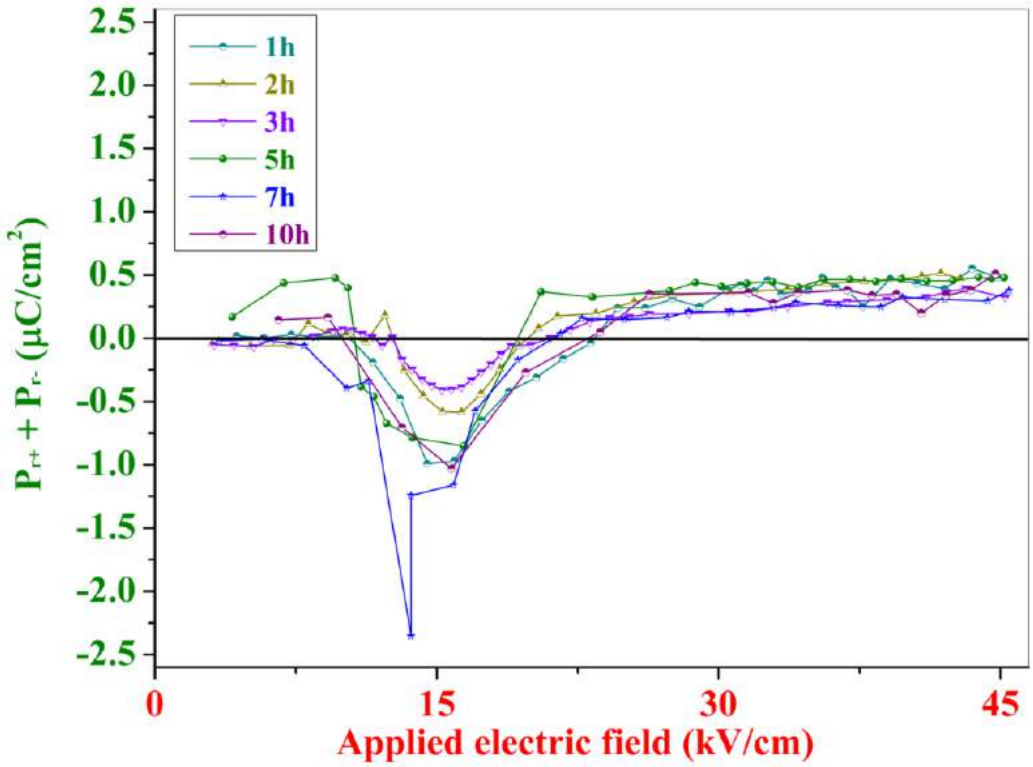

Fig. 5.19 *Change in the shape symmetry of P-E loops, calculated from the remnant polarization of unpoled PLZT ceramics, milled for different durations, measured at 45 kV/cm, 1 Hz and 25°C.*

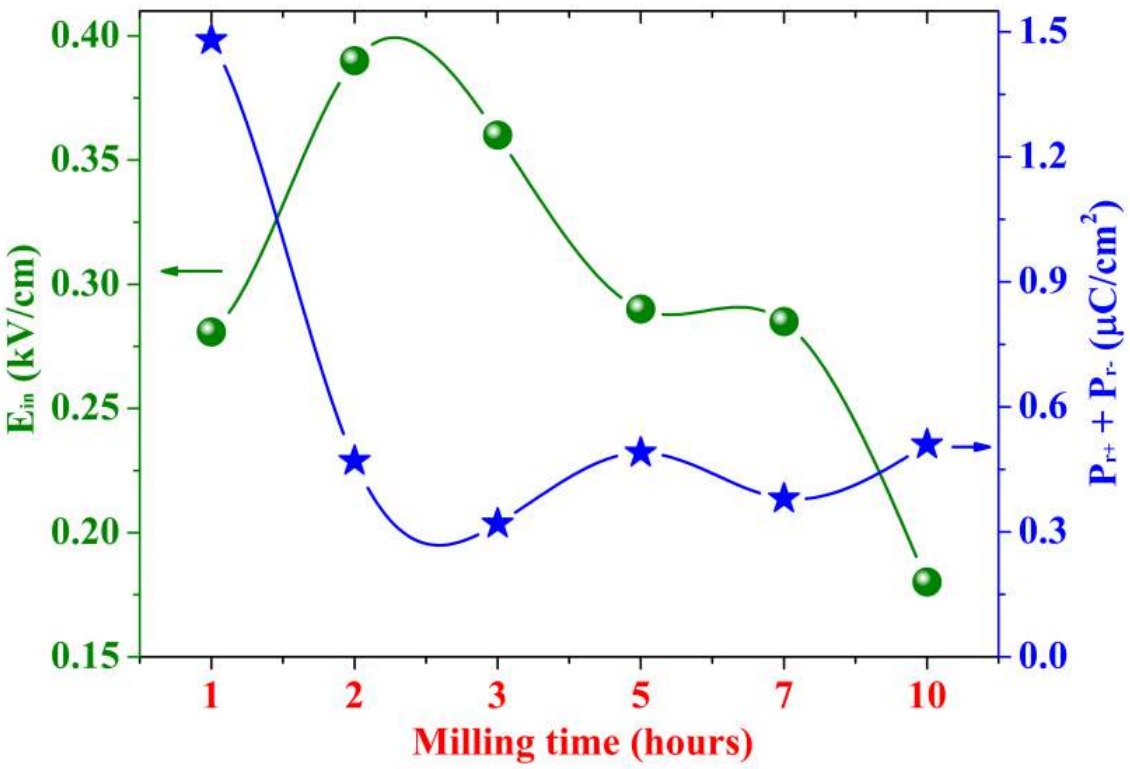

Fig. 5.20 *Change in E_{in} and (P_{r+} + P_{r-}) as a function of milling time of unpoled PLZT ceramics measured at 45 kV/cm, 1 Hz and 25^{o}C.*

Figs. 5.18, 5.19 and 5.20 are related to the symmetry of P-E hysteresis loops of PLZT 8/60/40 ceramics that were milled for different durations. Above mentioned figures shows the deviation of P-E loops from their ideal symmetry. These deviations can be calculated in terms of E_{in} and (P_{r+} + P_{r-}), as discussed in section 5.4.1. More the change in these values from the X-axis, more the asymmetry in the P-E loops. Figs. 5.18 and 5.19 confirm that the shape of P-E loop of 5 hours milled PLZT 8/60/40 ceramics is more symmetric. Ferroelctric properties of PLZT 8/60/40 ceramics are listed in Table-5.3.

Table-5.3 *Ferroelectric properties of PLZT 8/60/40 ceramics milled for different durations, measured at 45 kV/cm.*

Milling time	P_r (μC/cm^2)	E_c (kV/cm)	I_{max} (mA)
1h	24.7	14.3	0.54
2h	30.1	13.0	0.91
3h	30.6	13.2	1.15
5h	34.0	12.0	2.06
7h	32.2	13.6	1.26
10h	26.2	14.0	0.62

5.5 Electric field induced strain vs. electric field (S-E) hysteresis loop studies

The S-E hysteresis loops provide information about the piezoelectric nature of ferroelectrics. In this chapter, unipolar S-E hysteresis curves of poled PLZT ceramics were studied, which can be used for the indirect measurement of the low and high field piezoelectric charge coefficient (d_{33}).

5.5.1 Compositional dependence of S-E loops in the PLZT system

In the previous section 5.4.1, polarization vs. electric field hysteresis loops were studied for the different compositions of PLZT ceramics. In the current section, the effect of lanthanum substitution on the electric field induced, unipolar strain vs. electric field is discussed.

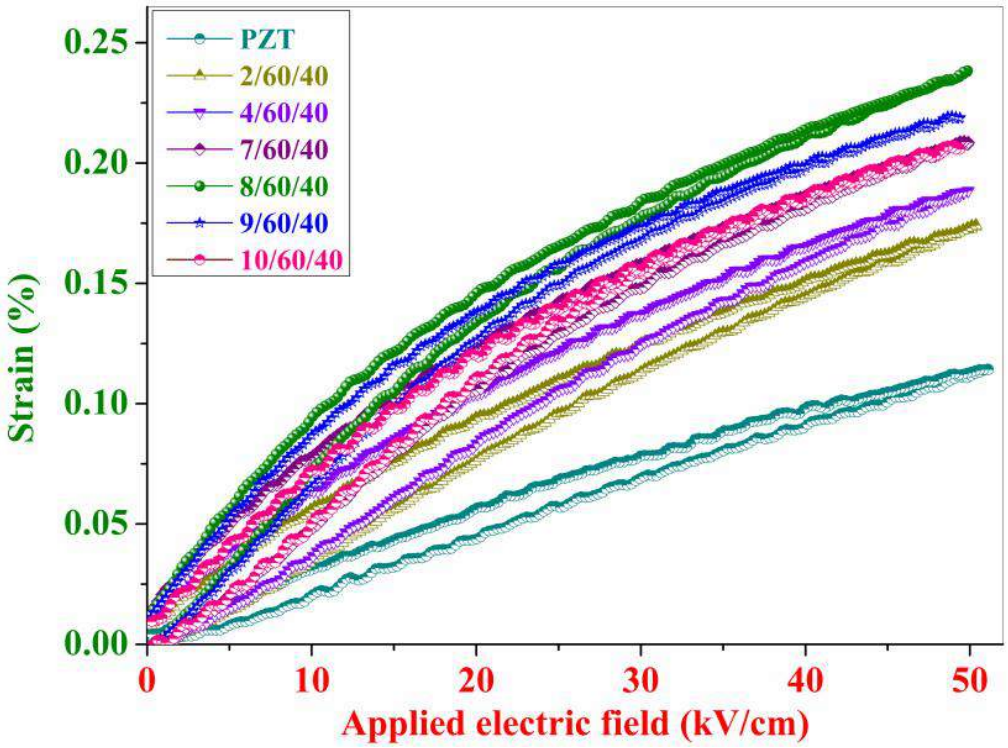

Fig. 5.21 *Unipolar S-E hysteresis curves for poled PLZT x/60/40 ceramics measured at 1 Hz, 25°C.*

Fig. 5.21 shows electric field induced unipolar strain hysteresis curves for different compositions of PLZT electro-ceramics. Fig. 5.22 shows the maximum strain and strain hysteresis as a function of lanthanum substitution, measured at 50 kV/cm.As discussed in the Chapter-2, strain hysteresis in PLZT ceramics from the S-E curves can be calculated by using the eq-(7).

$$\textbf{Strain hysteresis}\ (\%) = \frac{\Delta \mathbf{x}}{\mathbf{x_{max}}} \times \mathbf{100} \quad \ldots\ldots\ldots\ldots\ldots\ldots\ldots\ldots\ldots\ldots\ (7)$$

where x_{max} is the maximum strain in the specimen when subjected to the maximum applied field, Δx is the difference between the strain values in both directions at ½ E_{max} field.

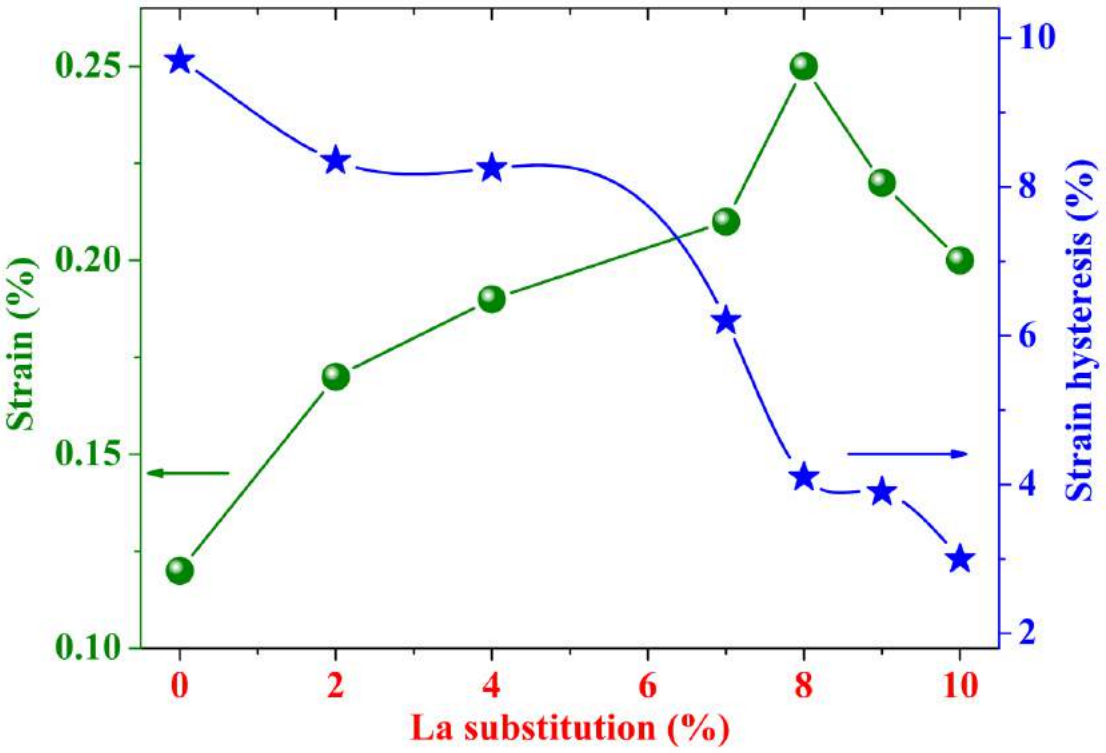

Fig. 5.22 *Change in strain (%) and strain hysteresis (%) as a function of lanthanum substitution as measured at 50 kV/cm, 1 Hz and 25°C.*

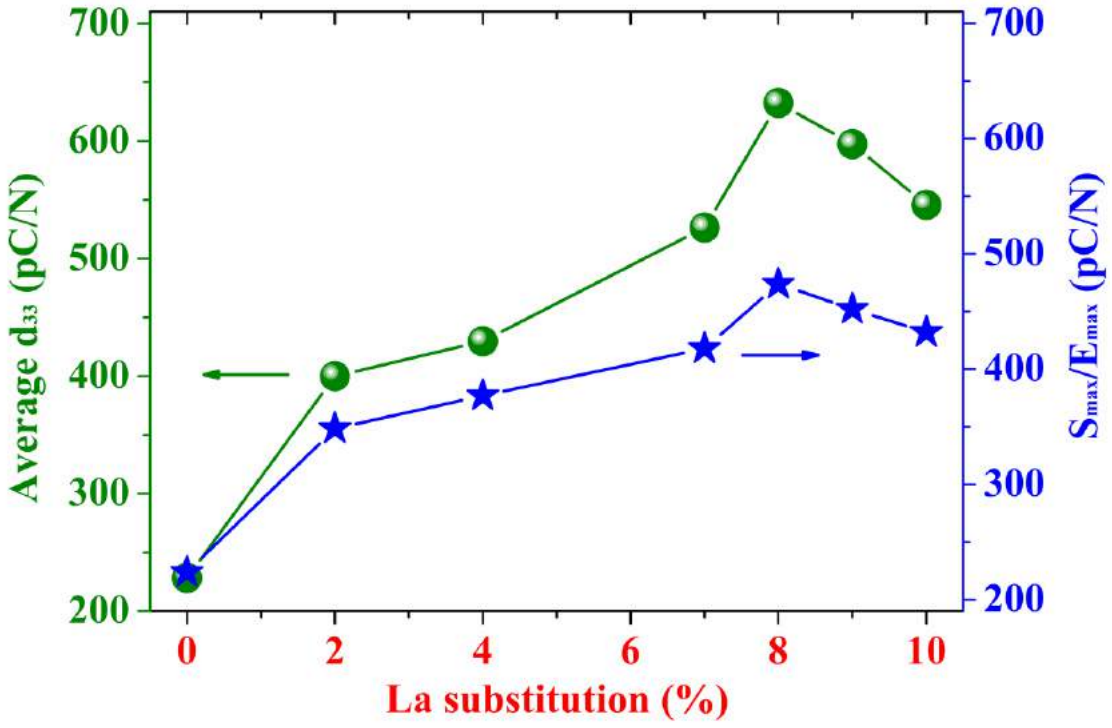

Fig. 5.23 *Change in the (a) average piezoelectric charge coefficient (d_{33}) calculated from the slope of SE curve and (b) maximum strain divided by maximum applied electric field as a function of lanthanum substitution as measured at 50 kV/cm, 1 Hz and 25°C.*

From figs. 5.21 and 5.22, it is clear that basic PZT system shows less strain, but as the amount of lanthanum substitution increases, the unipolar strain also increases. At the high electric field, the alignment of domains saturates and the hysteresis loss, which is represented by the area of the loop decreases. The PLZT 8/60/40 electro-ceramic exhibited a ~0.25% strain with low hysteresis loss of ~4% at ~50 kV/cm, due to increasing alignment of domains.

Piezoelectric charge coefficient (d_{33}) of piezoelectric materials can be calculated from the S-E hysteresis curves. The S-E measurements were performed on PLZT 8/60/40 electro-ceramic in a unipolar direction to calculate the piezoelectric charge coefficient (d_{33}). For unipolar measurements where the total displacement is of interest, an average d_{33} can be defined as the slope of the displacement vs. electric field hysteresis loop in the low field region and these were found to be almost same as the ones determined from the d_{33} meter. Fig. 5.23 shows the average d_{33} value calculated from the slope of S-E hysteresis loops in low field region and normalized strain coefficient (S_{max}/E_{max}) as a function of lanthanum substitution. PLZT 8/60/40 ceramics shows the highest d_{33} and normalized strain coefficient (S_{max}/E_{max}) value. Some important parameters that are derived from S-E hysteresis loops are given in Table-5.4.

Table-5.4 *Ferroelectric properties of PLZT x/60/40 ceramics measured at 50 kV/cm.*

Compositions	Max. Strain (%)	Avg. d_{33} (pC/N)	Strain hysteresis (%)
PZT 60/40	0.12	228	9.7
PLZT 2/60/40	0.17	400	8.1
PLZT 4/60/40	0.19	430	8.4
PLZT 7/60/40	0.21	526	6.2
PLZT 8/60/40	0.25	632	4.1
PLZT 9/60/40	0.22	597	3.9
PLZT 10/60/40	0.20	545	3.0

5.5.2 PLZT 8/60/40 ceramics milled with different vials

The effect of lanthanum substitution on the S-E hysteresis loops of PZT ceramics was studied in section 5.5.1. PLZT 8/60/40 ceramics shows the highest strain, high d_{33} and low strain hysteresis. This composition was again used for the study of the effect of milling vials on S-E hysteresis loops. PLZT 8/60/40 was milled by using different milling vials made of agate and zirconia respectively. Some of the important ferroelectric parameters of PLZT 8/60/40 ceramics milled with different vials are given in Table-5.5. It shows that PLZT 8/60/40 ceramics milled with zirconia vial have a high strain, d_{33} and less strain hysteresis than agate milled ceramics.

Table-5.5 *Ferroelectric properties of PLZT 8/60/40 ceramic milled with different vials and measured at 50 kV/cm.*

Milling vials	Max. Strain (%)	Avg. d_{33} (pC/N)	Strain hysteresis (%)
Zirconia vial	0.27	712	3.3
Agate vial	0.25	632	4.1

5.5.3 PLZT 8/60/40 ceramics milled for different durations

In this section effect of milling time on the S-E hysteresis loops of PLZT ceramics was studied. Electric field induced unipolar strain vs. electric field hysteresis curves were measured for PLZT 8/60/40 ceramics that were milled for different durations.

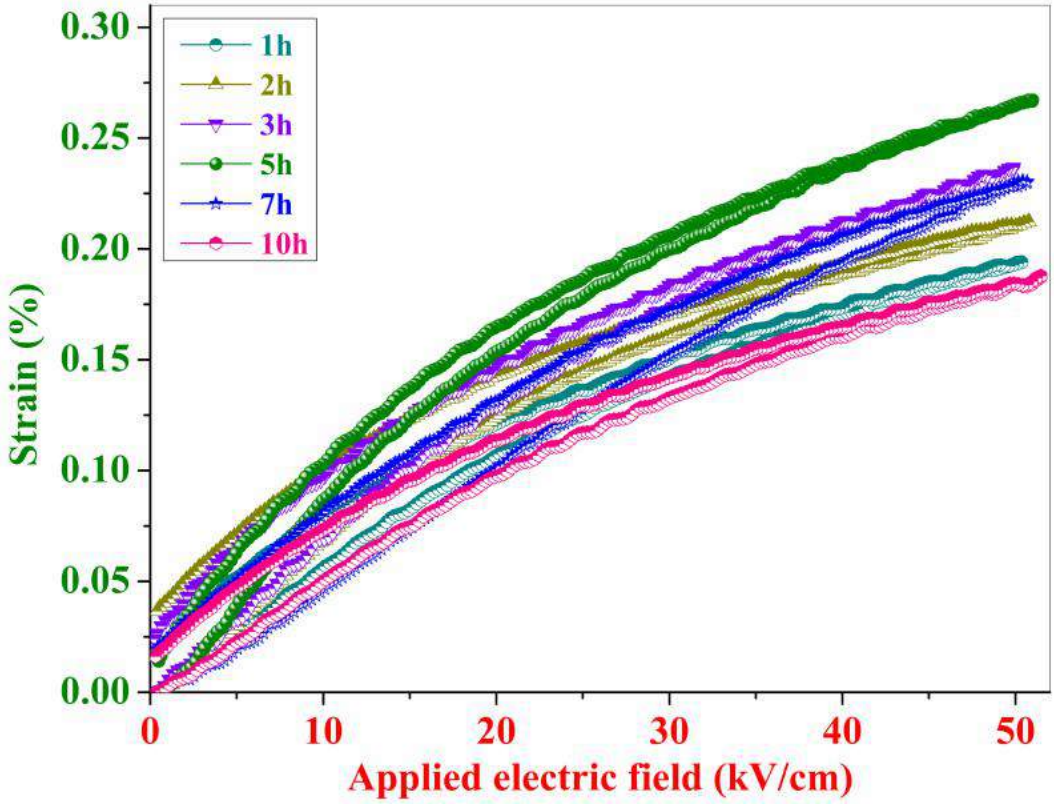

Fig. 5.24 *Strain vs. electric field (S-E) hysteresis curves for poled PLZT 8/60/40 ceramics milled for 1h, 2h, 3h, 5h, 7h and 10h, measured at 50 kV/cm, 1 Hz and 25°C.*

Fig. 5.24 shows the S-E hysteresis curves for PLZT 8/60/40 ceramics, milled for different durations. Fig. 5.25 shows the maximum strain and strain hysteresis as a function of milling time, measured at 50 kV/cm. Figs. 5.24 and 5.25 show that unipolar strain is increased, and strain hysteresis is decreased as a function of milling time. Both the parameters show their optimum value for 5 hours milled PLZT 8/60/40 ceramics. In this present case, a maximum strain of ~0.27% was achieved at a

field of 50 kV/cm, which is much higher than the previous reports, not only for the same composition but also for other PLZT compositions **[27-30]**. The strain hysteresis loss (%) value was calculated from fig. 5.24 using equation-(7) and was found close to ~3%. The strain values were observed at high electric fields, and these ceramics showed good dielectric strength. If one compares these strain values with other ceramic systems in same electric field range, PLZT 8/60/40 ceramics showed improved strain.

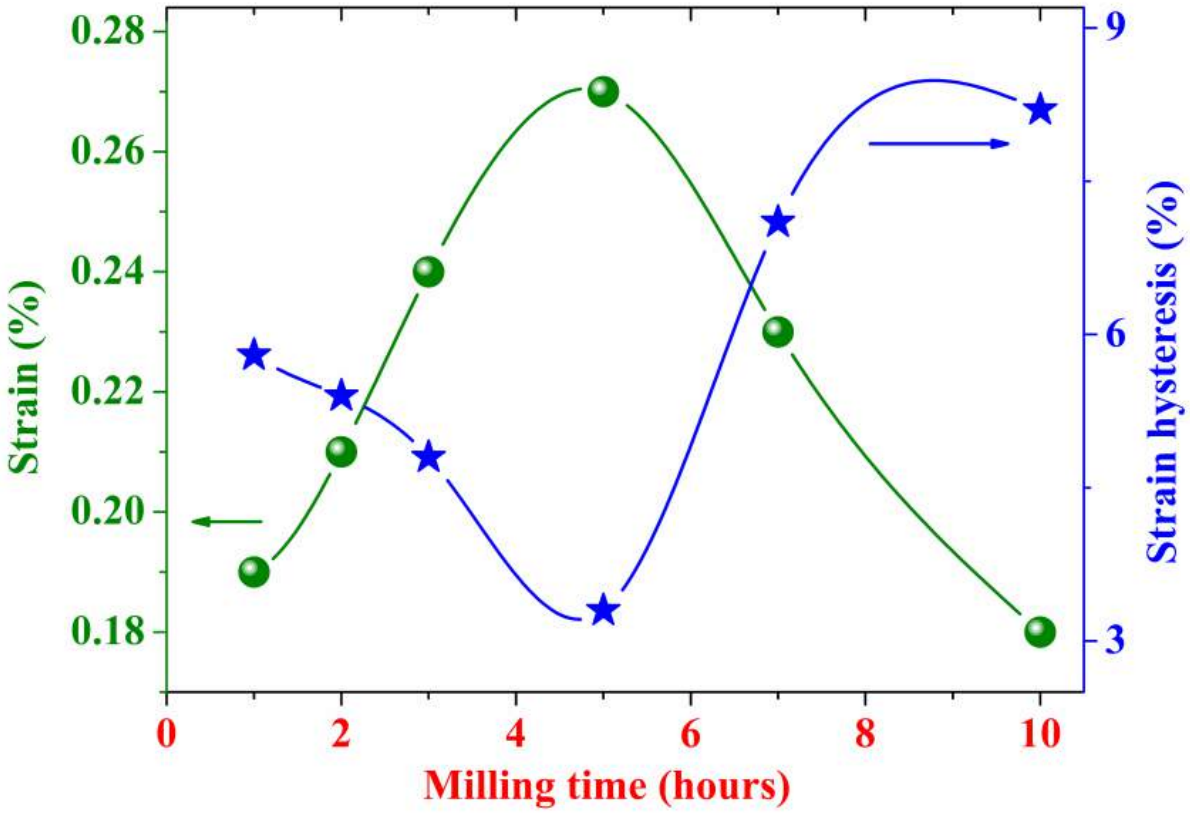

Fig. 5.25 *Change in strain (%) and strain hysteresis (%) as a function of milling time, measured at 50 kV/cm, 1 Hz and 25^{o}C.*

As per the previous section 5.5.1, piezoelectric charge coefficient (d_{33}) was calculated from the unipolar S-E hysteresis curves of poled PLZT 8/60/40 ceramics. An average d_{33} can be defined as the slope of the displacement vs. electric field hysteresis loop in the low field region. Fig. 5.26 shows the average d_{33} value, which was calculated from the slope of S-E hysteresis loop in low field region and normalized strain coefficient (S_{max}/E_{max}) as a function of milling time. PLZT 8/60/40 ceramics that were milled for 5 hours show the highest d_{33} and normalized strain coefficient (S_{max}/E_{max}) value. Some important parameters derived from S-E hysteresis loops are given in Table-5.6.

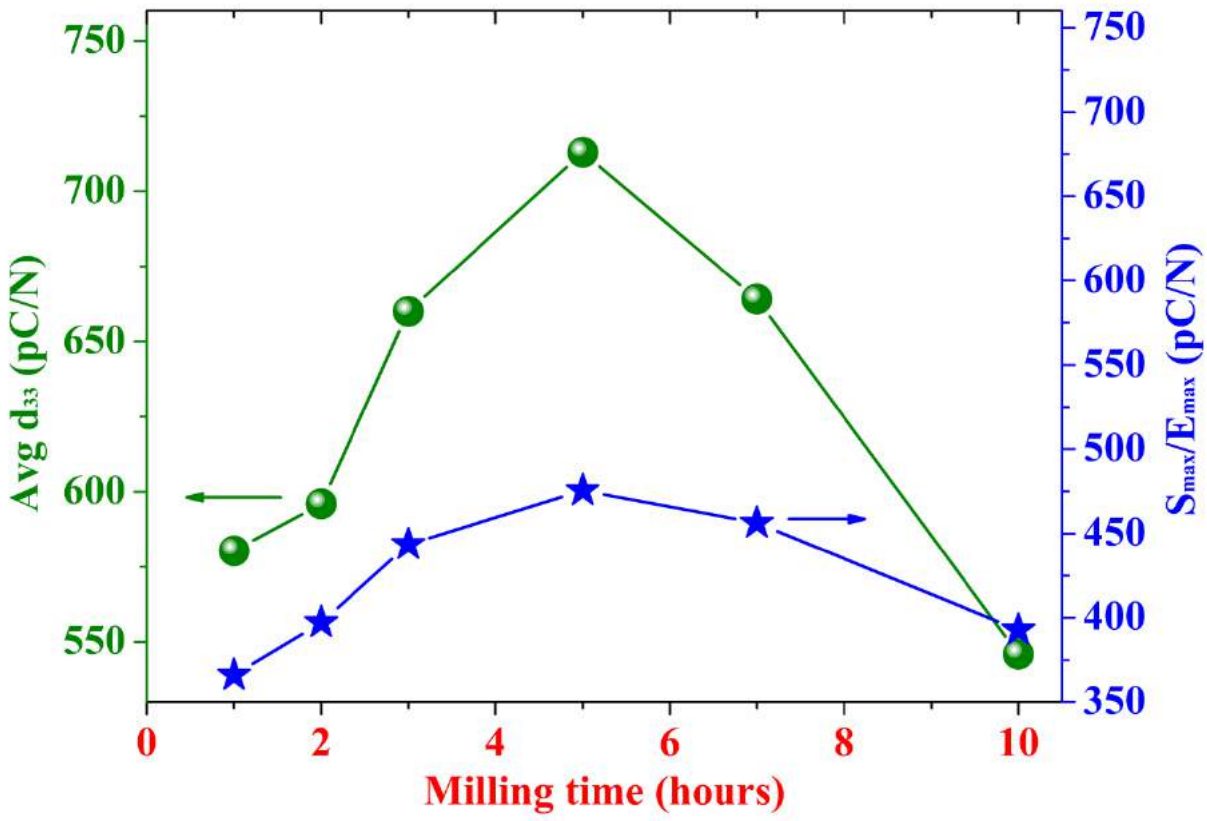

Fig. 5.26 *Variation in the (a) average piezoelectric charge coefficient (d_{33}) calculated from the slope of SE curve and (b) maximum strain divided by maximum applied electric field as a function of lanthanum substitution while measured at 50 kV/cm, 1 Hz and 25°C.*

Table-5.6 *Ferroelectric properties of PLZT 8/60/40 ceramics milled for different durations, measured at 50 kV/cm.*

Milling time	Strain (%)	Avg. d_{33} (pC/N)	Strain hysteresis (%)
1h	0.19	580	5.8
2h	0.21	596	5.4
3h	0.24	660	4.8
5h	0.27	712	3.3
7h	0.23	664	7.1
10h	0.18	546	8.2

5.6 Temperature dependent ferroelectric studies of PLZT 8/60/40 ceramics

In this section, ferroelectric hysteresis loops were measured for PLZT 8/60/40 ceramics at different temperatures. The dielectric measurements of electrically poled PLZT ceramics suggest that the La modification in PZT ceramics results in a deviation from the nature of ferroelectric phase transition from normal to the diffuse type phase transition (DPT). To support this study, polarization vs. electric field measurement were also performed on PLZT 8/60/40 ceramics within the temperature range of 30^{o}C to 170^{o}C. The temperature dependent P-E hysteresis loop can be used to understand the ferroelectric phase transition of PLZT 8/60/40 electro-ceramics. Temperature dependent S-E hysteresis loops were also measured and studied.

5.6.1 Temperature dependent P-E hysteresis loops

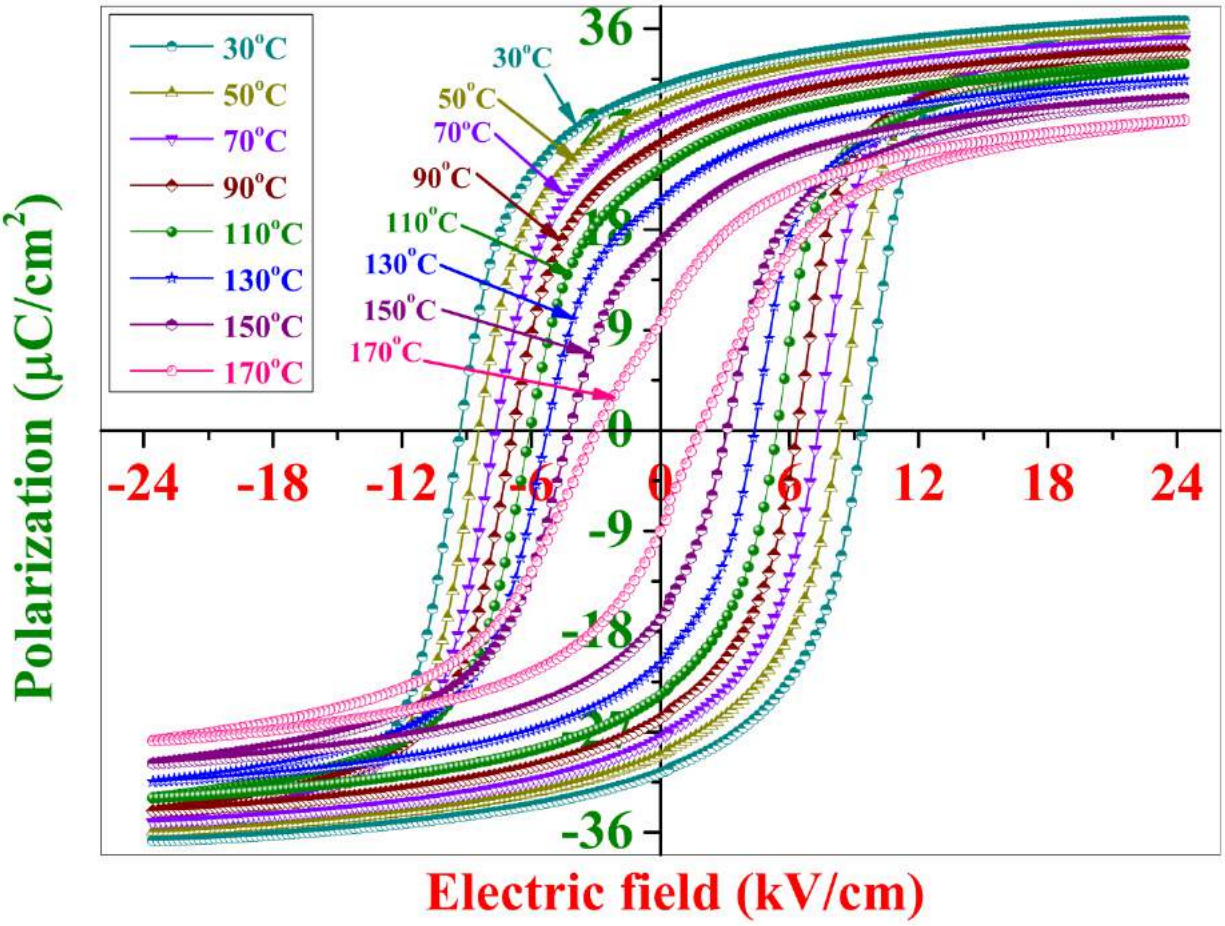

Fig. 5.27 *Temperature dependent polarization vs. electric field hysteresis loops for PLZT 8/60/40 electro-ceramics, measured at 1 Hz in the temperature range of 30^{o}C to 170^{o}C.*

The effect of temperature on the hysteresis behaviour of P-E loops for the PLZT ceramics was studied in detail. The change in the polarization of the PLZT 8/60/40 ceramics (5 hours milled in Zr-vial) with respect to applied electric field at different temperatures (from 30°C to 170°C) is shown in fig. 5.27. The well saturated P-E hysteresis loop with sharp edges confirms the ferroelectric nature of PLZT 8/60/40 ceramics at room temperature. The values of remnant polarization (P_r) and coercive field (E_c) at room temperature were found to be ~30.7 μC/cm^2 and 9.4 kV/cm, respectively at maximum applied electric field of 25 kV/cm. Fig. 5.27 shows that the shape of the P-E hysteresis loop changes with increasing temperature. With further increase in temperature, the P-E loops of PLZT ceramic become slimmer as in the case of the P-E loop for a dielectric material **[24]**.

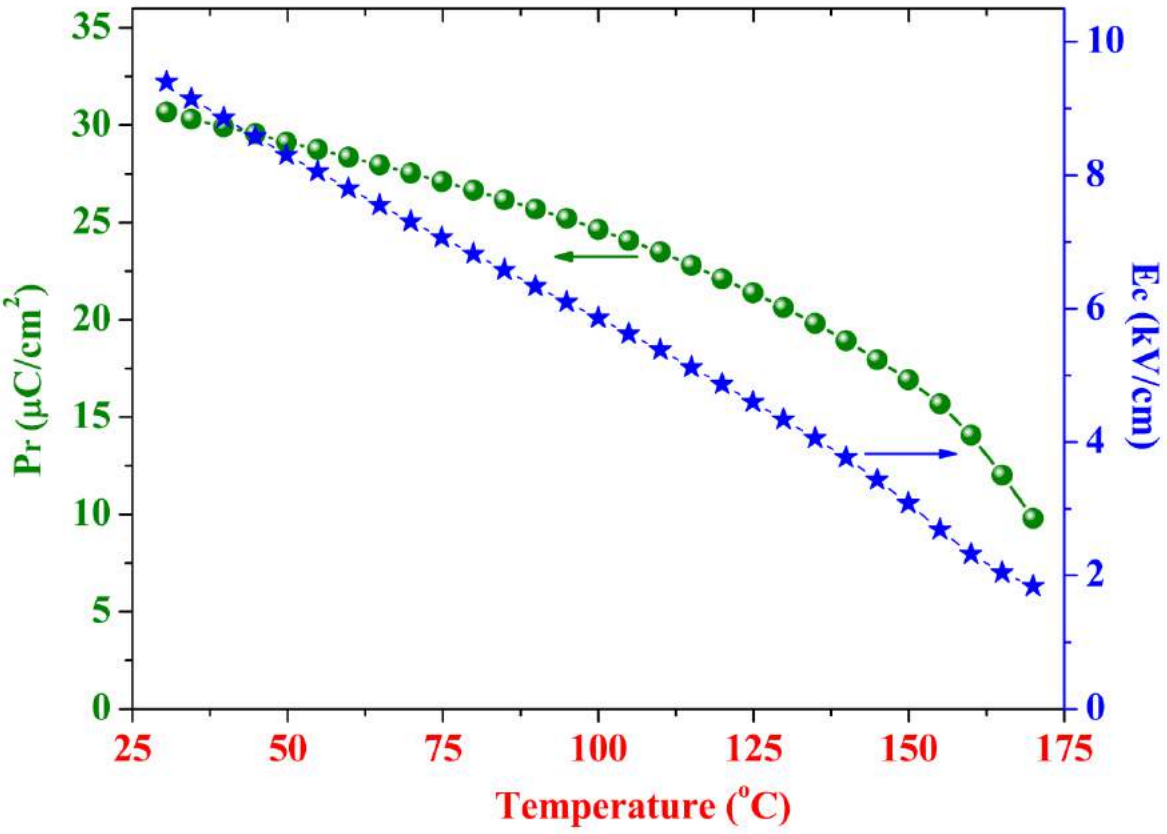

Fig. 5.28 *Change in remnant polarization and coercive field of PLZT 8/60/40 ceramics as a function of temperature.*

For the ferroelectric materials the values of maximum polarization (P_{max}), remnant polarization (P_r) and coercive field (E_c) decreases with an increase in temperature. Figs. 5.27 and 5.28 show the effect of temperature on ferroelectric properties such as the shape of P-E hysteresis loops, remnant polarization and coercive field of PLZT 8/60/40 electro-ceramics. At the transition temperature (T_c), normal ferroelectric show zero polarization. On the other hand ferroelectrics, which show the relaxor or DPT type transitions, have non-zero polarization, even after crossing the T_c. Fig. 5.27 shows the P-E hysteresis loop of PLZT 8/60/40 ceramics, measured at high temperature 170°C,

which is close to the transition temperature. The high value of P_r (~10 μC/cm^2) of PLZT 8/60/40 ceramics at 170^{o}C shows the possibility of non-zero remnant polarization even beyond the transition temperature. The coercive field value was also found to be very less at high temperature. This non-zero remnant polarization, which is a necessary condition for the existence of ferroelectricity and coercive field above the dielectric maxima temperature confirms the DPT type phase transition for PLZT 8/60/40 ceramics.

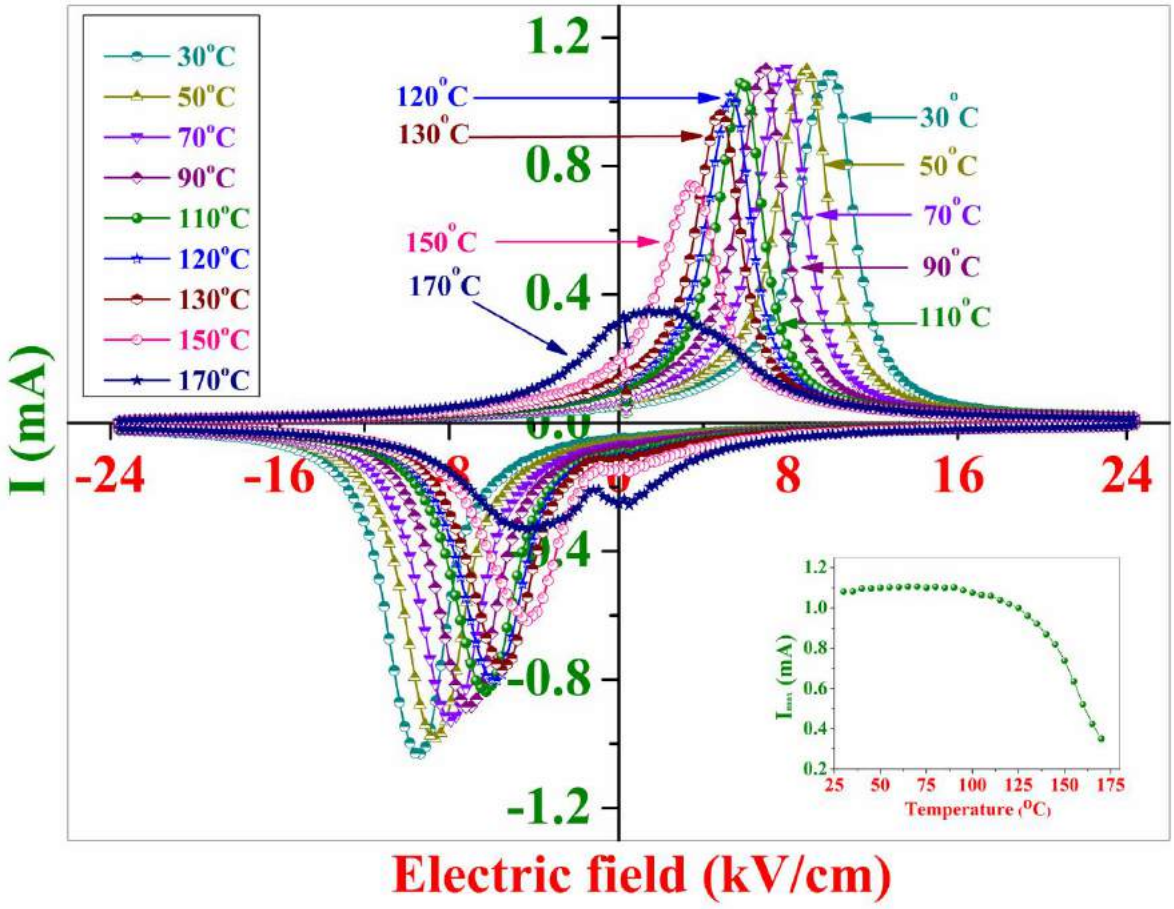

Fig. 5.29 *Temperature dependent I-E loops for PLZT 8/60/40 electro-ceramics, measured at 1 Hz from 30^{o}C to170^{o}C. Inset of the fig. shows the change in peak current with temperature.*

Fig. 5.29 shows the temperature dependent current vs. electric field (I-E) curves of PLZT 8/60/40 ceramics in the same temperature range, from 30^{o}C to170^{o}C. Room temperature I-E curve shows a sharp domain switching peak. As the temperature increases, the shape of the I-E curves changes and domain switching peak shifts towards the lower end. Fig. 5.29 show the change in domain switching peak current (I_{max}) as a function of the temperature of PLZT 8/60/40 electro-ceramics. The shape of I_{max} is sharp at room temperature and has the value of ~1.1 mA. As the temperature increases, the sharpness of the peak decreases, and it becomes broader. At 170^{o}C, the value of I_{max} is ~0.3 mA. The existence of domain switching current peak and non-zero I_{max} value, near to the transition temperature again confirms the DPT type phase transition for PLZT ceramics.

Fig. 5.27 shows the P-E hysteresis loops of the unpoled PLZT ceramics within the temperature range of 30°C-170°C, measured at 1 Hz. The profiles of the P-E hysteresis loops are related to the structure of polycrystalline PLZT ceramics with the temperature evolution. The quantification of changes in the hysteresis behavior of the PLZT ceramics can be derived from the following equation **[31-32]**

$$R_{sq} = \frac{P_r}{P_{sat}} + \frac{P_{1.1E_c}}{P_r} \quad \text{..... (8)}$$

Where R_{sq} is related to the squareness of P-E hysteresis loop, $P_{1.1Ec}$ is corresponding to the polarization, which was measured at 1.1 times the coercive field (E_c). For an ideal P-E hysteresis loop, R_{sq} is equal to 2.0.

The value of (P_{sat}, P_r) is related to the volume fraction of back switched domain (V_{back}), which is a kind of "switchable domain" and back switched when the value of electric field reduces to zero **[32]**

$$V_{back} \propto P_{sat} - P_r \quad \text{..... (9)}$$

Fig. 5.30 shows the change in R_{sq} and V_{back} as a function of temperature. It can be seen that the R_{sq} value is maximum at room temperature (R_{sq}=1.28). As the temperature increases, R_{sq} decreases and the volume fractions of back switching domains (V_{back}) is increases.

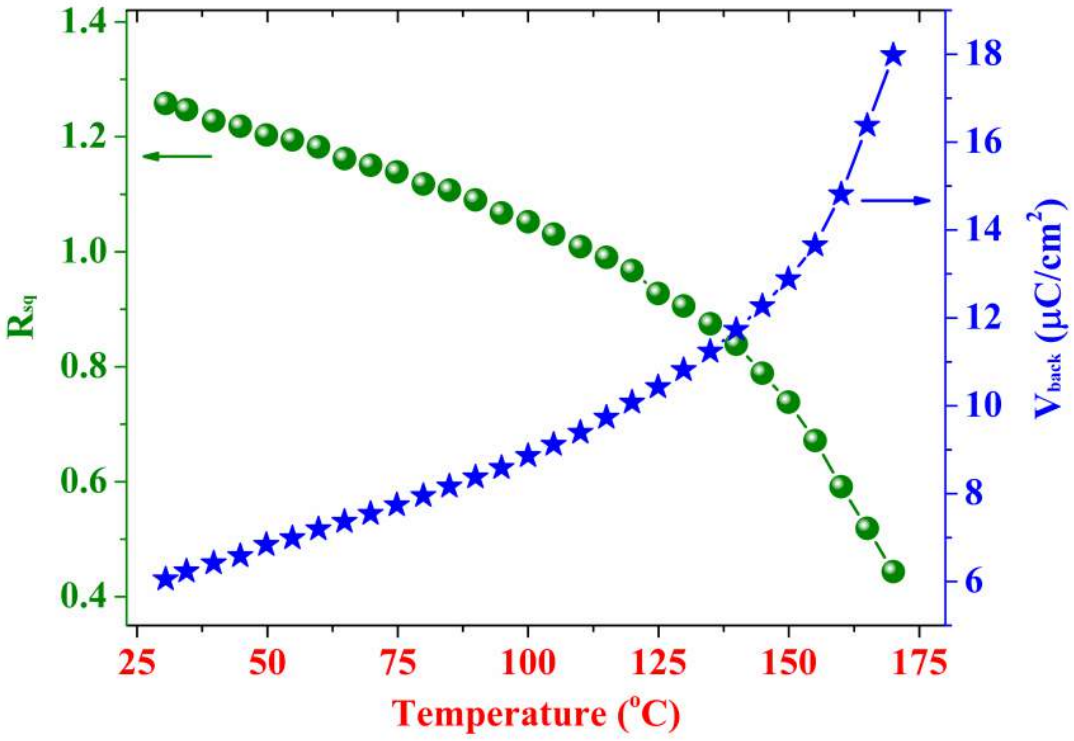

Fig. 5.30 *Effect of temperature on the squareness of P-E hysteresis loops and volume of back switched domains of PLZT 8/60/40 electro-ceramics.*

5.6.2 Temperature dependent S-E hysteresis loops

Electric field induced S-E hysteresis loops were measured for the PLZT 8/60/40 (5 hours milled in Zr-vial) ceramics from room temperature (30^{o}C) to the temperature (170^{o}C) that is close to a ferroelectric phase transition. Fig. 5.31 shows the temperature dependent S-E hysteresis curve for the PLZT ceramics. The shape of S-E loop and strain is changing as a function of temperature. The maximum strain value at room temperature was found to be ~0.09% at the maximum applied electric field of 40 kV/cm.

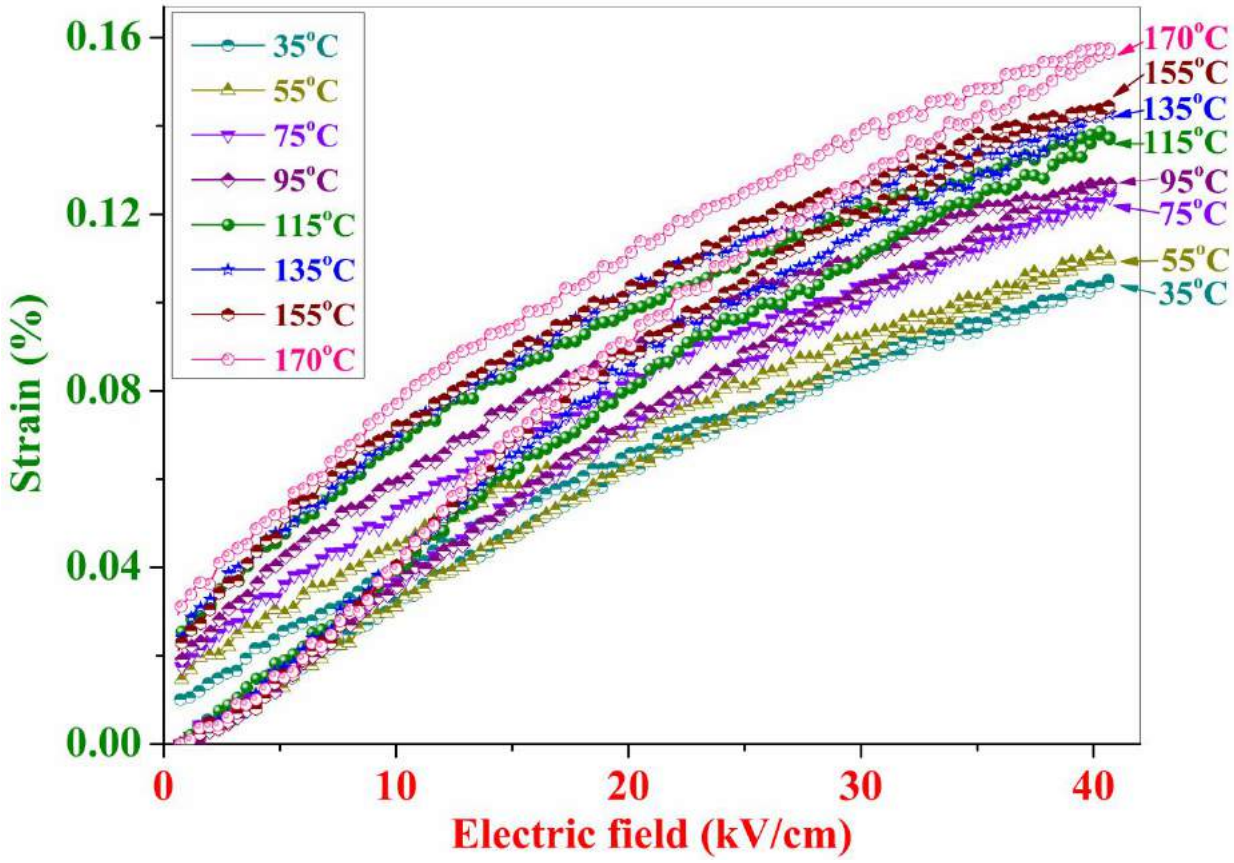

Fig. 5.31 Temperature dependent strain vs. electric field loops for PLZT 8/60/40 electro-ceramics, measured at 1 Hz in the temperature range of 30^{o}C to170^{o}C.

Fig. 5.32 shows the effect of temperature on (a) strain (%) (b) strain hysteresis (c) an average d_{33} and (d) S_{max}/E_{max} for PLZT 8/60/40 ceramics. All the above parameters were calculated from the fig. 5.31 and show an increase with temperature. The strain hysteresis value first shows an increase as a function of temperature then almost constant value at high temperature.

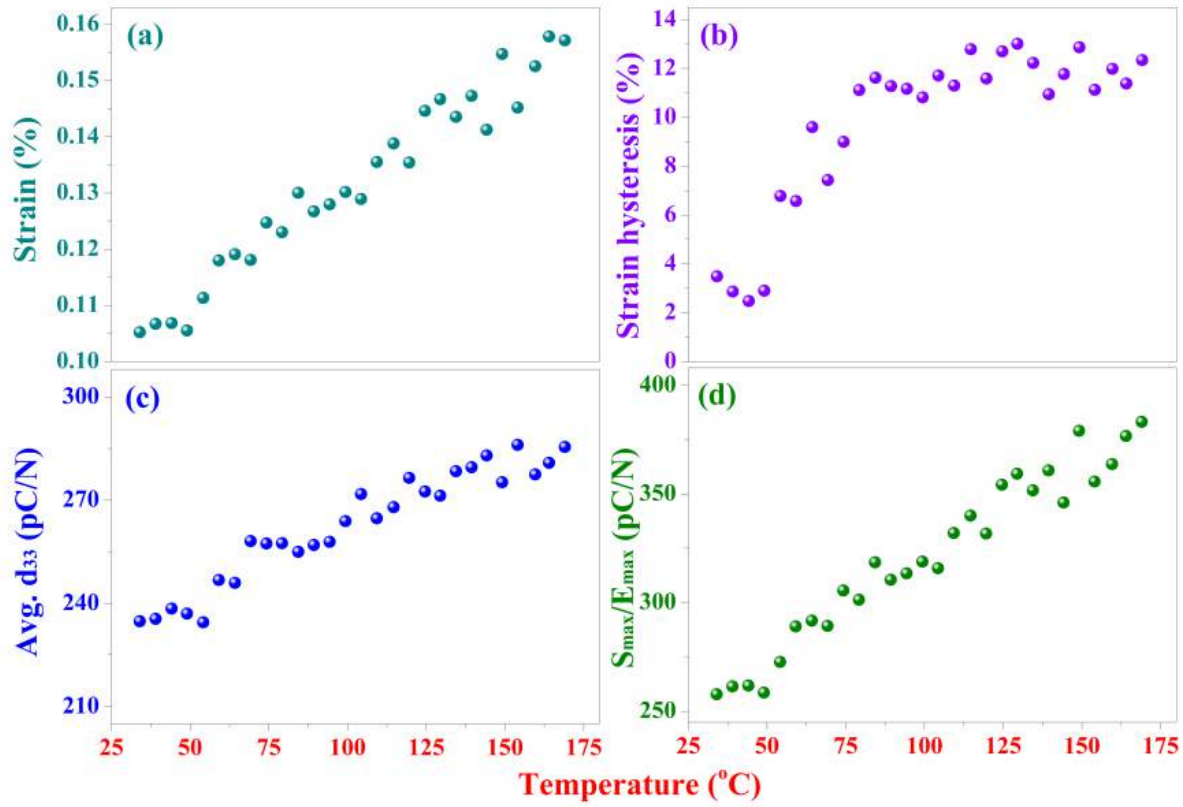

Fig. 5.32 Effect of temperature on (a) strain (%) (b) strain hysteresis (c) average d_{33} and (d) S_{max}/E_{max} for PLZT 8/60/40 electro-ceramics.

5.7 Discussion

Figs. 5.1 and 5.2 show the P-E, I-E and unipolar S-E hysteresis loops for PLZT 8/60/40 ceramics that were prepared using a mortar pestle and the results were compared with high energy milled ceramics. Mortar pestle prepared ceramics to show lower electrical properties than the high energy milled ceramics possibly due to the differences between their microstructure, as discussed in chapter-3.

Figs. 5.3, 5.7, 5.12 and 5.16 show the typical saturated P-E hysteresis loop and I-E curves at room temperature for (i) PLZT x/60/40 ceramics and (ii) PLZT 8/60/40 unpoled ceramics that were milled for different durations. When an electric field is applied to ferroelectric materials, the total current response consists of different types of signals as discussed previously. However, domain switching phenomena dominates the other ones **[11, 22-24]**. The occurrence of a peak in the current signal before reaching the maximum electric field is an indication of switching of ferroelectric domains inside ferroelectric materials. The appearance of a domain switching current peak (as evidenced in Figs. 5.7 and 5.16) in both positive and negative electric field directions, while measuring I-E curves, confirms the ferroelectric nature of PLZT ceramics. As the number of switched

domains increases with an increase in applied electric field, the magnitude of domain switching current peak also increases and finally gets saturated. The magnitude of other components of total current at the maximum applied electric field is very low compared to the magnitude of domain switching peak current. The corresponding P-E hysteresis curve shows high shape symmetry and squareness. The coercive field E_c value as determined from the saturated P-E and I-E loops is almost equal and can be used for further studies.

The variation of the domain switching current as a function of hysteresis electrical field amplitude of PLZT x/60/40 ceramics is also shown in fig. 5.7. The domain switching current, which was measured during the switching field cycles, is different from the leakage current which is generated when the ceramic experienced a high electric field. The domain switching current peaks, observed in both forward and reversed switching electric field cycles are an indication of the ferroelectricy in the electro-ceramics. In the case of PLZT ceramics, it can also be observed from the I-E plots that the current distribution is symmetrical for both negative and positive fields. This is a very important feature of electro-ceramics, as no remarkable change in the conductance of PLZT ceramics, when the direction of switching cycle changes was observed. Other important observed characteristics in PLZT ceramics is the stability and repeatability of the data under repeated cycling, which proves the potential of this material for cyclic high field applications.

The magnitude of domain switching current peak increases with an increase in lanthanum substitution (Fig. 5.7) and as a function of milling time (Fig. 5.16). These show the maximum value for PLZT 8/60/40 ceramics milled for 5 hours because the 5 hours milled PLZT 8/60/40 ceramics have the highest density, fine grain size and dense microstructure. The corresponding P-E hysteresis curves also show an improvement in squareness and symmetry.

Figs. 5.4, 5.5, 5.13 and 5.14 show the variation of remnant polarization and coercive field as a function of applied electric field, measured at room temperature for (i) PLZT x/60/40 ceramics and (ii) PLZT 8/60/40 unpoled ceramics that were milled for different durations. Figs. 5.6 and 5.8 show the change in P_r, E_c and I_{max} as a function of lanthanum substitution. Similarly figs. 5.15 and 5.17 show the change in P_r, E_c and I_{max} as a function of milling time. The highest values of all the above parameters were found for PLZT 8/60/40 ceramics; that was milled for 5 hours. As we know that even a low electric field, which is applied in the opposite direction of polarization over a long time is capable of switching the polarization in the opposite direction **[11]**. Polycrystalline ferroelectric materials contain different domain states, out of that some are clamped and do not contribute to the total polarization. The available domain states decide the magnitude of the remnant polarization (P_r) of ferroelectric materials. Apart from that the shape symmetry of the P-E loops, remnant polarization, coercive field are affected by many factors such as preparation conditions, mechanical stresses, charged defects, and thermal treatment **[2, 11]**.

The PLZT 8/60/40 composition is close to the morphotropic phase boundary, which provides the 14 available domain orientation states in perovskite structured ferroelectrics as per the

crystallographic point of view. These 14 domains states are the combination of 6 states in tetragonal and 8 states in rhombohedral phases, which contain a number of 180^o and non-180^o (90^o) domains. 180^o domain reversal is easier than the non-180^o domain switching. The 180^o domain reversal requires minimal structural strains or electric field, however, the switching of non-180^o domains linked with the larger deformation or higher electric field. In the presence of an external electric field both 180^o and non-180^o domains try to align in the electric field direction. However, switching of domains, which is separated by 180^o domain walls plays an important role and has a major contribution to the P_r value. Initially, the rapid increase in polarization refers to 180^o domain reversal and further increases refer to the switching of non-180^o domains. The switching of non-180^o domains contributes more to the strain but less in polarization **[33]**. A similar trend for P_r and E_c parameters as a function of applied electric field was found. Almost same switching characteristics at same electric field suggest the dependence of both parameters on the switching of 180^o domain wall. Figs. 5.4, 5.5, 5.13 and 5.14 shows the both P_r and E_c are highly electric field dependent. Hence, the saturated P-E and I-E loops should be used for the coercive field determination.

Figs. 5.9 to 5.11 and 5.18 to 5.20 are related to the symmetry of P-E hysteresis loops. All of the above figures show the change in E_{in} and (P_{r+} + P_{r-}) as a function of applied electric field, lanthanum substitution and milling time. Both the values shows less variation for 5 hours milled PLZT 8/60/40 ceramics. The asymmetric P-E loops suggest that the difference in positive and negative part of the coercive field, which leads to a high value of E_{in} i.e. the internal electric field (E_{in}), which can also induce or switch ferroelectric polarization. E_{in} arise due to thermal strain (ceramics preparation) that can introduce defect dipoles. A mass of these dipoles introduces a macroscopic internal electric field (E_{in}).

Figs. 5.21 to 5.26 show the electric field induced unipolar S-E hysteresis loops and their derived parameters as a function of applied electric field, measured at room temperature for (i) PLZT x/60/40 ceramics and (ii) PLZT 8/60/40 ceramics that was milled for different durations. Fig. 5.22 and 5.25 show the change in strain and strain hysteresis in PLZT ceramics as a function of lanthanum substitution and milling time. The strain hysteresis loss (%) value was calculated from fig. 5.21 and 5.24 using eq.-(7). Fig. 5.23 and 5.26 show the piezoelectric charge coefficient (d_{33}) and the normalized strain coefficient (S_{max}/E_{max}) as a function of lanthanum substitution and milling time. It is known that electro-ceramics also contain non-180^o domains and the movement and switching of non-180^o walls involve a significant change in dimensions of the ceramics, in addition to the pure piezoelectric response. The strain values increase with applied electric field, due to an increase in the alignment of domains. The fine grained ceramic show high remnant strain compared with coarse grained materials. As the grain growth occurs, the remnant strain decreases. The decrease in the area of S-E hysteresis loops as a function of an electric field indicates the easy domain switching in large grains ceramics.

From the above figures, it is observed that strain, d_{33} and S_{max}/E_{max} increases while strain hysteresis decrease as a function of lanthanum substitution and milling time. The 5 hours milled PLZT ceramics show the highest strain, d_{33} and S_{max}/E_{max} and low hysteresis loss. The strain values were observed at high electric fields and these ceramics showed good dielectric strength. The high piezoelectric response in ferroelectric ceramics can be explained on the basis of the grain sizes. The effect of fine grain sizes on the properties of electro-ceramics can be explained by the internal stress. Tuttle et al. **[34]** observed multiple 90^o domain walls for grains larger than 1 μm. It was observed that the domain width also decreased with a decrease in grain size.

The PLZT 8/60/40 ceramics milled for 5 hours show the maximum strain ~0.27% and minimum loss (~3%) at the electric field around 50 kV/cm (as shown in Fig. 5.24). The ultra-high strain and low hysteresis in PLZT ceramics make them promising candidates for the applications in which hysteresis loss results in the heating of peripheral electronics. As we know that the hysteresis loss necessitates the use of the additional circuitry in the feedback network which again increase the cost and the complexity of the device. Hence, the use of PLZT ceramics which show the decrease in the area of the hysteresis loop helps to minimize the addition of extra circuitry **[25, 35]**. The well saturated loops with high shape symmetry, low coercive field, high remnant polarization, high strain level and low hysteresis loss of PLZT ceramics can be attributed to uniform distribution of composition, uniform distribution of grain sizes, fewer imperfections and defects in the crystallites **[11, 28-29, 36]**.

The temperature dependent ferroelectric properties of PLZT 8/60/40 ceramics was also studied. The P-E (Fig. 5.27) and I-E loops (Fig. 5.29) were measured at the different temperature and their derived parameters P_r, E_c and I_{max} (Fig. 5.28 and Inset of 5.29) were plotted as a function of temperature. When ferroelectric ceramics undergo low symmetry ferroelectric to a high symmetry paraelectric phase transition, the shape of the P-E hysteresis loops become slimmer. At transition temperature the value of P_r, E_c and I_{max} approach zero. In the presence of an electric field, the dipoles in ferroelectrics begin to orient in the direction of the electric field. This alignment is opposed by the thermal agitation which tends to randomize the dipoles. The average dipole moment contribution per dipole ($P^|$) within the range 0^o to 180^o is given by Langevin **[37-38]**

$$\boldsymbol{P^|} = \boldsymbol{p}\,\mathbf{coth}\left(\frac{\boldsymbol{pE}}{\boldsymbol{kT}}\right) - \frac{\boldsymbol{kT}}{\boldsymbol{pE}} \quad \text{..... (10)}$$

where E = applied electric field, T = temperature of the ceramic, p = dipole moment, k = Boltzmann constant.

Eq-(10) show the two possibilities for the polarization in ferroelectrics (i) in the case of high applied electric field and low temperature, a maximum number of dipoles align along the direction of the electric field and (ii) The second case is related to the increase in temperature of the ferroelectric

ceramics. As the temperature increases, the total polarization of the ceramics starts decreasing due to the domains inside the ceramics grains, which start getting randomly oriented. At a certain temperature known as the Curie or transition temperature (T_c), the total polarization of ferroelectrics disappears continuously or sometimes discontinuously.

At the T_c, the polarization is zero for a normal ferroelectric and non-zero for ferroelectrics that show relaxor or DPT type transitions. The presence of ferroelectricity at temperature, close to T_c can also be noted from the figs. 5.27 and 5.29, in which the P-E and I-E loop were measured near to T_c. The persistence of ferroelectricity at this temperature may be due to the existence of polar regions. The temperature dependent ferroelectric measurements were performed by immersing the PLZT ceramic sample in silicone oil which breaks down at temperatures beyond 170^{o}C. This condition limits the measurement of P-E and I-E loops within the temperature range of 30^{o}C to 170^{o}C, which is less than the transition temperature of the PLZT 8/60/40 ceramics. However, the high Pr (~10 μC/cm^2, Fig. 5.28) and I_{max} (~0.3mA, Inset of fig. 5.29) values of PLZT ceramics at 170^{o}C show the possibility of non-zero remnant polarization with low coercive field value even beyond the transition temperature. This non-zero remnant polarization, which is a necessary condition for the existence of ferroelectricity and coercive field above the dielectric maxima temperature confirms the DPT type phase transition for PLZT 8/60/40 ceramics.

The ferroelectric studies further corroborated the dielectric studies (Chapter-4), which indicate the deviation of phase transition from Curie-Weiss behavior. The existence of ferroelectricity beyond the transition temperature is a common phenomenon which is already reported by several researchers **[39-41]**. The non-zero polarization may be attributed to the following reasons; oxygen deficiency in various regions within the ceramics, which leads to electric heterogeneity, disruption of the ferroelectric long-range order, which is usually, caused by the chemical disorder, grain boundary contributions, etc. These compositional gradients and different types of defects and imperfections related to the ceramic grain boundaries create local random fields. Since fine grained polycrystalline ceramics have the high density of grain boundaries **[42]** the grain boundaries and various defect structures play an important role in this mechanism. The volume fraction of back switching domains of P-E hysteresis loops are increasing (Figs. 5.33 and 5.30), and squareness of the P-E loops is decreasing (Fig. 5.30) as a function of temperature because at high temperature, domains become unstable and ferroelectric ceramics approach the phase transition.

The performance of ferroelectric material based devices shows considerable changes when operated over a wide temperature range. These changes are due to the temperature dependence of strain characteristics of the ferroelectric material. The effects of temperature on electric field induced unipolar strain, measured at an electric field of 40 kV/cm have been investigated between 35^{o}C to 170^{o}C for PLZT 8/60/40 ceramics, which was 5 hours milled in Zr vial (Fig. 5.31). The value of

maximum strain (%), average d_{33} and normalized strain coefficients (Fig. 5.32 (a)-(c)) shows an increase as a function of temperature, whereas the strain hysteresis is stable at higher temperatures (Fig. 5.32 (d)). The available reports which show temperature dependent piezoelectric properties of polycrystalline PZT based ceramics will be discussed here. Jaffe et al. **[17]** discovered that the piezoelectric charge coefficient (d_{33}) increases with temperature. Zhang et al. **[18]** reported that an increase in piezoelectric charge coefficient by a factor of ~2.5 when the temperature was increased from 50 to 300 K. Experimental results from Paik et al. **[19]** in the temperature range of 30 and 300 K showed many fold enhancement in the d_{33}, which again depends on the PLZT composition. Here in our study, we found that the strain, d_{33} and normalized strain was increased by a factor of ~1.5 times when the temperature of the ceramics was increased from 35^{o}C to 170^{o}C. However, the increase in strain hysteresis value shows saturation at high temperatures.

5.8 Summary

Polarization versus electric field (P-E) and strain vs. electric field (S-E) hysteresis loops was measured for two cases (i) different compositions of PLZT ceramics (ii) milling of PLZT 8/60/40 ceramics at different time durations. Based on the above hysteresis curves, the nature of the PLZT ferroelectric material was studied. Along with these hysteresis loops, I-E loops were also measured. Optimized PLZT 8/60/40 compositions show the maximum value of remnant polarization (~29.1 μC/cm^2), domain switching current (~2 mA) and low coercive field (~9.40 kV/cm). The PLZT 8/60/40 electro-ceramics exhibited the highest strain of 0.25% with low hysteresis loss of ~4% and an average d_{33} value of ~632 pC/N. This optimized PLZT 8/60/40 composition shows the highest properties when it was milled for 5 hours with P_r ~34 μC/cm^2, E_c ~12 kV/cm, I_{max} ~2.06 mA, strain ~0.27%, hysteresis loss ~3% and an average d_{33} value of ~712 pC/N. Ultra-high strain properties, coupled with low hysteresis loss, demonstrate the suitability of PLZT material for cyclic and high electric field applications. The symmetry of the P-E hysteresis loops is studied by using the internal macroscopic electric field (E_{in}) and (P_{r+} + P_{r-}) parameters and highly symmetrical PE loop was found for the PLZT 8/60/40, 5 hours milled ceramics. The P-E and S-E hysteresis loops along with I-E loops of PLZT 8/60/40 ceramics were also measured as a function of temperature to understand the behavior of ferroelectric material at elevated temperatures. It shows the squareness (R_{sq}) of the P-E loops is decreased and the volume fraction of back switching (V_{back}) domains increased as temperature increases. High shape symmetry of P-E loops, low hysteresis loss in S-E loops and high remnant polarization at high temperatures suggests that the PLZT 8/60/40 ceramics are promising materials for high temperature applications.

References

[1] B. Jaffe, W.R. Jr. and H. Jaffe, Piezoelectric Ceramics, Academic Press, New York, (1971).

[2] G.H. Haertling, J. Am. Ceram. Soc., **82** (1999) 797.

[3] W.J. Merz, Phys. Rev., **95** (1954) 690.

[4] A. Gruverman, D. Wu and J.F. Scott, Phys. Rev. Lett., **100** (2008) 097601.

[5] A.K. Tagantsev, I. Stolichnov, N. Setter, J.S. Cross and M. Tsukada, Phys. Rev. B, **66** (2002) 214109.

[6] J. Li, B. Nagaraj, H. Liang, W. Cao, C.H. Lee and R. Ramesh, Appl. Phys. Lett., **84** (2004) 1174.

[7] V.L. Ginzburg, ZhEksp. Teor. Fiz. 15, 739 (1945) [J. Phys. X 107, (1946)].

[8] S. Ducharme, V.M. Fridkin, A.V. Bune, S.P. Palto, L.M. Blinov, N.N. Petukhova et al., Phy. Rev. Lett., **84** (2000) 175.

[9] W.J. Merz, J. Appl. Phys., **27** (1956) 938.

[10] M.E. Lines and A.M. Glass, Principles and Applications of Ferroelectrics and Related Materials, Clarendon Press Oxford, Great Britain, Ch. 11 (1977).

[11] D. Damjanovic, Rep. Prog. Phy., **61**(1998) 1267.

[12] K. Uchino, Piezoelectric actuators and ultrasonic motors. Boston, MA: Kluwer; (1997).

[13] K. Lubitz, C. Schuh, T. Steinkopff and A. Wolff, editor: N. Setter, Piezoelectric Materials in Devices, Lausanne: EPFL, (2002) 183.

[14] W. Wersing, editor: N. Setter, Piezoelectric Materials in Devices, Lausanne, EPFL, (2002) 29.

[15] J. Zheng, S. Takahashi, S. Yoshikawa, K. Uchino and J.W.C. de Vries, J. Am. Cer. Soc., **79** (1996) 3193.

[16] H. Kungl and M.J. Hoffmann, Sensor Actuator A, submitted for publication.

[17] H. Jaffe and D.A. Berlincourt, Proc. IEEE, **53** (1965) 1372.

[18] Q.M. Zhang, H. Wang, N. Kim and L.E Cross, J. Appl. Phys.,**75** (1994) 454.

[19] D.S. Paik, S.E. Park, T.S. Shrout and W.J. Hackenberger, Mater. Sci., **34** (1999) 469.

[20] H. Kungl and M.J. Hoffmann, Acta Mater., **55** (2007) 5780.

[21] J.C. Burfoot and G.W. Taylor, Polar Dielectrics and Their Applications, London: Macmillan, (1979).

[22] Hysteresis software version 2.4.0.0 user manual, aixACCT GmbH, Germany.

[23] B. Tareev, Physics of Dielectric Materials, English Translation, Meer Publishers, Moscow, Second Edition, Ch. 3 (1979).

[24] H. Yan, F. Inam, G. Viola, H. Ning, H. Zhang, Q. Jiang, T. Zeng, Z. Gao and M.J. Reece, J. Adv. Diel., **1 [1]** (2011) 107.

[25] M.L.V. Mahesh, V.V.B. Prasad and A.R. James, J. Elect. Mat., **42** (2013) 12.

[26] X. Chen,Y.Zou,G. Yuan, M. Zeng, J.M. Liu, J. Yin and Z. Liu, J. Am. Ceram. Soc., **96 [12]** (2013) 3788.

[27] A.R. James, J.P. Praveen, M.P. Kumar and V.V. Bhanu Prasad, Mater. Res. Bul., **47 [11]** (2012) 3459.

[28] A.R. James, J. Subrahmanyam and K.L. Yadav, J. Phys. D: Appl. Phys., **39** (2006) 2259.

[29] M.B. Rauls, W. Dong, J.E. Huber and C.S. Lynch, Acta Mater., **59** (2011) 2713.

[30] A.R. James, B.S.S. Chandra Rao, S.V. Kamat, J. Subrahmanyam, K. Srinivas and O.P. Thakur, Smart Mater. Struct., **17** (2008) 035020.

[31] W. Chaisan, R. Yimnirun, and S. Ananta, Phys. Scr., **T129** (2007) 205.

[32] Y. Tian, X. Chao, L. Wei, P. Liang and Z. Yang, J. Appl. Phys., **113** (2013) 184107.

[33] H. Du, F. Tang, F. Luo, W. Zhou, S. Qu and Z. Pei, Mater. Sci. Eng. B, **137** (2007) 175.

[34] B.A. Tuttle, T.J. Garino, J.A. Voigt, T.J. Headley, D. Dimos, M.O. Eatough, Science and Technology of Electroceramic Thin Films, Editors: O. Auciello and R. Waser (Dordrecht: Kluwer) (1995) p 117.

[35] H. Janocha, Actuators: Basics and Applications, Berlin: Springer, (2004).

[36] A. Kumar, V.V.B. Prasad, K.C.J. Raju and A.R. James, J. Alloys Comp., **599** (2014) 53.

[37] A. Kumar, V.V.B. Prasad, K.C.J. Raju and A.R. James, J. Mater. Sci.: Mater. Electron., **26** (2015) 3757.

[38] M.A. Wahab, Solid State Physics: Structure and Properties of Materials, Narosa Publishing House, New Delhi, India, Ch. 14 (2013).

[39] M.L.V. Mahesh, V.V.B. Prasad and A.R. James, J. Mater Sci: Mater Electron **24** (2013) 4684.

[40] M. Deluca, C.A. Vasilescu, A.C. Ianculescu and D.C. Berger, J. Eur. Ceram. Soc., **32** (2012) 3551.

[41] C. Ciomaga, M. Viviani, M.T. Buscaglia, V. Buscaglia, L. Mitoseriu, A. Stancu, and P. Nanni, J. Eur. Ceram. Soc., **27** (2007) 4061.

[42] I. Bunget and M. Popescu, Physics of Solid Dielectrics, Elsevier, New York, (1978).

Chapter- VI

Identification of the optimum poling conditions for PLZT 8/60/40 ceramics

6.1 Introduction

Ultra high strain $(Pb_{0.92}La_{0.08})(Zr_{0.60}Ti_{0.40})O_3$ (PLZT 8/60/40) piezoelectric ceramics were synthesized via a combinatorial approach of mechanical activation, followed by a cold isostatic pressing. The PLZT ceramics were structurally investigated and the coercive field was determined from the ferroelectric P-E hysteresis loops. The electrical properties of the piezoelectric ceramics are greatly influenced by the poling conditions. Therefore to get the highest electrical properties in piezo-ceramics the poling conditions should be optimized. Present study deals with the identification of the optimum poling conditions for the PLZT 8/60/40 ceramics. The effect of poling conditions on the piezoelectric and dielectric properties will be discussed here. Optimization of poling conditions can be done in three possible ways (1) Poling electric field (2) Poling time (3) Poling temperature. In this chapter, all three conditions have been described and the results presented. The effect of each of the three conditions on the dielectric, ferroelectric and piezoelectric properties are discussed. The dielectric constant (K), and loss (D) along with piezoelectric charge coefficient (d_{33}) and electromechanical coupling factor (k_p) were measured at different combinations of poling parameters. Since the high strain and the high piezoelectric charge (d_{33}) of the electro-ceramics are interdependent so it is necessary to find optimum poling conditions for electro-ceramics.

Generally, poling of piezoelectric materials is done by applying an electric field higher than their coercive fields. However, in this study, the values of K, D, d_{33} and k_p parameters show that PLZT 8/60/40 ceramics can be poled at ~5 kV/cm (< 0.5 E_c), which is contrary to common practice of poling. Moreover, the induced high piezoelectricity of PLZT ceramics was not compromised. This involved optimization of two other important poling parameters, viz poling temperature and poling time. The effect of ceramic sample thickness on the said properties was also studied. Additionally, the effect of aging on the electrical properties was studied for ceramics poled at $0.6E_c$ and $3E_c$, in detail.

6.2 Literature survey

Lanthanum modified PZT system is an important material, which has been widely used for highly reliable and repeatable dielectric, ferroelectric, piezoelectric, electro-optic and pyroelectric properties. These outstanding electrical properties of PLZT ceramics are intensively used for different technological applications. Some of them are different types of sensors, transducers, Surface Acoustic Wave filters, actuators, micro-electromechanical systems, nano-positioners, and high frequency devices **[1-3]**. PLZT 8/60/40 is a composition close to the MPB **[4]** and shows the highest strain [**5**] and better piezoelectric coefficients and coupling factors **[6]**. At the MPB, the six domain states of the tetragonal phase (90^o and 180^o domains) coexist with eight domain states of the rhombohedral phase (71^o, 90^o and 180^o domains), which results in 14 possible available directions of spontaneous

polarization. All the aforementioned factors make the properties show a maximum around the MPB **[3]**. Piezoelectric properties of the PLZT ceramics not only depend on the microstructure and morphology **[7-9]** but also on poling conditions **[10-14]**.

When a polycrystalline piezoelectric ceramic cools from the paraelectric to the ferroelectric state, ferroelectric domains are formed to minimize the electrostatic energy of the depolarizing field **[3-5]**. These domains are randomly reoriented at room temperature with zero net polarization termed as piezoelectrically inactive. With the application of dc poling electric field at high poling temperature, domains of the ferroelectric ceramics can be aligned to show piezoelectric properties. Thermal energy facilitates the motion of ferroelectric domains, which results in the reorientation of spontaneous polarization within each grain, leading to a net polarization along the direction of the poling field **[15]**.

In perovskite structure based ferroelectrics, non-180° domain walls are both ferroelastically and ferroelectrically functioning while 180° domain walls only are ferroelectrically active. Both 180° and non-180° domain walls contribute to the dielectric response. However, the piezoelectric response is only due to the 180° domain walls. The Rayleigh law explains the linear change in dielectric permittivity and piezoelectric coefficient as a function of electric field. For ferroelectric materials, the Rayleigh law can be expressed as **[16]**

$$d_{33} = d_{int} + \alpha_d E_0 \qquad (1)$$

$$\varepsilon_r = \varepsilon_{int} + \alpha_\varepsilon E_0 \qquad (2)$$

where d_{33} is the piezoelectric coefficient, E_0 is the amplitude of the driving field, ε_r is the relative permittivity, d_{int} and ε_{int} are the reversible dielectric and piezoelectric Rayleigh coefficients. α_ε and α_d are the irreversible Rayleigh coefficients for the dielectric and piezoelectric properties.

A detailed poling study not only for lead free ceramics **[11, 17-19]** but also for lead based materials **[10-12, 17-19]** is available in the literature. However, very few reports on poling are available for the PZT and PLZT ceramics. Available reports suggest that to get the excellent piezoelectric properties, the poling field should be higher than the coercive field. The carefully optimized poling conditions for PLZT ceramics helps to get outstanding piezoelectric properties. The three important poling parameters are poling electric fields, temperature and time; however, this study includes the thickness of the PLZT ceramic sample as an additional parameter. The purpose of this study is to identify the optimum poling conditions for PLZT 8/60/40 electro-ceramics and also to investigate the effect of poling conditions on the dielectric and piezoelectric properties.

6.3 PLZT ceramics preparation for poling optimization study

Preparation conditions for PLZT 8/60/40 ceramics, poling procedure and poling setup was already explained in detail in Chapter-2. All the characterization techniques that preceded the poling studies such as XRD, SEM, density, dielectric constant, dielectric loss, d_{33}, k_p, P-E and S-E were also discussed in Chapter-2.

Ceramics should fulfill minimum structural requirements such as pure phase, grain size and density, suggested by Kong et al. **[20]**. The PLZT 8/60/40 sintered ceramics shows a pure perovskite single phase, uniform grain sizes with well defined grain shapes and density >98% relative to the theoretical density and fit for further electrical characterizations.

It is known that the poling electric field is related to the coercive field of the ferroelectrics, which can be evaluated from the polarization vs. electric field P-E and I-E curves. Fig. 6.1 shows the saturated P-E and I-E loops for PLZT 8/60/40 un-poled ceramics. The coercive field (E_c) value, which was identified from the saturated P-E and I-E loops, is almost same and was found to be ~12 kV/cm. These values were borne in mind while performing further poling studies.

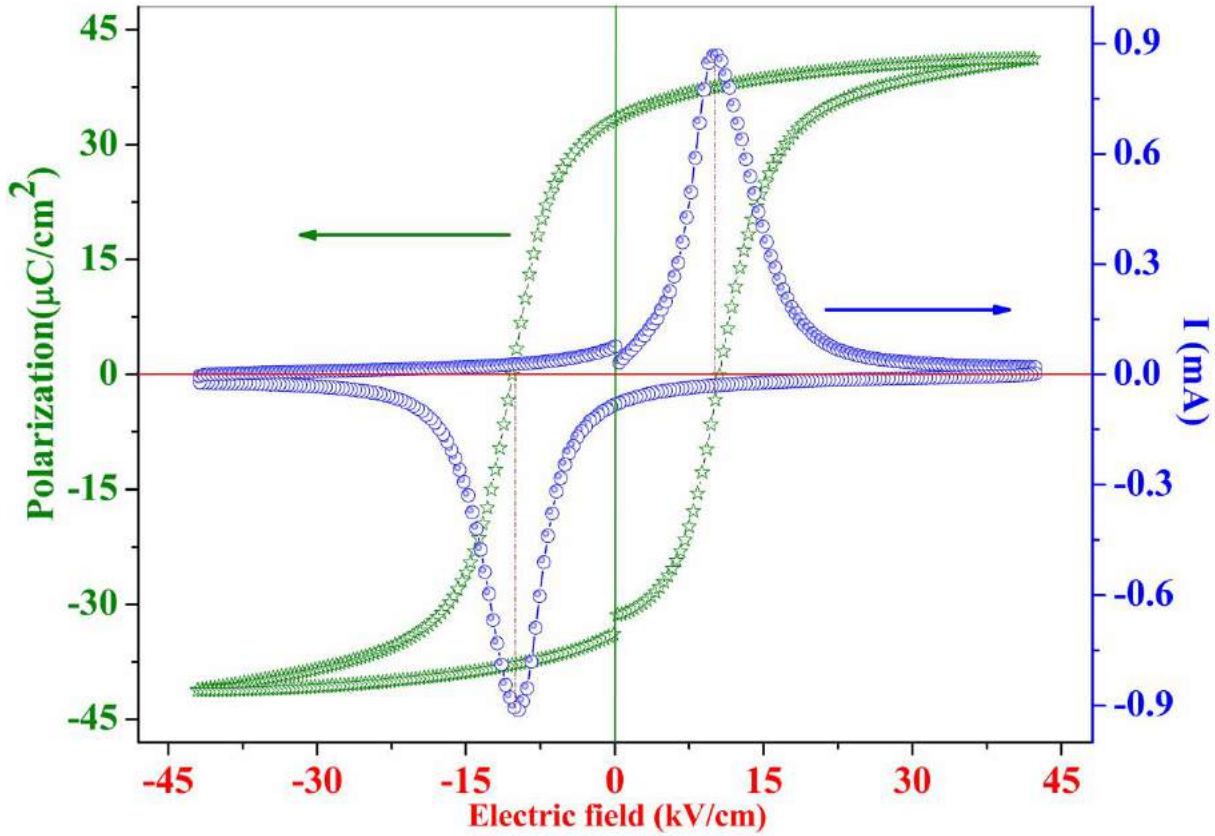

Fig. 6.1 *Polarization vs. electric field (P-E) and current vs. electric field (I-E) curves for the PLZT 8/60/40 un-poled ceramic sample at 1 Hz. A dotted line shows the electric field value at domain switching current peak that matches with polarization reversal field* ***[14]****.*

6.4 Effect of poling parameters on the piezoelectric properties of PLZT 8/60/40 ceramics

6.4.1 Effect of poling electric fields

Fig. 6.2 shows the change in piezoelectric coefficients of PLZT 8/60/40 ceramics as a function of poling field, confirming the influence of poling field on the aforesaid properties. The electric field, which was used for the poling process causes the switching and re-orientation of domains in ferroelectrics and make them piezoelectrically active. After the poling process, remnant polarization in polycrystalline ferroelectrics depends on the available domain states. Ferroelectrics containing only 180^o domains show P_r ~0.25 P_s. The ferroelectrics having tetragonal, rhombohedral and orthorhombic symmetries contain six, eight and twelve domain states, respectively and the corresponding P_r are ~0.83 P_s, ~0.87 P_s and ~0.91 P_s. The above discussion is based on the assumption that all ferroelectric domains reorient by the poling field. However, many domains cannot reorient due to their complex set of internal stresses and electric fields in grains **[3]**. During the poling process, the spontaneous strain of piezoelectric materials is affected only by non-180^o domains. The switching of 180^o domains does not have any contribution in strain thereby the switching of 180^o domains is easier than non-180^o domains.

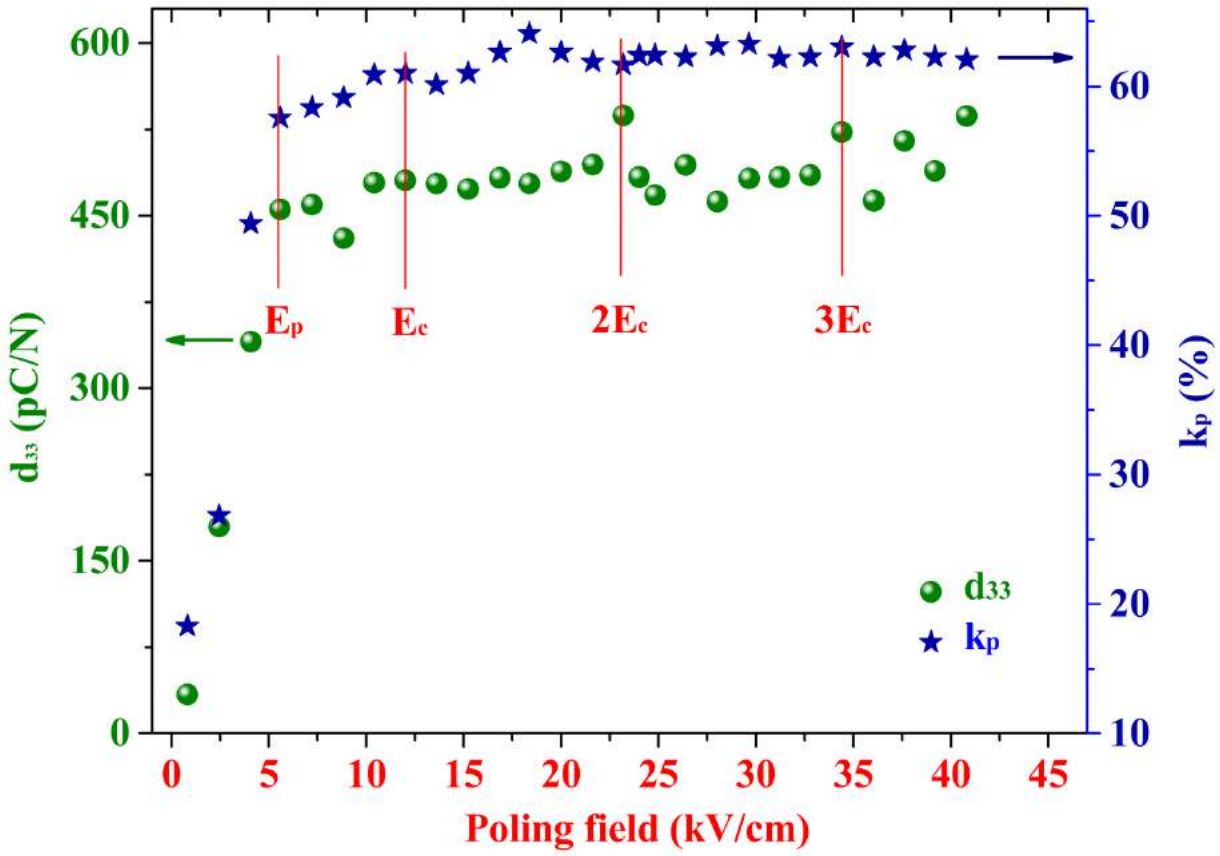

Fig. 6.2 *Variation in piezoelectric charge coefficient (d_{33}) and electromechanical coupling factor (k_p) with respect to the poling electric field.*

Fig. 6.2 shows the change in d_{33} and k_p as a function of poling electric field for PLZT 8/60/40 ceramics. The value of parameters increases rapidly with the poling electric field over the range of ~0.8 to ~5 kV/cm, which is less than half of the coercive field. However, when the poling electric field exceeds ~5 kV/cm, not much significant change was observed in piezoelectric parameters. The rapid increase in d_{33} and k_p may be attributed to the switching of 180^o domains at lower poling electric fields due to their easier switching, than non-180^o domains.

The PLZT 8/60/40 composition is close to the morphotropic phase boundary, which provides 14 possible domain orientation states in perovskite structured ferroelectrics from a crystallographic perspective. These 14 domains states are a combination of 6 states in tetragonal and 8 states in rhombohedral phases, which contain a number of 180^o and non-180^odomains. The 180^o domain reversal is easier than the non-180^o domain switching. The 180^o domain reversal requires minimal structural strains or electric field, however, the switching of non-180^o domains is linked with the larger deformation or higher electric field. In the presence of an external electric field, both 180^o and non-180^o domains try to align in the electric field direction **[12]**.The dipoles in ferroelectrics possess minimum potential energy only when they are aligned in the direction of the electric field. The average dipole moment contribution per dipole ($P^|$) within the range 0^o to 180^o is given by **[21]**

$$\boldsymbol{P^|} = \boldsymbol{p}\,\mathbf{coth}\left(\frac{\boldsymbol{pE}}{\boldsymbol{kT}}\right) - \frac{\boldsymbol{kT}}{\boldsymbol{pE}} \quad \text{..... (3)}$$

where p=dipole moment, E=applied electric field, k = Boltzmann's constant, T= ceramic temperature

Eq-(3) explained the effect of the poling electric field on the piezoelectric properties of PLZT 8/60/40 ceramics. When the applied electric field is very high at low temperature, maximum number of dipoles align along the direction of the electric field. However, this high external electric field results in collisions between the free electrons. The accumulated energy leads to an increase in temperature of the piezoelectric ceramics, which results in the fall in piezoelectric properties, and final thermal breakdown. Due to the quantum tunneling effect, free electrons of piezoceramics may move from the forbidden band to the conduction band, which speeds up the electron impact ionization in a high field and an increase in an electric leakage current **[10]**. Thereafter this results in the decline of poling dependent electrical properties and eventually breakdown of ceramics.

The application of high electric field increases the number of aligned dipoles the direction of the electric field. However, in PLZT 8/60/40 ceramics, when the electric field exceeded 40 kV/cm, they show electrical as well as physical breakdown. The ceramics show visible cracks on the surface. This may be due to vacancy defects, pores (which were not seen in SEM image in Chapter-3), and other physical flaws in the ceramics. These flaws and defects can move easily at high electric field compared with the coercive field of PLZT ceramics ~12 kV/cm (~40 kV/cm), and results in an increase in electrical conductivity.

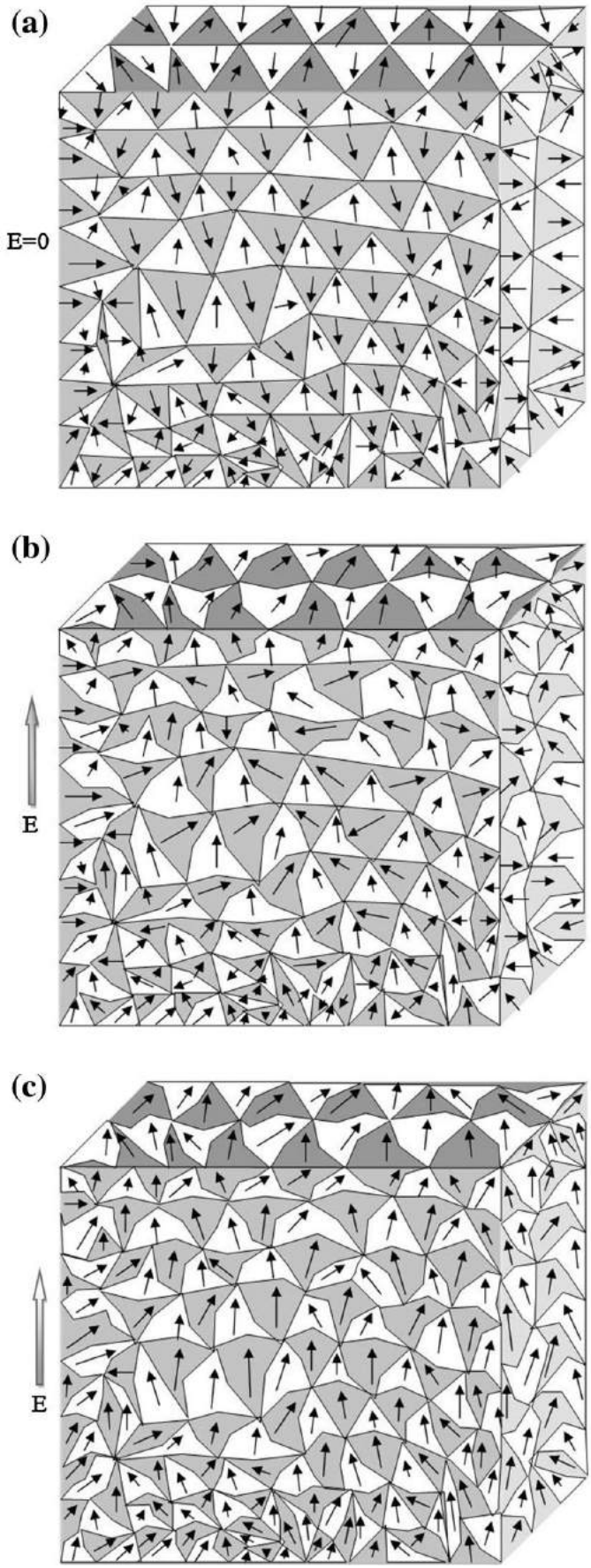

Fig. 6.3 *Schematic representation of the ferroelectric domains orientation for (a) un-poled, (b) sufficiently poled (~0.5E_c) and (c) excess poled (~3E_c) PLZT ceramics, respectively* ***[13]***.

Figs. 6.3 (a), (b) and (c) show the schematic representation of ferroelectric domains orientation inside the grains which are (a) un-poled, (b) sufficiently poled (~$0.5E_c$) and (d) excess poled (~$3E_c$), respectively. At first, when the applied electric field is zero, domains of the sintered and un-poled PLZT ceramics are randomly oriented as shown in fig. 6.3 (a). As the electric field increases, domains begin to align in the electric field direction. When the electric field reaches its threshold value, a large number of domains suddenly switch into the direction of applied electric field as shown in fig. 6.3 (b) as well as fig. 6.2 (~5 kV/cm, ~0.5Ec). When most of the domains are switched, there is not much difference in the piezoelectric properties of PLZT ceramics with an increase in an electric field as shown in fig. 6.3 (c).

Available reports suggest that the poling electric field should be higher than the coercive field of the ceramics **[10-12, 19]**. However, the optimum poling field for PLZT ceramics was found to be half of the coercive field, which is very less compared to conventional poling. The poling of ferroelectrics at significantly reduced poling voltages is very advantageous if the samples have poor resistivity or high conductivity, which is a common problem at high temperature. The study was done by Hinterstein et al. **[7]**, in which the thermal parameter of the lead atom shows its maximum value less than the coercive field can be correlated with the present results.

6.4.2 Effect of poling temperature on the piezoelectric properties

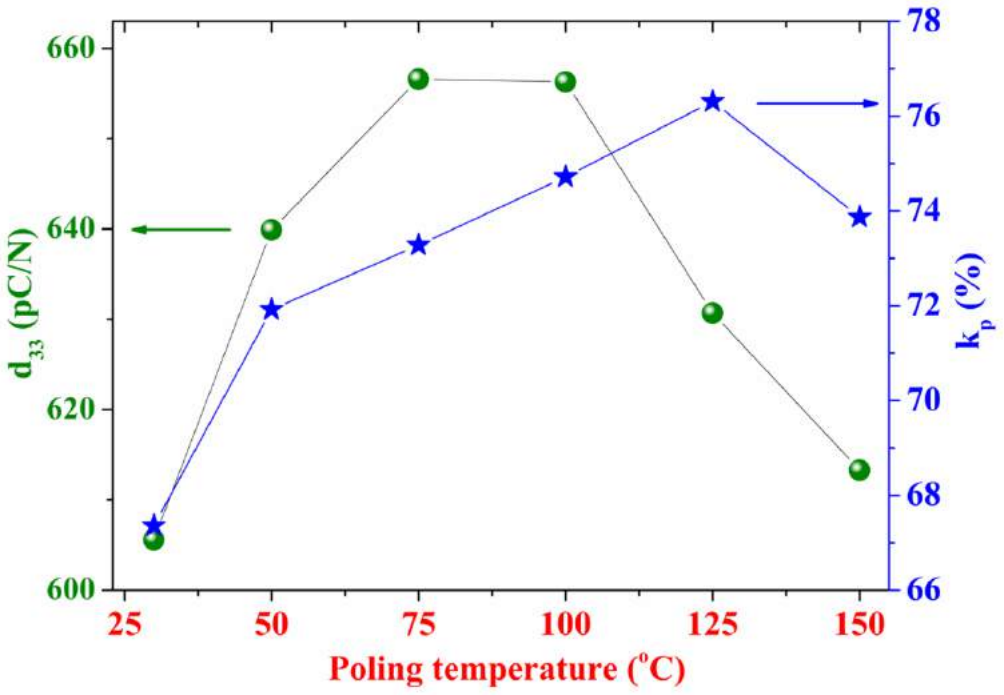

Fig. 6.4 *Variations in piezoelectric charge coefficient (d_{33}) and electromechanical coupling factor (k_p) values as a function of poling temperature with applied electric field of ~5 kV/cm.*

To study the of the effect of poling temperature on piezoelectric properties, PLZT ceramics samples were poled at different poling temperatures keeping the poling field (~0.5E_c) and poling time un-changed. Fig. 6.4 shows the change in piezoelectric charge coefficient (d_{33}) and electromechanical coupling factor (k_p) as a function of poling temperature for PLZT 8/60/40 ceramics. At first, both d_{33} and k_p values increase as a function of poling temperature. The d_{33} and k_p parameters show their highest value at 75°C and 125°C, respectively. Usually, high poling temperature enhanced the domain motion. An increase in poling temperature facilitates switching of domains, which results in an increase in electrical properties. However, when the poling temperature of PLZT ceramics exceeds the temperature, at which the ceramics show their highest values, the piezoelectric properties start decreasing. At sufficiently high temperature, the increase in leakage current is the main reason of remarkable decrease in said parameters.

6.4.3 Effect of poling time on the piezoelectric properties

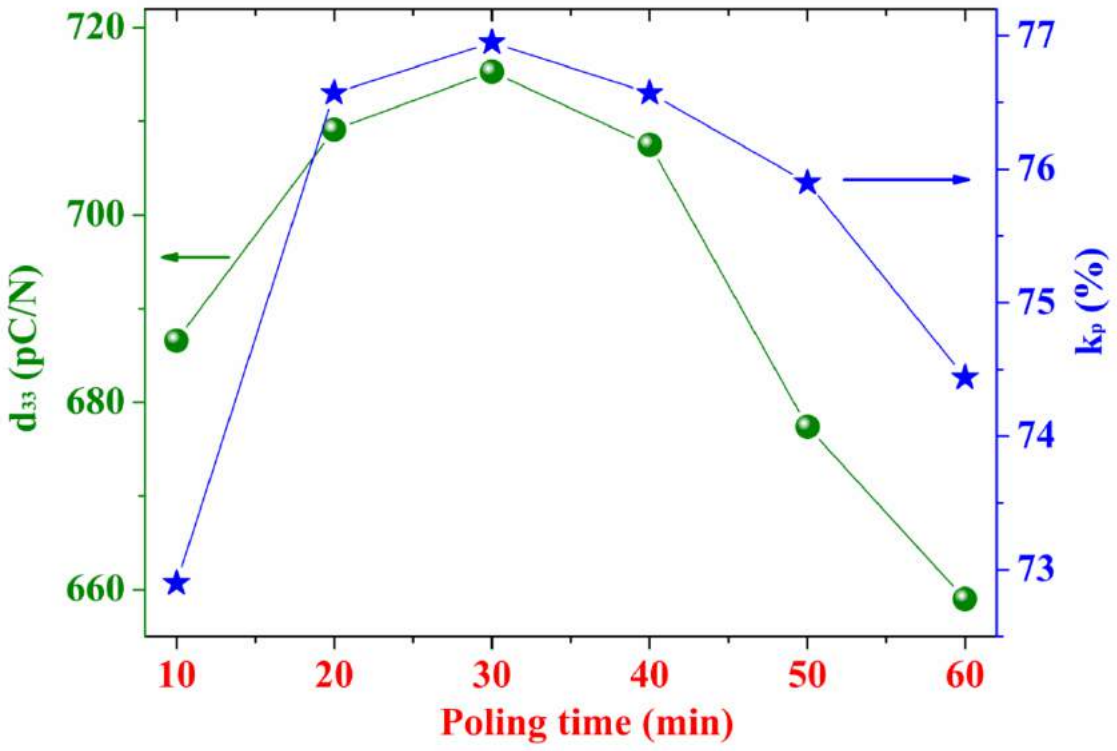

Fig. 6.5 *Variations in piezoelectric charge coefficient (d_{33}) and electromechanical coupling factor (k_p) values as a function of poling time with applied electric field of ~5 kV/cm.*

Fig. 6.5 shows the change in d_{33} and k_p values as a function of poling time for PLZT ceramics. While doing the poling time study, the applied poling electric field and the poling temperature was

same for the all ceramic samples. The d_{33} and k_p parameters both show the same trend as in the case of poling field and time. At first, both k_p and d_{33} parameters show an increase with increasing in poling time, which is due to the switching of 180^o domains. At the initial duration of poling, switching of 180^o domains is easier than non-180^o domains. When the poling time exceeds 30 min, the piezoelectric properties (k_p and d_{33}) of PLZT ceramics starts decreasing. Prolonged poling time may result in the unleashing of leakage current that is responsible for lowering of piezo properties. The application of high electric filed for a longer duration (poling time) results in the generation of free electrons. The number of these free electrons increases with increase in poling duration. The generated electrons get accelerated and collide with other atoms and release more charge carriers, which results in increased leakage current or conduction of the PLZT ceramics. The temperature of local regions rises due to an increase in electric current **[15]**. Thereafter, there is a decline of poling time dependent piezoelectric properties of PLZT ceramics, and subsequently, the breakdown of ceramics occurs.

6.4.4 Effect of sample thickness on piezoelectric properties

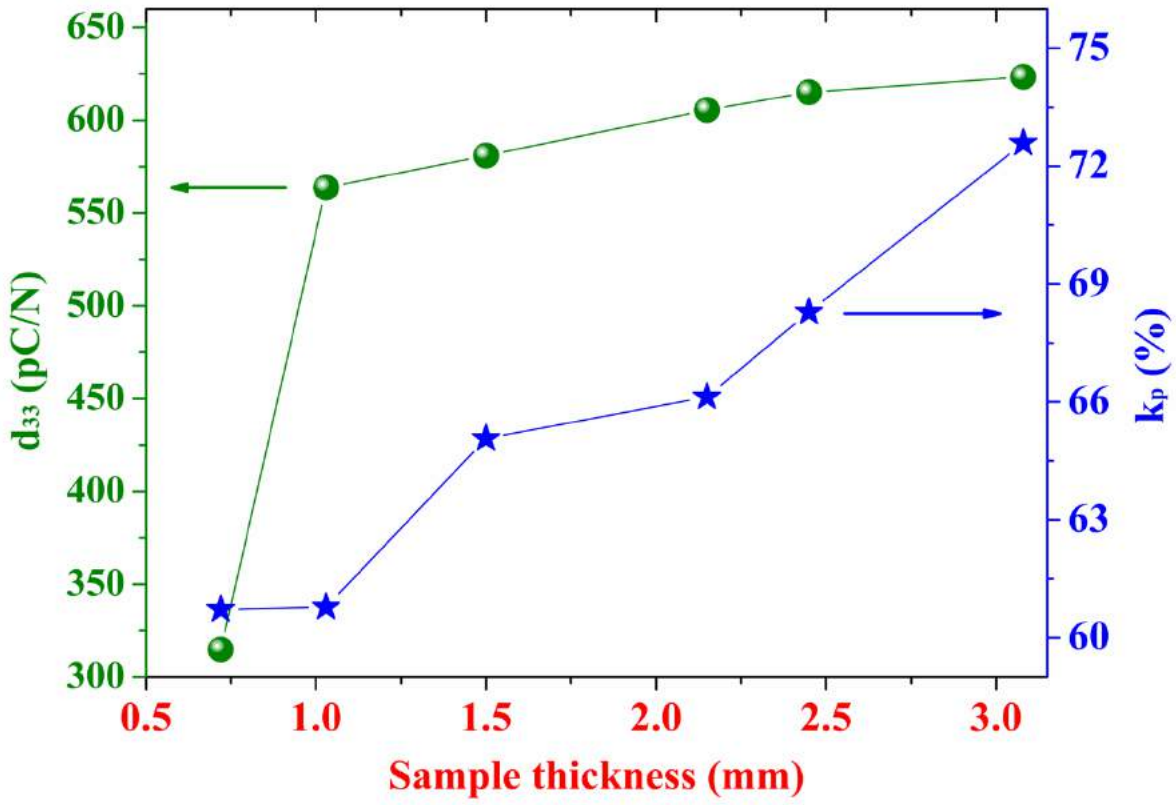

Fig. 6.6 *Variations in piezoelectric charge coefficient (d_{33}) and electromechanical coupling factor (k_p) values as a function of ceramic sample thickness, measured at 25^oC.*

Apart from the above three important poling parameters, another additional parameter the thickness of PLZT ceramic samples also has an effect on the piezoelectric parameters. According to the IEEE standards [27], for the measurements of the piezoelectric parameters ceramic sample should have a minimum thickness. In this study, the maximum possible thickness of the PLZT sample was taken. Fig. 6.6 shows the change in d_{33} and k_p values as a function of ceramic sample thickness of PLZT 8/60/40 ceramics. The piezoelectric charge coefficient (d_{33}) and electromechanical coupling factor (k_p) showed an increase with an increase in thickness of the PLZT ceramics and reached saturation. Ceramics with different thicknesses were used in this study. Thicker samples were difficult to pole with the existing poling setup. The highest thickness of the ceramic sample which was poled for the study is ~1/3 of the sample diameter. The PLZT ceramics with increased sample dimensions showed improvement in piezoelectric coefficients which may be due to the availability of more domains in the ceramics with an increase in thickness. Thus the ceramics sample with appropriate dimensions should be used for the stable and accurate piezoelectric coefficient determination. Optimized poling parameters are given in Table-6.1.

Table-6.1 *Optimized poling parameters for PLZT 8/60/40 ceramics.*

Parameters	Value
Optimum poling field (E_p)	~5 kV/cm
Optimum poling temperature	~75^{o}C
Optimum poling time	30 minutes
Sample thickness	1/3 of diameter
Piezoelectric charge coefficient (d_{33})	715 pC/N
Electromechanical coupling coefficient (k_p)	77 %

6.5 Effect of poling conditions on dielectric properties of PLZT 8/60/40 ceramics

Figs. 6.7 (a), (b), (c) and (d) show the change in dielectric constant and loss of PLZT 8/60/40 ceramics which were poled at the different poling electric field, poling temperature, poling time and ceramic sample thickness, respectively. Figs. 6.7 (a)-(d) shows the dielectric constant of PLZT ceramics increases quickly as a function of poling parameters and reaches its maximum value at optimum poling conditions. The reverse trend was also observed for the dielectric loss of the PLZT ceramics but shows the same optimum poling parameters. Du et al. **[19]** reported that the diffraction peaks of ceramics after poling shift towards the lower 2θ angles, which indicates an increase in lattice constant of the ceramics after poling. The increase in lattice constant can be correlated with an increase in dielectric constant. Figs. 6.7 (a), (b), (c) and (d) show a trend that is similar to the figs. 6.2, 6.4, 6.5 and 6.6. Once the poling process is completed, the crystallites are clamped along the poling

direction yielding a higher value of dielectric constant in the direction perpendicular to the clamped direction. Along the clamped direction the crystal would be less polarizable.

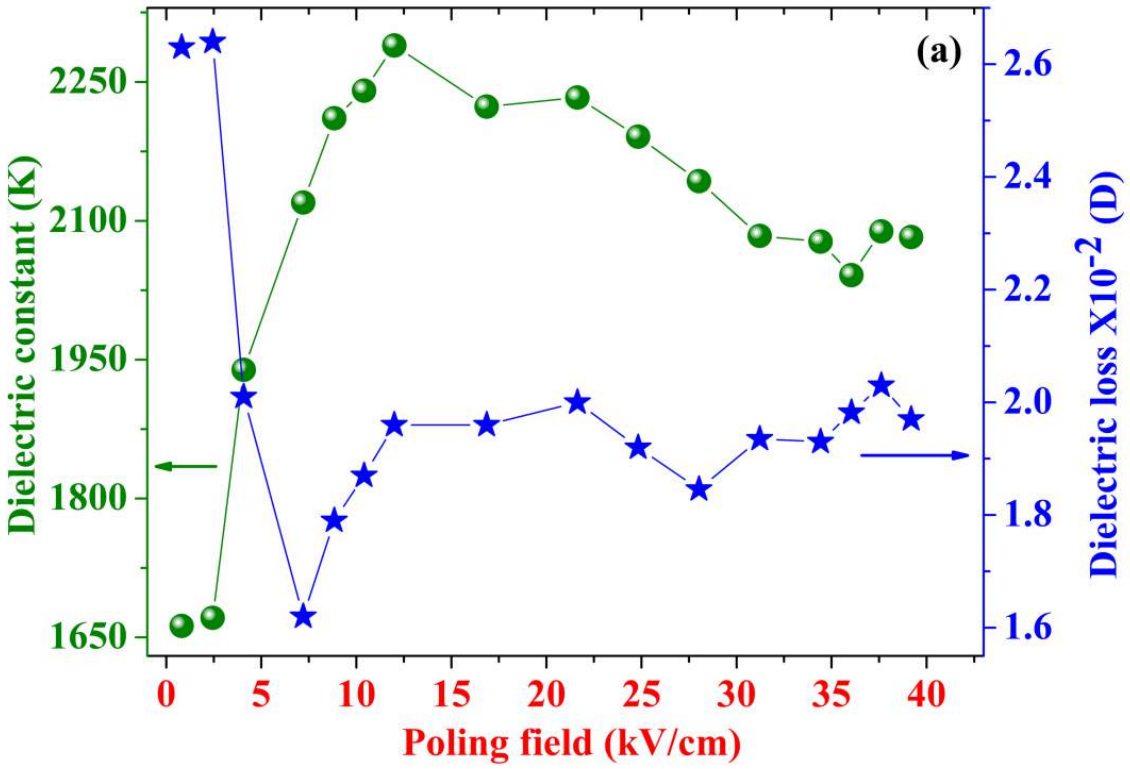

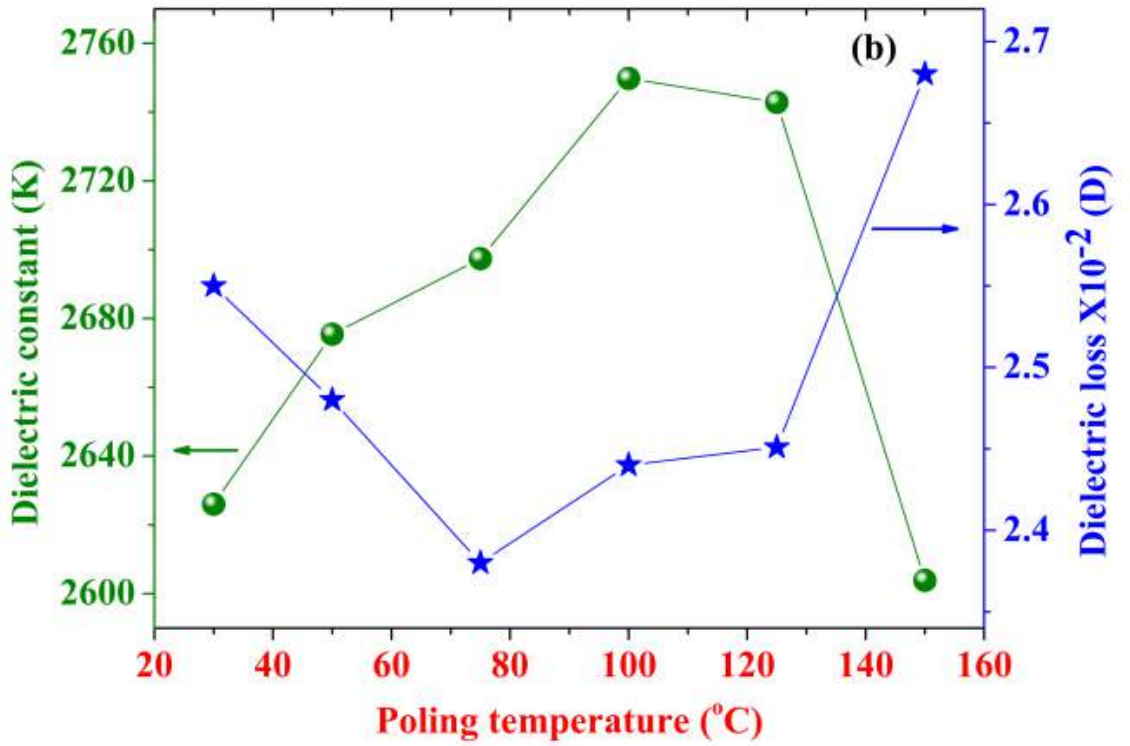

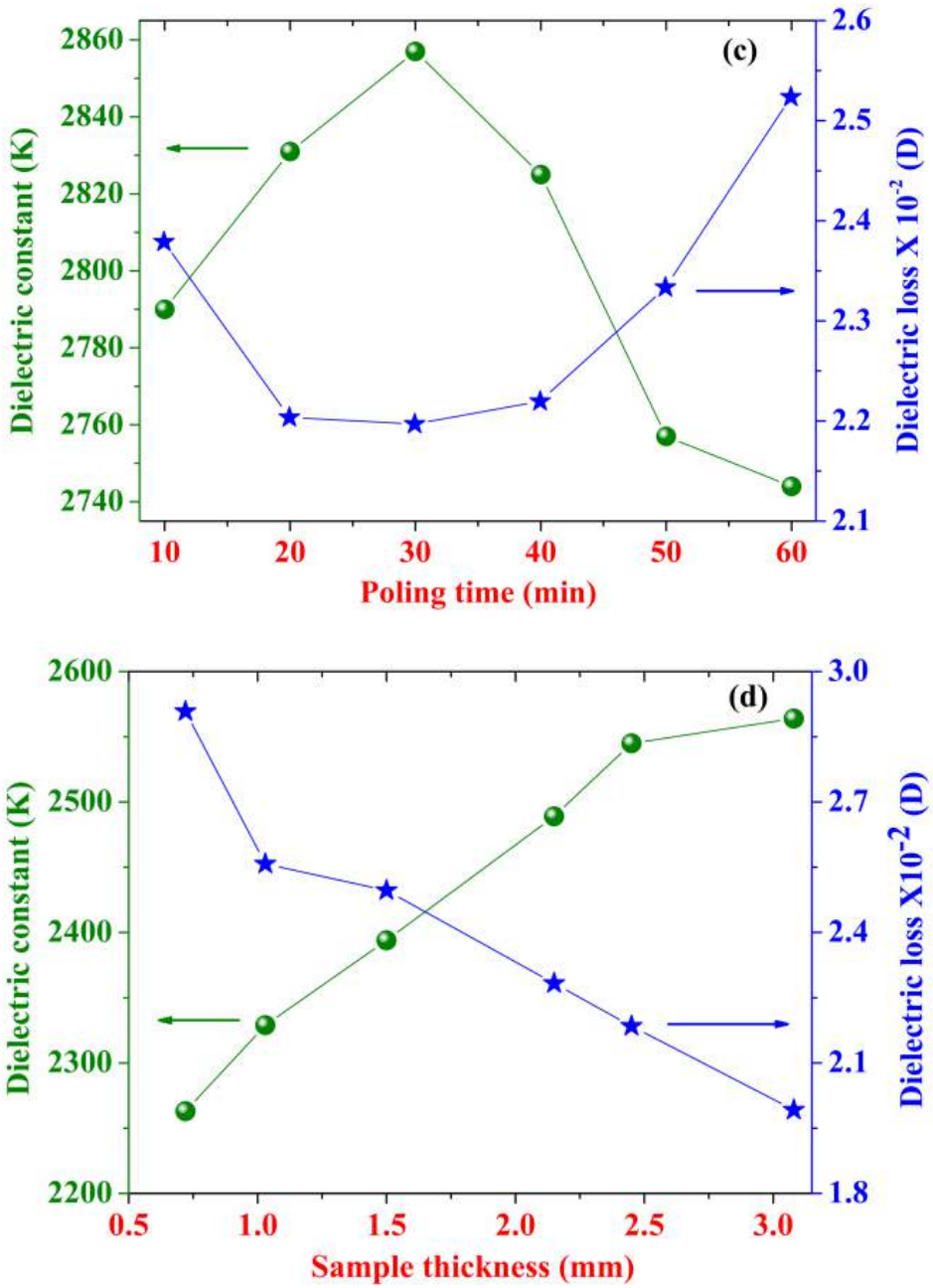

Fig. 6.7 *Change in Dielectric constant and loss as a function of (a) poling field, (b) poling temperature (c) poling time and (d) ceramic sample thickness, measured at a frequency of 1 kHz, 25^{o}C.*

For PLZT ceramics which have sufficient sample thickness, the dielectric constant was found to be stable, which is consistent with the domain textures that are almost saturated at this stage. The poled PLZT 8/60/40 ceramics shows the high dielectric constant when compared with un-poled ceramic samples. The total increase of ~31% was found for the poled PLZT ceramics. Therefore, these dielectric studies also can be used for the identification of the optimal electrical poling conditions. Previously Li et al. **[22]** studied the effect of mechanical as well as electrical poling on the dielectric properties of PZT and $BaTiO_3$ ceramics. The changes in dielectric constant before and after poling are given in Table-6.2.

Table-6.2 *Dielectric properties of unpoled and poled PLZT ceramics, measured at 1 kHz and 25^{o}C.*

Samples	K (Before poling)	K_{max} (After poling)	% Change
At different poling field	1743	2290	31
At different poling temperature	2612	2750	5
At different poling time	2745	2857	4
At different thickness	2338	2564	10

6.6 Ageing in piezoelectric and dielectric properties of PLZT 8/60/40 ceramics

This study suggests that the use of low poling electric field also can give high piezoelectric properties for PLZT ceramics, which is contrary to the previous reports. These reports suggest the use of high electric field due to the stability issue for lower field poled ceramics. However, low electric field poled ceramics shows the almost same properties as in the case of use of high poling field. If the ceramics are subjected to the higher electric field, the probability of electrical breakdown is more compared with low field poling, which is already discussed in previous sections. The piezoelectric properties of the PLZT ceramics are also affected by the high leakage current at high poling fields.

All the aforementioned factors necessitate consideration for not only achieving the good piezoelectric and electromechanical properties but also for the stability issue. In general, electro-ceramics, which are poled at $2E_c$ and more, give the best aligned domain configuration with high stability. To support our findings and experimental results, which suggest the use of the low poling field, the ageing factor can be considered here as reliable evidence. To study the ageing phenomenon in PLZT ceramics, two sets of ceramic samples were poled at different poling field, $0.6E_c$ and $3E_c$, respectively. During the course of poling of ceramics, poling temperature and poling time was kept constant.

Instead of optimized poling field (~$0.5E_c$), here we poled the first set of PLZT ceramic sample at a slightly higher electric field of $0.6E_c$. The second set of ceramic samples was poled at five time's higher field ($3E_c$). Figs. 6.8 (a) to (c) and 6.10 (a) to (c) show the effect of ageing on the piezoelectric, electromechanical and dielectric properties of PLZT 8/60/40 ceramics, poled at $0.6E_c$ and $3E_c$ respectively. The time for the ageing study taken here is ~300 days, and the values of all the parameters were measured at random intervals. The PLZT ceramics show the almost same properties for both sets of the ceramic sample. The ceramic sample dimension can affect the electrical properties as seen in figs. 6.6 and 6.7 (d). Therefore certain changes in the properties of both sets of ceramics arise due to slight variation in their dimensions.

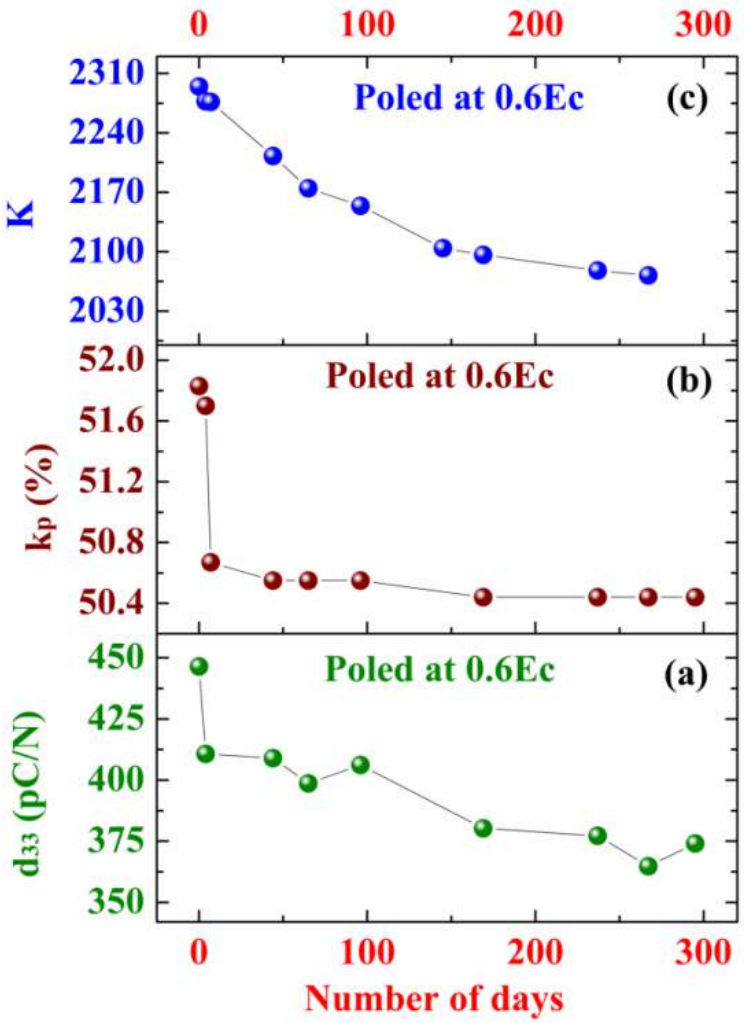

Fig. 6.8 *Study of ageing in (a) piezoelectric charge coefficient (d_{33}) (b) electro-mechanical coupling factor (k_p) and (c) dielectric constant (at 1 kHz) for 0.6E_c poled PLZT 8/60/40 ceramics.*

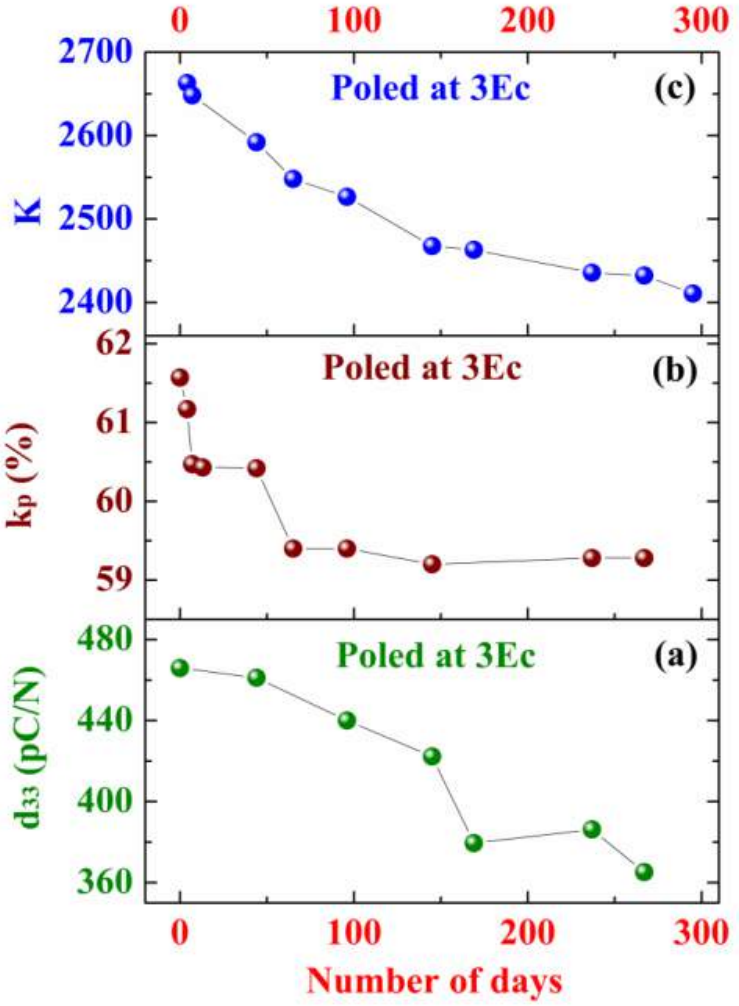

Fig. 6.9 *Study of ageing in (a) piezoelectric charge coefficient (d_{33}) (b) electromechanical coupling factor (k_p) and (c) dielectric constant (at 1 kHz) for 3E_c poled PLZT 8/60/40 ceramics.*

Hence all the dielectric and piezoelectric properties of electro-ceramics should be discussed in relative terms. Figs. 6.10 (a)-(c) shows the relative change in piezoelectric charge coefficient, electromechanical coupling factor and dielectric constant for PLZT 8/60/40 ceramics, which was poled at $0.6E_c$ and $3E_c$. The d_{33} and k_p for $0.6E_c$ poled ceramics are relatively more stable than $3E_c$ poled ceramics. However, dielectric constant for both sets of ceramic samples show an almost same rate of change even after 300 days. The $0.6E_c$ poled PLZT ceramics show less rate of change compared to $3E_c$ poled ceramics. The measurement conditions affect the electrical parameters of PLZT ceramics such as humidity, temperature, instrument errors, human error, etc., which are the reason for fluctuations in the measured values shown in figs. 6.8, 6.9 and 6.10.

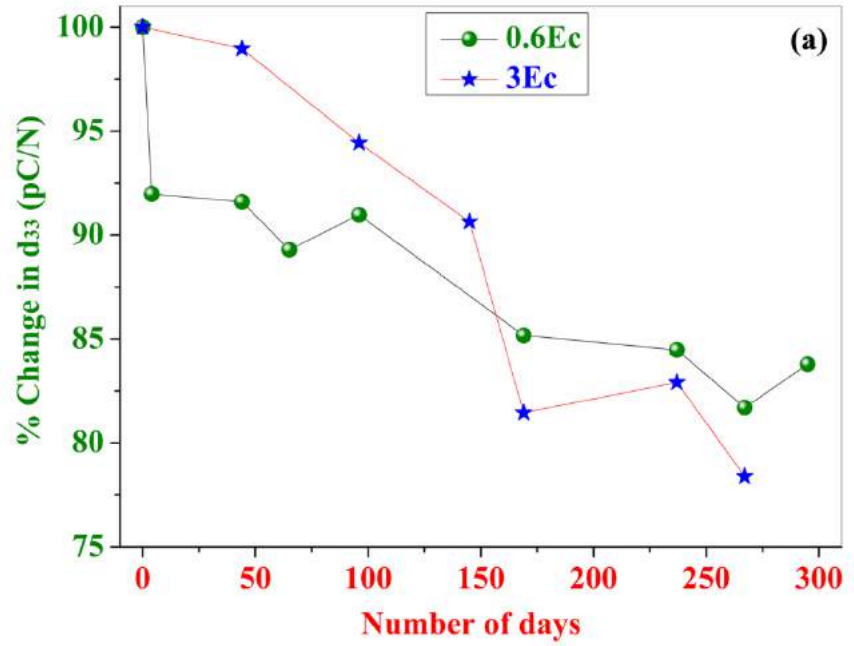

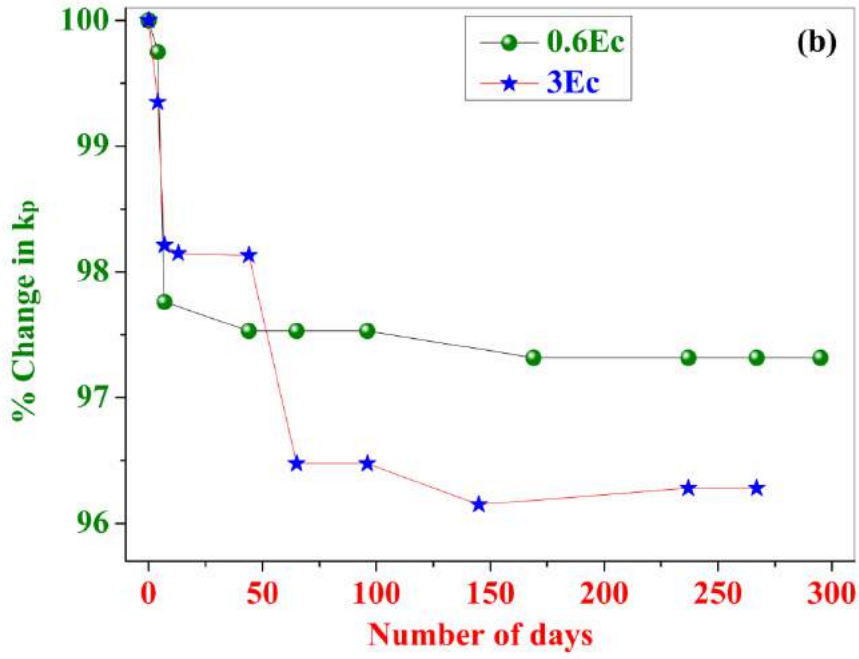

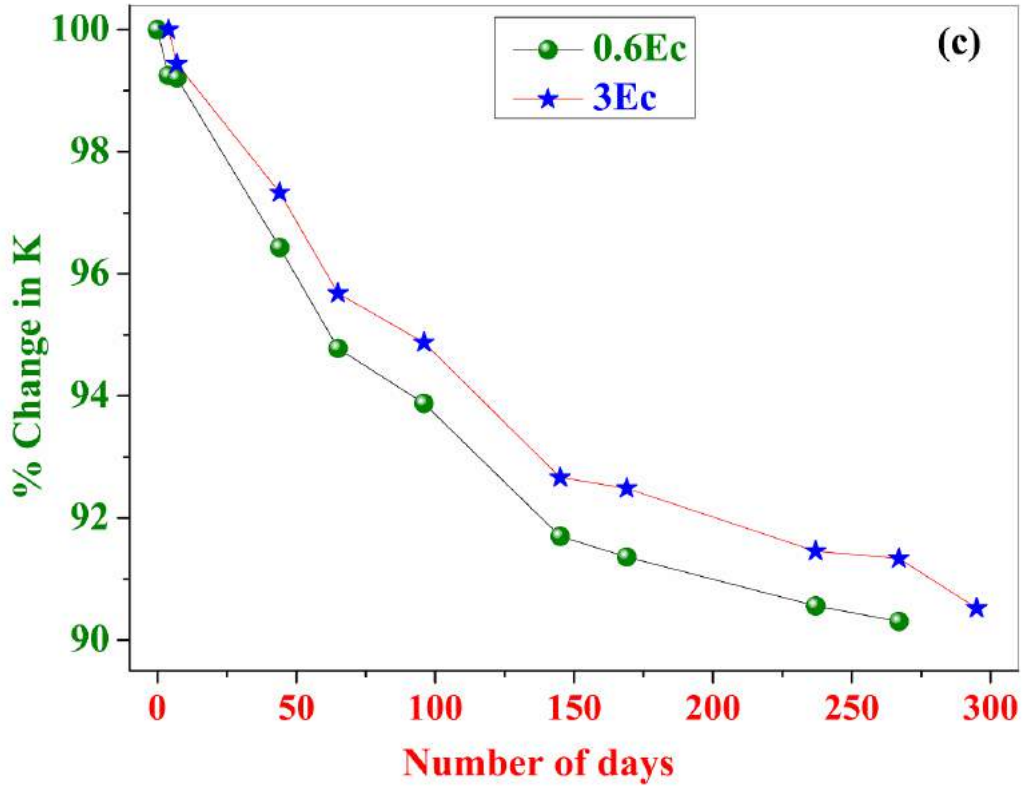

Fig. 6.10 *% decrease in (a) d_{33} (b) k_p and (c) dielectric constant at 1 kHz frequency, values for PLZT 8/60/40 ceramics poled at 0.6Ec and 3Ec, respectively.*

6.7 Summary

PLZT 8/60/40 ceramics with pure perovskite phase and dense microstructure were successfully prepared by mechanical activation. The SEM and P-E studies were done to check the microstructure and to measure the coercive field. PLZT ceramics were poled by varying the poling conditions to identify the optimum poling parameters. Poling electric field studies suggest that the PLZT ceramics can be poled at ~5 kV/cm while the coercive field is ~12 kV/cm. This shows that the poling of PLZT ceramics at the significantly low electric field could be very advantageous if the samples show low resistivity or high conductivity. The poling temperature range for the PLZT ceramics is from 75^{o}C to 120^{o}C while the T_c is 190^{o}C. The optimum poling time was found to be 30 minutes which is also much less compared to the normally employed time in hours. The ageing study for PLZT ceramics also supports the poling at the lower electric field. The d_{33} and k_p values for PLZT 8/60/40 ceramics, which was measured at optimum poling conditions were found to be ~715 pC/N and ~77 %, respectively. These values are found to be far superior to conventionally synthesized piezoceramics and even the well known PMN-32PT composition. This goes to show that the work embodied in this thesis has successfully achieved significant improvement in electrical property output through suitable processing and optimized poling of ceramics.

References

[1] G.H. Haertling, J. Am. Ceram. Soc., **82** (1999) 797.

[2] A.J. Moulson and J.M. Herbert, Electroceramics: Materials, Properties & Applications, Chapman & Hall, London (1990).

[3] D. Damjanovic, Rep. Prog. Phy. **61** (1998) 1267.

[4] G.H. Haertling and C.E. Land, J. Am. Ceram. Soc., **54** (1971) 1.

[5] A. Kumar, V.V.B. Prasad, K.C.J. Raju, A.R. James, J. Allo. Comp., **599** (2014) 53.

[6] A.R. James, J.P. Praveen, M.P. Kumar and V.V.B. Prasad, Mater. Res. Bul., **47** (2012) 3459.

[7] M. Hinterstein, K.A. Schoenau, J. Kling, H. Fuess, M. Knapp, H. Kungl and M.J. Hoffmann, J. Appl. Phy., **108** (2010) 024110.

[8] G. Viola, K.B. Chong, M. Eriksson, Z. Shen, J. Zeng, Q. Yin et. al., Appl. Phys. Lett., **103** (2013) 182903.

[9] T.M. Kamel and G. deWith, J. Euro. Ceram.Soc., **28** (2008) 851.

[10] L. Zhang, Q. Sun, W. Ma, Y. Zhang and H. Liu, J. Mater. Sci.: Mater. Electron., **23** (2012) 688.

[11] Y. Zhao, R. Huang, R. Liu and H. Zhou, Ceram. Inter., **38** (2012) 6067.

[12] S. Su, R. Zuo, S. Lu, Z. Xu, X. Wang and L. Li, Curr. Appl. Phy., **11** (2011) S120.

[13] A. Kumar, V.V.B. Prasad, K.C.J. Raju and A.R. James, J. Mater. Sci.: Mater. Electron., **26** (2015) 3757.

[14] A. Kumar, V.V.B. Prasad, K.C.J. Raju and A.R. James, Europ. Phy. J. B, **88** (2015) 287.

[15] T.M. Kamel, F.X.N.M. Kools and G. deWith, J. Eur. Ceram. Soc., **27** (2007) 2471.

[16] S.T. McKinstry, N.B. Gharb and D. Damjanovic, Appl. Phy. Lett., **88** (2006) 202901.

[17] M.C. Ehmke, J. Glaum, M. Hoffman, J.E. Blendell and K.J. Bowman, J. Am. Ceram. Soc., **96 [12]** (2013) 3805.

[18] H. Guo, C. Ma, X. Liu and X. Tan, Appl. Phy. Lett.,**102** (2013) 092902.

[19] H. Du, F. Tang, F. Luo, W. Zhou, S. Qu and Z. Pei, Mater. Sci.Eng. B, **137** (2007) 175.

[20] L.B. Kong, J. Ma and T.S. Zhang, J. Mater. Res., **16** (2001) 1636.

[21] M.A. Wahab, Solid State Physics: Structure and Properties of Materials, Narosa Publishing House, New Delhi, India, Ch. 14 (2013).

[22] Y. Li, Y. Sun and F. Li, Ceram. Inter., **39** (2013) 8605.

Chapter-VII

Piezoelectric studies on PLZT ceramics

7.1 Introduction

Piezoelectric studies are very important to describe the electrical properties of piezo-ceramics, which deals with the piezoelectric coefficients such as charge (d_{33}) and voltage (g_{33}) coefficients as well as electromechanical coupling factor (k_p, k_{33} and k_{31}). The charge coefficients d_{33} is defined as the proportionality constant for the S-E relation or charge generated per Newton force in ferroelectric ceramics, whereas k_p is related to the conversion of applied mechanical energy to the generated electrical energy and vice-versa. High values of both d_{33} and k_p parameters decide the end application (actuator or transducer) of the electro-ceramics. Certain PLZT compositions are known to show high values for both the parameters d_{33} and k_p.

In this chapter, results of different compositions of PLZT ceramics that were prepared by substituting La at the A-site of perovskite PZT using high energy mechanical ball milling (mechanical activation), followed by cold isostatic pressing (CIP) are presented and discussed. The piezoelectric coefficients (d_{33} and g_{33}), electromechanical coupling factors (k_p, k_{33} and k_{31}) and elastic compliances were calculated for the above compositions. Ceramics showing the highest values were selected for further characterization experiments. The PLZT 8/60/40 composition is close to the MPB region. On account of this, it is expected that the increased number of directions of spontaneous polarization will help to improve the piezoelectric properties. The effect of milling time as well as milling vials on PLZT 8/60/40 composition on the said properties are also discussed in this chapter. The piezoelectric properties of the PLZT 8/6/40 ceramics are discussed based on many factors, such as different types of processing techniques, morphotropic phase boundary (MPB) conditions, the microstructure of the ceramics, which is usually related to the grain sizes and poling conditions. The processing technique that was used here resulted in improved density and ceramics retain their fine grain size, which in turn influence the domain wall motion and switching phenomena. All these factors help to improve the piezoelectric and electromechanical properties of PLZT ceramics.

To give the more details about the diffuse phase transition of PLZT ceramics, resonance data were taken from room temperature to high temperature (close to the transition temperature). This resonance data was used for the calculation of electromechanical coupling coefficients. Temperature dependent electromechanical coupling coefficient studies are also very useful, in order to understand the ferroelectric phase transition of PLZT 8/60/40 electro-ceramics.

7.2 Literature survey

From the time of the discovery of piezoelectric materials, they have been studied for their direct and indirect piezoelectric effects, for sensor and actuator applications. Piezoelectric materials develop surface charges due to the direct piezoelectric effect in response to an applied pressure. On

the other hand, the converse piezoelectric effect creates mechanical displacements or strain in the material in response to an applied electric field. Both the effects are useful in both sensors and actuators applications **[1-2]**. Lead based materials have significant practical and academic importance because of their reliable and repeatable, dielectric, ferroelectric and piezoelectric properties **[3-5]**. Recent literature **[6]** values for the PMN-PT relaxor ferroelectric materials show that these ceramics possess very high piezoelectric strain and piezoelectric coefficients. These huge strain levels and piezoelectric coefficients are multiple times that of PZT ceramics and can arise only under specific conditions and have very complex preparation methods. As an alternative, PLZT ceramics were synthesized relatively easy via suitable materials engineering approaches with electrical properties comparable with PMN-PT **[7]**. The PLZT system is less complex in preparation and the electrical properties which are comparable to other lead based systems show more repeatability.

Detailed literature surveys suggest that the piezoelectric properties of piezoelectric ceramics are affected by many factors. Some of them are the composition of piezoelectrics, MPB conditions [**8-10**], different processing techniques, grain sizes [**11-14**] and poling conditions [**15-19**]. Studies show that the different piezoelectric materials whose compositions are balanced at the MPB possess outstanding piezoelectric properties. These high properties can be attributed to the unique structural features of the MPB at which both the tetragonal and rhombohedral phases coexist. At the MPB, six domain states of the tetragonal phase along the (100) direction (90^o and 180^o domains) coexist with eight domain states of the rhombohedral phase along the (111) directions (71^o, 90^o and 180^o domains). This results in a total of 14 possible available directions of spontaneous polarization for the piezoelectric material at their MPB composition. The PLZT 8/60/40 composition is close to the MPB [**10**] and shows the highest strain, piezoelectric and coupling coefficients. The above mentioned reasons make PLZT ceramics to show its maximum properties around the MPB [**20**].

Micro-structural and morphological (XRD, SEM and density) results were examined carefully in Chapter-3. The PLZT 8/60/40 ceramics, those have the single-phase pure perovskite structure, fine grains and good density only were used for further electrical characterizations. The coercive field E_c was identified from the saturated P-E hysteresis loops. This coercive field value was used to pole the PLZT ceramics. Since electrical properties of the piezoelectric ceramics are greatly influenced by the poling conditions (poling electric field, time and temperature), PLZT ceramics were poled at optimized poling conditions as described in Chapter-6.

7.3 Piezoelectric coefficients (d_{33} and g_{33})

The piezoelectric charge coefficient, which is represented by symbol ‘d’ is related to the generation of total polarization when subjected to mechanical stress (T) in a piezoelectric material.

Alternatively, ‘d’ is related to the mechanical strain experienced by a piezoelectric material per unit applied an electric field. On the other hand, piezoelectric voltage coefficient, which is represented by the symbol ‘g’ is related to the generation of the electric field by per unit of applied mechanical stress in a piezoelectric material. Alternatively ‘g’ is related to the mechanical strain produced in a piezoelectric material when subjected to per unit of applied electric displacement. Both the piezoelectric constants that are defined above are discussed in detail in Chapter-1 and 2.

7.3.1 Compositional dependence of piezoelectric properties in PLZT system.

La substituted PZT ceramics $(Pb_{1-x}La_x)(Zr_{0.60}Ti_{0.40})O_3$ for different compositions (PLZT x/60/40; x=0.00, 0.02, 0.04, 0.07, 0.08, 0.09, 0.10) were synthesized via mechanical activation and CIP. The PLZT ceramic samples were electroded and poled at optimized poling conditions (Chapter-6). Poled PLZT samples were used to determine piezoelectric charge and voltage coefficients. Complete details regarding synthesis and characterization techniques have been given in Chapters-2 and 3. Effects of La substitution on the piezoelectric properties were also described in this chapter. Fig. 7.1 shows the variation of piezoelectric charge (d_{33}) and voltage (g_{33}) coefficients for PLZT x/60/40 ceramics, as a function of different lead compositions. Fig. 7.1 shows that the PLZT 8/60/40 ceramic system exhibit higher piezoelectric properties than other systems. All the piezoelectric parameters of PLZT x/60/40 ceramics are listed in Table-7.1

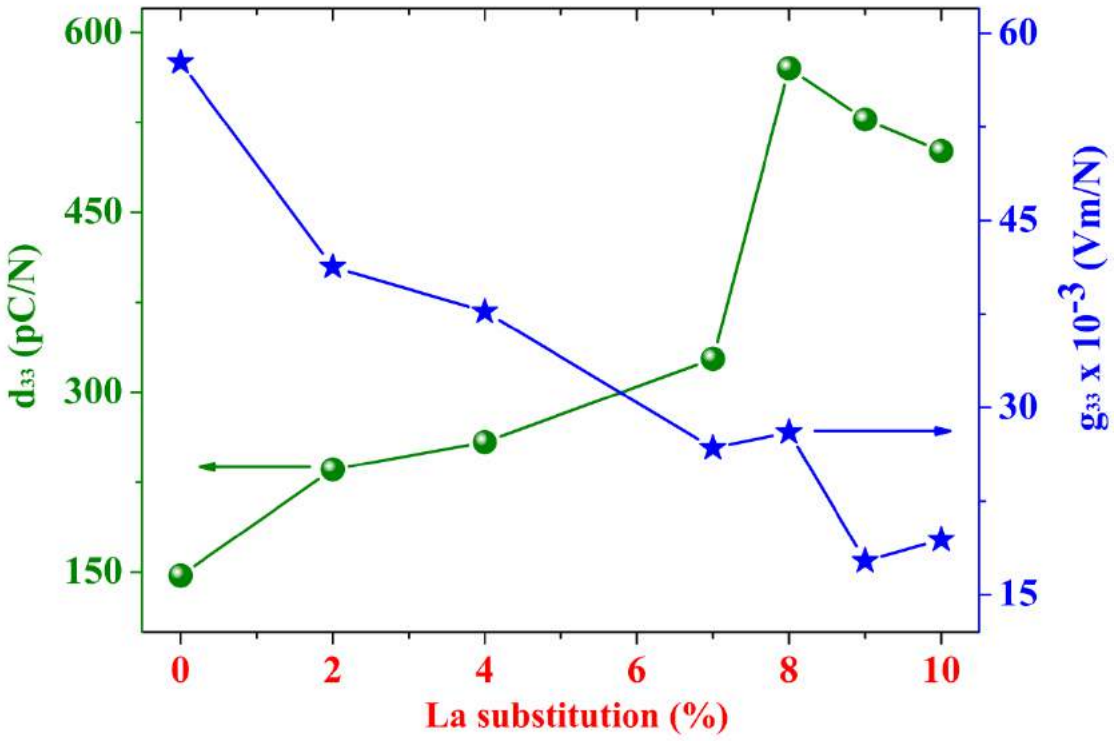

Fig. 7.1 *Piezoelectric charge (d_{33}) and voltage (g_{33}) coefficients for PLZT x/60/40 ceramics.*

Table-7.1 *Piezoelectric coefficients of PLZT x/60/40 ceramics.*

Compositions	d_{33} (pC/N)	g_{33} x 10^{-3} (Vm/N)
PZT 60/40	147	57.7
PLZT 2/60/40	236	41.3
PLZT 4/60/40	258	37.7
PLZT 7/60/40	328	26.8
PLZT 8/60/40	570	28.0
PLZT 9/60/40	528	17.7
PLZT 10/60/40	501	19.4

7.3.2 PLZT 8/60/40 ceramics milled with different vials

From the last section 7.3.1, it is clear that PLZT composition that was prepared by the substitution of 8% of lanthanum at the A-site of PZT (PLZT 8/60/40) shows the highest piezoelectric charge coefficient (d_{33}). Encouraged by these results, this composition was further used to study the effect of milling vial on piezoelectric properties. PLZT 8/60/40 was milled by using different milling vials made of agate and Zirconia respectively. Piezoelectric coefficients of PLZT 8/60/40 ceramics milled with different vials are given in Table-7.2. It shows that PLZT 8/60/40 ceramics milled in Zirconia vial have the better properties than agate milled ceramics.

Table-7.2 *Piezoelectric coefficients of PLZT 8/60/40 ceramic milled with different vials.*

Milling vials	~d_{33} (pC/N)	~g_{33} x 10^{-3} (Vm/N)
Zirconia vial	688	28.5
Agate vial	570	28.0

7.3.3 PLZT 8/60/40 ceramics milled for different durations

PLZT ceramics were processed using high energy ball milling. HEM results in very fine scale size and highly reactive nano-powders. The use of milling process results in the enhancement in better mixing and size reduction of the raw oxides and provides for an intimate interface in each collision, momentarily. The electrical properties of electro-ceramics are affected by the milling parameters such as milling vials, milling balls, milling time, etc. as discussed in Chapter-2. In this study, PLZT ceramics were ball milled for different durations for the optimization of milling time. In order to obtain the optimum electrical properties, it is necessary to mill the powder for an optimum duration of

time. Shorter milling times cannot trigger the chemical reaction and on the other hand, excess milling may cause contamination of the electro-ceramics powders.

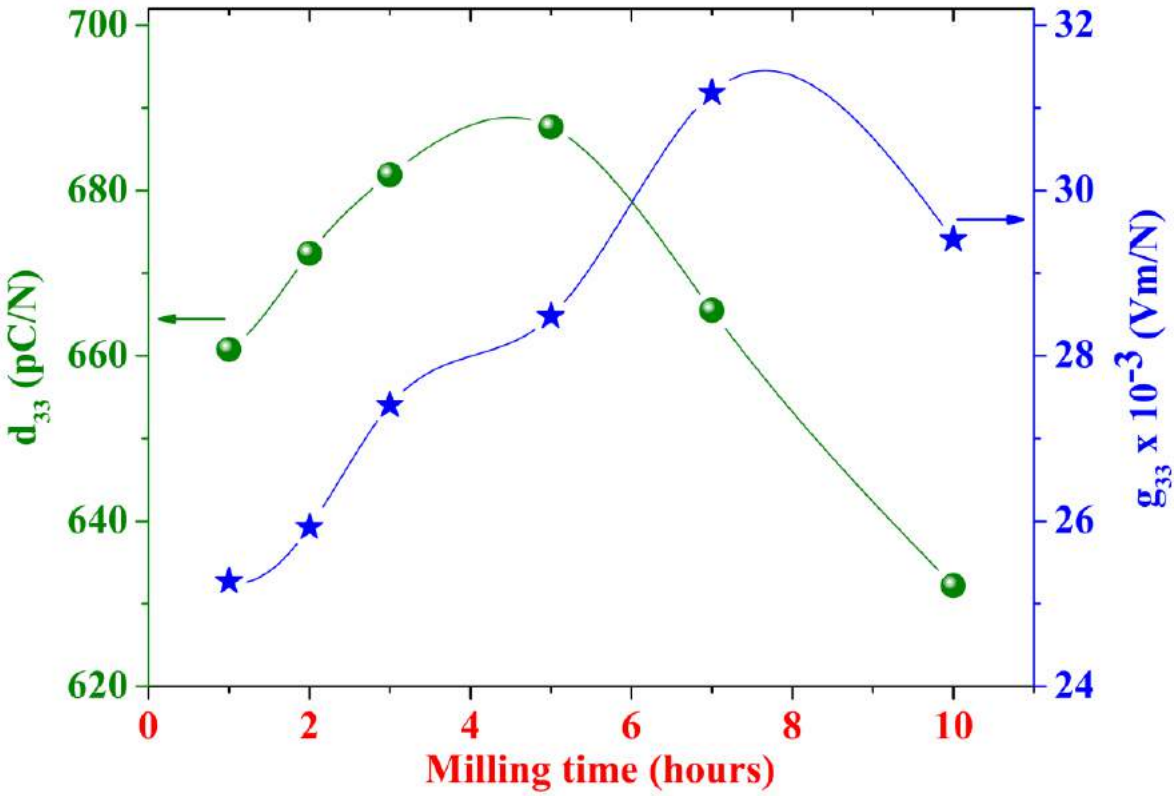

Fig. 7.2 *Piezoelectric charge (d_{33}) and voltage (g_{33}) coefficient for PLZT 8/60/40 ceramics as a function of milling time.*

Fig. 7.2 shows the piezoelectric charge (d_{33}) and voltage (g_{33}) coefficient for PLZT 8/60/40 ceramics, as a function of milling time, milled in Zirconia vial. As seen in figure 6.2 the PLZT 8/60/40 ceramics that were milled for 5 hours gave the best piezoelectric property. All the piezoelectric parameters of PLZT 8/60/40 ceramics are listed in Table-7.3.

Table-7.3 *Piezoelectric parameters of PLZT 8/60/40 ceramics milled for different durations.*

Milling durations	d_{33} (pC/N)	g_{33} x 10^{-3} (Vm/N)
1h	661	25.3
2h	672	25.9
3h	682	27.4
5h	688	28.5
7h	666	31.2
10h	632	29.4

7.4 Electromechanical coupling factors (k_p, k_{33} and k_{31})

Electromechanical coupling factors (k_p, k_{33} and k_{31}) are an indicator of the effectiveness in which a piezoelectric material converts the applied input mechanical energy to the output electrical energy or converts applied input electrical energy to output mechanical energy. The first subscript to the symbol 'k' denotes the direction along with the electrical energy is applied; the second subscript denotes the direction along with the mechanical energy is developed. A high k is usually desirable for efficient energy conversion. Hence it is very important to have these values in mind before going to the selection of these materials for specific applications. Resonance measurements were used to calculate several electromechanical properties of PLZT ceramics. The electromechanical coupling factors (k_p, k_{33} and k_{31}), resonance (f_r) and anti-resonance (f_a) frequencies were determined from the first maxima and first minima of the admittance vs. frequency graphs. The equations that were used for the calculation of electromechanical coupling coefficients (k_p, k_{33} and k_{31}) are given Chapter-2.

7.4.1 Compositional dependence of coupling factors in PLZT system

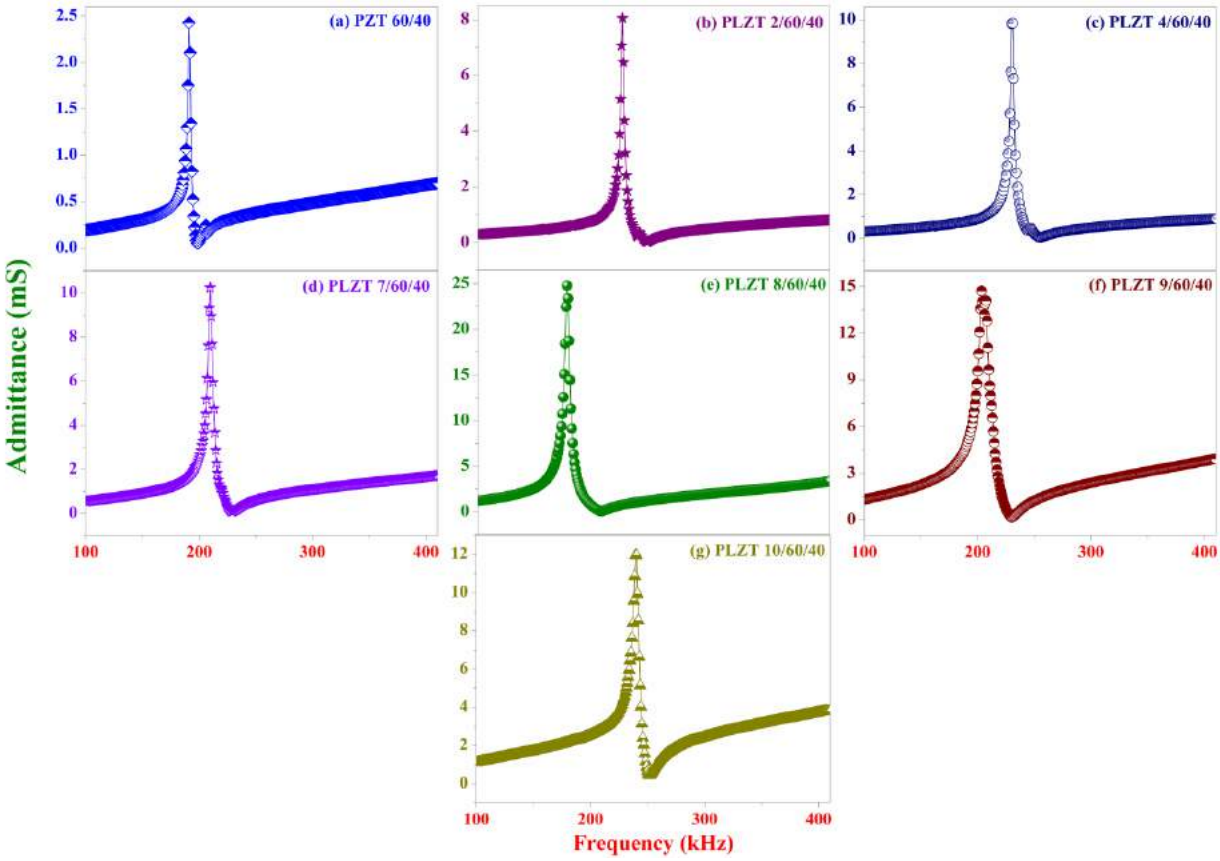

Fig. 7.3 *(a-g) Admittance vs. frequency graphs for mechano-chemical processed PLZT x/60/40 poled ceramics, sintered at 1200^{o}C, showing resonance and anti-resonance peaks.*

PLZT x/60/40 ceramics of different compositions were electrically poled and admittance data were recorded with respect to frequency. Figs. 7.3 (a)-(g) shows the admittance-frequency graph for the poled PLZT 60/40, 2/60/40, 4/60/40, 7/60/40, 8/60/40, 9/60/40 and 10/60/40 compositions with their resonance (f_r) and anti-resonance (f_a) frequencies. The values of f_r and f_a were measured from the fig. 7.3 and these values were used for the calculation of electromechanical coupling factors.

Fig. 7.4 shows the electro-mechanical coupling factors (k_p, k_{33} and k_{31}) for PLZT x/60/40 ceramics, as a function of lanthanum substitution. As seen in the figure, PLZT 8/60/40 ceramic composition shows the highest value of electromechanical factors as well as the piezoelectric coefficients. So here we can say that PLZT 8/60/40 is an optimum composition. All the electromechanical parameters of PLZT x/60/40 ceramics are also listed in Table-7.4.

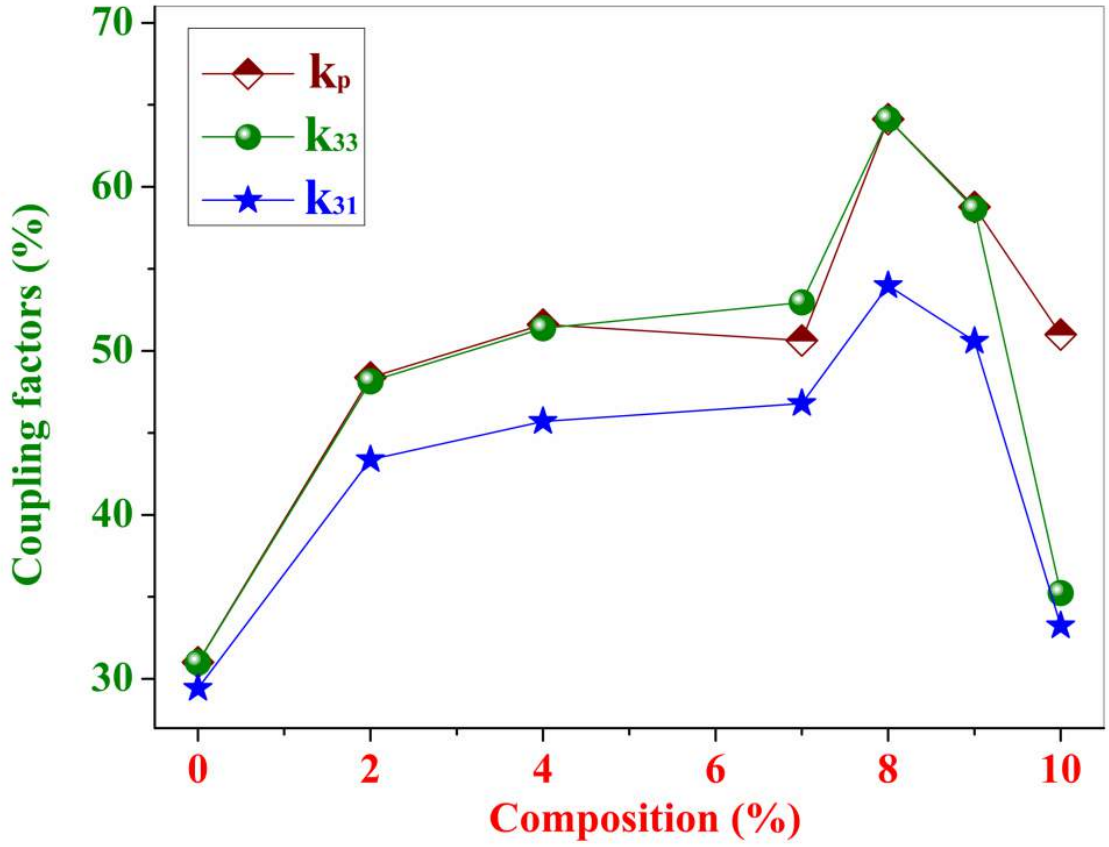

Fig. 7.4 *Electromechanical coupling factors (k_p, k_{33} and k_{31}) of PLZT x/60/40 ceramics.*

Table-7.4 *Electromechanical coupling factors of PLZT x/60/40 ceramics*

Compositions	k_p (%)	k_{33}(%)	k_{31} (%)
PZT 60/40	31.0	31.0	29.4
PLZT 2/60/40	48.4	48.1	43.4
PLZT 4/60/40	51.6	51.4	45.7
PLZT 7/60/40	50.6	52.9	46.8
PLZT 8/60/40	64.1	64.1	54.0
PLZT 9/60/40	58.8	58.7	50.6
PLZT 10/60/40	51.0	35.2	33.2

7.4.2 PLZT 8/60/40 ceramics milled with different vials

As we already discussed the effect of milling media on piezoelectric coefficients in the section 7.3.2, the same study was also done for the electromechanical coupling factors. The PLZT 8/60/40 showed the highest electromechanical coupling factors and milled by using different milling vials. Based on the results, it is clear that zirconia milled PLZT 8/60/40 ceramics show the better properties. Electromechanical coupling factors of PLZT 8/60/40 ceramics milled with different vials are given in Table-7.5.

Table-7.5 *Electromechanical coupling factors (k_p, k_{33} and k_{31}) of PLZT 8/60/40 ceramics, milled with different vials.*

Milling vials	k_p (%)	k_{33} (%)	k_{31} (%)
Zirconia vial	75.8	76.3	60.7
Agate vial	64.1	64.1	54.0

7.4.3 PLZT 8/60/40 ceramics milled for different durations

Admittance data of electrically poled PLZT 8/60/40 ceramic samples, milled for different duration were acquired with respect to frequency. Figs. 7.5 (a)-(f) shows the admittance vs. frequency plots for the poled PLZT 8/60/40 ceramics milled at 1h, 2h, 3h, 5h, 7h, and 10h with their resonance (f_r) and anti-resonance (f_a) frequencies. The values of f_r and f_a were measured from the fig. 7.5 and these values were used to calculate electromechanical coupling factors. Figs. 7.5 (a)-(c) and (e) shows the three resonance-antiresonance peaks compared to the figs. 7.5 (d) and (f) that shows only two peaks. These are due to the different dimensions of the PLZT ceramic samples.

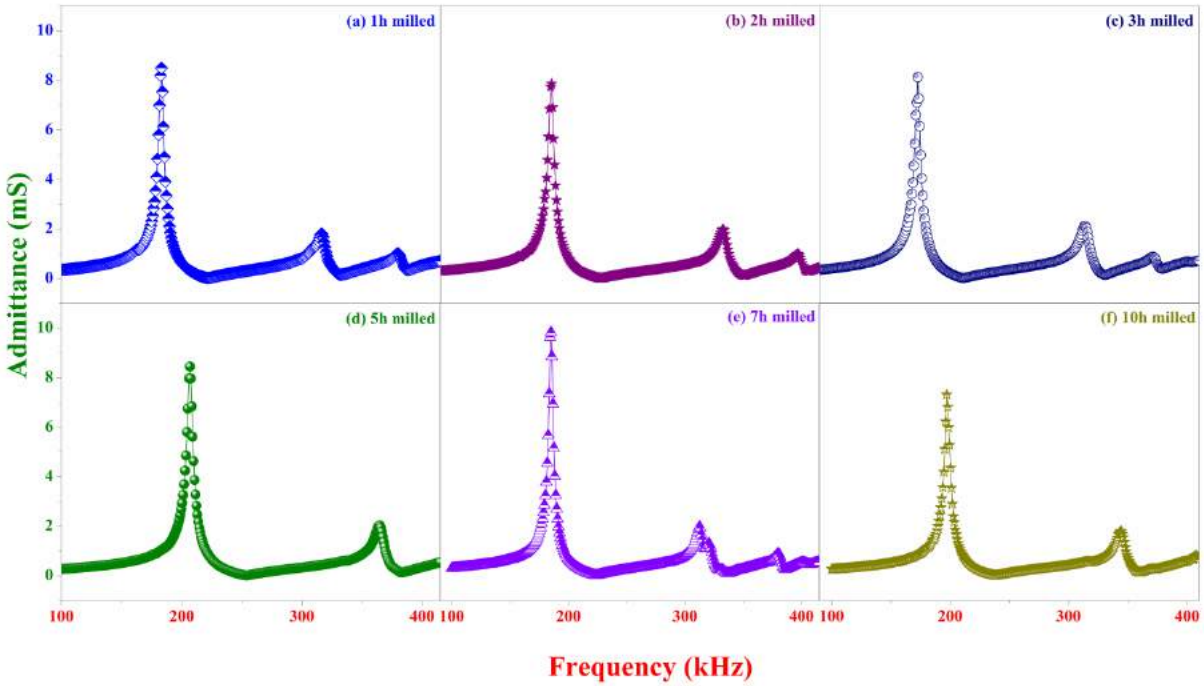

Fig. 7.5 *Admittance vs. frequency graphs for poled PLZT 8/60/40 ceramics milled for (a) 1h, (b) 2h, (c) 3h, (d) 5h, (e) 7h and (f) 10h, showing resonance and anti-resonance peaks.*

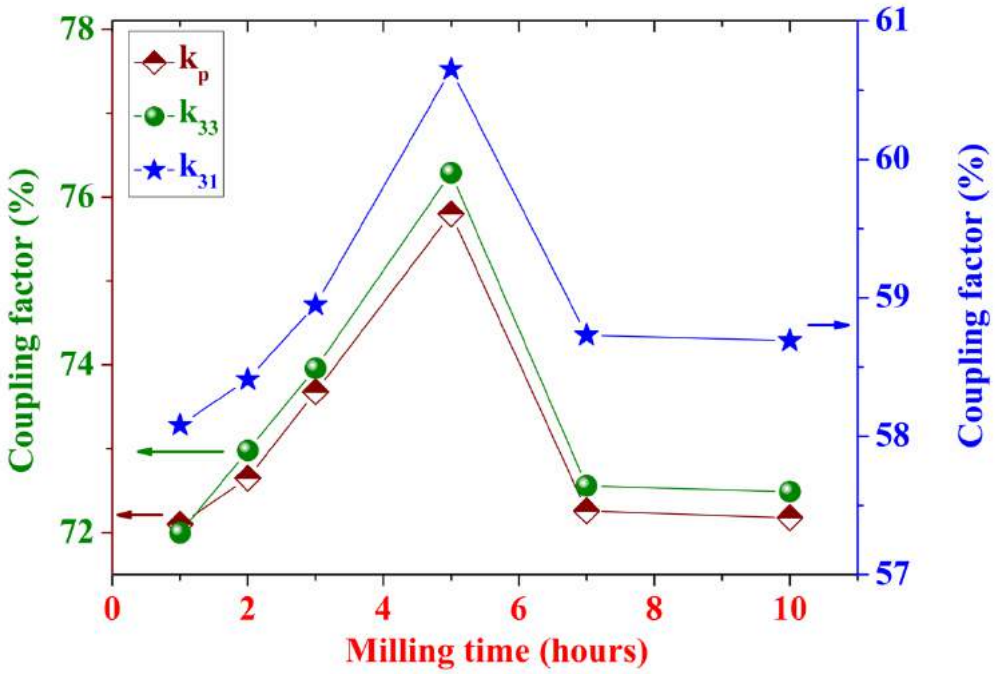

Fig. 7.6 *Change in electromechanical coupling factors (k_p, k_{33} and k_{31}) of PLZT 8/60/40 ceramics as a function of milling time.*

Fig. 7.6 shows the electromechanical coupling factors (k_p, k_{33}, k_{31}) for PLZT 8/60/40 ceramics, milled for different durations. As seen in the figures, the ceramic composition milled for 5 hours gives the highest value of electromechanical coupling factors same as the piezoelectric

coefficients. So it is clear that to get the highest piezoelectric and electromechanical properties of PLZT ceramics, it should be milled for 5 hours. All the electromechanical parameters of PLZT 8/60/40 ceramics, milled for different durations are listed in Table-7.6

Table-7.6 *Electromechanical coupling factor (k_p, k_{33} and k_{31}) of PLZT 8/60/40 ceramics milled for different durations.*

Milling durations	k_p (%)	k_{33}(%)	k_{31} (%)
1h	72.1	72.0	58.1
2h	72.7	72.9	58.4
3h	73.7	73.9	58.9
5h	75.8	76.3	60.7
7h	72.3	72.6	58.7
10h	72.2	72.5	58.7

7.5 Elastic Compliances

Elastic compliances are the ratio of a material's change in dimensions (strain) to an externally applied load (stress) in ferroelectric materials. These parameters show the inverse relation with the Young's modulus. For a given piezoelectric material, the parallel or perpendicular strain to the poling axis decides the elastic compliance along with electrical boundary conditions [**21-22**]. Here s^E is the compliance under a constant electric field (short circuit) and s^D is the compliance under a constant electric displacement (open circuit). The first subscript indicates the direction of strain; the second is the direction of stress. The equations that were used for the calculation of elastic compliances are given in Chapter-2.

7.5.1 Compositional dependence of elastic compliances in PLZT system

Table-7.7 *The elastic compliance coefficients of different compositions of PLZT ceramics.*

Compositions	S_{33}^D (10^{-12} m^2/N)	S_{33}^E (10^{-12} m^2/N)	S_{11}^E (10^{-12} m^2/N)	S_{11}^D (10^{-12} m^2/N)	C_{33}^D (10^{11} N/m^2)	C_{33}^E (10^{11} N/m^2)
PZT 60/40	5.968	6.593	6.434	5.877	1.676	1.517
PLZT 2/60/40	5.100	6.638	6.095	4.948	1.961	1.507
PLZT 4/60/40	5.072	6.891	6.210	4.913	1.610	1.185
PLZT 7/60/40	6.574	9.136	7.986	6.237	1.521	1.095
PLZT 8/60/40	5.715	9.708	7.740	5.484	1.750	1.030
PLZT 9/60/40	6.184	9.428	8.004	5.955	1.617	1.061
PLZT 10/60/40	5.753	6.569	6.345	5.644	1.738	1.522

7.5.2 PLZT 8/60/40 ceramics milled with different vials

Table-7.8 *The elastic compliance coefficients for PLZT 8/60/40 ceramics milled using different vials.*

Milling vials	S_{33}^{D} (10^{-12} m^2/N)	S_{33}^{E} (10^{-12} m^2/N)	S_{11}^{E} (10^{-12} m^2/N)	S_{11}^{D} (10^{-12} m^2/N)	C_{33}^{D} (10^{11} N/m^2)	C_{33}^{E} (10^{11} N/m^2)
Zirconia vial	5.715	9.708	7.740	5.484	1.750	1.03
Agate vial	6.236	14.916	9.418	5.953	1.604	0.671

7.5.3 PLZT 8/60/40 ceramics milled for different durations

Table-7.9 *The elastic compliance coefficients of PLZT 8/60/40 ceramics milled for different durations.*

Milling durations	S_{33}^{D} (10^{-12} m^2/N)	S_{33}^{E} (10^{-12} m^2/N)	S_{11}^{E} (10^{-12} m^2/N)	S_{11}^{D} (10^{-12} m^2/N)	C_{33}^{D} (10^{11} N/m^2)	C_{33}^{E} (10^{11} N/m^2)
1h	6.371	13.738	9.354	6.089	1.570	0.728
2h	6.390	13.673	9.360	6.107	1.565	0.731
3h	6.360	13.189	9.230	6.081	1.572	0.758
5h	6.236	14.916	9.418	5.953	1.604	0.671
7h	5.797	12.243	8.460	5.542	1.725	0.816
10h	6.410	13.515	9.350	6.129	1.560	0.740

7.6 Temperature dependent electromechanical factor of PLZT ceramics

Fig. 7.7 shows the change in electromechanical coupling factor (k_p) of poled PLZT 8/60/40 ceramics as a function of temperature, which was calculated from the resonance and antiresonance frequencies. The non zero k_p value in fig. 7.7, above dielectric maxima temperature, is due the existence of nano-polar regions, which gives the resonance phenomena. That may also cause an increase in a dielectric constant near the transition temperature and peak in a dielectric loss at 500 kHz. The inset of fig. 7.7 shows the existence of resonance at 210^{o}C, which is above T_c.

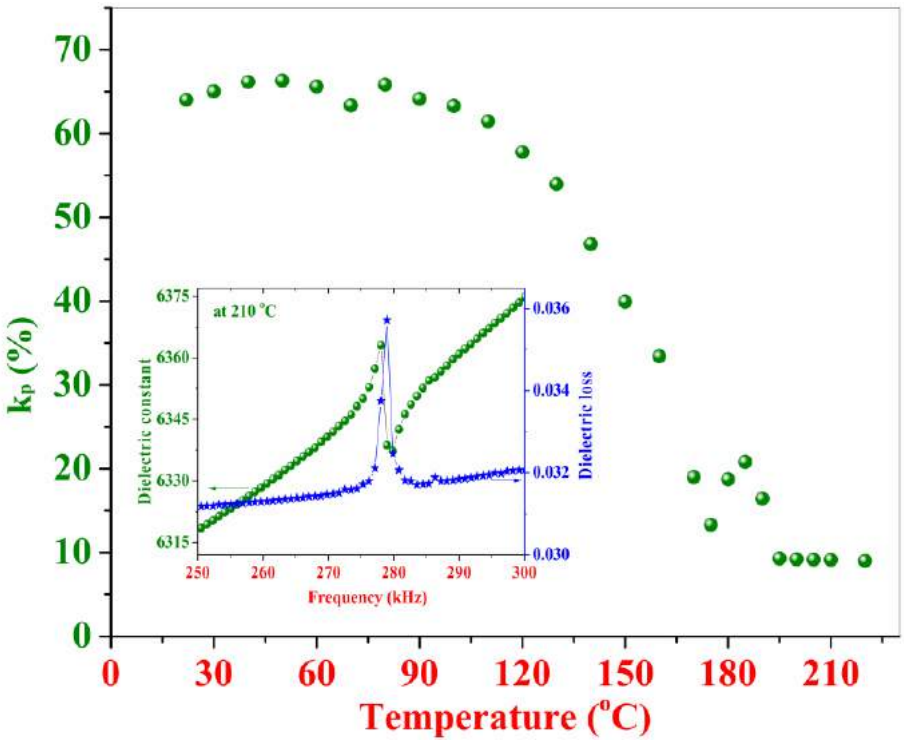

Fig. 7.7 Electromechanical coupling factor (k_p) vs. temperature graph for poled PLZT 8/60/40 ceramics showing non zerok_p after crossing the dielectric maxima temperature. The inset shows the resonance and anti-resonance peaks at 210^{o}C (>T_m).

7.7 Discussion

In this study, the effects of lanthanum substitution variation (at the A-site of PZT ceramic) on the piezoelectric and electromechanical properties were studied for PLZT electro-ceramics. The effect of milling parameters such as milling vial and milling time on the said properties of PLZT ceramic were studied in detail. Elastic compliances were also calculated for PLZT ceramics.

Figs. 7.1 and 7.4 shows that the measured and calculated values of both d_{33} and k_p parameters are very less for PLZT x/60/40 ceramics with low lanthanum substitutions (x=0, 2 and 4%) (d_{33} ~327 pC/N and k_p~ 50.64%). However, for PLZT 8/60/40, PLZT 9/60/40 and PLZT 10/60/40 ceramics there is a rapid improvement in piezoelectric properties. The highest values of d_{33} and k_p are exhibited by for PLZT 8/60/40 ceramics with values of ~570 pC/N and ~64.13%, respectively. The calculated values of other electromechanical coupling factors (k_{33} and k_{31}) for PLZT x/60/40 ceramics also shows the same trend as seen in Fig. 7.4. The highest values of k_{33} and k_{31} were found to be 64.1%, 54.0%, respectively for PLZT 8/60/40 ceramics. Fig. 7.1 shows that the piezoelectric voltage coefficient (g_{33}) is decreasing with an increase in lanthanum substitution. Since as per the definition, the value of g_{33} depends upon the ratio of piezoelectric charge coefficient (d_{33}) and permittivity (ε) of

the material. From Chapter-4, it was found that with an increase in lanthanum substitution, the permittivity (ε) of PLZT ceramics increases. However, pure PZT has very low d_{33} but a small value of ε that makes the g_{33} comparably high. Figs. 7.3 (a)-(g) shows the admittance vs. frequency graphs for poled PLZT x/60/40 ceramics. Here we can see that the shape of the graphs is changing with the change in lanthanum substitution. With an increase in lanthanum, peaks are getting sharper and clear. For the PLZT 8/60/40 ceramics, admittance vs. frequency graph shows a clear and sharp resonance and anti-resonance peaks with highest admittance values.

The PLZT 8/60/40 ceramics were also milled using agate and zirconia milling vials. The highest piezoelectric properties were achieved for the zirconia milled PLZT ceramics. There is a large difference in the density of the milling vials. Agate has the density in the range of ~2.58-2.64 gm/cm^3 and a Mohs scale hardness of ~6.5-7 but for the zirconia, the same parameters are ~6.0-6.2 gm/cm^3 and ~8, respectively. So the zirconia vials provide more impact for the milling balls resulting in fine size final powders with higher properties. It is also understandable that as Zirconia gives only Zr pick-up which is already present in PLZT while the use of agate vial will lead to picking up of impurities like Si which can alter the properties of this ceramics.

Figs. 7.2 and 7.6 show the piezoelectric coefficients (d_{33} and g_{33}) and electro-mechanical coupling factors (k_p, k_{33} and k_{31}) for PLZT 8/60/40 ceramics, as a function of milling time. As seen in these figures, PLZT 8/60/40 ceramics that was milled for 5 hours with zirconia vials show the highest piezoelectric and electromechanical parameters. The piezoelectric charge (d_{33}) and voltage (g_{33}) coefficients for PLZT 8/60/40 ceramics was found to be ~688 pC/N and ~28.48 x 10^{-3} (Vm/N), respectively. The calculated values of electromechanical coupling factors k_p, k_{33} and k_{31} was found to be 75.8%, 76.3% and 60.7% respectively. In this study we have achieved the highest reported values for all parameters. Figs. 7.5 (a)-(g) shows the admittance vs. frequency graphs for poled PLZT 8/60/40 ceramics milled for different durations. As seen in figs. 7.5 (a)-(g), here also we can see the change in the shapes of the graphs with milling durations. Since PLZT 8/60/40 ceramics milled for optimum milling duration has the highest density and better microstructure, that result in sharp and clear resonance and anti-resonance peaks.

Like other electro-ceramics, piezoelectric properties of the PLZT ceramics depend upon many factors, such as the composition of piezoelectrics, MPB conditions [**8-10**], different processing techniques, grain sizes [**11-14**], poling conditions [**15-19**], etc. However, it is remarkable that the conditions, which gives good dielectric properties yielded excellent piezoelectric properties for piezoelectric material. The crystallites in the ferroelectric materials, under these conditions seemingly evidence near single crystal like environment with minimum constraints. Hence to obtain the best electrical properties of ferroelectric materials, these conditions can be identified as the optimized conditions. To enhance the piezoelectric properties of PLZT ceramics a combinatorial approach of mechanical activation and cipping were used. Mechanical activation and CIP together improve the material's density (≥ 98%) and help to retain their optimum grain sizes. The switching phenomena of

domain walls and domain wall motion are both influenced by the grain sizes. In this study, the reason of high piezoelectric and electromechanical coefficients in PLZT 8/60/40 ceramics can be correlated with the switching and movement of non-180^o domains walls. This phenomenon was experimentally shown by Tsurumi et al. **[23]**. The switching and the movement of domain walls are greatly influenced by the presence of inter-granular phases, quality of grain boundaries and porosity **[20]**.The effects of grain size on the electrical properties of ferroelectrics can be explained on the basis of residual internal stresses. The presence of multiple 90^o domain walls for grains larger than 1 μm was observed by Tuttle et al. **[24]**.

In this study it was found that PLZT ceramics, having high density and fine grain sizes show reasonably good piezoelectric properties that can be achieved by optimizing the lanthanum substitution, milling vials and milling durations. PLZT ceramics that were 8% lanthanum substituted, milled in zirconia vials for 5 hours milling duration and sintered at 1200^{o}C showed a grain size of ~1.4 μm. These, in turn, resulted in uniform grain sizes, clearly visible grain boundaries, low porosity and optimum electrical properties. Domain wall reorientation or movement can be restricted due to their imperfections, defects, complex set of internal stresses and electric fields within the grains.

Strain in the piezoelectric materials increases with an increase in electric field on account of the reorientation of ferroelectric domains. It reaches its maximum value at highest possible electrical fields but these strains in piezoelectric materials at high fields are not stable. Thus the removal of the applied electric field causes these unstable domains to switch back to their original state. In this case, material, therefore, goes through repeated cycling in the form of poling and de-poling, though strains can be large in such a situation. Fine grain ceramics have higher, low field properties because their domains remain more completely aligned after removal of the electric field. This means there is a lesser strain at high fields due to fewer contributions from domain reorientations **[25]** because most of the domains in the piezo-ceramics are already aligned.

The ferroelectric domains of electro-ceramics are formed to minimize the electrostatic energy of the depolarizing field, which arises due to the surface charge and elastic energy associated with mechanical constraints. Both 90^o and 180^o domain walls help to reduce the effect of depolarization electric fields . However, only 90^o domain walls participate in minimizing the elastic energy [**19**]. The PLZT 8/60/40 composition is located near the MPB region. On account of this, it is expected that the increased number of directions of spontaneous polarization will help to improve the piezoelectric properties. As discussed in Chapter-6 on poling, the tetragonal and rhombohedral phase possesses a total number of six (90^o and 180^o domain walls) and eight (180^o, 71^o and 109^o domain walls) polarization directions, respectively. Since at the MPB, for polycrystalline ferroelectric materials, the number of available directions of spontaneous polarization are 14 (6+8=14) resulting in the highest piezoelectric properties. However the observed (low) polarization is attributed to the complex set of internal stresses and electric fields within grains of ferroelectrics, which restricts many domains to

reorient. On the other side after the electric field removal, many domains switched back to their virgin states **[20]**.

The high value of piezoelectric properties reported in the present study could be attributed to any or all of the following: uniform distribution of composition, uniform distribution of grain size in the samples, low defect density, high relative density, etc. **[5]**. Ferroelectric materials always contain elastic and electrical defects along with imperfections. All of these affect the switching and movement of domain walls along with polarization within individual grains. Domain wall movement can be restricted by defects and imperfections. The reason for higher piezoelectric values for the PLZT 8/6040 ferroelectric material obtained in this thesis work could be due to fewer defects and imperfections in the crystallites **[20]**.

The piezoelectric and electromechanical properties of PLZT ceramics are greatly influenced by the poling conditions. Therefore to get the highest electrical properties in piezo-ceramics the poling conditions should be optimized. In Chapter-6 the optimum poling conditions of PLZT 8/60/40 ceramics were carefully identified by changing the (1) Poling electric field (2) Poling time (3) Poling temperature and (4) the ceramic sample thickness. Poling field studies suggest that ceramics can be poled at ~5 kV/cm even though the coercive field is ~12 kV/cm within a temperature range from 75^{o}C to 120^{o}C. This shows that the PLZT ceramics can be poled at significantly reduced poling voltages. The optimum poling time was found to be 30 minutes which is very less compared to what has been reported in literature, often several hours long. The ageing study also supports the hypothesis of poling of PLZT ceramics at lower electric fields than the coercive field. Since the high strain and the high piezoelectric charge (d_{33}) of the electro-ceramics are interdependent, it is necessary to find optimum poling conditions for electro-ceramics and the results should be discussed in conjunction with the strain vs. electric field curves (Chapter-5).

7.8 Summary

In this study, different compositions of PLZT ceramics were prepared by substituting lanthanum at the A-site of the PZT system. PLZT 8/60/40 composition shows the piezoelectric charge coefficients ($d_{33}\cong 570$ pC/N, $g_{33}\cong 28.03 \times 10^{-3}$ Vm/N) and electromechanical coupling factors ($k_p = k_{33} = 64.13\%$ and $k_{31} = 53.99\%$). Optimized PLZT 8/60/40 composition was milled using an agate and zirconia vials. PLZT 8/60/40 ceramics milled for 5 hours with zirconia vial shows the improvements in electrical properties and shows the highest piezoelectric charge coefficients ($d_{33}\cong 688$ pC/N, $g_{33}\cong 28.48 \times 10^{-3}$ Vm/N) and electromechanical coupling factors ($k_p = 75.8\%$, $k_{33} = 76.29\%$ and $k_{31} = 60.65\%$). The values of elastic compliances for the optimized PLZT ceramics were also found to be good. The diffuse phase transition in PLZT ceramics was also studied by temperature dependent electromechanical coupling factor (k_p) measurements within the temperature range 30^{o}C to 210^{o}C, respectively. The results of these measurements have been reported in this chapter.

References

[1] B. Jaffe, J. Am. Ceram. Soc., **41 [11]** (1958) 494.

[2] G.H. Haertling, J. Am. Ceram., **82** (1999) 797.

[3] B.G. Kim, S.M. Cho, T.Y. Kim and H.M. Jang, Phy. Rev. Lett., **86 [15]** (2001) 3404.

[4] A.R. James, J.P. Praveen, M.P. Kumar and V.V. Bhanu Prasad, Mater.Res. Bul., **47 [11]** (2012) 3459.

[5] A.R. James, J. Subrahmanyam and K.L. Yadav, J. Phys. D: Appl. Phys., **39** (2006) 2259.

[6] S.H. Baek, M.S. Rzchowski, V.A. Aksyuk, MRS Bulletin, **37** (2012) 1022.

[7] S.L. Swartz, T.R. Shrout, Mater. Res. Bull., **17** (1982) 1245.

[8] L. Pdungsap, N. Udomkan, S. Boonyuen and P. Winotai, Sensors and Actuators A: Physical, **122** (2005) 250.

[9] M. Hinterstein, K.A. Schoenau, J. Kling, H. Fuess, M. Knapp, H. Kungl and M.J. Hoffmann, J. Appl. Phys, **108** (2010) 024110.

[10. G.H. Haertling and C.E. Land, J. Am. Ceram. Soc., **54** (1971) 1.

[11] G. Viola, K.B. Chong, M. Eriksson, Z. Shen, J. Zeng and Q. Yin et. al., Appl. Phys. Lett., **103** (2013) 182903.

[12] T.M. Kamel and G. deWith, J. Euro. Ceram.Soc., **851** (2008) 28.

[13] B.M. Jin, J. Kim and S.C. Kim, Appl. Phys. A, **65** (1997) 53.

[14] C.A. Randall, N. Kim, J.P. Kucera, W. Cao and T.R. Shrout, J. Am. Ceram. Soc., **81** (1998) 677.

[15] L. Zhang, Q. Sun, W. Ma, Y. Zhang and H. Liu, J. Mater. Sci.: Mater. Electron., **23** (2012) 688.

[16] Y. Zhao, R. Huang, R. Liu and H. Zhou, Ceram. Inter., **38** (2012) 6067.

[17] S. Su, R. Zuo, S. Lu, Z. Xu, X. Wang and L. Li, Curr. Appl. Phy., **11** (2011) S120.

[18] A. Kumar, V.V.B. Prasad, K.C.J. Raju and A.R. James, J. Mater. Sci.: Mater. Electron., **26** (2015) 3757.

[19] A. Kumar, V.V.B. Prasad, K.C.J. Raju and A.R. James, Europ. Phy. J. B, **88** (2015) 287.

[20] D. Damjanovic, Rep. Prog. Phy., **61** (1998) 1267.

[21] W.A. Smith, proc. 6th Int. Symp. Ampl. Ferroelectrics, (1986) 249.

[22] L. Swartz, IEEE Trans. Electrical Insulation, **25** (1990) 935.

[23] T. Tsurumi, Y. Kumano, N. Ohashi and O. Fukunaga, Jpn. J. Appl. Phys., **36** (1997) 5970.

[24] B.A. Tuttle, T.J. Garino, J.A. Voigt, T.J. Headley, D. Dimos and M.O. Eatough, Science and Technology of Electroceramic Thin Films, Editosr: O. Auciello and R. Waser (Dordrecht: Kluwer) (1995) p 117.

[25] W. Hackenberger, M.J. Pan, V. Vedula, P. Pertsch, W. Cao and C. Randall, T.R. Shrout, SPIE Conf. on Smart Mater. Tech., San Diego, CA, March Proc. SPIE 3324 (1998) 28.

Chapter-VIII

Evidence of monoclinic phase at morphotropic phase boundary of PLZT ceramics and its variation with temperature

8.1 Introduction

$(Pb_{0.92}La_{0.08})(Zr_{0.60}Ti_{0.40})O_3$ (PLZT 8/60/40) was synthesized by substituting 8% lanthanum on the A-site of lead zirconate titanate (PZT) electro-ceramics by using high energy mechano-chemical ball milling and cold isostatic pressing. Complete details of PLZT ceramics preparation have already been discussed in chapter-2. After phase analysis and micro-structural studies (Chapter-3), dielectric studies (Chapter-4), ferroelectric studies (Chapter-5) and piezoelectric studies (Chapter-7), we confirmed that PLZT 8/60/40 ceramics that were milled for 5 hours, show single and pure perovskite phase, uniform grain sizes with visible grain shapes and dense micro-structure indicating a polycrystalline microstructure with average grain size <1.5 μm with highest electrical (dielectric, ferroelectric and piezoelectric) properties. Poling field studies for the PLZT 8/60/40 ceramic suggest that ceramics can be poled below the coercive field. Polarization and strain in PLZT ceramics were measured as a function of electric field, which show an improvement in ferroelectric properties such as shape of the hysteresis loop, remnant polarization (~34 μC/cm^2), coercive field (~12 kV/cm) as well as strain (0.29%), strain hysteresis loss (<3%) with piezoelectric charge coefficient (~750 pC/N) and electromechanical coupling factor (~75%).

In this chapter, the origin of these ultra high electrical parameters, high strain and piezoelectric properties are discussed. Since we know that PLZT 8/60/40 ceramic composition is close to MPB, even a slight change in phase can cause a huge variation in their electrical properties. This phase variation of PLZT ceramics can be detected by studying the XRD patterns. A detailed study of XRD patterns by using Rietveld analysis is required for the same. In this current study slow scan X-ray, diffraction data was collected from a PLZT sample at room temperature, by varying temperature of the ceramics. This data is refined and analyzed by Rietveld refinement method. The refined XRD patterns for the PLZT 8/60/40 ceramics shows the presence of coexistence of two phases, instead of the previously reported single tetragonal phase at MPB. These two phases have the tetragonal (P4mm) and monoclinic (Cm) symmetries. This structural change is correlated with the ultra high piezoelectric strain in PLZT ceramics.

8.2 Morphotropic phase boundary studies for PZT and PZT based electro-ceramics

Ferroelectric ceramics for piezoelectric applications historically have been used for different applications **[1]**. Perovskite ABO_3 type materials always possess high piezoelectric coefficients and electromechanical coupling factors, which can be further improved by doping or substitution at A-site or B-site. The composition ratio between the B-cations decides the morphotropic phase boundary (MPB) of the ceramics. Examples are $xPb(Mg_{1/3}Nb_{2/3})O_3$-$(1-x)PbTiO_3$ (PMN-PT), $xPb(Zn_{1/3}Nb_{2/3})O_3$-$(1-x)PbTiO_3$ (PZN-PT), $Pb(Zr_xTi_{1-x})O_3$ (PZT), $(Pb_ySr_{1-y})(Zr_xTi_{1-x})O_3$ (PSZT), $(Pb_yBa_{1-y})(Zr_xTi_{1-x})O_3$

(PBZT) and $(Pb_yLa_{1-y})(Zr_xTi_{1-x})O_3$ (PLZT) solid solutions **[1-2]**. Before going to study the detailed Rietveld analysis of PLZT 8/60/40 ceramics from XRD patterns, some important points are discussed here.

Like other electro-ceramics an optimum piezoelectric activity in PZT solid solutions was found at MPB, which separates rhombohedral (R3c) phase and tetragonal (P4mm) phase **[3]**. The MPB of electro-ceramics has been the subject of intense scientific studies to understand its behavior. The solid solution of $Pb(Zr_xTi_{1-x})O_3$ (PZT) displays a complex phase diagram (fig. 8.1), which shows a high-symmetry, primitive cubic structure at high temperatures and lower temperatures a variety of cation shifts, octahedral tilts and deformations occur leading to different structures. At room temperature $PbZrO_3$ (Ti=0%) shows the lower-symmetry, anti-ferroelectric, orthorhombic (A_O) structure **[4]**. With increasing Ti content (0 to 100%), two ferroelectric, rhombohedral phases, FR_{LT} and FR_{HT}, are observed up to x=0.48 where there is a transition to a ferroelectric tetragonal phase, F_T, continuing to the end $PbTiO_3$ (Zr=0%) **[5]**. Both rhombohedral and tetragonal ferroelectric regions of PZT phase diagrams have been of considerable technological importance for their applications in different applications.

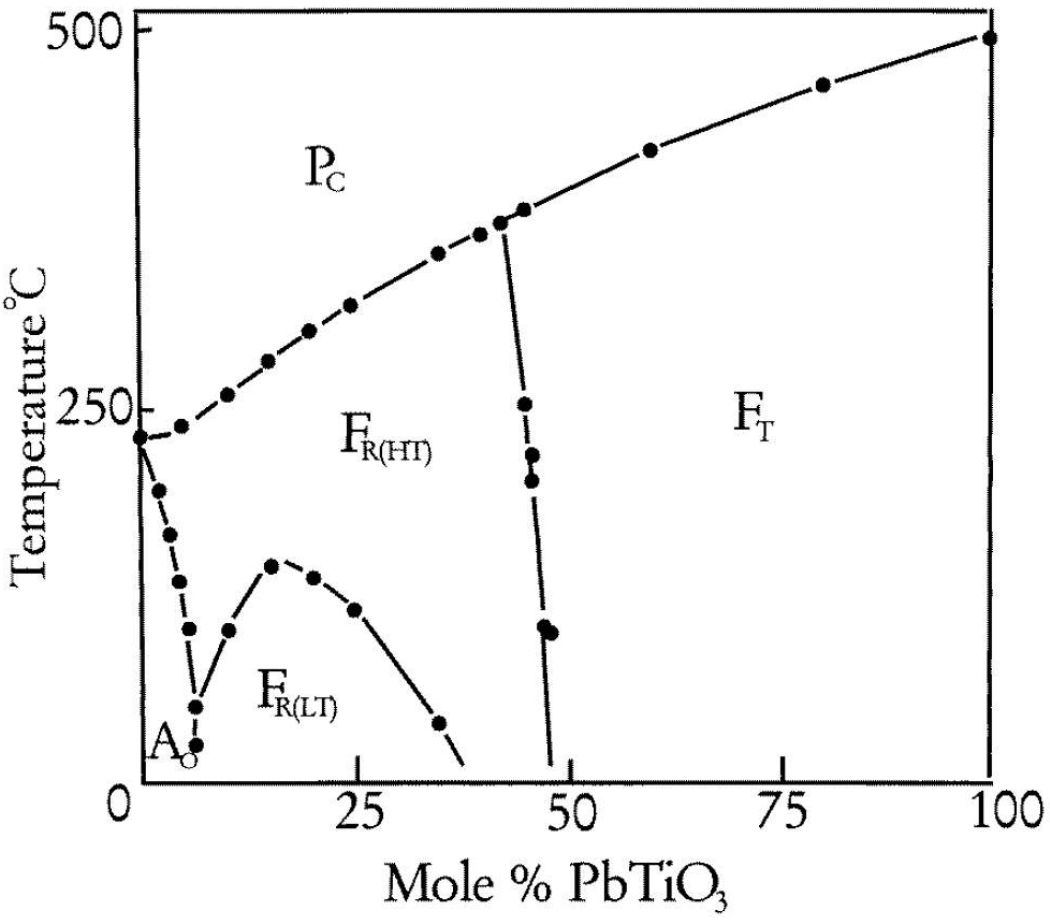

Fig. 8.1 *The phase diagram of the $Pb(Zr_xTi_{1-x})O_3$ (PZT) solid solution **[3]**.*

The high resolution synchrotron XRD data of PZT ceramics shows the existence of monoclinic phase with space group Cm at the MPB **[6-9]**. However, PMN-PT **[10]** and PZN-PT **[11]** ceramics show the monoclinic Pm phase. The monoclinic phase fraction depends on the average composition and temperature of the ceramics **[12]**. The monoclinic Cm phase relieves the stress in PZT ceramics, which was generated due to the interaction between R3m and P4mm phases at MPB **[13]**. The discovery of stable monoclinic phase at MPB provides a new perspective to view the rhombohedral to tetragonal phase transformation not only for the PZT system [**7]** but also for the PMN-PT and PZN-PT **[8]**, which has the similar phase boundaries. The presence of this monoclinic phase plays a key role to explain the high piezoelectric response in PZT as well as other systems with similar MPBs. The polar axis of this monoclinic phase is in the (110) plane along a direction between the tetragonal and rhombohedral polar axes **[7]**. After investigation of several compositions at MPB, Guo et. al. **[14]** has shown a modified PZT phase diagram as shown in fig. 8.2 **[8, 14]**.

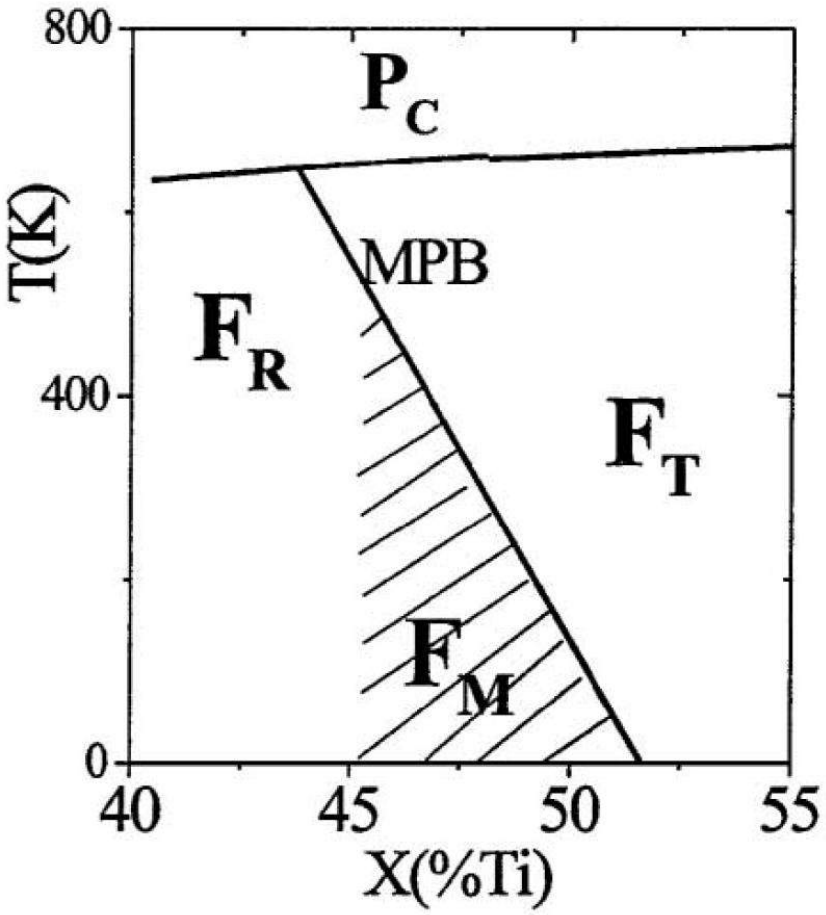

Fig. 8.2 *Schematic of the PZT phase diagram at MPB showing the monoclinic region* ***[14]****.*

Previous studies have revealed the existence of a phase boundary in PZT that separates the titanium-rich region from the zirconium-rich region. A second phase boundary has been theoretically predicted to exist since calculations have shown that the piezoelectric effect of PZT increases towards

such a boundary. However, this boundary, which was predicted to lie between the zirconium-rich region and a region containing lead atoms observed by Zhanget al. **[15]**. The nature of the crystal structure of PZT was investigated, and this missing boundary can explain why PZT is such a good piezoelectric material, and also provides insight into how to optimize its piezoelectric response. The studies revealed that the region containing lead is composed of two types of structures. In one structure, the lead atoms have a lot of space to move around, allowing them more room to be affected by an external mechanical stress. In the other structure, the lead atoms do not have nearly as much space to move. This finding indicates that the first type of structure is strongly preferable for maximizing the piezoelectric response in PZT material, helping explain why the piezoelectric response increases near this boundary. There are two possible monoclinic phases, which are denoted by M_A and M_B, where the atomic displacements lie within {110} mirror planes. The M_A monoclinic phase has cation displacements between the R and T positions, whereas the M_B monoclinic phase can be found between R and O regions. The structural data point of PZT ceramics is a mixture of an average rhombohedral structure with disordered lead atom displacements along with long-range monoclinic structure, which is consistent with Rietveld refinement results **[16]**. Fig. 8.3 shows the new phase diagram of PZT ceramics proposed by Zhang et. al. **[15]**.

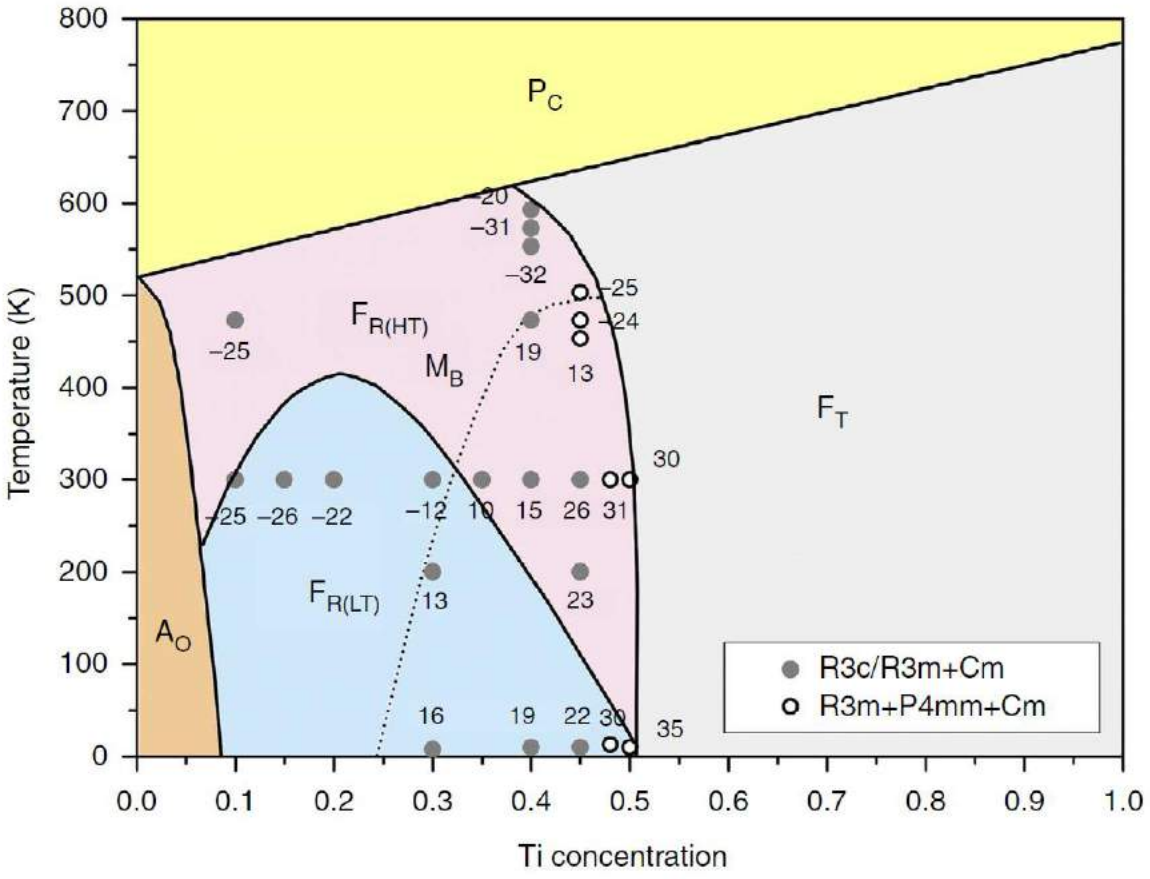

Fig. 8.3 *The new phase diagram for PZT. The crossover between M_A and $M_B$region is separated by a dashed line. The phase regions, which are shown in fig. are cubic (P_C), orthorhombic (A_O) tetragonal (F_T), rhombohedral ($F_{R(LT)}$ and $F_{R(HT)}$)* ***[3, 15]****.*

Fig. 8.4 shows the PLZT phase diagram, which shows the reduction of the T_c with increasing La substitution, due to decrease in ferroelectric phase stability in favour of the paraelectric and anti-ferroelectric phases, as indicated by the red line. The cross-hatched area represents a region of diffuse and metastable relaxor phases, which can be brought to ferroelectric phase by application of electric field. In this region, ceramics shows a quadratic strain and electro-optic behavior. The solubility of La in the PZT lattice is related to the amount of PT as indicated by the dashed line adjacent to the mixed-phase region (double cross-hatched area) in fig. 8.4 **[2]**.

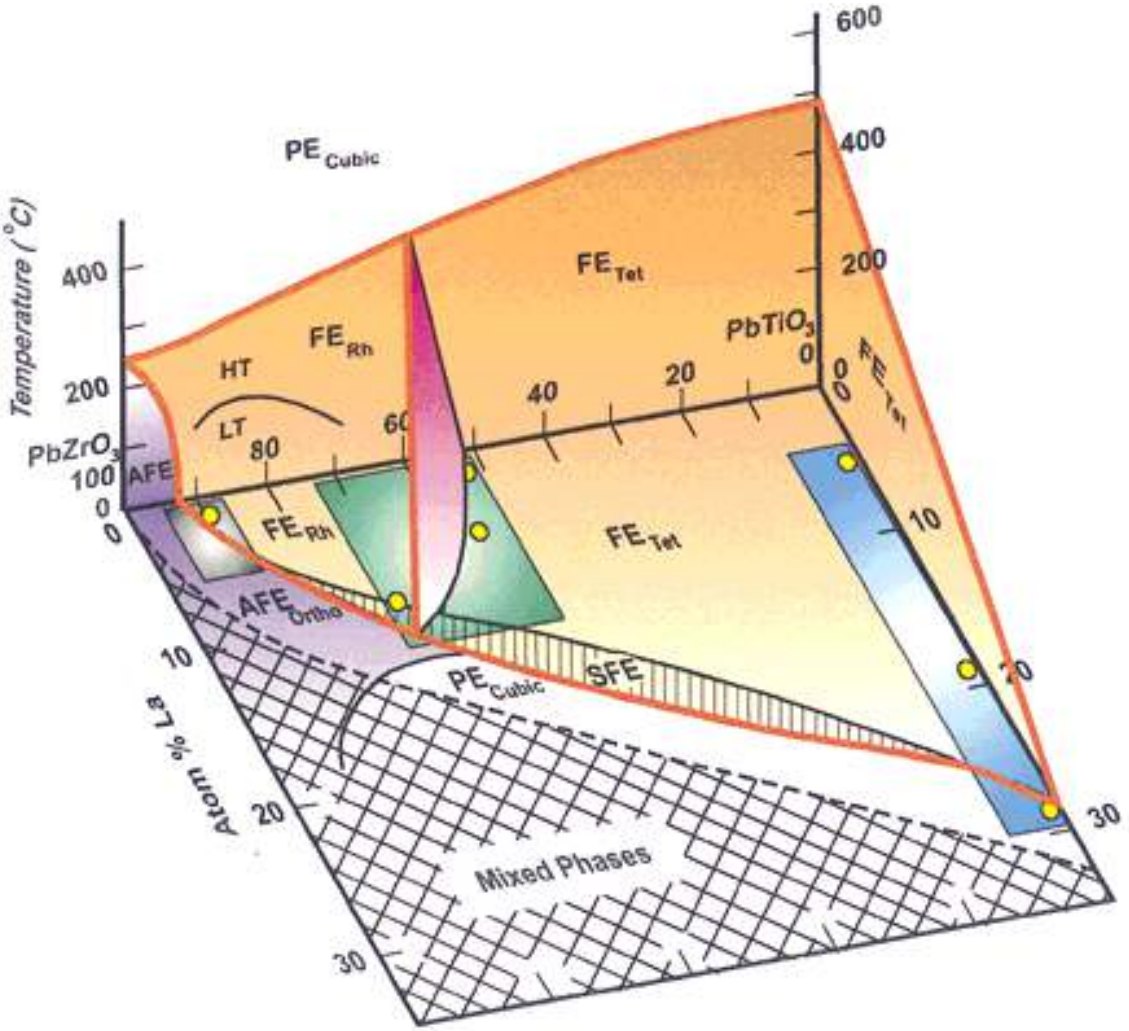

Fig. 8.4 *The phase diagram of the* $(Pb_yLa_{1-y})(Zr_xTi_{1-x})O_3$ *(PLZT) solid solution system* ***[2]****.*

8.3 Origin of high piezoelectric response in PLZT 8/60/40 electro-ceramics

Two theories are widely accepted to explain the mechanism behind the enhanced piezoelectric and electro-mechanical response at MPB of electro-ceramics, (i) the field induced polarization rotation within the unit cell **[7, 14, 17-22]** and (ii) the adaptive phase model (formation of a high density of low energy domain walls) **[23-25]**. Both theories help to see the different side of the same problems to understand the high piezoresponse.

8.3.1 Polarization rotation model

Origin of high piezoelectric response for perovskite oxides has been interpreted by Fu and Cohen **[20]** via a "polarization rotation" between the adjacent R3c and P4mm phases through an intermediate monoclinic phase. This polarization rotation model helped to understand the remarkable high piezoelectric properties of PZT and other lead based perovskite systems. The easy rotation of the polarization vector on the application of electric field helps in attaining enhanced properties. The intermediate monoclinic phase near MPB was experimentally first observed for PZT by Noheda et. al. **[7-9]**.

In a polarization rotation model, a high piezoelectric response is associated with the availability of a continuous pathway for the rotation of polarization vector on the application of electric field as provided by low symmetry (monoclinic/triclinic) distortions/phases **[20]**. For example, in lead-zirconate titanate (PZT), the polarization is contained in a mirror plane $(1\bar{1}0)_{pc}$ of the monoclinic M_A phase **[26-27]**. This monoclinic M_A phase is one of the three possible monoclinic space groups Cm (M_A and M_B) and Pm (M_C), predicted by the Vanderbilt and Cohen **[26]**. The rotation pathway is determined by the anisotropic flattening of the free energy profile, near a ferroelectric-ferroelectric critical point, induced either by composition, pressure or temperature **[28-30]**. This theory has also been invoked to explain the strong piezoelectric response obtained after poling ferroelectric crystals along non-polar directions and to explain the strong shear coefficient near inter-ferroelectric instabilities **[31-33]**. First principles calculations **[31]** have shown the feasibility of electric field induced paths in PZT via intermediate low symmetry phases. Davis et al. **[34-35]** suggested that the key feature of the polarization rotation mechanism is the ferroelectric-ferroelectric phase transformation.

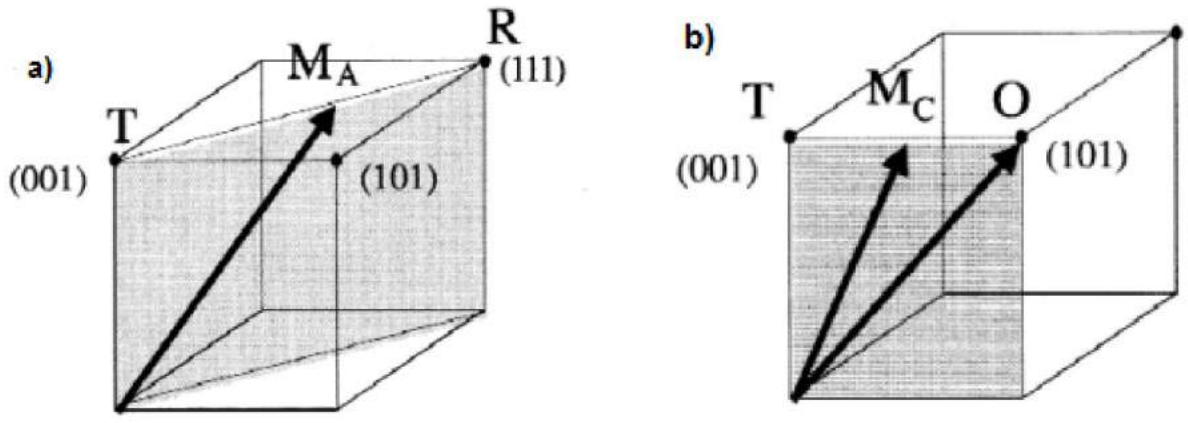

Fig. 8.5 *Schematic of the perovskite unit cell with a polarization vector (solid arrow) in the (a) Monoclinic M_A phase rotating between the rhombohedral (R) and tetragonal (T) phase in the $(101)_C$ plane (shaded), (b) Monoclinic (M_C) phase rotating between tetragonal (T) and orthorhombic (O) phases in $(010)_C$ plane (shaded)* ***[36-37]***.

In PZT, the monoclinic phase is Cm (M_A) with unit cell parameter a_m, b_m, c_m, β. Monoclinic lattice parameter a_m and b_m lie along the tetragonal $(101)_C$ directions ($a_m \approx b_m \approx a_t\sqrt{2}$), and c_m is close to the (001) axis ($c_m \approx c_t$), as illustrated in fig. 8.5 (a). The monoclinic cell has b_m as the unique axis, and the angle between a_m and c_m is β. The monoclinic polarization is contained in the monoclinic plane $(101)_C$, pointing along a direction in between $[001]_C$ and $[111]_C$. It represents the structural bridge between the tetragonal (P4mm) and the rhombohedral (R3m) phases through the common mirror symmetry element, $(101)_C$ plane. Similarly, for PMN-PT and PZN-PT, the monoclinic phase is Pm (Mc) with polar vector lies in $(010)_C$ plane, shown in fig. 8.5 (b) **[37]**.

8.3.2 Adaptive phase model:

In this adaptive phase model, the monoclinic symmetry is considered as an adaptive phase resulting from the coherent scattering by a superlattice of nano-sized twinned regions of the high symmetry tetragonal or rhombohedral phases. This theory is based on the assumption of a dramatic decrease in domain wall energy near an inter-ferroelectric phase transition. According to this theory, the large piezoresponse arises due to the easy motion of low-energy domain walls on the application of external stimuli (stress or electric field). The adaptive phase model is still a matter of considerable debate as many reports are available in support and against it **[38-40]**. According to this model, an adaptive phase is a particular case of miniaturized stress accommodating domain microstructure observed in the conventional martensitic phase. This kind of domain configuration becomes possible provided the domain wall energy is significantly low. The relation between the domain wall energy (γ) and the domain width (D) is; **[23-24]**

$$\boldsymbol{D} \propto \sqrt{\boldsymbol{\gamma}} \quad \ldots\ldots(1)$$

According to the above relation, domain wall energy is directly proportional to the square of the domain wall width, which implies that the decrease in domain wall energy considerably decreases the domain width. Further, the low domain wall energies transform the domain configurations into a mixed state that comprises of inhomogeneous nanoscale (<10 nm) domains and homogeneous macroscale (>10 μm) domains **[37]**.

8.4 Aim of the present study

From the existing literature and in our work **[41-45]** it has been observed that the PLZT 8/60/40 composition shows ultra high piezo parameters and strain values. There are plenty of explanations based on microstructure are already given (Chapter-3), but the adequate explanation for the fundamental understanding of the excellent piezoelectric properties of PLZT 8/60/40 is still lacking and needs more details. The origin of the widely applicable piezoelectric properties of PZT ceramics, one of the most common piezoelectric materials is not fully understood. This lack of

understanding is due to the complex nature of the material's underlying crystal structure, which is responsible for its physical properties.

Substitution of La ion at the A-site (lead ion) in PZT solid solution system results in improved microstructural, ferroelectric and dielectric properties. In addition to that lanthanum, substitution can also modify the MPB reported by Haertling **[2]** and found that the following composition $(Pb_{0.92}La_{0.08})(Zr_{0.60}Ti_{0.40})O_3$ (PLZT 8/60/40) is located near the MPB region separating the tetragonal and rhombohedral crystal structures. The aim of this study is to give a satisfactory explanation to understand the origin of ultra high piezoelectric response and the structural details of PLZT 8/60/40 electro-ceramics in the vicinity of the MPB. The present study deals with the confirmation of monoclinic phase in 8% La-substituted $Pb(Zr,Ti)O_3$ solid solution by Rietveld analysis using Full Prof Software and its variation with temperature. This can be correlated with the observed higher electrical properties of the PLZT system.

8.5 Phase variation study of PLZT 8/60/40 ceramics at different temperatures

The PLZT 8/60/40 ceramic sample which was used for the structural analysis was prepared by using optimum preparation conditions (milling parameters, CIP, etc., already discussed in detail in Chapter-2). The high resolutions slow scan XRD data for PLZT 8/60/40 ceramics were taken from 25^{o}C to 350^{o}C. Fig. 8.6 shows the XRD plots of PLZT ceramics from room temperature to 350^{o}C. During the heat treatment process of compact ceramics, the reaction between unreacted oxides leads to desired PLZT perovskite phase. Room temperature XRD pattern of PLZT shows the formation of pure perovskite single phase free from any secondary phases, which was confirmed by JCPDS (53-0698) file, indicating the completion of the chemical reaction. This file shows that PLZT 8/60/40 has a tetragonal symmetry at room temperature with lattice parameters a = b = 4.005 Å and c = 4.010 Å.

It is well known that when the ferroelectric ceramics are heated from room temperature to high temperature, the material undergoes a ferroelectric phase transition from low symmetry tetragonal phase to high symmetry cubic phase. Dielectric studies (Chapter-4) for the PLZT 8/60/40 ceramics show that this structural phase transition occurs at ~200^{o}C. Structural lattice parameters of the ceramics also change as a function of temperature. These small changes give valuable information about the crystal structure of piezoelectric ceramics. Rietveld refinement is widely accepted for crystallographic studies. In this study also, Rietveld refinement of XRD data was used to study the effect of temperature on the lattice parameters, crystal structure and phase variation.

Before going for the Rietveld refinement of PLZT ceramics, it is necessary to study the available literature to find out the possible crystal structure and the initial value of several parameters such as lattice parameters, atomic positions, occupancy, etc. The approximate values of these starting parameters are required for the good refinement. As we know after the ferroelectric phase transition

temperature (T_c~200^{o}C), ceramics possess a cubic structure so cubic fitting should be used at high temperature (>T_c). However, in this study, several crystal symmetries were used for the Rietveld refinement of PLZT ceramics at room temperature. The χ^2 parameter was used to find out the best fitting, which should be minimum (For ideal fitting χ^2 =1).

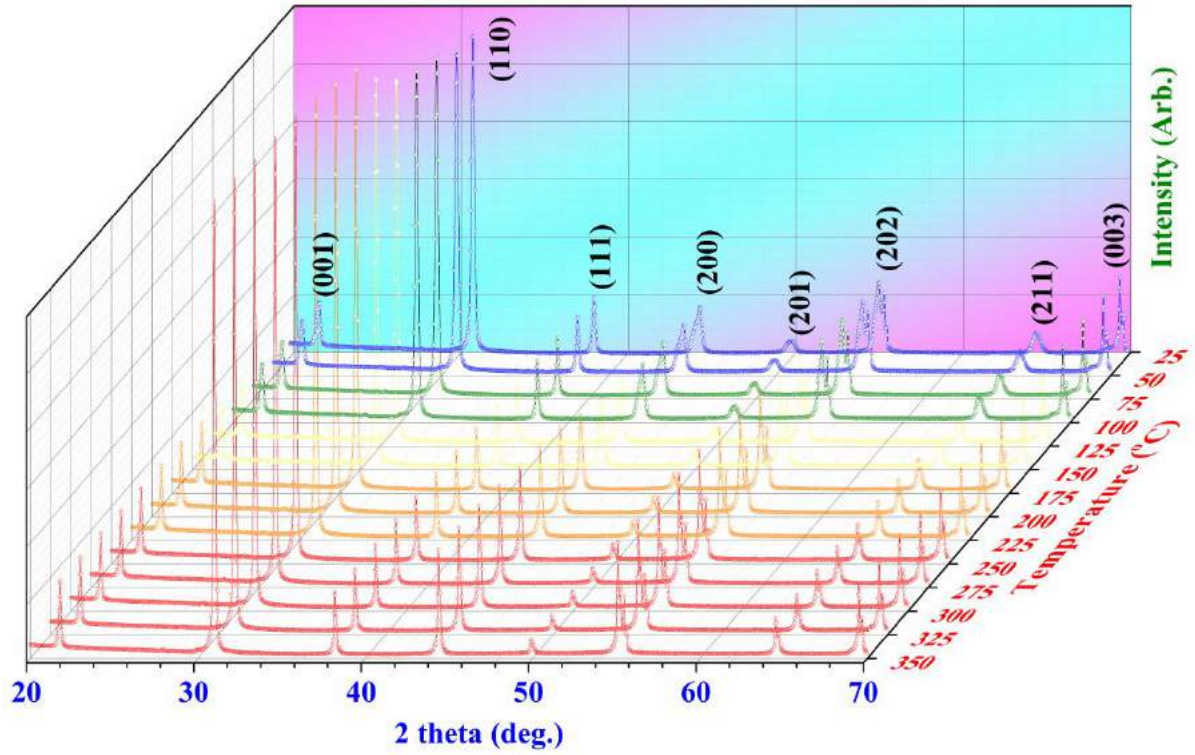

Fig. 8.6 *XRD patterns of PLZT 8/60/40 ceramics at a different temperature.*

For the tetragonal and rhombohedral crystal symmetries, their respective space groups are P4mm and R3m. However, the monoclinic crystal structure has two space groups C1m1 and P1m1. The Rietveld refinement was done in two steps; single phase (for example Tetragonal, Rhombohedral, and Monoclinic) as well as double phase refinement (For example Tetragonal+Rhombohedral, Tetragonal+Monoclinic). The approximate initial values for all the starting parameters with their respective crystal symmetries were taken from the existing literature **[46]**. These approximate initial values are required for the convergence of Rietveld refinement and given in Table-8.1 to 8.5.

The information regarding atomic coordinates and occupancy and how the atomic coordinates and occupancy are selected/calculated is given in International Tables for Crystallography in detail **[47]**. All of these involve Wyckoff positions, multiplicity, etc. Generally, the occupancy of an atom is calculated by site occupancy/General multiplicity. The Rietveld refinement of PLZT ceramics was done as per the guidelines **[48]**. The refinement parameters are Scale, Background, Instrument, Cell parameters (a, b, c, α, β, γ), FWHM (U, V, W), shape, Asymmetry, Isothermal, Displacement,

Occupancy and Atomic coordinates (X, Y, Z). The scale factor is related to the intensity of XRD peak and U, V, W parameters are related to the width of the peak.

Table-8.1 *Approximate initial values of important parameters for tetragonal symmetry with P4mm space group, which were used for Rietveld refinement.*

Atom	**Valance state**	**Lattice parameters**	**Atomic Coordinates**			**B_{iso}**	**Occupancy**
			X	**Y**	**Z**		
Pb	Pb+2	a=b=4.0635Å c=4.0959 Å	0	0	0	2.14718	0.92*1/8=0.115
La	La+3		0	0	0	2.14718	0.08*1/8=0.010
Zr	Zr+4		0.5	0.5	0.45625	0.0258	0.60*1/8=0.075
Ti	Ti+4		0.5	0.5	0.45625	0.0258	0.40*1/8=0.050
O_1	O-2		0.5	0.5	-0.03878	0.0258	1.00*1/8=0.125
O_2	O-2		0.5	0	0.56754	0.0258	2.00*1/8=0.250

Table-8.2 *Approximate initial values of important parameters for rhombohedral symmetry with R3m space group, which were used for Rietveld refinement.*

Atom	**Valance state**	**Lattice parameters**	**Atomic Coordinates**			**B_{iso}**	**Occupancy**
			X	**Y**	**Z**		
Pb	Pb+2	a= b=5.7550 Å c=7.0495 Å γ=89.86°	0	0	0	2.14718	0.92*1/6=0.1533
La	La+3		0	0	0	2.14718	0.08*1/6=0.0133
Zr	Zr+4		0.5	0.5	0.45625	0.0258	0.60*1/6=0.1000
Ti	Ti+4		0.5	0.5	0.45625	0.0258	0.40*1/6=0.0666
O	O-2		0.5125	0.5125	0.03878	0.0258	3.00*1/2=0.5

Table-8.3 *Approximate initial values of important parameters for monoclinic symmetry with P1m1 space group, which were used for Rietveld refinement.*

Atom	**Valance state**	**Lattice parameters**	**Atomic Coordinates**			**B_{iso}**	**Occupancy**
			X	**Y**	**Z**		
Pb	Pb+2	a= 5.7739Å b=5.7652 Å c=4.0559 Å β=89.86°	0	0	0	2.14718	0.92*2/4=0.460
La	La+3		0	0	0	2.14718	0.08*2/4=0.04
Zr	Zr+4		0.495	0.5	0.4951	0.26392	0.60*2/4=0.30
Ti	Ti+4		0.495	0.5	0.4951	0.26392	0.40*2/4=0.20
O_1	O-2		0.495	0.0	0.4951	0.36392	1.0*2/4=0.50
O_2	O-2		0.495	0.50	0.0125	0.36392	1.0*2/4=0.50
O_3	O-2		0.125	0.50	0.4950	0.45865	2.0*2/4=1.00

Table-8.4 *Approximate initial values of important parameters for monoclinic symmetry with C1m1space group, which were used for Rietveld refinement.*

Atom	Valance state	Lattice parameters	Atomic Coordinates			B_{iso}	Occupancy
			X	Y	Z		
Pb	Pb+2	a= 5.7739Å b=5.7652 Å c=4.0559 Å β=90.17°	0	0	0	2.14718	0.92*2/4=0.460
La	La+3		0	0	0	2.14718	0.08*2/4=0.040
Zr	Zr+4		0.495	0	0.495	0.26392	0.60*2/4=0.300
Ti	Ti+4		0.495	0	0.495	0.26392	0.40*2/4=0.200
O_1	O-2		0.495	0	0.200	0.36392	1.00*2/4=0.500
O_2	O-2		0.255	0	0.4750	0.76392	2.00*2/4=1.000

Table-8.5 *Approximate initial values of important parameters for cubic symmetry with $Pm\bar{3}m$ space group, which were used for Rietveld refinement.*

Atom	Valance state	Lattice parameters	Atomic Coordinates			B_{iso}	Occupancy
			X	Y	Z		
Pb	Pb+2	a=b=c=4.0766 Å	0	0	0	3.14718	0.92*1/8=0.115
La	La+3		0	0	0	3.14718	0.08*1/8=0.010
Zr	Zr+4		0.5	0.5	0.5	0.8258	0.60*1/8=0.075
Ti	Ti+4		0.5	0.5	0.5	0.8258	0.40*1/8=0.050
O	O-2		0.5	0.5	0	4.0258	3.00*1/8=0.375

Figs. 8.7 (a) to (f) shows the Rietveld refinement for XRD data and fitting of tetragonal (P4mm), monoclinic (Cm), monoclinic (Pm), tetragonal+rhombohedral (P4mm+R3m), tetragonal+monoclinic (P4mm+Cm) and cubic ($Pm\bar{3}m$) crystal symmetries respectively. Figs. 8.7 (a) to (e) refinements were done for room temperature XRD data (30°C). However, cubic fitting was used at high temperature (>200°C), after crossing the transition temperature.

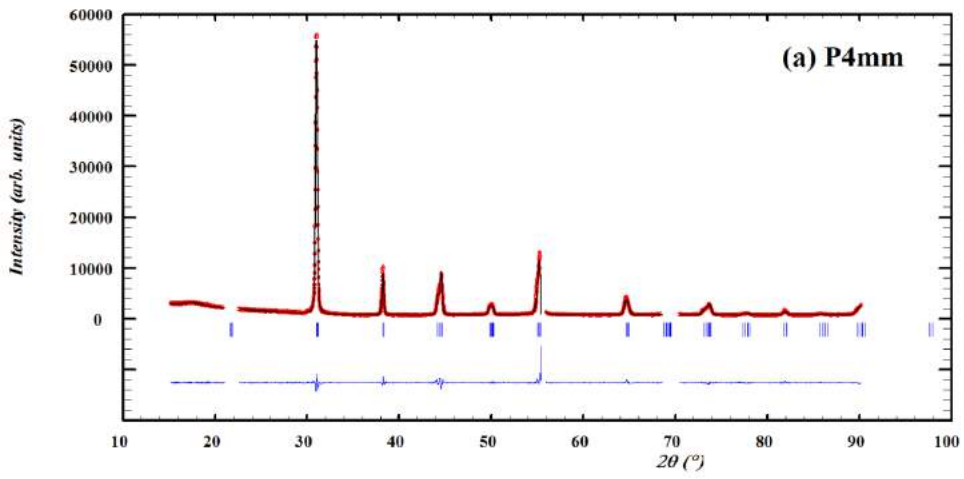

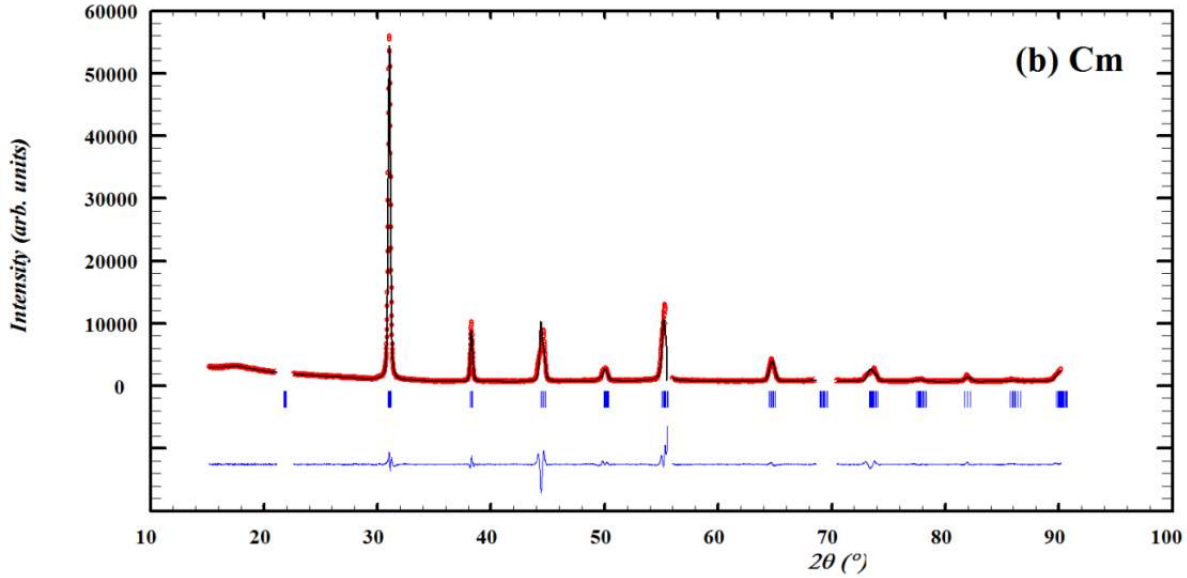
(b) Cm
Intensity (arb. units)
2θ (°)

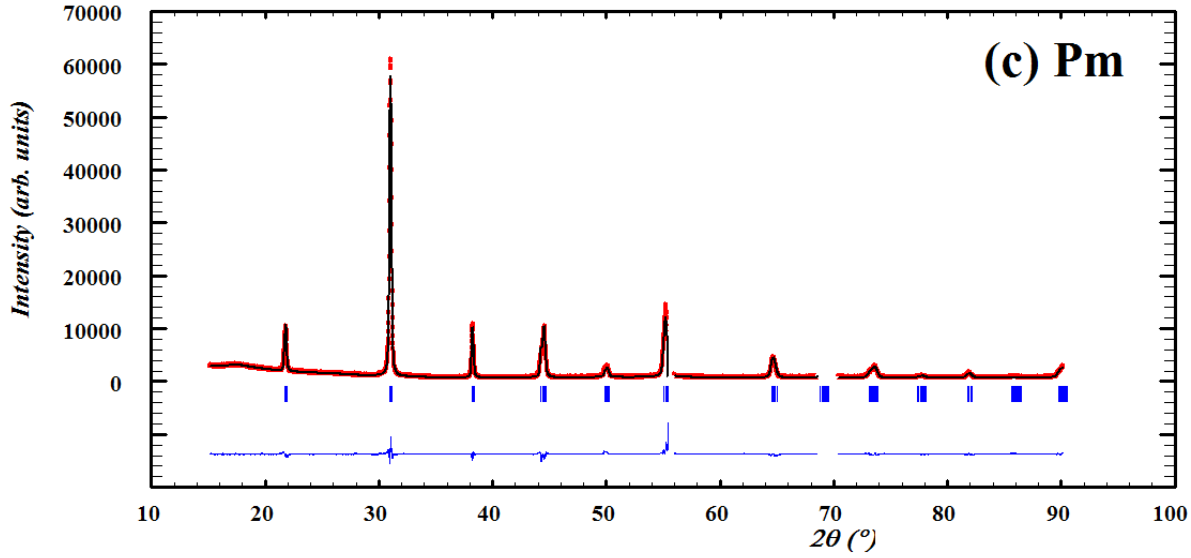
(c) Pm
Intensity (arb. units)
2θ (°)

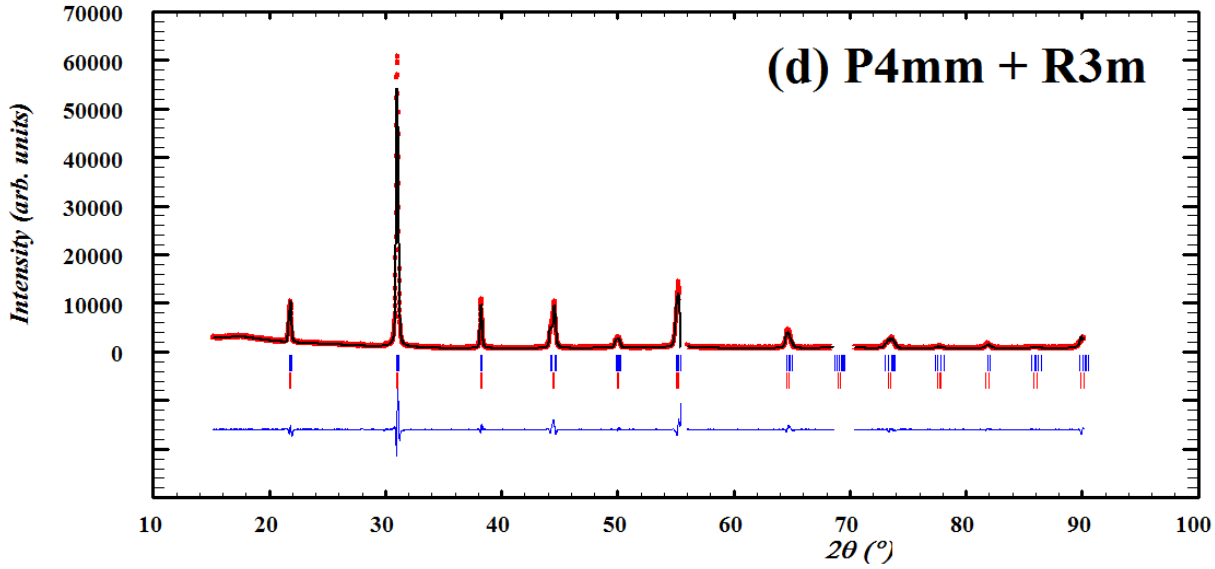
(d) P4mm + R3m
Intensity (arb. units)
2θ (°)

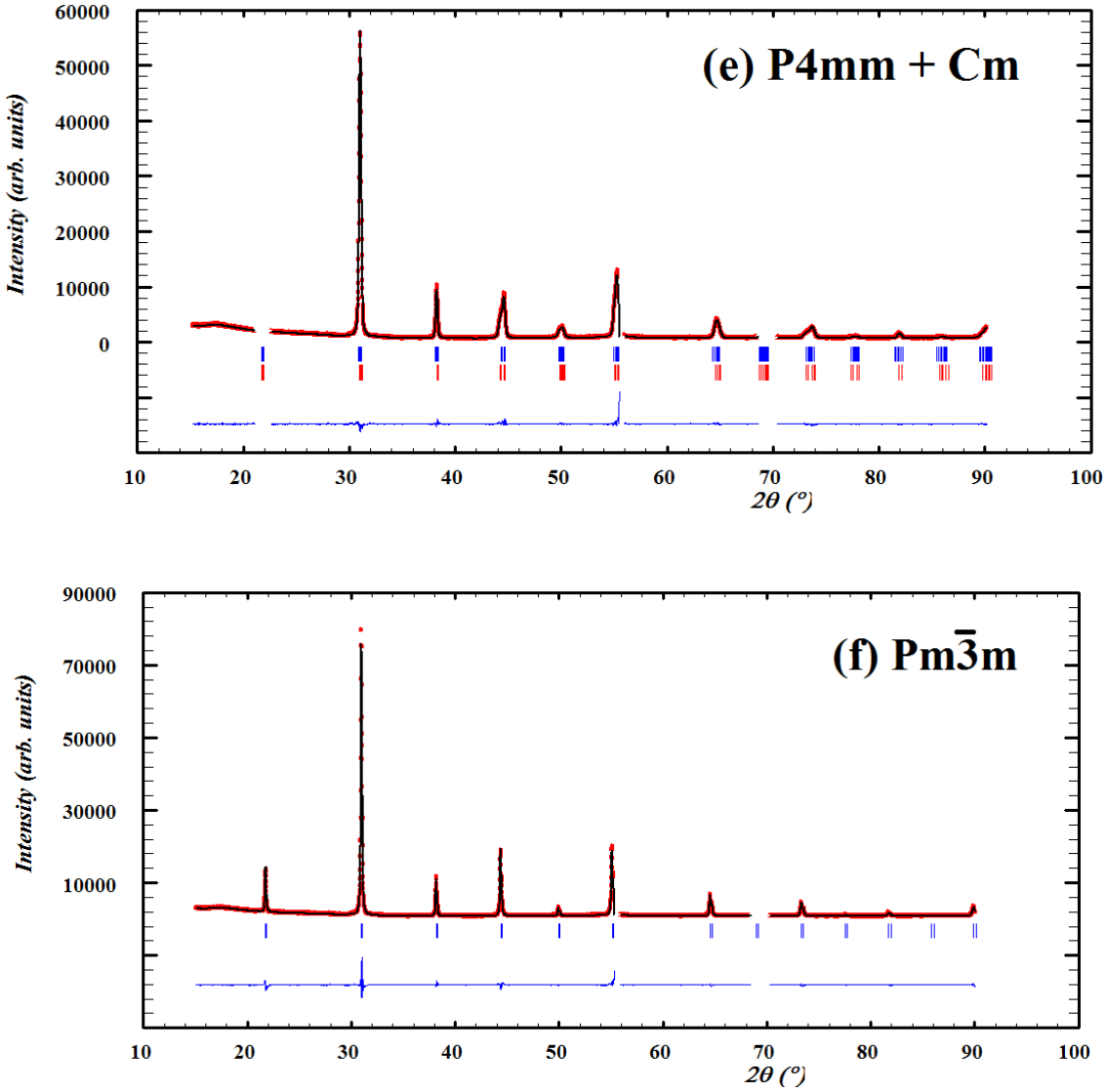

Fig. 8.7 *Rietveld refinement of PLZT 8/60/40 ceramics using (a) P4mm, (b) Cm, (c) Pm, (d) P4mm+R3m, (e) P4mm+Cm and (f) Pm$\bar{3}$m crystal structure. Pm$\bar{3}$m refinement was done for high temperature XRD data.*

Figs. 8.8 (a) to (e) shows the fitting for (200) peak using tetragonal (P4mm), monoclinic (Cm), monoclinic (Pm), tetragonal+rhombohedral (P4mm+R3m), tetragonal+monoclinic (P4mm+Cm). All above fitting was done using room temperature XRD data. However, cubic (Pm$\bar{3}$m) crystal symmetry was used for the refinement of high temperature XRD data. It is clear that the P4mm+Cm fitting at room temperature shows the best fitting (Fig. 8.8 (e)). After transition temperature Pm$\bar{3}$m symmetry fitted well for the PLZT 8/60/40 ceramics. Hence from room temperature to transition temperature, Rietveld refinement was done by using the two phase (P4mm+Cm) symmetries and the results are given in Table-8.5. The refinement results for the cubic structure are given in Tables-8.6 and 8.7.

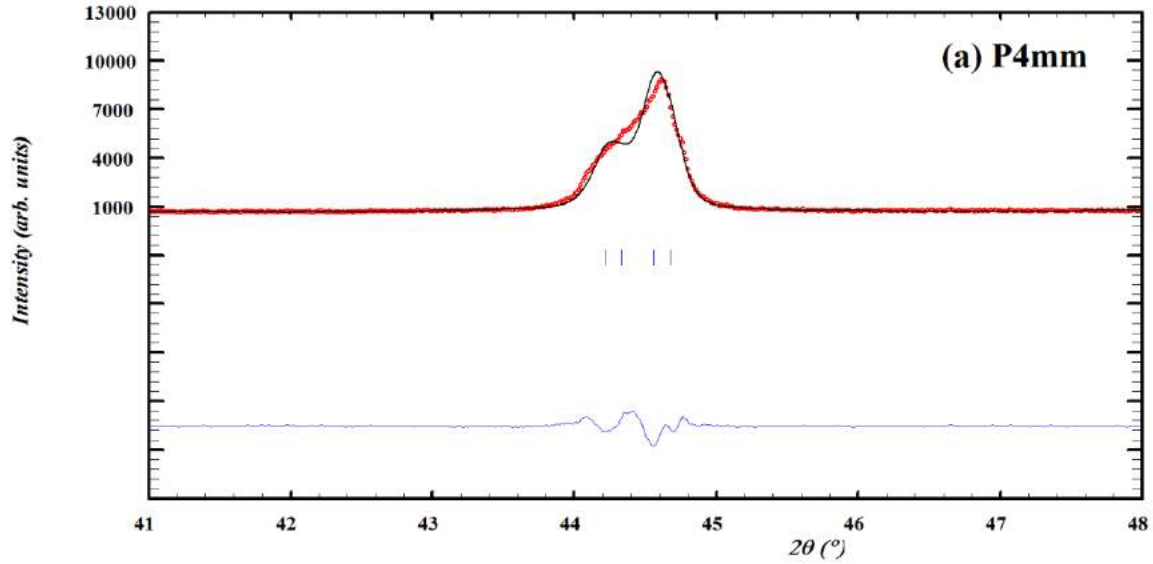
(a) P4mm
Intensity (arb. units)
13000
10000
7000
4000
1000
41
42
43
44
45
46
47
48
2θ (°)

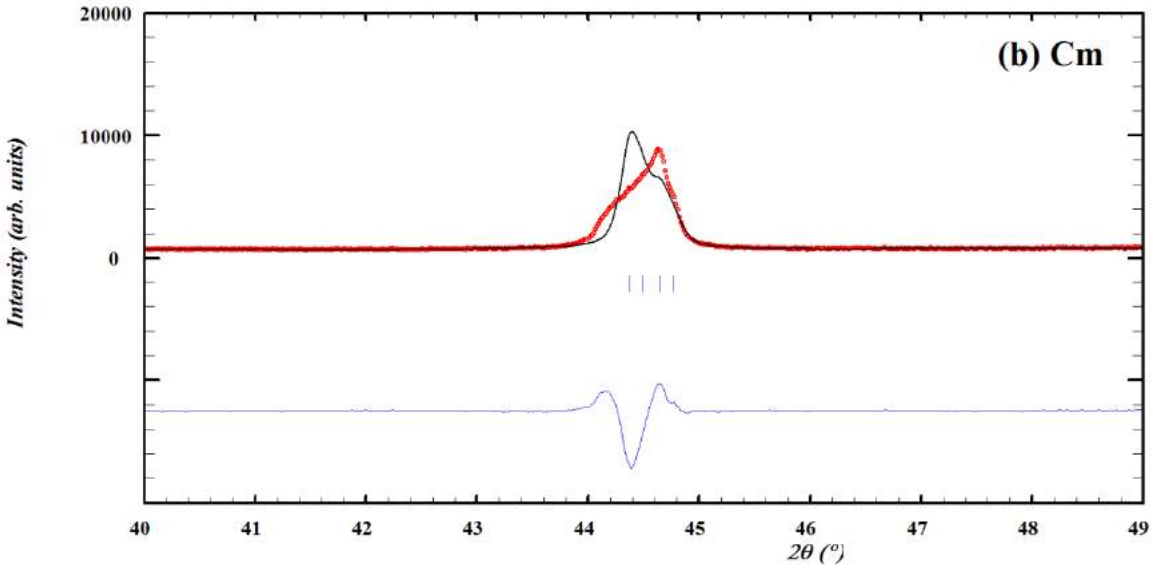
(b) Cm
Intensity (arb. units)
20000
10000
0
40
41
42
43
44
45
46
47
48
49
2θ (°)

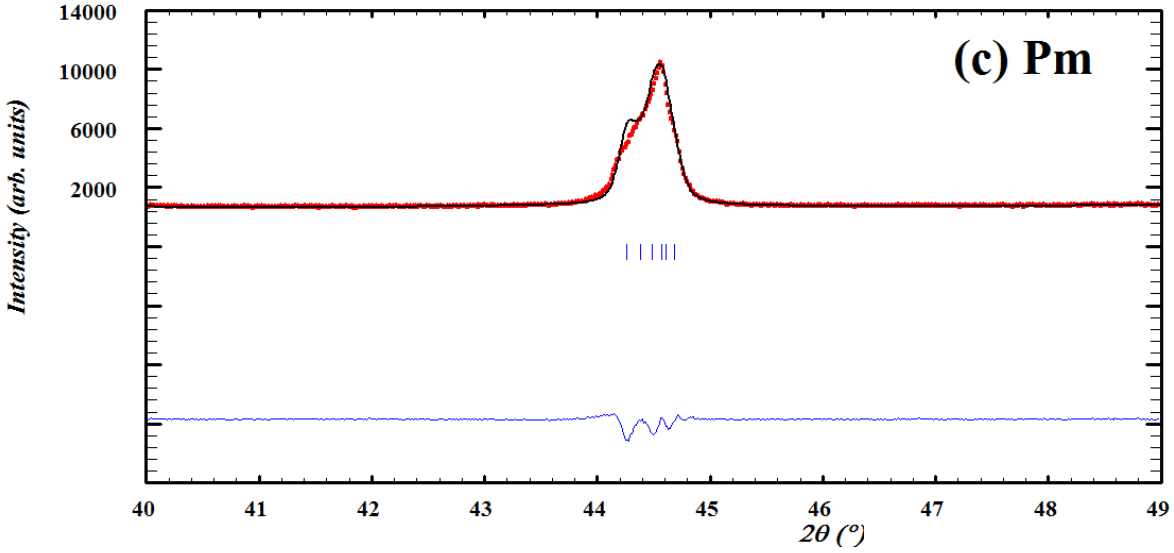
(c) Pm
Intensity (arb. units)
14000
10000
6000
2000
40
41
42
43
44
45
46
47
48
49
2θ (°)

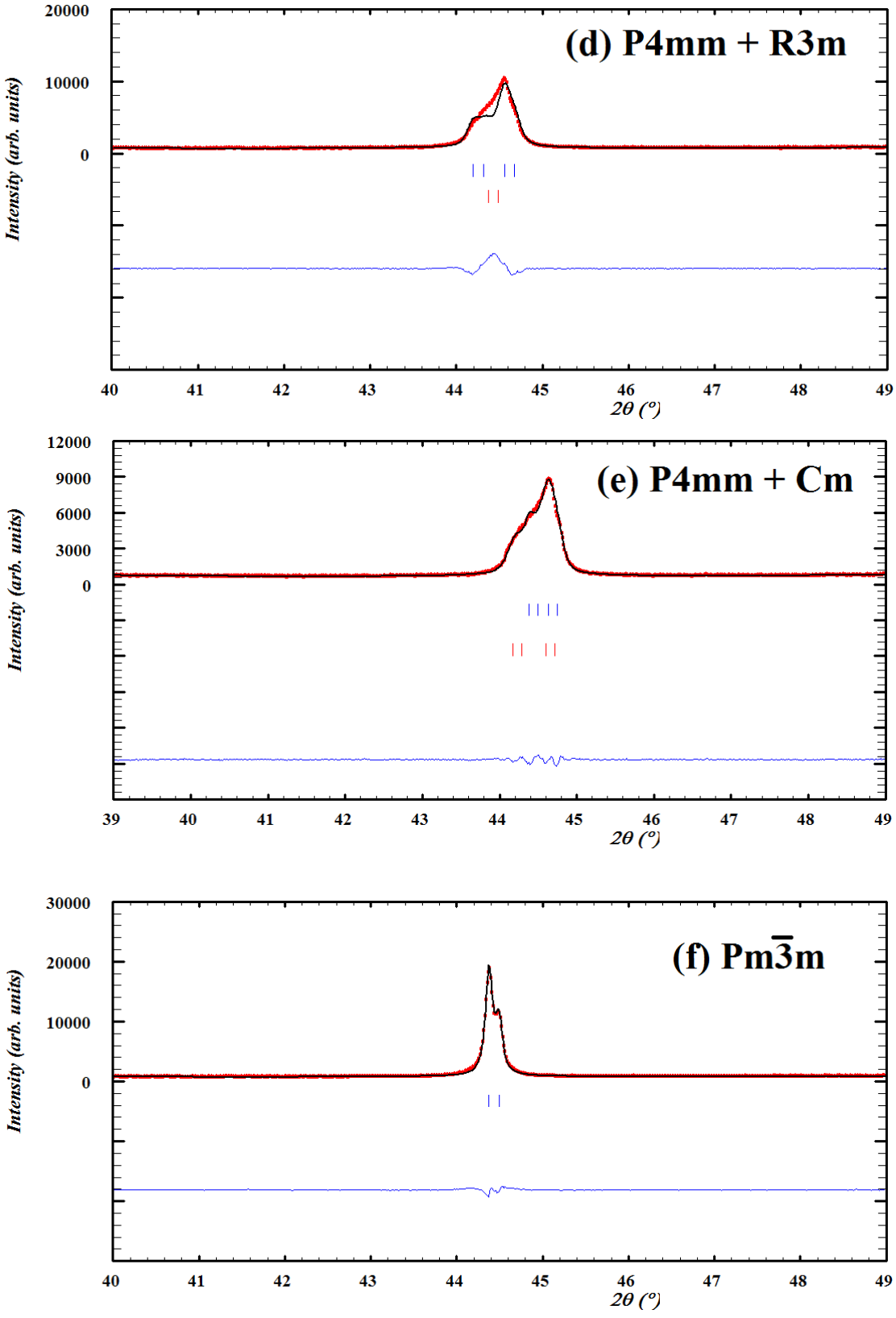

Fig. 8.8 *Rietveld refinement fitting for (200) peak of PLZT 8/60/40 ceramics using (a) P4mm, (b) Cm, (c) Pm, (d) P4mm+R3m, (e) P4mm+Cm and (f) Pm$\bar{3}$m crystal structure. Pm$\bar{3}$m refinement was done for high temperature XRD data.*

Table-8.6 *Rietveld refinement results of PLZT ceramics with tetragonal and monoclinic fitting (30°C to 175°C).*

		a (Å)	b (Å)	c (Å)	β (°)	Phase (%)	Volume (Å)^3	χ^2
30°C	Monoclinic	5.7752	5.7612	4.0574	89.899	31.42	135.0001	2.669
	Tetragonal	4.0602	4.0602	4.0970		68.58	67.5394	
50°C	Monoclinic	5.7752	5.7612	4.0574	89.899	31.42	134.9986	2.120
	Tetragonal	4.0602	4.0602	4.0970		68.58	67.5396	
75°C	Monoclinic	5.7734	5.7629	4.0610	89.898	26.59	135.1141	2.165
	Tetragonal	4.0630	4.0630	4.0947		73.41	67.5957	
100°C	Monoclinic	5.7717	5.7632	4.0633	89.915	22.93	135.1588	2.279
	Tetragonal	4.0647	4.0647	4.0925		77.07	67.6150	
125°C	Monoclinic	5.7697	5.7633	4.0655	89.935	17.23	135.1891	2.583
	Tetragonal	4.0666	4.0666	4.0900		82.77	67.6378	
150°C	Monoclinic	5.7684	5.7613	4.0678	89.951	25.80	135.1867	3.115
	Tetragonal	4.0675	4.0675	4.0872		74.20	67.6209	
175°C	Monoclinic	5.7632	5.7662	4.0719	90.063	14.15	135.3147	4.682
	Tetragonal	4.0718	4.0718	4.0857		85.85	67.7366	

Table-8.7 *Rietveld refinement results of PLZT ceramics with cubic fitting (200°C to 350°C).*

	a (Å)	Volume (Å)^3	χ^2
200°C	4.07662	67.749	4.05
225°C	4.07709	67.772	3.70
250°C	4.07772	67.804	3.56
275°C	4.07836	67.835	3.50
300°C	4.07898	67.867	3.27
325°C	4.07973	67.904	3.06
350°C	4.08049	67.942	3.41

Figs. 8.9 and 8.10 show the change in lattice parameters, the volume of the unit cell, phase fractions and pseudo monoclinic angle as a function of temperature. For tetragonal structure lattice parameter, 'a' is increasing and 'c' is decreasing with an increase in temperature. The volume of the tetragonal, monoclinic and cubic unit cells shows an increase with temperature. The pseudo monoclinic lattice parameters 'a_{pm}' and 'c_{pm}' were calculated from the relations

$$\boldsymbol{a_{pm}} = \frac{\boldsymbol{a_m}}{\sqrt{\boldsymbol{2}}}, \qquad \boldsymbol{c_{pm}} = \frac{\boldsymbol{c_m}}{\sqrt{\boldsymbol{2}}} \quad \text{..... (2)}$$

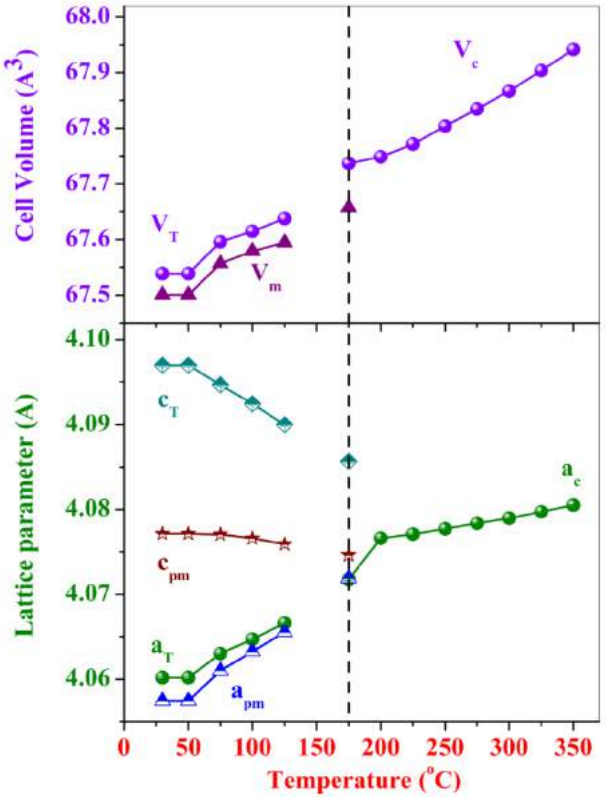

Fig. 8.9 *Change in lattice parameters and volume of PLZT unit cell as a function of temperature for tetragonal and monoclinic phase and a cubic phase.*

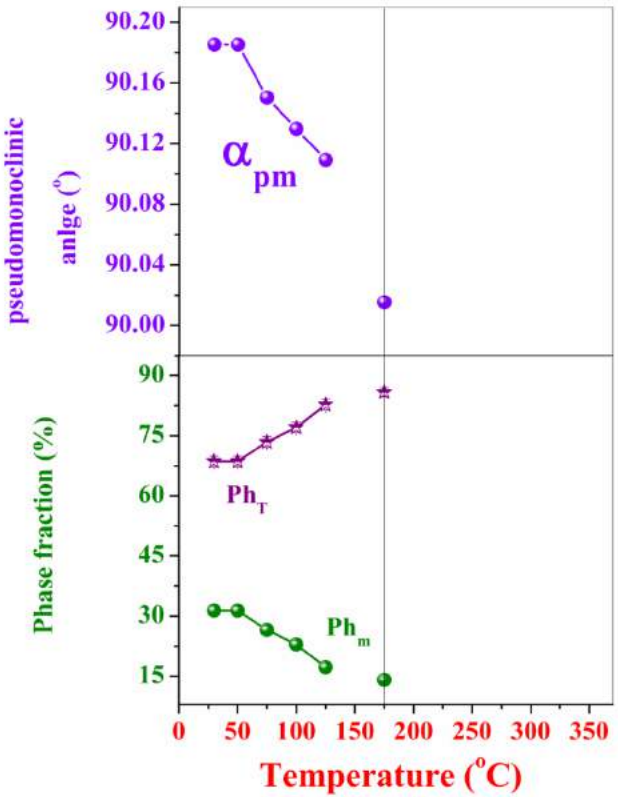

Fig. 8.10 *Change in phase fractions (%) and pseudo monoclinic angle as a function of temperature.*

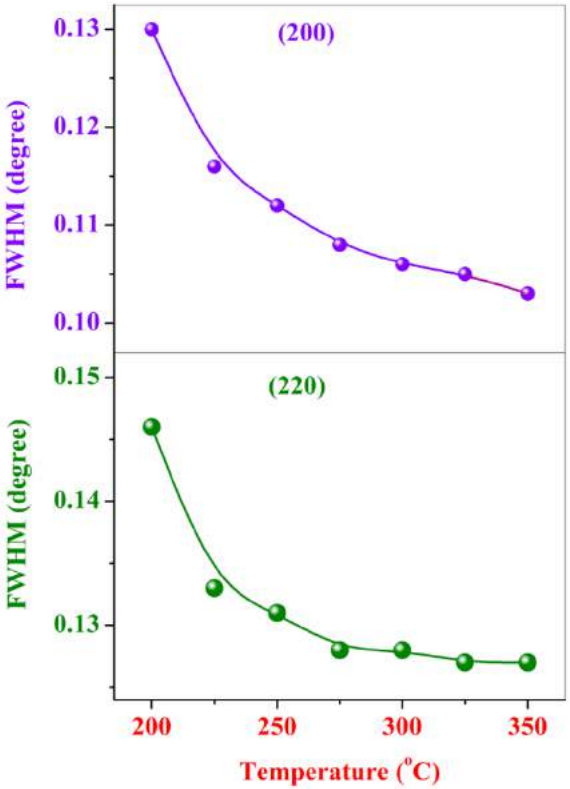

Fig. 8.11 *Change in Full Width at Half Maxima for (200) and (220) peak as a function of temperature for cubic structure.*

The pseudo monoclinic angle also shows a decrease with temperature. The decrease in monoclinic phase and an increase in tetragonal phase with increasing temperature show that the structural transformation follows a low symmetry to high symmetry path as seen in fig. 8.10, where the monoclinic phase fraction is decreasing at the cost of tetragonal phase. Fig. 8.11 shows a decrease in Full Width at Half Maxima for (200) and (220) peak as a function of temperature for cubic structure. When the temperature increases diffraction, peaks become very sharp. When the PLZT ceramics are subjected to high temperature, lattice defects and strains in the materials reduce with increase in temperature. It shows a lattice relaxation which leads to an increase in the volume of the unit cell. Here we also have seen that the lattice parameters of PLZT ceramics increased with temperature. Materials become more and more defect free and strains reduce at high temperatures.

Fig. 8.12 shows the crystal structure for the PLZT ceramics after Rietveld refinement. FP Studio software was used for the same. The refined parameters were used as an input file for FP studio to draw the crystal structure. Figs. 8.12 (a) and (b) show the room temperature crystal structure for single phase tetragonal and double phase tetragonal + monoclinic structure. Fig. 8.12 (c) shows a cubic structure after phase transition.

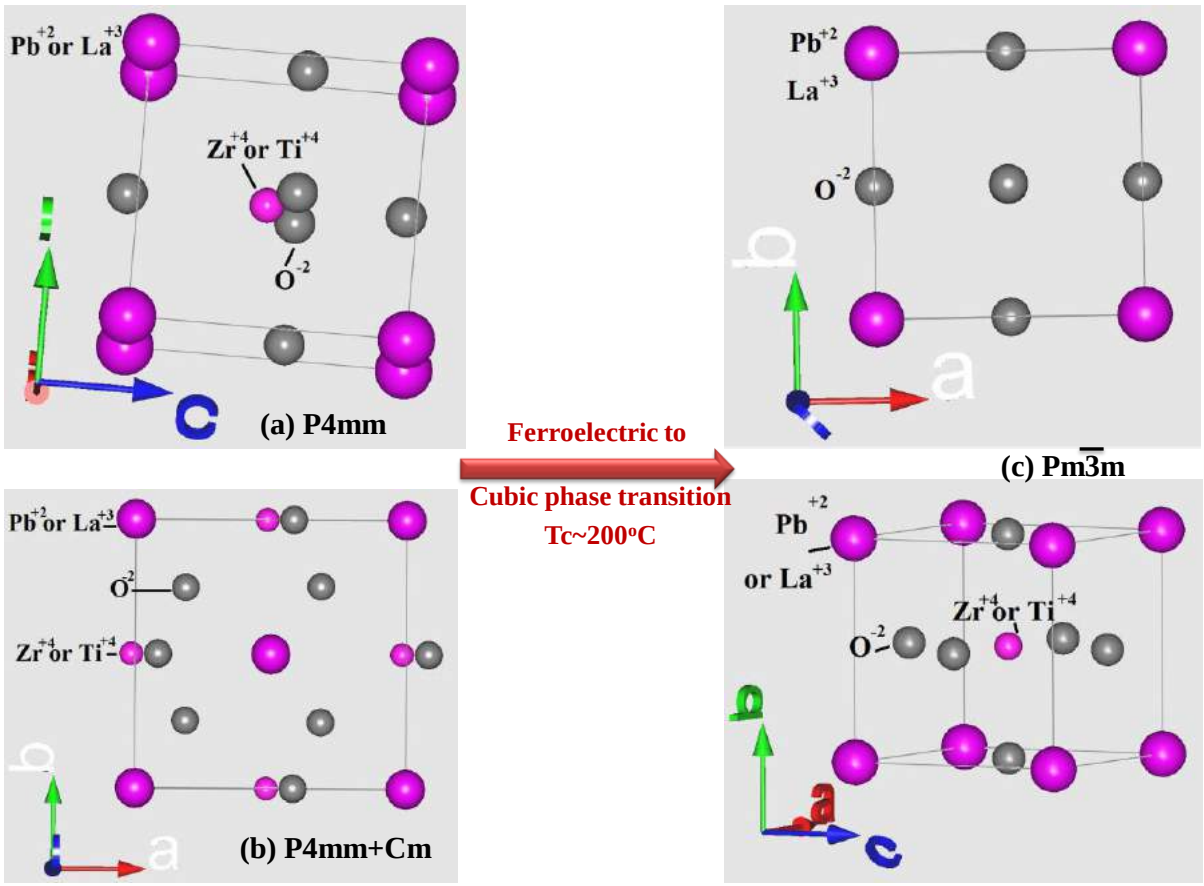

Fig. 8.12 *Crystal structure of PLZT ceramics having (a) P4mm (b) P4mm+Cm and (c) Pm$\bar{3}$m symmetries.*

In the previous section 8.5, the co-existence of the monoclinic phase along with the tetragonal phase was discovered at the MPB of PLZT ceramics. Hitherto this was also discovered in PZT ceramics. From the time of discovery of PZT ceramics, the high electrical properties of PZT ceramics have been the centre of considerable debate. Many researchers have tried to explain the above properties based on micro-structural point of view. However, the discovery of low symmetry phase at the MPB of PZT ceramics gave more comprehensive details to understand the origin of high piezoelectric and ferroelectric properties. Based on the above crystallographic studies the enhanced properties of PZT ceramics are successfully explained. In this work, we have studied PLZT ceramics, which was prepared by La substitution at the A-site of PZT ceramics. PLZT ceramics show the ultra high ferroelectric and piezoelectric properties, multiple times that of PZT ceramics. Micro-structural studies were done (Chapter-3) and were also correlated with the above properties. However, it was felt that the MPB of PLZT ceramics should be explored from a crystallographic perspective as in the case of PZT ceramics. The detailed crystallographic studies helped to discover the monoclinic phase at MPB of PLZT ceramics, which is believed to be the reason for enhanced properties. As discussed in section 8.3, two models, polarization rotation and adaptive phase model explained the importance of the existence of monoclinic phase at MPB.

At first the effect of the monoclinic phase on the dielectric properties of PLZT 8/60/40 ceramics, which shows the high dielectric constant of ~2335, measured at room temperature, will be discussed here. The good density and the improved microstructure of PLZT 8/60/40 ceramics are the reason behind the high value of dielectric constant. However, the monoclinic phase plays a key role, when the ceramics are under the influence of an electric field. It was found that different electro-ceramics show a change in their dielectric constant after the poling process. The increase and decrease in the dielectric constant again depend upon the phase of the ceramics. The same ceramic materials with different phases show different changes in dielectric constant. Here MPB also plays an important role. The effect of the poling electric field on the dielectric properties of PLZT 8/60/40 ceramics has been discussed in Chapter-6. In the case of PLZT 8/60/40 ceramics, which is close to the MPB, the dielectric constant shows an increase after poling. There are some reports for the PZT **[49-51]** and BSPT **[52-53]** compositions which are close to the MPB, show an increase in dielectric constant after poling. Lalitha et al. **[27]** studied the effect of electric field on BSPT ceramics in four cases, that is ceramics having (a) tetragonal structure which is far away from the MPB, (b) tetragonal structure which is close to the MPB, (c) monoclinic structure at the MPB and (d) and monoclinic structure close to the MPB. It was found that the relative permittivity decreased after poling for a tetragonal composition far away from the MPB. However, for tetragonal compositions, which are close to the MPB, an increase in the relative permittivity after poling was found. The BSPT compositions with the monoclinic structure at MPB also show an increase in relative permittivity after poling (maximum change in dielectric constant). The monoclinic composition just outside of the MPB also exhibits an increase in relative permittivity after poling (less change in dielectric constant compared to MPB composition). For the PLZT 8/60/40 ceramics, which is close to the MPB, an increase in relative permittivity was found after

poling **[37, 54]**. The possible adaptive nature of monoclinic Cm phase in PZT arises due to the nanodomains of rhombohedral (R3m) phase **[55]**. However, within the MPB range of PZT, the nanodomains were reported to be stable under an electric field. Hinterstein et. al. **[40]** has reported that an electric field increases the monoclinic fraction in soft PZT ceramics. If the rhombohedral nanodomains are responsible for the monoclinic phase, after poling an increase in the volume fraction of rhombohedral nanodomains leads to an increase in monoclinic phase fraction. The increase in permittivity of the poled MPB compositions can correspondingly be attributed to this increase in the nanodomain volume fraction. The formation of monoclinic phase and the flattening of the energy landscapes, both are mutually related phenomena **[34]**. The drastic reduction in the domain wall formation energy due to a flattened energy landscape causes the miniaturization of the domains leading to an enhanced extrinsic contribution to the dielectric and piezoelectric effect **[23, 56]**. At equilibrium, the monoclinic phase was formed due to nanodomains. The polarization correlation length is related to the two phenomena: (i) field induced phase transformation and (ii) growth of the ferroelectric domains.

The above discussions also help to unravel the microscopic mechanisms associated with the anomalous piezoelectric response in MPB ferroelectric systems for La-modified soft PZT. As previously discussed, the mechanism of enhanced piezo-response in MPB systems is explained by two competing theories, (i) polarization rotation model and (ii) adaptive phase model. The polarization rotation theory proposes low symmetry (monoclinic/triclinic) distortions of the perovskite cell which allows continuous pathway(s) for the rotation of the polarization vector on the application of electric field. In a generalized phenomenological framework, the rotation pathway is determined by the nature of anisotropic flattening of the free energy profile **[28, 57]**. The adaptive phase theory, on the other hand, argues that the additional scattering in diffraction patterns attributed to monoclinic distortion of the unit cell, which can as well arise from coherent scattering by suitably oriented nano-sized twinned regions of the high symmetry tetragonal or rhombohedral parent phase. As per this model, the higher piezo-response arises due to the easy motion of low-energy domain walls on the application of external stress or electric field.

The ferroelectrics show polarization and strain hysteresis under the application of electric field. The ferroelectrics at MPB, which has two degenerate ferroelectric phases, show hysteresis not only due to irreversible domain alignment (which is the case in a single phase ferroelectric material), but also due to one phase transforming to the other under the influence of an electric field and its incomplete recovery after switching off of the field. That is, the remnant strain/polarization would also be associated with the remnant irreversibly transformed phase. This offers a great scope to unravel the nature of electric field driven transformation pathways in MPB systems by comparing the structural states of specimens before and after application of electric field, i.e. by ex-situ diffraction experiments. Structural analysis using very high resolution X-ray powder diffraction data revealed the intrinsic mechanism to be a polarization rotation and polarization extension. The anomalous piezoelectric response in this system is therefore associated with the coupled phenomenon of (i) polarization-rotation-polarization-extension operating on the atomic

length scale and (ii) domain miniaturization on a coarser nano-length scale. The electric field driven structural changes in the PLZT 8/60/40 ceramics are discussed in detail and from results, it is evident that after poling, *c*-parameter of the tetragonal phase increases by ~0.15% and the *a*-parameter decreases by ~0.09%. The tetragonal strain ((*c/a)*-1) in PLZT ceramics was increased from ~0.80 from unpoled state to ~1.04 poled state (~ 30%). Since tetragonal strain scales as the square of polarization, hence the magnitude of polarization of the tetragonal phase increases remarkably. The unit cell volumes of tetragonal and monoclinic phase are nearly preserved after poling. The electric field not only changes in the cell dimensions but also irreversibly decreased the fraction of the tetragonal phase from 32% to 18% (~16%). A decrease in the tetragonal fraction by ~15% also reported by Hinterstein et. al. **[40]** for a similar system. The increase in the monoclinic phase fraction may be interpreted as the tendency of the polarization vector to rotate away from the [001]c pseudocubic direction in the $(1\bar{1}0)$c plane. The electric field not only rotates the polarization vector but also increases its magnitude in the tetragonal phase. The polarization rotation and extension phenomenon are responsible for the high piezo-response in electro-ceramics **[30]**. All of these results can be attributed to the high piezoelectric and ferroelectric properties of PLZT 8/60/40 ceramics.

8.6 Summary

PLZT 8/60/40 ceramics, which were prepared by mechanical activation and cold isostatic pressing show the best electrical properties. These can be attributed to the improved microstructure of the ceramics. However, to give the more detail about the origin of these ultra-high electrical parameters such as high stain and piezoelectric properties, XRD patterns of PLZT 8/60/40 ceramics were studied with the help of Rietveld refinement. XRD patterns were recorded from room temperature to higher temperatures with an interval of 25^{o}C. Rietveld refinement of these XRD patterns helped to found the existence of monoclinic phase along with tetragonal phase for the PLZT 8/60/40 ceramics, which is close to the MPB. The presence of monoclinic phase helps the rotation of polarization vector along the easy axis and is believed to be the origin of ultra-high electrical properties. The monoclinic phase along with the tetragonal phase is responsible for the high remnant polarization, strain, piezoelectric charge coefficient and electromechanical coupling factor with low coercive field and low strain hysteresis loss.

References

[1] B. Jaffe, J. Am. Ceram. Soc., **41 [11]** (1958) 494.

[2] G.H. Haertling, J. Am. Ceram., **82** (1999) 797.

[3] B. Jaffe, W. R. Cook Jr., and H. Jaffe, Piezoelectric Ceramics, Academic Press, London, U.K. and New York (1971).

[4] D.L. Corker, A.M. Glazer, J. Dec, K. Roleder and R. Whatmore, Acta Crystallogr. B, **53** (1997) 135.

[5] A.M. Glazer and S.A. Mabud, Acta Crystallogr. B, **34** (1978) 1065.

[6] A.K. Singh, D. Pandey, S. Yoon, S. Baik and N. Shin, Appl. Phys. Lett., **91** (2007) 192904.

[7] B. Noheda, D.E. Cox, G. Shirane, J.A. Gonzalo, L.E. Cross and S.E. Park, Appl. Phys. Lett., **74** (1999) 2059.

[8] B. Noheda, J.A. Gonzalo, L.E. Cross, R. Guo, S.E. Park, D.E. Cox and G. Shirane, Phys. Rev. B, **61** (2000) 8687.

[9] B. Noheda, D.E. Cox, G. Shirane, R. Guo, B. Jones and L.E. Cross, Phys. Rev. B, **63** (2001) 014103.

[10] B. Noheda, D.E. Cox, G. Shirane, J. Gao and Z.G. Ye, Phys. Rev. B, **66** (2002) 054104.

[11] B. Noheda, D.E. Cox, G. Shirane, S.E. Park, L.E. Cross and Z. Zhong, Phys. Rev. Lett., **86** (2001) 3891.

[12] J. Frantti, S. Ivanov, S. Eriksson, H. Rundlof, V. Lantto, J. Lappalainen and M. Kakihana, Phys. Rev. B, **66** (2002) 064108.

[13] V.Y. Topolev and A.V. Turik, J. Phys.: Condens. Matter, **13** (2001) 771.

[14] R. Guo, L.E. Cross, S.E. Park, B. Noheda, D.E. Cox and G. Shirane, Phys. Rev. Lett., **84 [23]** (2000) 5422.

[15] N. Zhang, H. Yokota, A.M. Glazer, Z. Ren, D.A. Keen, D.S. Keeble, P.A. Thomas and Z.G. Ye, Nature Communications, **5** (2014) 5231.

[16] H. Yokota, N. Zhang, A.E. Taylor, P.A. Thomas and A.M. Glazer, Phys. Rev. B, **80** (2009) 104109.

[17] S.E. Park and T.R Shrout, J. Appl. Phys., **82** (1997) 1804.

[18] J. Kuwata, K. Uchino and S. Nomura, Japan. J. Appl. Phys., **21** (1982) 1298.

[19] R.E. Eitel, C.A. Randall, T.R. Shrout, P.W. Rehrig, W. Hackenberger and S.E. Park, Japan. J. Appl. Phys., (2001).

[20] H. Fu and R.E. Cohen, Nature, **403** (2000) 281.

[21] D.E. Cox, B. Noheda, G. Shirane, Y. Uesu, K. Fujishiro and Y. Yamada, Appl. Phys. Lett., **79** (2001) 400.

[22] L. Bellaiche, A. Garcia and D. Vanderbilt, Phys. Rev. Lett., **63** (2001) 094108.

[23] Y.M. Jin, Y.U. Wang, A.G. Khachaturyan, J.F. Li and D. Viehland, Phys. Rev. Lett., **91** (2000) 197601.

[24] Y.M. Jin, Y.U. Wang, A.G. Khachaturyan, J.F. Li and D. Viehland, J. Appl. Phys. **94** (2003) 3629.

[25] Y.U. Wang, Phys. Rev. B, **76** (2007) 024108.

[26] D. Vanderbilt and M.H. Cohen, Phys. Rev. B, **63** (2001) 094108.

[27] K.V. Lalitha, A.K. Kalyani and R. Ranjan, Phys. Rev. B, **90** (2014) 224107.

[28] D. Damjanovic, J. Am. Ceram. Soc., **88** (2005) 2663.

[29] M.J. Haun, E. Furman, S.J. Jang and L.E. Cross, Ferroelectrics, **99 (**1989) 63.

[30] D. Damjanovic, Appl. Phys. Lett., **97** (2010) 062906.

[31] L. Bellaiche, A. Garcıa and D. Vanderbilt, Phys. Rev. B, **64** (2001) 060103.

[32] M. Budimir, D. Damjanovic and N. Setter, J. Appl. Phys., **94** (2003) 6753.

[33] M. Davis, M. Budimir, D. Damjanovic and N. Setter, J. Appl. Phys., **101** (2007) 054112.

[34] M. Davis, D. Damjanovic and N. Setter, Phys. Rev. B, **73** (2006) 014115.

[35] A.J. Bell, J. Appl. Phys., **89** (2001) 3907.

[36] B. Noheda, Curr. Opin. Solid State Mater. Sci., **6** (2002) 27.

[37] A.K. Kalyani, Electric field driven structural transformations in BaTiO3 and lead zirconate titanate (PZT) based Piezoceramics, Ph. D. Thesis, (2015).

[38] Y.U. Wang, Phys. Rev. B, **76** (2007) 024108.

[39] K.A. Schonau, M. Knapp, H. Kungl, M.J. Hoffmann and H. Fuess, Phys. Rev. B, **76** (2007) 144112.

[40] M. Hinterstein, J. Rouquette, J. Haines, P. Papet, M. Knapp, J. Glaum and H. Fuess, Phys. Rev. Lett., **107** (2011) 077602.

[41] A. Kumar, V.V.B. Prasad, K.C.J. Raju and A.R. James, J. Alloys Comp., **654** (2016) 95.

[42] A. Kumar, V.V.B. Prasad, K.C.J. Raju and A.R. James, J. Mater. Sci.: Mater. Electron., **26** (2015) 3757.

[43] A. Kumar, V.V.B. Prasad, K.C.J. Raju and A.R. James, Euro. Phys. J. B, **88** (2015) 287.

[44] A.R. James, J.P. Praveen, M.P. Kumar and V.V.B. Prasad, Mater. Res. Bul., **47 [11]** (2012) 3459.

[45] A.R. James, R. Kumar, M.P. Kumar, K. Srinivas, V. Radha, M. Vithal and M. Vijayakumar, J. Alloys Comp., **496** (2010) 624.

[46] F. Clemens, T. Comyn, J. Heiber, F. Nobre, A.C.E. Dent and C.R. Bowen, J. Mater. Sci., **46** (2011) 4517.

[47] International Tables for Crystallography, Volume A: Space-Group Symmetry, Editor: Theo Hahn, Reprint (2005).

[48] L.B. McCusker, R.B.V. Dreele, D. E. Cox, D. Louer and P. Scardi**,** J. Appl. Cryst., **32** (1999) 36.

[49] F. Xu, S.T. McKinstry, W. Ren, B. Xu, Z.L. Xie and K.J. Hemker, J. Appl. Phys., **89** (2001) 1336.

[50] J.E. Garcıa, R. Perez, D.A. Ochoa, A. Albareda, M.H. Lente and J.A. Eiras, J. Appl. Phys., **103** (2008) 054108.

[51] V. D. Kugel and L. E. Cross, J. Appl. Phys., **84** (1998) 2815.

[52] G. Tutuncu, D. Damjanovic, J. Chen and J.L. Jones, Phys. Rev. Lett., **108** (2012) 177601.

[53] R.E. Eitel, T.R. Shrout and C.A. Randall, J. Appl. Phys., **99** (2006) 124110.

[54] A.K. Kalyani, K.V. Lalitha, A.R. James, A. Finch and R. Ranjan, J. Phys.: Condens. Matter, **27** (2015) 072201.

[55] K.A. Schonau, M. Knapp, H. Kungl, M.J. Hoffmann and H. Fuess, Phys. Rev. B, **76** (2007) 144112.

[56] B. Noheda and D.E. Cox, Phase Transit., **79** (2006) 5.

[57] M.J. Haun, E. Furman, S.J. Jang and L.E. Cross, Ferroelectrics, **99** (1989) 63.

Chapter-IX

Summary and scope of future work

9.1 Summary

In this chapter, a brief summary of the results, which were obtained from the micro-structural and morphological, dielectric, ferroelectric, piezoelectric, poling as well as phase analyse studies are presented. The main objective of the work, which was discussed in this thesis is (1) To synthesize a material with properties comparable to PMN-PT and (2) To develop a synthesis technique which is inexpensive but at the same time shows properties comparable to the complex hot pressing method. As per these objectives, PZT system was chosen for this study and modified with lanthanum to achieve electrical properties close to the PMN-PT. La substitution was optimized based on different studies as discussed in Chapter-3 to Chapter-8. PLZT ceramics were prepared using high energy mechanical ball milling and cold isostatic pressing at significantly reduced calcination and sintering temperatures and times. In this study the optimized milling time was found to be 5 hours that is very less compared to available reports. Zirconia vials were used to avoid contamination and the results were promising. Another important objective of this study was to find the reason behind the ultra high piezoelectric properties of optimized PLZT ceramics, which was explained on the basis of Rietveld refinement.

The summary of the detailed study of PLZT ceramics is as follows:

In **Chapter-3,** the micro-structural and morphological studies of PLZT ceramics were discussed. It shows that the novel approach of HEM and CIP result in improved microstructure confirmed by density, XRD and SEM. HEM ball milling helps to prepare ceramics without excess PbO, with reduced calcination and sintering temperatures which help in turn to improve the electrical properties. High energy milled PLZT powders show the formation of the partial perovskite phase, which proves that partial chemical reaction took place at milling stage itself. Micro-structural properties of PLZT 8/60/40 HEM milled ceramics are found to be better than PLZT 8/60/40 mortar pestle mixed ceramics. PLZT 8/60/40 ceramics which were milled for 5 hours in zirconia vials have the highest density and best microstructure. Higher density and more uniform grain distributions were found for the optimum PLZT composition. TEM studies were used for the 5 hours milled PLZT 8/60/40 ceramics which show that the particle size of PLZT 8/60/40 milled powders deviates from the spherical shape. The average particle size of milled powders, relative density and grain size of sintered compacts were found to be ~25 nm, 97.23% and ~1.45 μm, respectively.

The temperature dependent dielectric measurements (**Chapter-4**) of PLZT x/60/40 (x=La=0 to 10%) and $(Pb_{0.92}La_{0.08})(Zr_{0.60}Ti_{0.40})O_3$ also known as PLZT 8/60/40 suggest that the La substitution affects the nature of ferroelectric phase transition of PZT. The PLZT Ceramics shows a deviation from normal to the diffuse type phase transition (DPT). This diffuse phase transition for the PLZT ceramics is explained based on many parameters such as the diffuseness parameter (γ), the degree of deviation from Curie-Weiss law (ΔT_m) and empirical parameters (ΔT_{diff}). All the said parameters were calculated at various frequencies from 1 kHz to 500 kHz by using different equations and fitting curves. The large value of diffuseness

parameter (γ) ($1<\gamma<2$) and empirical parameters (ΔT_{diff}) for PLZT ceramics at different frequencies confirms the deviation from normal phase transition and the high degree of disorderliness in the material. The maximum value of dielectric constant ~2336 was found for the 5 hours milled PLZT 8/60/40 ceramics.

In **Chapter-5**, the nature of the PLZT ferroelectric material was studied by using ferroelectric (P-E and S-E) hysteresis loops for (i) different compositions of PLZT ceramics (ii) milling of PLZT 8/60/40 ceramics at different durations. I-E loops were also used for the determination of coercive field. As per the objective, the optimized PLZT 8/60/40 composition, shows the highest P_r ~34 $\mu C/cm^2$, I_{max} ~2.06 mA, unipolar strain ~0.27%, hysteresis loss~3%, an average d_{33} ~712 pC/N and high shape symmetry with low E_c~12 kV/cm, when it was milled for 5 hours in a zirconia vial. Temperature dependent P-E, S-E and I-E loops of PLZT 8/60/40 ceramics show the existence of P_r and I_{max} near the dielectric maxima temperature. This is yet another evidence for the deviation from normal phase transition. The squareness (R_{sq}) of the P-E loops is decreased, the volume fraction of back switching (V_{back}) domains increases as temperature increases. High shape symmetry of P-E loops, low hysteresis loss in P-E as well as S-E loops and high remnant polarization at high temperature suggest that the PLZT 8/60/40 ceramics are promising materials for high temperature applications.

PLZT ceramics were poled by varying the poling conditions to identify the optimum poling parameters (**Chapter-6**). Poling electric field studies suggest that the PLZT ceramics can be poled at ~5 kV/cm while the coercive field is ~12 kV/cm. This shows that the poling of PLZT ceramics at the significantly low electric field could be very advantageous if the samples show low resistivity or high conductivity. The poling temperature range for the PLZT ceramics is from 75^{o}C to 120^{o}C while the T_c is 190^{o}C. The optimum poling time was found to be 30 minutes which is also much less compared to the normally employed time in hours. The ageing study for PLZT ceramics also supports the poling at the lower electric field. The d_{33} and k_p values for PLZT 8/60/40 ceramics, which was measured at optimum poling conditions were found to be ~715 pC/N and ~77 %, respectively.

Piezoelectric studies (**Chapter-7**) of PLZT ceramics show that PLZT 8/60/40 system has highest piezoelectric charge coefficients ($d_{33} \cong 570$ pC/N, $g_{33} \cong 28.03 \times 10^{-3}$ Vm/N) and electromechanical coupling factors ($k_p = k_{33} = 64.13\%$ and $k_{31} = 53.99\%$) when compared with remaining compositions. The PLZT 8/60/40 composition milled for 5 hours with zirconia vials shows an improvement in the electrical properties and also shows the highest piezoelectric charge coefficients ($d_{33} \cong 688$ pC/N, $g_{33} \cong 28.48 \times 10^{-3}$ Vm/N) and electromechanical coupling factors ($k_p = 75.8\%$, $k_{33} = 76.29\%$ and $k_{31} = 60.65\%$). The values of elastic compliances for the optimized PLZT ceramics were also found to be high. The existence of resonance phenomenon (for calculation of k_p) after dielectric maxima temperature for PLZT 8/60/40 ceramics suggests the DPT behavior.

In **Chapter-8**, the origin of ultra high strain and piezoelectric properties of PLZT ceramics are described. XRD pattern of PLZT ceramics was studied with the help of Rietveld refinement at room temperature as well as at higher temperature. The monoclinic phase was discovered at MPB of PLZT ceramics along with tetragonal phase. The presence of a monoclinic phase helps the rotation of the polarization vector along the easy axis and is believed to be the reason for the ultra high electrical properties.

9.2 Scope of future work

The current study deals with the improvement of electrical properties of La^{3+} substituted PZT ceramics. Mechanically activated and cold isostatically pressed PLZT ceramics show ultra high piezo properties. However, there are still more possibilities available for the further improvement of piezo properties by changing the synthesis route from conventional heating to microwave heating. Use of microwave radiation is advantageous in the saving of both time and energy consumption compared with conventional thermal processes. The future work in this field lies in the ability to minimize the problems and difficulties, which usually degrade the properties of lead based materials.

It is also felt that microwave dielectric properties of PLZT ceramics should be measured because broadband dielectric spectroscopy helps to understand the hardening and softening mechanisms of soft and hard PZT ceramics. In the frequency range below 20 GHz, the different contributions to the permittivity by domain wall motion were revealed in hard and soft materials.

The presence of monoclinic phase at MPB of PLZT ceramics, which was found in this study, is believed to be the origin of high piezo response. However, this field is still open for further exploration. The monoclinic phase variation with La substitution at different temperatures may give more information and understanding, which is still lacking since the time of discovery of PZT based ceramics.

In conclusion, it can be said that the PLZT ceramics which were milled for 5 hours in a zirconia vial show the optimum electrical properties. PLZT 8/60/40 system shows an ultra high unipolar strain (~0.27%) with minimal loss, which is the required condition for actuator applications. The high piezoelectric coefficients, as well as high electromechanical coupling factors of PLZT ceramics, are suitable for energy harvesting applications. High temperature ferroelectric studies suggest that PLZT 8/60/40 ceramics are promising materials for the high temperature applications. Such systems can be used for thin film preparation. These thin films have a further use in the miniaturization of the devices such as in MEMS applications.

List of Publications

Papers in International and National Journals:

1. "Ultra high strain properties of lanthanum substituted PZT electro-ceramics prepared via mechanical activation",

Ajeet Kumar, V.V. Bhanu Prasad, K.C. James Raju and A.R. James, J. Alloys and Comp., **599** (2014) 53.

2. "Poling electric field dependent domain switching and piezoelectric properties of mechanically activated $(Pb_{0.92}La_{0.08})(Zr_{0.60}Ti_{0.40})O_3$ ceramics ",

Ajeet Kumar, V.V. Bhanu Prasad, K.C. James Raju and A.R. James, J. Mater. Sci.: Mater. Electro., **26** (2015) 3757-3765.

3. "Optimization of poling parameters of mechanically processed PLZT 8/60/40 ceramics based on dielectric and piezoelectric studies",

Ajeet Kumar, V.V. Bhanu Prasad, K.C. James Raju and A.R. James, The Europ. Phys. J. B, **88** (2015) 287.

4. "Lanthanum induced diffuse phase transition in high energy mechanochemically processed and poled PLZT 8/60/40 ceramics",

Ajeet Kumar, V.V. Bhanu Prasad, K.C. James Raju and A.R. James, J. Alloys and Comp., **654** (2016) 95-102.

5. "Microwave sintering of fine grained PLZT 8/60/40 ceramics prepared via high energy mechanical milling",

Ajeet Kumar, Sivanagi Reddy Emani, V.V. Bhanu Prasad, K.C. James Raju and A.R. James, J. Europ. Ceram. Soc., **36** (2016) 2505-2511.

6. "Effect of lanthanum substitution on the structural, dielectric, ferroelectric and piezoelectric properties of mechanically activated PZT electroceramics",

Ajeet Kumar, V.V. Bhanu Prasad, K.C. James Raju, Rajdeep Sarkar, P. Ghoshal and A.R. James, Defence Science Journal, 66 [4] (2016) 360-367.

Submitted manuscripts in International Journals

7. "Microstructure and piezoelectric properties of mechanically processed $(Pb_{1-x}La_x)(Zr_{0.60}Ti_{0.40})O_3$ ceramics",

Ajeet Kumar, K.C. James Raju and A.R. James, Submitted to Mat. Chem. Phys.

8. "Investigation of diffuse phase transition in $(Pb_{1-x}La_x)(Zr_{0.60}Ti_{0.40})O_3$ ceramics fabricated using high energy mechano-chemical processing",

Ajeet Kumar, K.C. James Raju and A.R. James, Submitted to Mat. Chem. Phys.

9. "Ferroelectric properties of mechanically activated $(Pb_{1-x}La_x)(Zr_{0.60}Ti_{0.40})O_3$ ceramics",

Ajeet Kumar, K.C. James Raju and A.R. James, Submitted to Current Applied Physics.

10. "Temperature dependent ferroelectric and piezoelectric properties of PLZT 8/60/40 ceramics",

Ajeet Kumar, K.C. James Raju and A.R. James, Submitted to Mater. Lett.

Manuscript under preparation

11. "Evidence of monoclinic phase at morphotropic phase boundary of PLZT ceramics and its variation with temperature",

    Ajeet Kumar, K.C. James Raju and A.R. James

12. "Enhanced electrical properties of PLZT 8/60/40 ceramics milled with different vials",

    Ajeet Kumar, K.C. James Raju and A.R. James

13. "Microstructure, Dielectric, Ferroelectric and Piezoelectric properties of mechanically activated PLZT 8/60/40 ceramics prepared with different pressing techniques",

    Ajeet Kumar, K.C. James Raju and A.R. James

List of publications (not a part of the thesis work):

1. "Enhanced Microwave Dielectric Properties of $MgTiO_3$ Ceramics Prepared by Mechanochemical Method",

T. Santhosh Kumar, **Ajeet Kumar**, A.R. James and D. Pamu, J. Austra. Ceram. Soc., **47 [2]** (2011) 44.

2. "Strain-induced structural phase transition and its effect on piezoelectric properties of BZT-BCT-CeO_2 ceramics",

E. Chandrakala, J. Paul Praveen, **Ajeet Kumar**, A.R. James, Dibakar Das, J. Amer. Ceram. Soc., (2016) 1 doi: 10.111/jace:14409.

Papers in International Conference Proceedings

1. "Effect of milling media on structural and electrical properties of PLZT 8/60/40 ceramics prepared by high energy mechanochemical milling",

Ajeet Kumar, J. Paul Praveen, V.V. Bhanu Prasad and A.R. James, ICAM Conference Proceedings, (2011) 71-75.

2. "Dielectric and ferroelectric studies on lead free piezoelectric KNN ceramics",

P. Mahesh, **Ajeet Kumar**, A.R. James, and D. Pamu, AIP Conf. Proc., **62** (2013) 1512.

3. "Structural, vibrational and ferroelectric properties of $BaCaTiSi_2O_8$ ceramics",

S. K. Barbar, M. Roy, **A. Kumar**, and A. R. James, AIP Conf. Proc., **1536** (2013) 983.

4. "Enhanced piezo response in mechanically activated and microwave sintered PLZT 8/60/40 ceramics",

Ajeet Kumar, K.C. James Raju and A.R. James, ISAF conference proceddeings, Submitted.

Technical report:

"Pulsed Laser Deposition (PLD), Structural and Electrical Characterization of Ferroelectric Thin Films,"

A.R. James, M.L.V. Mahesh, **Ajeet Kumar**, V.V. Bhanu Prasad and S.V. Kamat, DRDO-DMRL-CCG-081-2015, February 2015.

Conferences/Workshops

1. **Ajeet Kumar** and A.R. James "Application of PLZT ceramics to develop Sensors and Actuators", National Conference on Sensors and Actuators: Science to Technology, March 11-12, 2011, Central Glass and Ceramic Research Institute, Kolkata. **(Poster presentation)**

2. **Ajeet Kumar**, J. Paul Praveen, V.V. Bhanu Prasad, A.R. James "Effect of milling media on structural and electrical properties of PLZT (8/60/40) Ceramics Prepared by high energy mechanochemical milling", International Conference on Advanced Materials, PSG College, Coimbatore, December 12-16, 2011.

3. **Ajeet Kumar**, V.V. Bhanu Prasad and A.R. James "Influence of high energy mechanochemical parameters on the structural, thermal and electrical properties of ultra high strain PLZT 8/60/40 piezoelectric ceramics", International Conference on Nano Science and Technology (ICONSAT-2012), January 20-23, 2012, ARCI, Hyderabad.

4. "Frontiers in Physics," September 27-29, 2012, School of Physics, University of Hyderabad.

5. Workshop on Machine drawing and machining, November 22-29, 2012, School of Physics, University of Hyderabad.

6. S.K. Barbar, M. Roy, **A. Kumar** and A.R. James, "Structural, vibrational and ferroelectric properties of $BaCaTiSi_2O_8$ ceramics", Recent Trends in Applied Physics and Material Science, Govt. College of Engineering & Technology, Bikaner, February 1-2, 2013. **(Poster presentation)**

7. **Ajeet Kumar**, V.V. Bhanu Prasad, K.C. James Raju and A.R. James, "Influence of lanthanum substitution on the structural and electrical properties of ultra high strain PZT ceramics", International Union of Materials Research Society-International Conference in Asia (IUMRS-ICA 2013), Indian Institute of Science, Bangalore, December 16-20, 2013. **Awarded with the best poster presentation award**

8. **Ajeet Kumar**, V.V. Bhanu Prasad, K.C. James Raju and A.R. James**,** "Microstructural, thermal, dielectric and ferroelectric properties studies for the ultra-high strain mechanical activated PLZT 8/60/40 ceramics"**,** International Conference On Nanomaterials and Technologies (CNT-2014), October 17-18, 2014**,** Vardhaman College of Engineering, Hyderabad.

9. **Ajeet Kumar**, V.V. Bhanu Prasad, K.C. James Raju and A.R. James, "The effect of poling conditions on the domain switching mechanism and piezoelectric properties of PLZT 8/60/40 ceramics prepared via high energy mechanical activation", International Conference on Frontier in Material Processing, Application, Research and

Technology, (FiMPART-2015), June 12-15, 2015, Novotel International Conventional Center, Hyderabad. **(Oral presentation)**

10. Attended a **"**Workshop On "Advanced Nanomaterials: Characterizations and Applications, (WANCA-2015)" 02-08 Nov., 2015, Department of Physics, Banaras Hindu University, Varanasi.

11. **Ajeet Kumar**, V.V. Bhanu Prasad, K.C. James Raju and A.R. James**, "**Preparation of ultra high strain PLZT 8/60/40 electro-ceramics for sensor and actuator applications via mechanical activation"**,** National Conference on Advances in Sensors: Lab to field (Sensors-2016), January 29-30, 2016, RCI, Hyderabad. **(Oral presentation)**

12. **Ajeet Kumar**, V.V. Bhanu Prasad, K.C. James Raju and A.R. James, "Structure-Property Correlations in ultra-high strain PLZT ceramics prepared via high energy mechanical milling", Frontiers in Physics-2016, March 28-29, 2016, School of Physics, University of Hyderabad. **(Poster presentation)**

13. **Ajeet Kumar**, V.V. Bhanu Prasad and A.R. James, "Prepartion of PLZT 8/60/40 thin films for device development", Conference on Emerging Materials (CEMAT-2016), July 18-19, 2016, Indian Institute of Science, Bangalore. **(Poster presentation)**

14. **Ajeet Kumar**, K.C. James Raju and A.R. James, "Enhanced piezo response in mechanical activated and microwave sintered PLZT 8/60/40 ceramics", IEEE International Symposium on the Applications of Ferroelectrics, European Conference on Applications of Polar Dielectrics & Workshop on Piezoresponse Force Microscopy (ISAF/ECAPD/PFM-2016), to be held on August 21-25, 2016, Technische Universität Darmstadt, Darmstadt, Germany. **(Selected for Oral presentation)**